Department of Phytopathology
Justus Liebig University of Gießen

Cell cycle regulation under pattern-triggered immunity

DISSERTATION

for the award of the doctoral degree (Dr. rer. nat.)
in the Faculty of Agricultural Sciences, Nutritional Sciences and Environmental Management at the Justus Liebig University of Gießen

submitted by
Sim Üstüner Uyumaz
from Çankaya, Turkey

Gießen, 2025

With the permission of the Faculty of Agricultural Sciences, Nutritional Sciences and Environmental Management of the Justus Liebig University of Giessen

Board of Examiners:

1st reviewer: Prof. Dr. Patrick Schäfer

2nd reviewer: Prof. Dr. Annette Becker

Examiner: Hon. Prof. Dr. Philip Lane

Examiner: Prof. Dr. Michael Frei

Chairperson: Prof. Dr. Jan Siemens

Date of the Disputation: 06.06.2025

Table of Contents

Authors declaration

I declare that the doctoral thesis here submitted is entirely my own work, written without any unauthorised help by a third party and solely with the assistance referred to in the thesis. I have indicated in the text those texts that have been quoted from already published sources, either verbatim or by analogy and all statements based on verbally conveyed information. During the research carried out by me and referred to in the doctoral thesis, I have at all times followed the principles of good scholarly practice as defined in the Statute of Justus Liebig University Giessen for Ensuring of Good Academic Practice.

Sim Üstüner Uyumaz

Parts of this work have already been published

Üstüner, S., Schäfer, P., & Eichmann, R. (2022). Development specifies, diversifies and empowers root immunity. *EMBO reports*, *23*(12), e55631.

Please note: Some parts of the introduction section of this thesis have been directly quoted from the above-mentioned article. Quotation marks have been applied where necessary and indicated with the citation "taken from Üstüner et al., 2022".

List of figures

List of tables

Abbreviations

A. thaliana	*Arabidopsis thaliana*
A. tumefaciens	*Agrobacterium tumefaciens*
APS	Ammonium persulfate
ATS	*Arabidopsis thaliana* salt
BAK1	BRI-ASSOCIATED RECEPTOR KINASE 1
BiFC	Bi-fluorescence complementation
BIK1	BOTRYTIS-INDUCED KINASE 1
BR	Brassinosteroid
BSA	Bovine serum albumin
CBB	Coomassie brilliant blue
CDK	Cyclin-dependent kinase
cDNA	Complementary DNA
CDS	Coding sequence
chi7	Active epitope of chitin
CYC	Cyclin
dai	Day after infiltration
DAMP	Damage-associated molecular pattern
dat	Day after treatment
DDR	DNA damage responses
DMSO	Dimethyl sulfoxide
dNTP	Deoxynucleotide triphosphates
DTT	Dithiothreitol
DZ	Differentiation zone
E. coli	*Escherichia coli*
e.g.	For example
elf18	Active epitope of elongation factor Tu
ETI	Effector-triggered immunity
ETS	Effector-triggered susceptibility
EZ	Elongation zone
flg22	Active epitope of bacterial flagellin
FLS2	FLAGELLIN SENSITIVE 2
G_1	Gap 1 phase
G_2	Gap 2 phase
GA	Gibberellic acid
gDNA	Genomic DNA
h	hour
hat	Hour after treatment
HR	Hypersensitive response
HRP	Horseradish peroxidase
HU	Hydroxyurea
I.I	Protein instability index
IPTG	Isopropyl β-D-1-thiogalactopyranoside
JA	Jasmonic acid
kDa	kiloDalton
L0, L1 and L2	Level 0, 1 or 2
LB	Lysogeny broth

LRR	Leucine-rich repeats
MAPK	MITOGEN-ACTIVATED PROTEIN KINASE
MS	Murashige and Skoog
N. benthamiana	*Nicotiana benthamiana*
NL	Nuclear protein localization
NLPs	Necrosis and ethylene-inducing peptide 1-like proteins
NLR	Nucleotide-binding/leucine-rich-repeat receptor
ns	No stop
o/n	overnight
P. parasitica	*Peronospora parasitica*
P. syringae	*Pseudomonas syringae*
PAMP	Pathogen-associated molecular patterns
PCR	Polymerase chain reaction
PIC	Protease inhibitor cocktail
PMSF	Phenylmethylsulfonyl fluoride
PRR	Pattern-recognition receptor
PTI	Pattern-triggered immunity
PTM	Post-translational modifications
PVDF	Polyvinylidene difluoride
QC	Quiescent centre
qRT-PCR	Quantitative real-time PCR
R proteins	Resistance proteins
RAM	Root apical meristem
Rel	Relative
Rep	Replicate
RGI	Root growth inhibition
RLK	Receptor-like kinases
RLP	Receptor-like proteins
RNA-seq	RNA sequencing
ROS	Reactive oxygen species
rpm	Revolutions per minute
RT	Room temperature
SA	Salicylic acid
SCR	SCARECROW
SDS	Sodium dodecyl sulfate
sec	seconds
seq	sequence
SHR	SHORTROOT
T-DNA	Transfer DNA
TBST	Tris buffered saline with Tween 20
tGFP	Turbo green fluorescent protein
UV	Ultraviolet
X-Gal	5-bromo-4-chloro-3-indolyl-beta-D-galactopyranoside

Summary

In a world with a constantly growing population, improving crop yields is necessary to ensure food security. However, plant diseases severely impact crop yields, and breeding efforts to enhance plant immunity can be limited by trade-offs between immune activation and growth. Yet, the molecular mechanisms behind these growth-immunity trade-offs remain largely unknown. Therefore, the aim of this work was to investigate the influence of pattern-triggered immunity (PTI) on mitotic cell cycle regulators during root growth inhibition (RGI).

Previous findings indicated that the intensity of the immunity-related RGI varies depending on the plant growth medium used. In this thesis, PTI responses in *Arabidopsis thaliana* (*A. thaliana)* roots grown on two standard growth media were compared. Depending on the medium, roots exhibited a much stronger response to elicitor flg22 (the active epitope of bacterial flagellin), in terms of RGI, reactive oxygen species production as well as immunity gene induction, and this was largely independent of gelling agent or media buffering. Using fluorescent PTI reporter lines, it was also shown that depending on the growth media used, different root zones responded to PTI elicitor treatment. Together, the findings that growth media can have a strong influence on PTI levels might be helpful for researchers to employ suitable growth conditions for PTI studies.

In the second part of this thesis, to gain a better understanding of the growth-immunity cross-talk, the expression of key cell cycle regulator genes was analyzed after PTI activation by exogenous application of the flg22 elicitor to *A. thaliana* roots. The results showed that the expression of various cell cycle regulators (e.g. *CYCLIN DEPENDENT KINASE B2;1* (*CDKB2;1*) and *CYCLIN D1;1* (*CYCD1;1*)) was reduced during flg22-induced PTI. Furthermore, the effect of flg22 treatment on key cell cycle regulator protein levels in *Nicotiana benthamiana* was investigated, and it was found that flg22-triggered PTI may disrupt protein accumulation (e.g. CYCD2;1).

Finally, it was shown that supporting the cell cycle by overexpressing some cell cycle regulators (e.g. *CDKB2;1*) could reduce root growth inhibition caused by flg22 treatment in *A. thaliana*. Together, these results support that during RGI, immune activation by flg22 treatment may directly affect cell cycle regulators and that over-activation of various cell cycle regulators can uncouple immunity- and growth-related processes. This may potentially help breeding strategies to obtain disease resistant crops with unimpaired growth.

Zusammenfassung

In einer Welt mit einer ständig wachsenden Bevölkerung ist die Verbesserung der Ernteerträge notwendig, um die Ernährungssicherheit zu gewährleisten. Pflanzenkrankheiten wirken sich jedoch stark auf die Ernteerträge aus, und Züchtungsbemühungen zur Verbesserung der Pflanzenimmunität können durch negative Wechselwirkungen zwischen Immunaktivierung und Wachstum eingeschränkt werden. Die molekularen Mechanismen hinter den negativen Wechselwirkungen zwischen Wachstum und Immunität sind jedoch weitgehend unbekannt. Ziel dieser Arbeit war es daher, den Einfluss der auf der Erkennung von konservierten molekularen Mustern basierenden Immunität (*Pattern-triggered immunity* (PTI)) auf mitotische Zellzyklusregulatoren während der Hemmung des Wurzelwachstums zu untersuchen.

Frühere Erkenntnisse deuteten darauf hin, dass die Intensität der immunitätsbedingten Hemmung des Wurzelwachstums je nach verwendetem Pflanzenwachstumsmedium variiert. In dieser Arbeit wurden PTI-Reaktionen in Wurzeln von *Arabidopsis thaliana* (*A. thaliana*) Pflanzen verglichen, die auf zwei Standardwachstumsmedien wuchsen. Im Allgemeinen zeigten die Wurzeln je nach Medium eine mehr oder weniger starke Reaktion auf Behandlung mit dem Elicitor flg22 (das aktive Epitop des bakteriellen Flagellins) hinsichtlich der Wurzelwachstumsinhibition, der Produktion von reaktiven Sauerstoffspezies und der Induktion von Immunitätsgenen, und dies war weitgehend unabhängig vom Geliermittel oder der Pufferung des Mediums. Mithilfe fluoreszierender PTI-Reporterlinien konnte außerdem gezeigt werden, dass je nach verwendetem Wachstumsmedium unterschiedliche Wurzelzonen auf die Behandlung mit PTI-Elicitor reagierten. Die Erkenntnis, dass Wachstumsmedien einen großen Einfluss auf die Pflanzenimmunität haben können, könnte für Forscher hilfreich sein, um geeignete Wachstumsbedingungen für PTI-Studien zu finden.

Im zweiten Teil dieser Arbeit wurde, um ein besseres Verständnis der Wechselwirkung zwischen Immunität und Wachstum zu erlangen, die Expression wichtiger Zellzyklusregulatoren nach PTI-Aktivierung durch exogene Anwendung des Elicitors flg22 auf *A. thaliana*-Wurzeln analysiert. Die Ergebnisse zeigten, dass die Expression verschiedener Zellzyklusregulatoren (z. B. *CYCLIN-DEPENDENT KINASE B2;1* (*CDKB2;1*) und *CYCLIN D1;1* (*CYCD1;1*)) während der durch flg22 induzierten PTI reduziert wurde. Darüber hinaus wurde die Wirkung der flg22-Behandlung auf die Proteinakkumulation wichtiger Zellzyklusregulatoren in *Nicotiana benthamiana* untersucht und es wurde festgestellt, dass die durch flg22 ausgelöste PTI die Proteinakkumulation (z. B. CYCD2;1) stören kann.

Schließlich konnte die Unterstützung des Zellzyklus durch Überexpression verschiedener Zellzyklusregulatoren (z. B. *CDKB2;1*) die durch die flg22-Behandlung in *A. thaliana* verursachte Wurzelwachstumshemmung reduzieren. Zusammen zeigen diese Ergebnisse, dass während der Wurzelwachstumshemmung die Immunaktivierung durch die flg22-Behandlung Zellzyklusregulatoren

direkt beeinflussen kann, und dass durch die Überaktivierung verschiedener Zellzyklusregulatoren die negativen Wechselwirkungen zwischen Immunität und Wachstum entkoppelt werden können. Dies könnte möglicherweise dabei helfen Züchtungsstrategien zu entwickeln, um krankheitsresistente Pflanzen mit ungestörtem Wachstum zu erhalten.

1 Introduction

1.1 Improving crop stress resistance under changing climates

The United Nations estimates that the growing world population will reach 9.7 billion by 2050 and 10.9 billion by 2100 (United Nations, 2019). It is anticipated that achieving food security, which aims to ensure access to sufficient, safe and nutritious food by all people, will be an extremely challenging for humanity. Factors like global warming, loss of culturable soil and arable land, loss of biodiversity will further enforce the need for more efficient food production (Tilman et al., 2011). The World Resources Institute predicts that to feed nearly 10 billion people in 2050, more than 50% more food will have to be produced compared to 2010 (World Resources Institute, 2019).

One of the imperatives to meet this demand is to be able to enhance crop yield. However, plant pathogens causing diseases can dramatically reduce crop yield. It was estimated that plant pathogens may cause around 14% of global crop loss per year (Vyska et al., 2016). Alarmingly, recent studies showed that climate change may further intensify plant diseases and their devastating effects on crops by increasing abundance and spreading of existing pathogens, promoting the emergence of new pathogenic strains, and changing host-pathogens interactions (Singh et al., 2023). This may result in dramatic plant disease outbreaks and severe crop loss. For example, a recent study predicted that under climate change, the *Triticum* pathotype of the fungal pathogen *Magnaporthe oryzae*, which leads to wheat blast disease, may dramatically spread especially in the Southern Hemisphere, considerably affecting global wheat production (Pequeno et al., 2024). Root diseases are expected to worsen due to global warming as well. For instance, Delgado-Baquerizo et al. projected a global atlas of soil-borne plant pathogens and future climate predictions, and showed that there might be a significant boost in the abundance of soilborne pathogens worldwide (Delgado-Baquerizo et al., 2020). In order to meet the increasing demand of food and ensure the global food security, it is vital to produce crops resistant to pathogens. To achieve this, it is crucial to have a comprehensive understanding of plant immunity.

1.2 Plant innate immunity

Plants encounter a diverse range of organisms during their lifetime. These organisms can affect plants in positive (growth-promoting mutualists, e.g. *Serendipita indica*), neutral (commensals) or negative ways (pathogens) (Raaijmakers et al., 2009; Yu et al., 2019b). To fight against pathogens, plants are in a continuous evolutionary arms race with microbes (Dodds & Rathjen, 2010; Jones & Dangl, 2006). Unlike mammals, plants lack an adaptive immune system as they neither have mobile specialized immune cells nor a circulatory system (Andolfo & Ercolano, 2015). Instead, they have a cell autonomous innate immunity, which relies on the detection of pathogens by receptors and the activation of defence responses (Andolfo & Ercolano, 2015; Jones & Dangl, 2006). Plant innate immunity is thought to be two-layered, encompassing pattern-triggered immunity (PTI) and effector-triggered immunity (ETI) (Jones & Dangl, 2006).

PTI is based on the recognition of conserved microbe-associated molecular patterns (MAMPs). There are many MAMPs in nature but some of the most studied and well-known ones are the following: a 22 amino acids long epitope of the bacterial flagellin protein (flg22), an 18 amino acid long epitope of elongation factor Tu (EF-Tu), necrosis and ethylene-inducing peptide 1-like proteins (NLPs), enigmatic MAMP of Xanthomonas (eMax), polygalacturonases, and active epitope of chitin (chi7) (Albert et al., 2015; Gómez-Gómez & Boller, 2000; Gust et al., 2007; Jehle et al., 2013; Kaku et al., 2006; Kunze et al., 2004). MAMPs are recognized by specific pattern-recognition receptors (PRRs) at the plasma membrane. PRRs are receptor-like kinases (RLKs) or receptor-like proteins (RLPs) (Newman et al., 2013). One of the well-studied RLKs is FLAGELLIN SENSITIVE 2 (FLS2), which was first identified in the model plant *A. thaliana* (Gómez-Gómez & Boller, 2000). FLS2 has an extracellular domain of 28 leucine-rich repeats (LRRs), which plays role in recognition of flg22, a transmembrane (TM) domain and an intracellular serine/threonine kinase domain (Gómez-Gómez & Boller, 2000). LRR and kinase domains were shown to be necessary for binding of flg22 (Gómez-Gómez et al., 2001). Binding of flg22 to FLS2 initiates recruitment of BRI-ASSOCIATED RECEPTOR KINASE 1 (BAK1), which forms a heteromeric complex with flg22-bound FLS2 (Albert & Felix, 2010; Sun et al., 2013). Upon pattern recognition, complex downstream signalling pathways are activated and a broad range of cellular responses occur such as increasing of Ca^{2+} in both cytoplasm and nucleus, reactive oxygen species (ROS) burst, MITOGEN-ACTIVATED PROTEIN KINASE (MAPK) phosphorylation, which activates a wide range of immune responses such as the expression of PTI-associate genes (Birkenbihl et al., 2017; Boudsocq et al., 2010; Jacobs et al., 2011; Jeworutzki et al., 2010; Zhou & Zhang, 2020). As a result, a broad-spectrum resistance is established to stop the pathogen.

In addition, upon biotic or abiotic stress, damage-associated molecular patterns (DAMPs) can trigger and likely amplify PTI responses as well (Boller & Felix, 2009; Chuberre et al., 2018; Rzemieniewski &

Stegmann, 2022). Unlike MAMPs, DAMPs are endogenous molecules of the host organism (Boller & Felix, 2009). Pep1 is one of the DAMPs that has been identified in *A. thaliana*. It is cleaved from the precursor protein PROPEP1, which is produced in response to abiotic and biotic stress and Pep1 is detected by the RLKs PEP-RECEPTOR 1 (PEPR1) and PEPR2 (Bartels et al., 2013; Huffaker et al., 2006; Krol et al., 2010; Saijo & Loo, 2020; Yamaguchi et al., 2006, 2010). The detection leads to the activation of similar signaling cascades as the ones triggered by the detection of flg22 (Bartels et al., 2013). However, when Pep1 is applied exogenously, stronger PTI responses are induced as compared to flg22 application (Poncini et al., 2017). For instance, AtPep1 treatment triggers a stronger activation of defense genes and a stronger root growth inhibition (Poncini et al., 2017).

Although most of the PTI studies have focused on aboveground organs, roots can sense pathogenic threats and activate effective immune responses just like leaves. Root immunity seems necessary as in the rhizosphere, roots are exposed to a highly diverse and abundant set of microorganisms, including potential pathogens (Chuberre et al., 2018). The receptors *FLS2*, *PEPR1* and *PEPR2* are expressed in roots and roots are capable of responding to flg22 and Pep1, just like leaves (Bartels et al., 2013; Beck et al., 2014; Jacobs et al., 2011; Millet et al., 2010; Poncini et al., 2017; Wyrsch et al., 2015). Furthermore, Wyrsch et al., demonstrated that cut-off *A. thaliana* roots were still able to induce PTI hallmarks responses after MAMP treatment, indicating that activation of root immunity is independent of signals from shoots (Wyrsch et al., 2015).

PTI is generally sufficient to prevent infection of nonadopted microbes. However, in order to overcome PTI, pathogens have evolved counter attack strategies. They can deliver effector proteins, also referred to as virulence factors, into the host cells. Effectors can manipulate PTI at different levels, leading to the impairment of immune responses (Cui et al., 2015; Deslandes & Rivas, 2012; Jones & Dangl, 2006). For instance, *Pseudomonas syringae (P. syringae)* effector AvrPto directly targets BAK1 and inhibits the association of FLS2 and BAK1 during infection. Therefore, the MAMP-signalling initiation cannot take place (Shan et al., 2008). Another *P. syringae* effector HopAI1, can target *A. thaliana* MAP KINASE KINASE5 (MKK2), which results in disruption of MAPK cascade (Wang et al., 2010). Pathogens evolve effectors to suppress PTI, however in return, plants employ so-called resistance (R) proteins, which are usually members of the intracellular nucleotide-binding/leucine-rich-repeat receptor (NLR) family, to detect effectors or effector activities (Cui et al., 2015). This R protein-mediated recognition induces ETI, which is stronger than PTI responses. ETI often leads to a hypersensitive response (HR) that involves a localized cell death and provides resistance to biotrophic or hemi-biotrophic pathogens (Jones & Dangl, 2006). For a long time, it was thought that PTI and ETI are induced at different times and at different response levels. Based on this, Jones and Dangl introduced “the zigzag model of plant-microbe interactions” (Jones & Dangl, 2006). In “the zigzag

model", MAMPs are recognized by PRRs, which leads to activation of PTI, then successful pathogens counteract PTI with the effectors, resulting in effector-triggered susceptibility (ETS). In response, plant cells can detect the effectors and launch ETI. The model highlights the fluctuating defence amplitude; PTI activation is depicted as raising response, followed by ETS as a falling response and ETI activates a stronger response (Jones & Dangl, 2006). However, accumulating evidence rather suggests that although PTI and ETI rely on two different classes of immune receptors, they are controlled by highly intertwined and overlapping pathways, instead of being separate "layers" of immunity. For instance, Ngou et al., investigated immune response read-outs upon selective induction of only PTI (by MAMP treatment), only ETI (by using an estradiol-inducible promoter for the expression of a bacterial effector, which is then recognized by matching R proteins) or both PTI and ETI in *A. thaliana*. When PTI and ETI were co-induced, the PTI responses were stronger than after PTI induction alone, and similarly, when both PTI and ETI were co-induced, ETI responses were stronger and lasted longer (Ngou et al., 2021). In another study, Yuan et al. used *A. thaliana* plants, which were PTI deficient because of various mutations in PPR- or co-receptor genes and showed that ETI-mediated resistance and HR were significantly impaired. They also showed that ETI-related ROS burst was severely impaired in PTI mutants. Furthermore, transcriptome analyses using RNA sequencing (RNA-seq) of either wild type or the PTI co-receptor mutants (*bak1, serk4/bak1- like 1 (bkk1) and chitin elicitor receptor kinase 1 (cerk1)*) revealed that in the PTI-impaired mutants, ETI could restore the expression of a subset of PTI genes (Yuan et al., 2021a). These two studies show the requirement of PTI signaling components to fully activate ETI, and in turn that ETI boosts PTI signaling components. Therefore, in order to launch a robust immunity, PTI and ETI appear to work synergistically (Bjornson & Zipfel, 2021; Tena, 2021). Due to accumulating evidence, which indicates the presence of a cross-talk between PRR- and NLR-mediated immune signaling, the widely accepted "zigzag" model needed to be revised. An updated model of the plant immune system can be seen in Figure 1 (Yuan et al., 2021b). In this model, PTI is the primary immune pathway, which is endogenously controlled to prevent autoimmunity, and, in the case of a compatible interaction, by pathogen effectors, which leads to effector-triggered susceptibility (ETS). Upon activation of ETI through effector recognition by NLRs, ETI amplifies PTI components to stop the attacking pathogen. Unlike "the zigzag model", ETI is not depicted as a separate immune pathway (Couto & Zipfel, 2016; Yuan et al., 2021a; Yuan, et al., 2021b; Ngou et al., 2021).

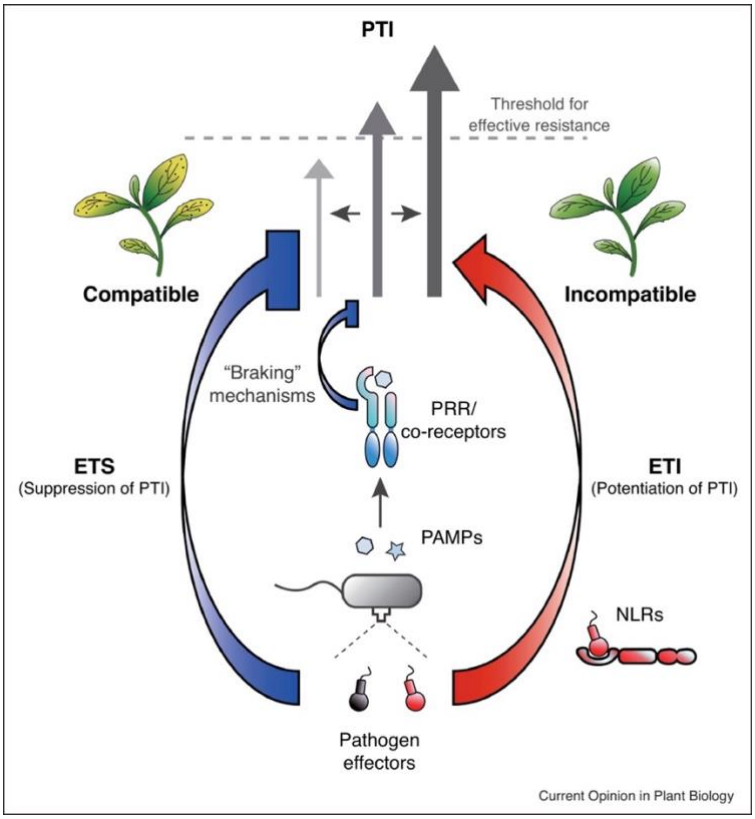

Figure 1: Model of the plant immune system: Pattern-triggered immunity (PTI) is acting as the primary immune response after perception of pathogen-associated molecular patterns (PAMPs) by pattern-recognition receptor (PRR) complexes: This is suppressed by endogenous "braking mechanisms" to prevent over activation (small blue arrow) or, in the case of a compatible plant-pathogen interaction, by bacterial effectors, which cause effector-triggered susceptibility (ETS) (big blue arrow). In an incompatible interaction, effector-triggered immunity (ETI) is activated through the recognition of pathogen effectors by nucleotide-binding domain leucine-rich repeat containing receptors (NLRs) and this recovers or potentiates PTI responses by upregulating PTI components (red arrow). The final resistance is equal to PTI minus the inhibition of PTI (by endogenous "braking mechanisms" or ETS) plus ETI. Taken from Yuan et al., 2021b.

1.3 Effect of immunity on plant growth

Although, plant immunity is necessary to stop pathogens, it is well documented that it can significantly impair plant growth in field-grown crops. This phenomenon has been reported for many different crops (Ning et al., 2017). For instance, the introduction of the *wheat streak mosaic virus resistance 1* (*Wsm1)* gene into wheat resulted in up to 21% yield reduction in the absence of a pathogen (Sharp et al., 2002). Or although the loss of the *Mildew-resistance locus O (Mlo)* gene of barley causes resistance to barley powdery mildew, its absence could lead to a reduction in grain yield by approximately 4.2% in the absence of the barley powdery mildew fungus (Jørgensen, 1992). Even regular activation of PTI by nonadopted microbes at the phyllosphere led to approximately 10% crop yield reduction in field-grown barley (Smedegaard-Petersen & Tolstrup, 1985). Many studies have shown the fitness cost of resistance in rice and maize as well (Goto et al., 2015; Kumar & Asino, 1994; Wang et al., 2021a). *Peronospora parasitica* (*P. parasitica*) -resistant genotypes of *Brassica napus* grew slower than *P. parasitica*-susceptible genotypes, even in the absence of the pathogen (Mitchell-Olds & Bradley,

1996). In addition, it has been reported that *A. thaliana* autoimmune mutants, which had a constitutively active immune system, showed a severe dwarfism phenotype (van Wersch et al., 2016). Yield penalties of disease resistance in crops may be as destructive as plant diseases (Eichmann & Schäfer, 2015). As mentioned in Section 1.1, in order to meet rising global food demands, we should maximize crop yield. Growth-immunity trade-offs might prevent us from achieving this goal as it can limit breeding efforts towards obtaining disease-resistant crops (He et al., 2022). Therefore, understanding the molecular mechanisms behind this cross-talk might help us to overcome it and increase both growth and disease resistance in crops. It is possible to induce growth-immunity trade-offs in lab-grown model plants as well. For instance, exogenous application of PTI elicitors flg22 or Pep1 reduces plant fresh weight and causes shorter primary roots in *A. thaliana* (Gómez-Gómez et al., 1999; Jacobs et al., 2011; Poncini et al., 2017). This can enable researchers to dissect and understand growth immunity cross-talk at the molecular level.

1.3.1 Potential causes of the growth-immunity antagonism

The first question that can come to mind is, "why does immunity inhibit plant growth?". Some researchers suggest that growth-immunity antagonism is a result of limited resources. "Since immunity and growth require a high amount of energy and other resources, it was hypothesized that growth-immunity trade-offs are the consequence of resource limitations and/or their imperfect reallocation. In such a model, plants would prioritize immunity over growth as cells and tissues may not be able to allocate sufficient resources to serve both processes at the same time (Brown, 2002; Herms & Mattson, 1992; Huot et al., 2014; Monson et al., 2022). Although resources might be limited under certain circumstances, the "reallocation model" might not be suitable to explain the phenomenon in general. While a range of MAMPs/DAMPs that are detected by RLK PRRs inhibit growth (e.g. flg22, elf18, Pep1), others such as chi7 or NLP (e.g. NLP20), which are ligands of RLP PRRs, do not (Böhm et al., 2014; Poncini et al., 2017; Pruitt et al., 2021)"(taken from Üstüner et al., 2022). Another commonly accepted hypothesis to explain growth-immunity antagonism is the autotoxicity of chemical defense. According to this theory, secondary metabolic changes during defense responses might be toxic to the plant itself and impair plant growth and development (Herms & Mattson, 1992; Neilson et al., 2013; Sestari & Campos, 2022). For instance, although methyl jasmonate plays important roles in defense signaling, high levels of methyl jasmonate can lead to growth inhibition in *A. thaliana* and be toxic to plant cells (Rehman et al., 2023; Staswick et al., 1992; Wasternack, 2007). Herms and Mattson proposed that in addition to "the resource reallocation model", growth-defense trade-offs can occur because the structural and secondary metabolic changes associated with defense responses can physiologically limit growth through cell division or cell expansion (Herms & Mattson, 1992).

However, in the light of recent studies, new theories that are contrary to the "the resource reallocation model" have been emerging. Kliebenstein (2016) has argued that "the resource reallocation model" is over simplified to explain the growth-immunity trade-offs as the theory assumes that all nutrients are equally limiting factors for both growth and immunity. However, in natural ecosystems, the situation might be more complicated. According to the author, growth and immunity do not necessarily require the same resources and in different ecosystems different nutrients might be the limiting factors. He proposed an alternative model in which growth and immunity are not in a "zero sum game" where growth or immunity wins and the other loses; rather they work together in a coordinated way to increase the fitness in changing environments. This regulation might be based on interfering signaling pathways, which sometimes work collaboratively and sometimes as trade-offs to ensure plants fitness (Kliebenstein, 2016)(See Section 1.3.2 for the intersecting compounds of growth and immunity).

Over 450-500 million years ago, early land plants have started to colonize land from aquatic life (Morris et al., 2018). Terrestrialization caused the exposure of the early land plants to different environmental stressors and potentially harmful microbes. Therefore, during evolution, plants developed sophisticated signaling components and metabolic pathways to survive stress and maintain growth. According to Sestari and Campos, the increasing complexity could have raised the chance of interference or cross-talk between pathways (Sestari & Campos, 2022). While "the resource reallocation model", explains growth immunity trade-offs based on resource limitations (Züst & Agrawal, 2017), as explained above, it may not be sufficient to explain the growth-immunity antagonism. In the conflicting signalling scenario, the intertwined nature of signaling and metabolic pathways controlling growth and defense increases the likelihood of pathway interference and leading to the trade-offs.

1.3.2 Intersecting compounds of growth and immunity

We are only just beginning to understand the interactions of growth and immunity and it appears that these interactions are sophisticated and occur at many different levels. It is thought that shared receptors and signaling components between plant hormones and immunity pathways may act as key mediators of the growth-immunity trade-off (Denancé et al., 2013; Eichmann & Schäfer, 2015; Guo et al., 2018; Huot et al., 2014; Lozano-Durán & Zipfel, 2015; Reitz et al., 2015; Smakowska et al., 2016). For instance, it is known that some components of the brassinosteroid (BR) signaling pathway such as BAK1, BOTRYTIS-INDUCED KINASE 1 (BIK1), or BRASSINOSTEROID-SIGNALLING KINASE 1 (BSK1) play roles in both immunity and plant growth (Chinchilla et al., 2007; Eichmann & Schäfer, 2015; Lin et al., 2013; Shi et al., 2013). An activated BR pathway induces the transcription factors *HOMOLOGUE OF BEE2 INTERACTING WITH IBH 1 (HBI1)* and *BRASSINAZOLE RESISTANT 1 (BZR1)*, which induce the

expression of growth-related genes and downregulate PTI genes. In addition, flg22 inhibits *HBI1* transcription (Fan et al., 2014; Lozano-Durán et al., 2013). Gibberellic acid (GA) promotes degradation of DELLA proteins, which normally repress growth-related transcription factors. flg22 treatment prevents GA-mediated DELLA degradation and this may cause flg22-induced growth inhibition (Huot et al., 2014; Navarro et al., 2008). Upon immunity activation, conflicting hormone signaling may redirect the growth (Eichmann & Schäfer, 2015). There are many examples of hormones as mediators of growth-immunity trade-offs but this is outside the scope of this work.

ROS signaling might be another one of the mediators of growth-immunity cross-talk. In addition to its roles in regulating the expression of growth and immunity, HBI1 controls the expression of ROS homeostasis-related genes as well (Neuser et al., 2019). In addition, MYB30, which is a ROS-responsive transcription factor, regulates gene networks involved in both root growth and plant immunity (Mabuchi et al., 2018; reviewed in Üstüner et al., 2022). Therefore, the antagonism between growth and defense programs might in parts be attributed to ROS homeostasis (Camejo et al., 2016; Dwivedi et al., 2021; Mase & Tsukagoshi, 2021; Neuser et al., 2019).

There has been a growing interest in plant growth regulatory peptides in the context of growth-immunity cross-talk. Recently, it has been shown that a peptide that is involved in plant development, GOLVEN2, could act as a positive regulator of PTI by increasing PRR abundance and increase antibacterial resistance in *A. thaliana* leaves (Stegmann et al., 2022). In addition, FERONIA (FER) and its RAPID ALKALINIZATION FACTOR (RALF) ligands regulate both plant growth/development and immune signaling pathways (Haruta et al., 2014; Stegmann et al., 2017; Xiao et al., 2019; Zhang et al., 2020).

1.3.3 Can growth-immunity trade-offs be uncoupled?

Growth-immunity antagonism that is due to intersecting signaling compounds/pathways rather than resource allocation would raise the possibility of genetically uncoupling growth and immunity from each other. Achieving this could also potentially address the problems outlined in Section 1.1, e.g. generation of highly resistant crops with unimpaired growth. Recent efforts to understand mechanism behind growth and immunity revolves around understanding the molecular nature of the natural genetic crop variants that are resistance to pathogens but show no reduced yield, rewiring the signaling pathways through genetic manipulation (He et al., 2022). The advancement of technologies e.g., in transcriptome sequencing and gene editing will undoubtedly strengthen these efforts.

Several studies have shown that natural genetic variations in crops exist that may lead to pathogen resistance without yield loss. Understanding those genetic variations may help us to overcome growth-immunity antagonism in crop plants (He et al., 2022). For instance, Deng et al. sequenced a rice variant that was resistant to rice blast without exhibiting yield loss. The authors found that this

rice variant had the *Pigm* locus, which contained various genes encoding NLRs. Among these receptors, PigmR and PigmS worked antagonistically to confer rice blast resistance without yield penalty (Deng et al., 2017). Similarly, in rice, a natural variant of the Ca^{2+} sensor *ROD1* caused resistance to pathogens without dampening grain yield (Gao et al., 2021).

To uncouple growth and immunity, ongoing efforts are based on genetic manipulation and for example, rewiring and re-combining growth and immunity signaling pathways (He et al., 2022). For example, light plays vital roles in plant growth and *A. thaliana* phytochrome B (*phyB*) mutants showed increased growth (Campos et al., 2016; He et al., 2022). On the other hand, jasmonic acid (JA) is a major phytohormone for immunity, and a polymutant in *JASMONATE ZIM-DOMAIN* (*jaz)* genes have constitutive JA signaling, accumulated defensive compounds but were impaired in growth (Betsuyaku et al., 2018). However, having *phyB* in *jaz* polymutants resulted in partial rescue of growth without losing the increased defense status (Campos et al., 2016; He et al., 2022). Salicylic acid (SA) is a well-known phytohormone, which is essential for immune signaling in plants. Although, overproduction of SA enhances disease resistance and abiotic stress tolerance, it negatively affects growth. Ortega et al. generated a set of *A. thaliana* transgenic lines, which produced different levels of SA and investigated the lines for plant growth, disease resistance and abiotic stress tolerance. They showed that high levels of SA downregulated *COLD-REGULATED (COR)* genes and that plants were smaller in normal conditions and grew even less at lower temperatures. However, overexpression of individual *COR* genes in plants producing high levels of SA could uncouple SA-mediated-growth and immunity trade-offs (Ortega et al., 2024). Similar attempts were also made for crop plants as well. For example, the transcription factor IDEAL PLANT ARCHITECTURE 1 (IPA1) of rice can balance growth and immunity in cooperation with WRKY45. Upon *Magnaporthe oryzae* infection, IPA1 was reversibly phosphorylated and upregulated the expression of *WRKY45*, which led to the activation of immune responses. Several hours after the infection, IPA1 was dephosphorylated again and supported growth (Wang et al., 2018). Interestingly, Liu et al. showed that overexpression of *IPA1* increased disease resistance but reduced crop yield, likely due to reduced GA levels. However, expressing *IPA1* under the pathogen-inducible promoter of *OsHEN1,* alleviated this effect, resulting in plants with high disease resistance and no loss in the yield. The authors also showed that increased resistance in the transgenic plants was partially due to DELLA protein accumulation, which is potentially mediated by GA pathway (Liu et al., 2019). Furthermore, editing disease susceptibility genes (S genes) could also reduce increase immunity without impairing growth. However, the observed lack of growth impairment could be unintended (secondary) consequence of gene (He et al., 2022). For instance, Li et al. generated wheat lines with mutations in the *MLO* locus using CRISPR-Cas9-mediated gene editing. Although, the mutations had broad-spectrum resistance to powdery mildew, they had impaired growth. However, one *MLO* mutant

line had an unintended mutation, which caused the overexpression of the *TONOPLAST MONOSACCHARIDE TRANSPORTER* gene *TaTMT3B*. Transgenic overexpression of *TaTMT3B* in *mlo* mutant background, rescued the impaired growth and retained resistance to mildew in both wheat and *A. thaliana* (Li et al., 2022). Taken together, many studies showed that in laboratory settings, it might be possible to uncouple growth and immunity by genetically manipulating the shared components of growth and immunity.

1.4 Root architecture and growth of root

"In longitudinal direction, the primary root is organised in root apical meristem (RAM), elongation zone (EZ) and differentiation zone (DZ) (Figure 2; Brady et al., 2007; Salvi et al., 2020)). At the very tip of the root (apical meristem), the root cap facilitates soil penetration and guides the direction of growth through the perception of gravity. The root cap also functions as an environmental sensor and protects the meristematic stem cell niche from damage (Kumpf & Nowack, 2015). The stem cell niche, a group of undifferentiated mitotically active stem cells (or initials), which is arranged around rarely dividing quiescent centre (QC) cells at the base of the RAM, is the root's organising centre from which all root tissues derive (Aichinger et al., 2012; Clowes, 1953; de Luis Balaguer et al., 2017; Dolan et al., 1993; Pardal & Heidstra, 2021; van den Berg et al., 1997). Cells that emerge from the stem cell niche subsequently divide in the RAM and then increase in length while passing through the EZ. Subsequently, cells differentiate and obtain specific genetically predestined functions. Emerging root hairs, for example, mark the beginning of the DZ (Datta et al., 2011; Topp & Benfey, 2012). The basis for the formation of lateral roots is also already being established when cells pass the RAM and EZ before they eventually emerge in the DZ (Banda et al., 2019; Laskowski & Ten Tusscher, 2017). Based on their specific transcriptional signatures, 15 different cell types with presumably different biological functions can be distinguished in *A. thaliana* roots (Birnbaum et al., 2003; Brady et al., 2007). Epidermis, cortex, endodermis and the pericycle around the vascular tissue (stele) are major cell types, which emerge from the stem cell niche and form cell files that appear as concentric rings in root cross-sections (Benfey & Scheres, 2000). Together with the root cap they form the core root body (Birnbaum, 2016; Dolan et al., 1993) (Figure 2). The stem cell niche determines this pattern of cell types as concentric files (Dolan et al., 1993; Pardal & Heidstra, 2021; van den Berg et al., 1997). In addition to root patterning, the stem cell niche functions in cell identity determination (Dinneny & Benfey, 2008). Stem cell divisions produce one cell with stem cell identity and a daughter cell that obtains cell type-specific identity depending on the position in the stem cell niche: Stem cells proximal to the QC found the stele in the centre of the root, which consists of the primary vascular tissues, procambium and pericycle (Brady et al., 2007; Tomescu, 2021). The ground tissue initials next to the stele initials generate two tissues, namely cortex and endodermis, following asymmetric cell divisions

(Cruz-Ramírez et al., 2012; Pardal & Heidstra, 2021). Casparian strip cell wall impregnations and suberin depositions are hallmarks of apoplastic diffusion barrier formation during endodermis differentiation (Barberon & Geldner, 2014; Geldner, 2013).“ (Taken from Üstüner et al., 2022). The plant root body plan is characterized by a precise organization based on cell types, which defines its structure and enables functional adaptability to environmental changes. Each cell type has a specific role in plant development (Petricka et al., 2012). Root cap cells primarily protect RAM, sense gravity and moisture, produce mucilage and facilitate phosphate uptake (Iijima et al., 2008; Kanno et al., 2016). Epidermis cells are involved in water and nutrient uptake as well as transport (Geldner, 2013). Cortex cells contribute to water and nutrient transport and help sense water potential gradient in soil (Barberon & Geldner, 2014; Dietrich et al., 2017; Geldner, 2013). Endodermis cells regulate selective nutrient uptake and form diffusion barrier (Geldner, 2013; Robbins et al., 2014). Pericycle cells are responsible for later root formation and play roles in xylem loading and phloem unloading (Beeckman & De Smet, 2014; Tegeder & Hammes, 2018). Finally, phloem and xylem cells are essential for the transport of water, nutrient and signalling molecules (Shabala et al., 2016).

Root growth is driven by the mitotic cell division and cell elongation regulated by the mitotic cell cycle and endocycle. Above the stem cell niche, cells proliferate rapidly via mitotic cell division. As the newly divided cell move away from the root tip, they stop dividing and enter to endocycle, where cells replicate DNA without cell division and they elongate (Breuer et al., 2014; Edgar et al., 2014; Heidstra & Sabatini, 2014; Sablowski & Carnier Dornelas, 2014; Sablowski & Gutierrez, 2022).

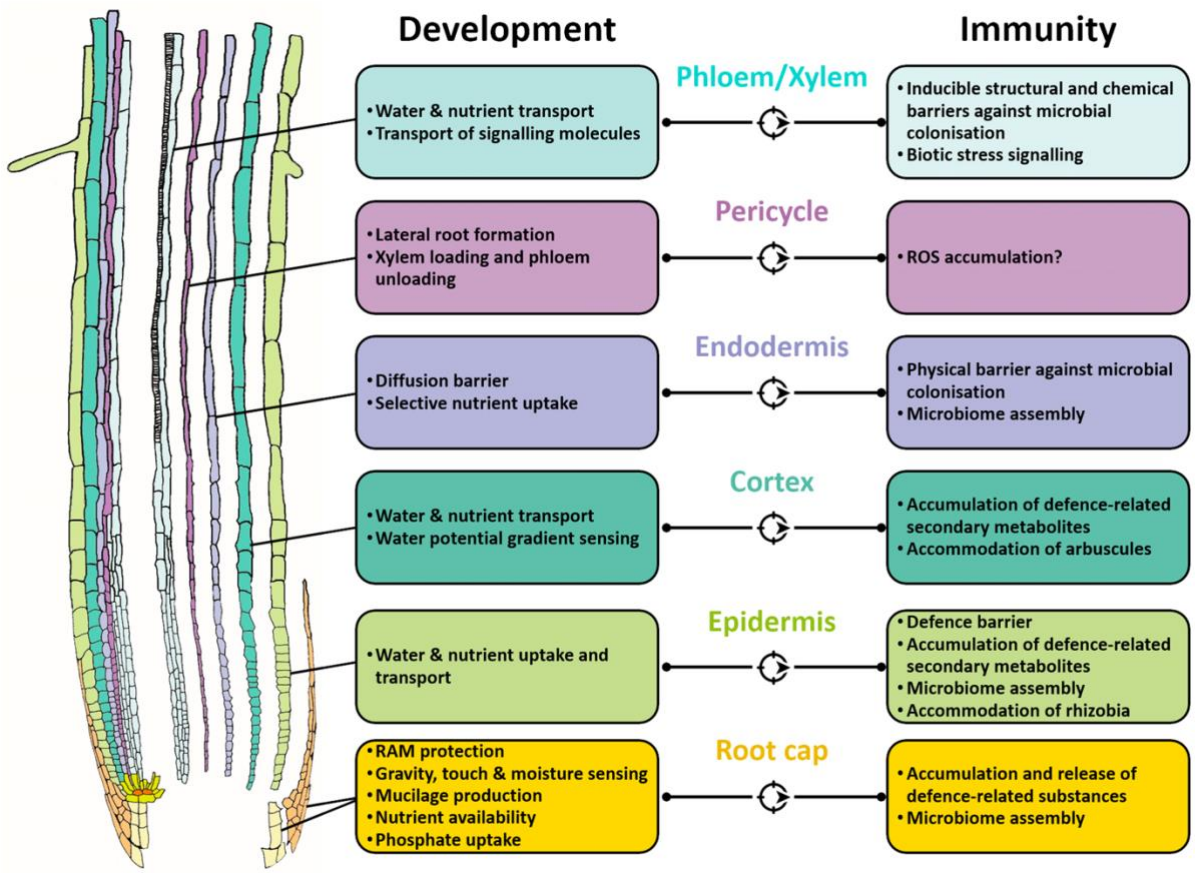

Figure 2: Functions of specific root cell types: Schematic longitudinal section of plant root and the functions of specific root cells. A strict cell type-based organization of root forms the plant root body plan, which determines the root´s structure. Root cap cells provide RAM protection, gravity, touch and moisture sensing, mucilage production and phosphate uptake. Epidermis cells are responsible from water and nutrient uptake. All cell types play role in water transport. In addition, cortex cells function in water potential gradient sensing. Endodermis cells provide selective nutrient uptake and diffusion barrier. Pericycle cells surround xylem and phloem and play roles in lateral root formation. The function of phloem and xylem cells is transportation of water, nutrient and signalling molecules. Taken from Üstüner et al., 2022.

1.5 The plant mitotic cell cycle

1.5.1 Plant cell cycle phases and the regulation of phase transitions

In plant cells, as in all eukaryotes, the cell cycle consists of specific phases: the DNA synthesis phase (S), during which DNA is duplicated, and the mitotic phase (M), where mitosis occurs. These phases are separated by the gap (G) phases: the G_1 phase takes place between the previous mitosis and the next S phase and G_2 separates the S phase from M phase. During the G_1 and G_2 phases, cells make sure that the previous phase has been fully completed without any errors. In order to preserve genome integrity and its transmission to the next generation, transition between the phases, particularly G_1 to S and G_2 to M phase transitions, are tightly regulated (Dewitte & Murray, 2003). The main regulators of the cell cycle are CYCLIN-DEPENDENT KINASES (CDKs), CYCLINS (CYCs) and CDK inhibitors. Various CDK-CYC complexes phosphorylate numerous substrates at the transition points to regulate the expression of the genes that play role in DNA replication and mitosis (Dewitte & Murray, 2003; Inzé & De Veylder, 2006).

The *A. thaliana* genome encodes 12 *CDK*s and more than 49 *CYC*s, which have been classified according to their sequences, and the classification reflects well with their functional diversity (De Veylder et al., 2007). Compared to mammals, plant genomes encode more cell cycle regulators. For example, mammalian genomes encode three types of *D-type CYCs*, whereas the *A. thaliana* genome encodes 10 (Inzé & De Veylder, 2006; Sherr, 1995). Extensive duplications of the plant genome might be one of the reasons for the higher number and complexity of plant CYCs (Simillion et al., 2002). In addition, the high number of plant CYCs might be attributed to the sessile lifestyle of plants, which requires significant developmental plasticity for the response to both internal and external cues (Inzé & De Veylder, 2006).

Plants have two major classes of CDKs: A-type and B-type CDKs. In *A. thaliana*, there is only one gene encoding an A-type CDK (*CDKA;1*) and four genes encoding B-type CDKs (*CDKB1;1, CDKB1;2*, *CDKB2;1* and *CDKB2;2*)(Dewitte & Murray, 2003). Transcript and protein levels of *CDKA;1* do not significantly fluctuate during the cell cycle. However, its kinase activity is post-translationally upregulated during the G_1/S and the G_2/M transitions (Dewitte & Murray, 2003; Iwakawa et al., 2006). In contrast, CDKB levels are dependent on the cell cycle phase and highest at G_2/M phase transition, where their kinase activities are needed (De Veylder et al., 2007).

It is thought that transcript levels of B1-type CDKBs reach the highest levels during S- to M-phase, whereas B2-type CDKBs transcripts accumulate from late G_2- to late M-phase (Oakenfull et al., 2002). The specificity and the temporal regulation of the CDKs are mainly controlled by CYCs. In plants, A-type (CYCA) and B-type (CYCB) CYCs control the S/G_2-phase and the G_2/M-phase transition, respectively (Polyn et al., 2015). Although it is widely accepted that CYCDs regulate G_1/S transition,

accumulating evidence suggests that they play a role in the G_2/M transition as well. Various *CYCD*s show a transcriptional peak at the G_2/M phase (Inzé & De Veylder, 2006)(See Section 1.5.2).

In addition to the CYCs, there are several other proteins that play a role in the control of cell cycle transitions. For instance, CDK-inhibitory proteins such as KIP-RELATED PROTEINS (KRPs) and SIAMESE (SIM)/SIM-RELATED PROTEINS (SMR), CDK-activating kinases (CDKD and CDKF) and ANAPHASE-PROMOTING COMPLEX/CYCLOSOME (APC/C) ubiquitin ligases, which proteolyze cyclins, are some of the proteins that regulate CDK activity in response to different stimuli (Churchman et al., 2006; Heyman & De Veylder, 2012; Polyn et al., 2015; Umeda et al., 2005). Before the G_1/S transition, RETINOBLASTOMA RELATED PROTEIN 1 (RBR1) binds to E2F and inhibits its dimerization with DIMERIZATION PARTNER (DP). During transition, a CYCD/CDKA;1 complex hyper-phosphorylates RBR1, which allows the dimerization of the E2F and DP transcription factors, which controls the expression of DNA synthesis genes (Magyar et al., 2012). At the G_2/M transition, CDKA;1/CYCB or CDKBs/CYCB complexes phosphorylate MYB3R transcription factors to control the expression of mitosis genes (De Veylder et al., 2007).

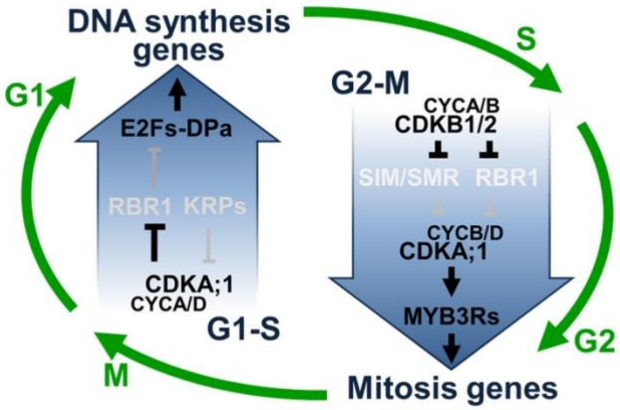

Figure 3: The plant mitotic cell cycle: The plant cell cycle consists of four phases; G_1, S, G_2, and M. The key regulator proteins are CDKs, CYCs and CDK inhibitors. G_1/S progression is promoted by the CDKA/CYCD complex hyper-phosphorylates RBR1, which relieves E2F-DPa repression. As a result, the transcription of S-phase genes are initiated. CDKA/CYCD complexes can be inhibited by KRP. S-phase progression is maintained by CYCA/B, which binds to CDKB1/2. SIM/SMR can target CDKB1/2 activity to provide a checkpoint mechanism during S-phase. G_2/M transitions is mediated by the interaction between CYCB/D and CDKA;1. The complex activates MYELOBLASTOSIS VIRUS transcription factor 3Rs (MYB3Rs), which regulate expression of mitotic genes. (Figure provided from Patrick Schäfer)

1.5.2 B-type CDKs and D-type CYCs in *A. thaliana*

The class of B-type CDKs is unique to plants as it has not been described in other organisms. CDKB1 and CDKB2 classes are characterized based on the presence of a PPTALRE or PPTTLRE hallmark motif, respectively (De Veylder et al., 2007). As mentioned in Section 1.5.1, B-type CDKs are thought to regulate G_2/M and play crucial roles in many developmental processes. For instance, CDKB1;1 is required to maintain the balance between mitotic cell division and endoreduplication (Boudolf et al., 2004b). In addition, CDKB1;1 plays a crucial role in the DNA damage responses (Weimer et al., 2016). CDKB1;1 and CDKB1;2 regulate the fate of stomatal cell lineages (Xie et al., 2010). CDKB2s on the other hand are required for shoot apical meristem integrity (Andersen et al., 2008).

The *A. thaliana* genome encodes 10 different *D-type CYC*s, which play roles in different phases of the cell cycle and control many embryonic and post-embryonic developmental processes in different plant tissues in response to internal and external signals. For instance, CYCD2;1 modulates auxin-induced lateral root formation together with INHIBITOR-INTERACTOR OF CDK/KIP-RELATED PROTEIN 2 (ICK2/KRP2) (Sanz et al., 2011). In leaves, CYCD3;1 controls the balance between cell proliferation and differentiation (Dewitte et al., 2003). The members of the CYCD3 family and CYCD7;1 regulate developmental rate during seed development (Collins et al., 2012; Sornay et al., 2016). Various members of CYCDs (such as CYCD4, CYCD3, CYCD5;1, CYCD7;1) are associated with stomatal development (Han et al., 2018; Kono et al., 2007; Weimer et al., 2018; Yang et al., 2014). The transcription factors SHORTROOT (SHR) and SCARECROW (SCR), which control ground tissue patterning, were shown to directly activate CYCD6;1, which is needed for proper root pattern formation (Sozzani et al., 2010).

It has been suggested that the expression of CYCDs is not necessarily dependent on a particular phase but rather correlates with internal and external factors. CYCDs are considered as the linkers of environmental factors to the cell cycle (De Veylder, 2019; De Veylder et al., 2007; Polyn et al., 2015). Early studies with *A. thaliana* cell suspension cultures showed that the expression of *CYCD2;1* and *CYCD3;1* was dependent on the presence of sucrose in the culture media, and sugar induced their gene expression (Riou-Khamlichi et al., 2000). Other studies showed that although the transcript levels of *CYCD2;1* and *CYCD3;1* dropped upon sugar removal, the protein level of CYCD2;1 was not changed, whereas the CYCD3;1 level dropped (Healy et al., 2001). Besides sugar, *CYCD3;1* expression showed strong responses to plant hormones (Dewitte & Murray, 2003; Oakenfull et al., 2002). Recent studies indicated that CYCDs form complexes with CDK inhibitors such as SMRs to inhibit CDKs in the case of stress (e.g. DNA damages) (De Veylder, 2019; Yi et al., 2014).

It is known that CDKBs and CYCDs form complexes to regulate G_2/M transitions. Kono et al. showed that CYCD4;1 is an interaction partner of CDKB2;1 via a yeast two-hybrid screening and *in vitro* Co-

immunoprecipitation, and they suggested that CDKB2;1 and CYCD4;1 form a complex to mediate G_2/M transition (Kono et al., 2003). Many studies have suggested protein-protein interactions between CDKBs and a large number of CYCDs using bi-fluorescence complementation (BiFC), yeast two-hybrid screening, *in vitro* Co-immunoprecipitation (Boruc et al., 2010; Kawamura et al., 2006; Kono et al., 2003; Van Leene et al., 2010; Veylder et al., 1997). It is important to note that little is known about the molecular mechanisms that regulate G_2/M transitions. Therefore, more functional studies are needed to reveal those molecular mechanisms.

1.5.3 Plant cell cycle and abiotic and biotic stress

"According to endogenous and exogenous changes, plants can regulate their cell cycle machinery (Pedroza-Garcia et al., 2022; Rymen & Sugimoto, 2012). This allows them to survive non-favourable conditions. CDKs and CYCs are thought to play a role in regulating cell division rates in response to environmental stress (Carneiro et al., 2021). It is known that abiotic stress, for instance, may lead to growth inhibition in plants by direct or indirect interference with the cell cycle. Salt treatment leads to root growth inhibition in an ABA-dependent manner (Geng et al., 2013). Recently it was shown that salt stress reduces the accumulation of CDKs (e.g. CYCB1;1) and some CYCs (e.g. CYCA2;1) in Arabidopsis [*A. thaliana*] roots (Carneiro et al., 2021; Qi & Zhang, 2019; West et al., 2004). In a similar way, biotic stress might affect cell cycle regulators and thus cell division. For instance, infection of Arabidopsis with geminiviruses changes the expression of cell cycle regulators, and overexpressing *CYCD3;1* or the cell cycle-promoting *E2F TRANSCRIPTION FACTOR 3* strongly increases plant resistance against geminivirus attack (Ascencio-Ibáñez et al., 2008). Little is known about biotic stress and cell cycle cross-talk. Hormones certainly take part directly or indirectly in underlying regulatory mechanisms. DELLA proteins, for instance, promote CDKA- and CDKB-inhibitors (Achard et al., 2009; Reitz et al., 2015), which may indicate a role of the defence hormone JA by its known function in growth inhibition based on its ability to downregulate CDKA1 and CYCB1;1 (Chen et al., 2011; Qi & Zhang, 2019)." (Taken from Üstüner et al., 2022)

The preliminary work conducted in the Schäfer lab indicated that flg22-induced PTI can interfere with cell cycle and inhibits root growth by affecting cell division. Eichmann et al. (unpublished) showed that the immune-elicitor flg22 caused shortening of the primary root without altering the overall root system architecture. The results demonstrated that the root meristem size was reduced after flg22 treatment and the root growth inhibition is FLS2-dependent as *fls2* mutants did not show the same phenotype. flg22-treatment did not affect stem cell niche function, but flg22 treated roots had less cortex cells in the meristem compare to the mock-treated roots, which implies that flg22 influences cell division. This was supported by reduced expression of GFP-tagged *CYCB1;1* (a cell division marker) and reduction in the levels of phosphorylated RBR1 after flg22 treatment (Eichmann et al.,

unpublished data). Additionally, Finch showed that flg22 or Pep1-induced PTI was associated with changes in relative abundance of various cell cycle marker gene transcripts in wild-type root tips (Finch, 2019). Further, the preliminary work done in the Schäfer lab indicated that overexpression of some cell cycle regulators in *A. thaliana* could abolish flg22-induced root growth inhibition. For instance, overexpressing *A. thaliana CDKB1;1* under Cauliflower mosaic virus 35S promoter exhibited reduced root growth inhibition upon flg22 treatment. The observed phenotype was dose-dependent; at higher concentrations of flg22 a slight root growth inhibition was observed. Importantly, the transgenic lines had still intact immune signaling and resistance against pathogens (Eichmann et al., unpublished data). Further screening which was conducted by J. Finch has showed that similar to CDKB1;1, overexpression of *A. thaliana CYCD1;1* also led to reduced sensitivity to flg22 treatment in terms of root growth (Finch, 2019). These results indicate that it might be feasible to uncouple growth and immunity by supporting various cell cycle regulators. Many previous studies investigated different aspects of the growth-immunity cross-talk (see above). The present work aimed at understanding the link between PTI signaling pathway and growth, with a focus on cell cycle regulation, and at investigating whether overexpression of other CDKBs and CYCDs leads to altered root growth after flg22-induced PTI activation (See Section 1.6 for objectives).

1.6 Objectives

In order to meet the world's increasing demand for food, researchers have focused on understanding various aspects of plant immunity and producing crops that are highly resistant to plant pathogens. However, breeding efforts to enhance plant immunity can be hampered by growth immunity trade-offs, where, due to unknown reasons, active plant immunity is accompanied by reduced growth. Previous findings indicated that plant immunity activated by the bacterial flg22 peptide may negatively interfere with the mitotic cell cycle, and that the negative effects of active immunity on root growth could be overcome by over-activation of cell cycle regulators.

The hypothesis of the thesis is that PTI induction influences cell cycle regulators in the root meristem, potentially explaining the RGI after flg22 treatment. The main aim of the thesis is to test this hypothesis and gain a deeper understanding of the molecular basis of the cross-talk between PTI and the mitotic cell cycle in *A. thaliana* roots with a particular focus on the cell cycle regulators B-type CDKs and D-type CYCs. Because the strength of the observed immunity-related root growth inhibition effect was dependent on the plant growth media used, first, it is aimed to determine which other kinds of immune response are affected by the choice of growth medium and to what extent. In addition, the properties of the different media that may account for the observed phenotypes will be tested.

Additionally, flg22-induced root growth inhibition could be overcome by supporting CDKBs and CYCDs. To test the hypothesis, the expression of all *CDKB* and *CYCD* genes will be analysed after immunity activation by flg22 treatment. Furthermore, all *CDKB* or *CYCD* coding sequences will be cloned as tagged versions under the control of strong constitutive promoters for transient and stable over-expression in plants. Transient over-expression in *N. benthamiana* leaves followed by flg22 treatment will be carried out to test whether flg22 treatment may affect protein abundance and thus function of cell cycle regulators during growth inhibition. Finally, root growth inhibition assays will be performed to examine if the stable overexpression of *CDKBs* or *CYCDs* alone or in combination can support root growth under flg22-triggered immunity and thus disentangle the growth-immunity antagonism.

2 Materials and Methods

2.1 Plant material and growth

Wild-type *A. thaliana* (Col-0) seeds were obtained from the Nottingham *Arabidopsis* Stock Centre. For the overexpressor lines generated and used in this study see Section 2.2.1. As PTI reporter lines, *pPER5::NLS-3xmVENUS* and *pMYB51::NLS-3xmVENUS* (Poncini et al., 2017) were used.

Surface sterilization of *A. thaliana* seeds was performed either with bleach (NaOCl) or with chlorine gas. For bleach sterilization, the required number of seeds were washed sequentially in 1 mL $H_2O_{0.02\%Tween20}$, 1 mL 70% ethanol, 1 mL 3% NaOCl, and sterile H_20 for 8 times. For the chlorine sterilization, the seeds were transferred into 2 mL Eppendorf tubes and the tubes were put in a rack with open lids. The rack was placed horizontally into a desiccator containing a glass beaker with 50 mL of 12% NaOCl solution. Under a fume hood, 3 mL of concentrated HCl were poured into the beaker, resulting in the immediate production of chlorine gas. The lid of desiccator was immediately closed and the seeds were incubated in chlorine gas for 3 h. After the incubation, seeds were washed once in $H_2O_{0.02\%Tween20}$ and 4 times in sterile H_2O. Sterilised seeds were transferred into 1 mL of 0.2% Gelrite™ (Duchefa Biochemie) or 0.2% phyto agar (Duchefa Biochemie). Stratification took place at 4°C for 2 days in the dark. Afterwards, under sterile conditions, seeds were transferred onto vertical square Petri dishes containing ATS medium (Lincoln et al., 1990) supplemented with 4.5 g l^{-1} Gelrite™, or with ½ "Murashige and Skoog basal salts with minimal organics MS medium" (½ MS) (Sigma, cat. M6899) with 0.05% (w/v) MES hydrate (Sigma Aldrich, cat. # M2933) containing 7 g l^{-1} Phytoagar (Duchefa Biochemie). Plants were grown in a 22°Cday/18°C night cycle, in 10 h light at 120 $\mu molm^{-2}s^{1}$. For *A. thaliana* seed propagation, plants were sown in a 5:1 soil-sand mix, supplemented with nematodes (*Steinernema feltiae*) as pest control. After 2 days of stratification at 4°C, plants were first grown in 22°C day/18°C night cycle with 8 h light. 5-6 weeks later, they were transferred into 24°C day/18°C night cycle with 16 h (long-day conditions) and grown until harvest. *Nicotiana benthamiana* (*N. benthamiana*) plants were grown in a soil-sand mix in the long-day conditions (see above).

2.2 Generation of transgenic *A. thaliana* lines

2.2.1 Generation of overexpression lines

2.2.1.1 Golden Gate Cloning

Golden Gate Cloning (Engler et al., 2014) was used to generate overexpression constructs of *CDK*Bs and *CYCD*s for *Agrobacterium tumefaciens* (*A. tumefaciens* or *Agrobacterium*)-mediated stable transformation of *A. thaliana,* and also for *A. tumefaciens*-mediated transient transformation of *N. benthamiana* leaves (see Table 2 for all plasmids used and generated). To generate the Level 0 (L0) no stop codon (ns) *tGFP* construct for C-terminal tagging, the coding sequence (CDS) of *tGFP* was amplified from pICSL80005 (for all Golden Gate vectors see Engler et al., 2014 and

https://www.addgene.org/) by using tGFP-specific primers removing the stop codon and including BpiI restriction enzyme recognition sites, as well as 4 bp overhangs for L0 (pAGM9121) ligation (see Table S1 for the primers used in this study). The PCR reaction mix was as follows: 32.5 µL ddH_2O, 10 µL 5x Q5 reaction buffer (New England Biolabs, cat. # M0491S), 2.5 µL 10 µM forward and reverse primer, 1 µL 10 mM dNTPs, 1 µL of 2 ng/µl plasmid template, 0.5 µL Q5 High-Fidelity DNA polymerase (New England Biolabs, cat. # M0491S). Thermal profile: 30 s at 98°C, 35 cycles of [10 s at 98°C, 20 s at 58°C, 20 s at 72°C], 5 min at 72°C. The amplification was confirmed by 1.2% agarose gel electrophoresis.

A number of L0 plasmids used in this study were produced by Jessica Finch (Finch, 2019). For the remaining plasmids, CDS fragments of the corresponding genes were synthesized by Integrated DNA Technologies. The stop codons were removed for C-terminal tagging. The illegal BsaI or BpiI restriction enzyme sites in the native sequences were removed with silent point mutations and corresponding overhangs for the ligation were added (see Table 1 for full sequences).

Ligation of *tGFP* PCR products or synthesised DNA fragments were ligated into L0 universal acceptor vector (pAGM9121) or L0 acceptor for CDS1 no stop modules (pAGM1287), respectively. The combined restriction enzyme digest and ligation reaction mix was as follows: 2 insert:1 acceptor molar ratio, 1.5 µL 10x T4 ligase buffer (New England Biolabs, cat. # M0202A), 1.5 µL bovine serum albumin (BSA, stock: 1 mg/mL), 0.5 µL T4 ligase (New England Biolabs, cat. # M0202S), 0.5 µL BpiI (Thermo Scientific, cat. # ER1011), topped up to 20 µL with ddH_2O. Thermal profile: 20 s at 37°C, 26 cycles of [3 min at 37°C, 4 min at 16°C], 5 min at 50°C, 5 min at 80°C, hold at 8°C. Ligation products were transformed into competent *Escherichia coli* DH5α cells and extracted from successfully transformed colonies (Section 2.2.1.2).

The corresponding L0 parts “promoter + 5’ untranslated region (UTR)”, “CDS of the gene of interest”, the corresponding “C-terminal tag”, and “3’ UTR modules” were ligated into L1 plasmid as follows: 100 ng of each L0 parts, 1.5 µL 10x T4 ligase buffer, 1.5 µL BSA, 0.5 µL T4 ligase, 0.5 µL BsaI (Thermo Scientific, cat. # ER0291), topped up to 20 µL with ddH_2O. The thermal profile was the same as for the L0 ligation reaction. Ligation products were again transformed into competent *E. coli* DH5α cells and extracted after confirmation (Section 2.2.1.2).

L1 plasmids were assembled into L2 acceptor vectors by using the same protocol as for L1 plasmid ligation but with a different restriction enzyme (BpiI instead of BsaI).

Table 1: Sequences synthesised for Golden Gate cloning: Green: BpiI recognition site, brown: 4 bp overhang. Red: domestication, silent point mutation

Gene name (AGI code)	Synthesised coding sequence
CDKB2;1 (AT1G76540)	GCAGGCTCCCTTGAAGACAAAATGGACGAGGGAGTTATAGCAGTTTCCGCCATGGATGCTTTCGAGAAGCTTGAGAAAGTTGGTGAAGGGACATACGGGAAAGTTTA CAGAGCCAGAGAGAAAGCTACCGGGAAAATCGTCGCTCTAAAGAAAACGCGTCTCCATGAGGACGAAGAAGGCGTTCCTTCCACCACTCTCCGCGAGATCTCCATTTTG CGAATGCTCGCTCGTGATCCTCACGTCGTCAGGTTAATGGATGTTAAGCAAGGACTAAGCAAAGAAGGCAAAACTGTACTGTACCTGGTTTTTGAATACATGGACACTG ATGTCAAGAAATTCATCAGAAGTTTCCGTAGCACTGGCAAGAACATTCCAACCCAAACTATCAAGAGCTTGATGTATCAACTATGCAAAGGTATGGCATTCTGCCATGG TCACGGGATATTGCACAGAGATCTCAAGCCTCACAATCTCTTGATGGATCCCAAGACAATGAGGCTCAAAATAGCAGATCTTGGTTTAGCCAGAGCCTTCACTCTGCCA ATGAAGAAGTATACCCATGAGATATTAACTCTTTGGTATAGAGCTCCAGAGGTTCTTCTTGGTGCCACCCATTACTCTACAGCTGTGGATATGTGGTCTGTTGGCTGCAT ATTTGCTGAACTTGTGACCAACCAAGCAATCTTTCAGGGAGACTCTGAGCTCCAACAGCTCCTCCATATTTTCAAGTTGTTTGGGACACCCAATGAAGAAATGTGGCCAG GAGTGAGCACACTCAAGAACTGGCATGAATACCCACAGTGGAAACCATCGACTCTATCCTCTGCTGTTCCAAACCTCGACGAGGCTGGAGTTGATCTTCTATCTAAAAT GCTGCAGTACGAGCCAGCGAAACGAATCTCAGCAAAGATGGCTATGGAGCATCCTTACTTTGATGATCTGCCAGAAAAGTCCTCTCTTTCGTTGTCTTCAACACCCAGCT TTC
CDKB2;2 (AT1G20930)	GCAGGCTCCCTTGAAGACAAAATGGACAACAATGGAGTTAAACCCGCTGTTTCCGCCATGGAAGCCTTTGAAAAGCTTGAGAAAGTAGGTGAAGGGACTTATGGGAA AGTTTACAGAGCAAGAGAGAAAGCTACTGGGATGATCGTTGCTTTGAAGAAAACGCGTCTCCATGAGGATGAAGAAGGTGTTCCTCCCACTACTCTTCGCGAGATCTCT ATCTTGCGTATGCTCGCTCGTGATCCTCACATCGTTAGGTTGATGGATGTTAAGCAAGGAATAAACAAAGAAGGAAAAACTGTACTTTACCTTGTTTTCGAGTATGTTG ATACTGATCTCAAGAAATTCATCAGAAGCTTTCGTCAAGCTGGACAGAACATTCCACAAAATACTGTCAAGTGCTTGATGTACCAGTTATGCAAAGGCATGGCTTTTTG CCATGGTCATGGAGTGTTGCACAGGGATCTTAAGCCTCACAATCTCTTGATGGACCGTAAGACAATGACGCTCAAAATAGCAGATCTTGGATTAGCCAGAGCCTTCACT CTCCCAATGAAAAAGTATACACATGAGATTCTAACTCTATGGTATAGAGCTCCGGAAGTTCTTCTTGGAGCAACCCATTACTCTACTGGAGTGGATATGTGGTCTGTTG GCTGTATTTTTGCTGAACTAGTGACCAAGCAAGCAATCTTTGCGGGAGACTCTGAGCTCCAACAGCTCCTCCGTATATTCAGGTTGTTGGGAACACCAAACGAAGAAGT TTGGCCTGGAGTAAGCAAACTCAAGGACTGGCATGAATACCCGCAATGGAAACCGTTGAGTCTCTCCACAGCTGTGCCAAACCTCGACGAGGCTGGACTTGATCTCTTA TCTAAAATGCTGGAGTACGAGCCAGCAAAACGAATCTCAGCAAAGAAAGCTATGGAGCATCCTTACTTCGATGATTTGCCTGACAAGTCCTCTCTTTCGTTGTCTTCAAC ACCCAGCTTTC
CYCD5;1 (ATG37630)	GCAGGCTCCCTTGAAGACAAAATGGGTGAGCCTAAAGACAGTCTCGCTCTCTTCCTCTGCCACGAATCGGAATCTTCTCTAAACGAAGATGACGACGAGACGATTGAGA GATCTGATAAGCAAGAACCTCACTTTACTACTACGATCGATGATGAAGATTATGTGGCAGACCTTGTTCTTAAAGAGAATCTCCGATTCGAAACCCTACCCTCTAAAAC GACGTCGTCATCCGATAGATTGATTGCCATCGATTGGATTCTCACTACAAGAACAAGATTTGGGTTCCAACATCAAACAGCTTACATTGCAATCTCATACTTCGATCTGT TTCTCCACAAAAGATTCATCGGTTTGCAGAAAGATGAAACATGGGCGATGCGATTGTTATCAGTAGCTTGTTTATCATTAGCTGCTAAAATGGAGGAACGTATTGTTCC TGGTTTATCACAATACCCTCAAGATCATGACTTCGTTTTCAAACCCGATGTCATTCGTAAAACTGAACTGTTGATTCTATCCACATTGGACTGGAAGATGAACTTGATCA CTCCTTTTCATTACTTCAACTACTTCCTTGCTAAAATCTCTCAGGACAACCATTCTGTTTCTAAAGACTTGGTGTTGTTAAGATCCTCTGATTCTCTTCTTGCTTTAACTAAA GAGATAAGTTTTACGGAGTATCGACAGTTTGTTGTTGCTGCTGTTACTACATTGCTAGCTTCTTCTTCTACCTCATCGGATATTAGATTGACTAGAGAAGAGATAGCTAA CAAGTTTGGTTCGATCTCTTGGTGGACTTCTAATGAGAATGAAAATGTATATTTGTGTTATCAGAGAACGCTAGAGATTGAGGAGAGGAAACATATGACACCTCCACC GGAAATAGCGGTTTCTCGCGAACCGCCGGCTTCAGGAAGTGGCGCTAAACGCCGATTGTCTTTTGATGATTCTGATCAAAGTTCTCCACCAGCCAAGAGAATGCGTAGG CTAGGTTCGTTGTCTTCAACACCCAGCTTTC

Table 1 Cont.

Gene name (AGI code)	Synthesised coding sequence
CYCD6;1 (AT4G03270)	GCAGGCTCCCTTGAAGACAAAATGGAGTTTCATCTTGAACATCCTCTCTCACATTCTTCACTCCACAATAACTTCAACGACGACACAGACTATGAAACTTTACCACACTC TCTCTTCCTCGTCGAGTTTCAACACATGCCTTCTTCTCATTACTTCCATAGCCTCAAGTCCTCTGCTTTTCTTCTCTCTAATCGAAACCAAGCCATTTCTTCAATCACTCAGT ATTCAAGAAAATTCGACGACCCATCTCTGACGTATCTTGCTGTGAATTATCTAGACAGGTTCTTGTCTAGCGAAGATATGCCGCAGTCAAAGCCCTGGATTCTTAAGCT CATATCTCTCTCTTGTGTCTCTTTGTCTGCAAAAATGAGGAAACCAGACATGTCTGTTTCTGATCTTCCGGTGGAAGGTGAGTTTTTTGATGCTCAGATGATAGAGAGA ATGGAGAATGTGATTCTAGGAGCTCTTAAATGGAGGATGCGCTCTGTTACTCCTTTCTCCTTTTTGGCCTTTTTCATTAGTCTCTTTGAGCTCAAAGAAGAAGATCCTTT ACTACTAAAACATTCCCTCAAATCTCAAACCAGTGATCTTACTTTCAGTCTCCAACATGATATCAGTTTCCTCGAGTTTAAACCATCGGTGATTGCAGGCGCGGCACTTC TCTTTGCTTCTTTCGAGCTCTGTCCTCTACAGTTTCCATGTTTCAGTAACAGAATCAACCAATGCACATATGTAAATAAGGATGAGTTAATGGAGTGTTACAAAGCAAT ACAAGAGAGAGATATTATAGTTGGAGAAAACGAAGGAAGCACTGAAACAGCAGTAAATGTGCTTGATCAGCAATTCTCGAGTTGTGAAAGCGATAAGAGCATCACA ATCACAGCTTCTTCTTCACCTAAGAGGAGGAAAACTAGTACTCGTCGTTACGGTTCGTTGTCTTCAACACCCAGCTTTC
CYCD7;1 (AT5G02110)	GCAGGCTCCCTTGAAGACAAAATGGATAATCTACTCTGCGAAGAATCTTGGCCCGCGAGTCCTTTAACCCCGGAGCCTTTACCAAACTTCCGTCACCGTTCTCACGACAA TGACGTCGTGAAGATGTATCCAGAGATAGACGCAGCGACGATGGAGGAAGCCATTGCTATGGACTTAGAGAAAGAATTATGTTTTAACAATCATGGAGACAAGTTT GTTGAGTTTTTCGTCTCAAAGAAGTTAACCGATTATAGGTTCCATGCGTTTCAATGGCTAATCCAGACTCGGAGTCGGCTAAATCTTTCATATGAAACGGTATTTTCCG CCGCTAATTGTTTTGATCGGTTCGTCTACATGACTTGCTGTGACGAATGGACGAATTGGATGGTGGAACTAGTTGCGGTAACTTCATTATCGATCGCATCAAAGTTCAA TGAAGTTACCACTCCATTACTCGAAGAACTTGAAATGGAAGGTTTAACTCATATGTTTCACGTTAATACAGTTGCTCAGATGGAACTCATAATTTTGAAAGCTCTCGAA TGGCGTGTGAACGCGGTTACGAGTTATACTTTTTCGCAAACCCTTGTGTCGAAGATCGGTATGGTTGGGGATCATATGATCATGAATCGAATTACAAATCATCTGCTTG ATGTTATATGCGATTTAAAAATGCTTCAATACCCACCAAGCGTTGTGGCCACTGCTGCTATATGGATTCTCATGGAAGATAAGGTGTGTCGAGAAAGTATCATGAATC TCTTTGAACAAAATCATAAGGAAAAAATCGTGAAATGTGTTGATGGGATGAAAAATCGAGACATTGATCATCAGTCGTCGAGAAGAAGATACAGTGAAGGGAGGA GTATTCTGAGTCTGTTGCAGCGAGGCGATGTGATGAATATGAATGGGGATTATAACGTTGAAGATCTCTCTAAAATCTTTCAGATTTTCCGATACGAAAAGAAGAAG AGGGATAGAGGAAACCACCAAGACAACATTCGTCCGGCAAAAAGAATGACAATTGAAATGTCAAATTACATTGGTTCGTTTGTCTTCAACACCCAGCTTTC

Table 2: Plasmids generated and used in this study

Name	Description	Source
Golden Gate Vectors		
pAGM9121	Universal level 0 acceptor, spectinomycin resistance.	MoClo Plant Tool Kit
pAGM1287	Level 0 acceptor for CDS1 no stop modules, spectinomycin resistance.	MoClo Plant Tool Kit
pICH47732	Level 1 acceptor, position 1 (L1P1), carbenicillin resistance.	MoClo Plant Tool Kit
pICH47751	Level 1 acceptor, position 3 (L1P3), carbenicillin resistance.	MoClo Plant Tool Kit
pICSL4723	Level 2 acceptor, kanamycin resistance.	MoClo Plant Tool Kit
L0 modules		
pICH51277	0.4 kb promoter, 35S *(CaMV)* + 5'UTR, Ω *(TMV)*.	Golden Gate Plant Parts Kit
pICH87644	AtAct2 promoter (*A. thaliana*) +5'UTR, *Ω (TMV)*.	Golden Gate Plant Parts Kit
pICSL80005	Variant of *turboGFP (tGFP)* codon-optimised for plants (*Pontellina plumata*) CDS.	Golden Gate Plant Parts Kit
pL0_tGFP	*tGFP* gene from pICSL80005 in level 0 acceptor pAGM9121.	This study
pL0_CDKB1;2	*CDKB1;2* CDS without stop codon in pAGM1287 backbone.	This study
pL0_CDKB2;1	*CDKB2;1* CDS without stop codon in pAGM1287 backbone.	This study
pL0_CDKB2;2	*CDKB2;2* CDS without stop codon in pAGM1287 backbone.	This study
pL0_CYCD1;1	*CYCD1;1* CDS without stop codon in pAGM1287 backbone.	Finch J
pL0_CYCD2;1	*CYCD2;1* CDS without stop codon in pAGM1287 backbone.	Finch J
pL0_CYCD3;1	*CYCD3;1* CDS without stop codon in pAGM1287 backbone.	Finch J
pL0_CYCD3;2	*CYCD3;2* CDS without stop codon in pAGM1287 backbone.	Finch J
pL0_CYCD3;3	*CYCD3;3* CDS without stop codon in pAGM1287 backbone.	Finch J
pL0_CYCD4;1	*CYCD4;1* CDS without stop codon in pAGM1287 backbone.	Finch J
pL0_CYCD4;2	*CYCD4;2* CDS without stop codon in pAGM1287 backbone.	Finch J
pL0_CYCD5;1	*CYCD5;1* CDS without stop codon in pAGM1287 backbone.	This study
pL0_CYCD6;1	*CYCD6;1* CDS without stop codon in pAGM1287 backbone.	This study
pL0_CYCD7;1	*CYCD7;1* CDS without stop codon in pAGM1287 backbone.	This study
pL0_HA-FLAG_C-tag	C-terminal 3xHA-FLAG tag in pAGM9121 backbone.	Finch J
pICSL50010	C-terminal 4xMYC tag.	Golden Gate Plant Parts Kit
pICH41421	3'UTR, polyadenylation signal/terminator, *nos (A. tumefaciens)*.	Golden Gate Plant Parts Kit
pICSL70008	pFAST-R selection cassette (monomeric tagRFP from *E. quadricolor* fused to the CDS of *OLE1 (A. thaliana)*.	Golden Gate Plant Parts Kit
pICSL80005	TurboGFP (*Pontellina plumata*) codon-optimised for plants, CDS	MoClo Plant Tool Kit
pICH41766	End-link 3 for assembling 3 L1 part into a L2 acceptor.	MoClo Plant Tool Kit
L1 modules		Golden Gate Plant Parts Kit
pL1P1_35S::tGFPHAFLAG	35S+ 5'UTR promoter from pICH51277+*tGFP* gene from pL0_tGFP, tagged with C-terminally with 3xHA-FLAG from pL0_HA-FLAG_C-tag+3'UTR+nos terminator from pICH41421 cloned into L1P1 plasmid (pICH47732).	This study
pL1P3_35S::tGFPMYC	35S+ 5'UTR promoter from pICH51277+*tGFP* gene from pL0_tGFP, tagged with C-terminally with 4xMYC from pICSL50010 +3'UTR+nos terminator from pICH41421 in L1P3 plasmid (pICH47751).	This study
pL1P1_35SCDKB1;1FLAGHA	35S+ 5'UTR promoter from pICH51277+*CDKB1;1* gene from pL0_CDKB1;1 tagged with C-terminally with 3xHA-FLAG from pL0_HA-FLAG_C-tag+3'UTR+act2 terminator from pICH44300 cloned into L1P1 plasmid (pICH47732).	Finch J

Table 2: Cont.

Name	Description	Source
pL1P1_35S::CDKB1;2FLAGHA	35S+ 5'UTR promoter from pICH51277+*CDKB1;2* gene from pL0_ CDKB1;2, tagged with C-terminally with 3xHA-FLAG from pL0_HA-FLAG_C-tag+3'UTR+nos terminator from pICH41421 cloned into L1P1 plasmid (pICH47732).	This study
pL1P1_35S::CDKB2;1FLAGHA	35S+ 5'UTR promoter from pICH51277+*CDKB2;1* gene from pL0_ CDKB2;1, tagged with C-terminally with 3xHA-FLAG from pL0_HA-FLAG_C-tag+3'UTR+nos terminator from pICH41421 cloned into L1P1 plasmid (pICH47732).	This study
pL1P1_35S::CDKB2;2FLAGHA	35S+ 5'UTR promoter from pICH51277+*CDKB2;2* gene from pL0_ CDKB2;2, tagged with C-terminally with 3xHA-FLAG from pL0_HA-FLAG_C-tag+3'UTR+nos terminator from pICH41421 cloned into L1P1 plasmid (pICH47732).	This study
pL1P3_35S::CYCD1;1MYC	35S+ 5'UTR promoter from pICH51277+*CYCD1;1* gene from pL0_CYCD1;1, tagged with C-terminally with 4xMYC from pICSL50010+3'UTR+nos terminator from pICH41421 in L1P3 plasmid (pICH47751).	This study
pL1P3_35S::CYCD2;1MYC	35S+ 5'UTR promoter from pICH51277+*CYCD2;1* gene from pL0_CYCD2;1, tagged with C-terminally with 4xMYC from pICSL50010+3'UTR+nos terminator from pICH41421 in L1P3 plasmid (pICH47751).	This study
pL1P3_35S::CYCD3;1MYC	35S+ 5'UTR promoter from pICH51277+*CYCD3;1* gene from pL0_CYCD3;1, tagged with C-terminally with 4xMYC from pICSL50010+3'UTR+nos terminator from pICH41421 in L1P3 plasmid (pICH47751).	This study
pL1P3_35S::CYCD3;2MYC	35S+ 5'UTR promoter from pICH51277+*CYCD3;2* gene from pL0_CYCD3;2, tagged with C-terminally with 4xMYC from pICSL50010+3'UTR+nos terminator from pICH41421 in L1P3 plasmid (pICH47751).	This study
pL1P3_35S::CYCD3;3MYC	35S+ 5'UTR promoter from pICH51277+*CYCD3;3* gene from pL0_CYCD3;3, tagged with C-terminally with 4xMYC from pICSL50010+3'UTR+nos terminator from pICH41421 in L1P3 plasmid (pICH47751).	This study
pL1P3_35S::CYCD4;1MYC	35S+ 5'UTR promoter from pICH51277+*CYCD4;1* gene from pL0_CYCD4;1, tagged with C-terminally with 4xMYC from pICSL50010+3'UTR+nos terminator from pICH41421 in L1P3 plasmid (pICH47751).	This study
pL1P3_35S::CYCD4;2MYC	35S+ 5'UTR promoter from pICH51277+*CYCD4;2* gene from pL0_CYCD4;2, tagged with C-terminally with 4xMYC from pICSL50010+3'UTR+nos terminator from pICH41421 in L1P3 plasmid (pICH47751).	This study
pL1P3_35S::CYCD5;1MYC	35S+ 5'UTR promoter from pICH51277+*CYCD5;1* gene from pL0_CYCD5;1, tagged with C-terminally with 4xMYC from pICSL50010+3'UTR+nos terminator from pICH41421 in L1P3 plasmid (pICH47751).	This study
pL1P3_35S::CYCD6;1MYC	35S+ 5'UTR promoter from pICH51277+CYCD6;1 gene from pL0_CYCD6;1, tagged with C-terminally with 4xMYC from pICSL50010+3'UTR+nos terminator from pICH41421 in L1P3 plasmid (pICH47751).	This study
pL1P3_35S::CYCD7;1MYC	35S+ 5'UTR promoter from pICH51277+CYCD7;1 gene from pL0_CYCD7;1, tagged with C-terminally with 4xMYC from pICSL50010+3'UTR+nos terminator from pICH41421 in L1P3 plasmid (pICH47751).	This study
pL1P3_AtAct2::tGFPMYC	AtAct2+ 5'UTR promoter from pICH87644+*tGFP* gene from pL0_tGFP, tagged with C-terminally with 4xMYC from pICSL50010+nos terminator from pICH41421 in L1P3 plasmid (pICH47751).	This study
pL1P3_AtAct2::CYCD1;1MYC	AtAct2+ 5'UTR promoter from pICH87644+*CYCD1;1* gene from pL0_CYCD1;1, tagged with C-terminally with 4xMYC from pICSL50010+nos terminator from pICH41421 in L1P3 plasmid (pICH47751).	This study
pL1P3_AtAct2::CYCD2;1MYC	AtAct2+ 5'UTR promoter from pICH87644+*CYCD2;1* gene from pL0_CYCD2;1, tagged with C-terminally with 4xMYC from pICSL50010+nos terminator from pICH41421 in L1P3 plasmid (pICH47751).	This study
pL1P3_AtAct2::CYCD3;1MYC ::CYCD4;1MYC	AtAct2+ 5'UTR promoter from pICH87644+*CYCD3;1* gene from pL0_CYCD3;1, tagged with C-terminally with 4xMYC from pICSL50010+nos terminator from pICH41421 in L1P3 plasmid (pICH47751).	This study
pL1P3_AtAct2::CYCD4;1MYC	AtAct2+ 5'UTR promoter from pICH87644+*CYCD4;1* gene from pL0_CYCD4;1, tagged with C-terminally with 4xMYC from pICSL50010+nos terminator from pICH41421 in L1P3 plasmid (pICH47751).	This study

Table 2: Cont.

Name	Description	Source
pL1P3_AtAct2::CYCD4;2MYC	AtAct2+5'UTR promoter from pICH87644+CYCD4;2 gene from pL0_CYCD4;2, tagged with C-terminally with 4xMYC from pICSL50010+nos terminator from pICH41421 in L1P3 plasmid (pICH47751).	This study
pL1P3_AtAct2::CYCD5;1MYC	AtAct2+5'UTR promoter from pICH87644+CYCD5;1 gene from pL0_CYCD5;1, tagged with C-terminally with 4xMYC from pICSL50010+nos terminator from pICH41421 in L1P3 plasmid (pICH47751).	This study
pL1P3_AtAct2::CYCD6;1MYC	AtAct2+5'UTR promoter from pICH87644+CYCD6;1 gene from pL0_CYCD6;1, tagged with C-terminally with 4xMYC from pICSL50010 +nos terminator from pICH41421 in L1P3 plasmid (pICH47751).	This study
pL1P3_AtAct2::CYCD7;1MYC	AtAct2+5'UTR promoter from pICH87644+*CYCD7;1* gene from pL0_CYCD7;1, tagged with C-terminally with 4xMYC from pICSL50010 +nos terminator from pICH41421 in L1P3 plasmid (pICH47751).	This study
pL1P2_FASTR	FAST-R selection cassette from pICSL70008 was cloned into L1P2 plasmid (pICH47742).	Finch J
L2 modules		
pL2_35S::tGFPHAFLAG_AtAct2::tGFPMYC	L2 acceptor (pICSL4723) carrying 35S::tGFP-FLAG-3xHA from pL1P1_35S::tGFPFLAGHA in position 1+FAST-R from pL1P2_FASTR in position 2+AtAct2::tGFP-4XMYC from pL1P3_AtAct2::tGFPMYC in position 3 with L1P3 linker (pICH41766).	This study
pL2_35SCDKB1FLAGHA	L2 acceptor (pICSL4723) carrying 35S::CDKB1;1-FLAG-3xHA from pL1P1_35SCDKB1FLAGHA in position 1+FAST-R from pL1P2_FASTR in position 2+AtAct2::tGFP-4XMYC from pL1P3_AtAct2::tGFPMYC in position 3 with L1P3 linker (pICH41766).	This study
pL2_35S::CDKB1;2FLAGHA	L2 acceptor (pICSL4723) carrying 35S::CDKB1;2-FLAG-3xHA from pL1P1_35S::CDKB1;2FLAGHA in position 1+FAST-R from pL1P2_FASTR in position 2+AtAct2::tGFP-4XMYC from pL1P3_AtAct2::tGFPMYC in position 3 with L1P3 linker (pICH41766).	This study
pL2_35S::CDKB2;1FLAGHA	L2 acceptor (pICSL4723) carrying 35S::CDKB2;1-FLAG-3xHA from pL1P1_35S::CDKB2;1FLAGHA in position 1+FAST-R from pL1P2_FASTR in position 2+AtAct2::tGFP-4XMYC from pL1P3_AtAct2::tGFPMYC in position 3 with L1P3 linker (pICH41766).	This study
pL2_35S::CDKB2;2FLAGHA	L2 acceptor (pICSL4723) carrying 35S::CDKB2;2-FLAG-3xHA from pL1P1_35S::CDKB2;2FLAGHA in position 1+FAST-R from pL1P2_FASTR in position 2+AtAct2::tGFP-4XMYC from pL1P3_AtAct2::tGFPMYC in position 3 with L1P3 linker (pICH41766).	This study
pL2_AtAct2::CYCD1;1MYC	L2 acceptor (pICSL4723) carrying 35S::tGFP-FLAG-3xHA from pL1P1_35S::tGFPFLAGHA in position 1+FAST-R from pL1P2_FASTR in position 2+AtAct2::CYCD1;1-4XMYC from pL1P3_AtAct2::CYCD1;1MYC in position 3 with L1P3 linker (pICH41766).	This study
pL2_AtAct2::CYCD2;1MYC	L2 acceptor (pICSL4723) carrying 35S::tGFP-FLAG-3xHA from pL1P1_35S::tGFPFLAGHA in position 1+FAST-R from pL1P2_FASTR in position 2+AtAct2::CYCD2;1-4XMYC from pL1P3_AtAct2::CYCD2;1MYC in position 3 with L1P3 linker (pICH41766).	This study
pL2_AtAct2::CYCD3;1MYC	L2 acceptor (pICSL4723) carrying 35S::tGFP-FLAG-3xHA from pL1P1_35S::tGFPFLAGHA in position 1+FAST-R from pL1P2_FASTR in position 2+AtAct2::CYCD3;1-4XMYC from pL1P3_AtAct2::CYCD3;1MYC in position 3 with L1P3 linker (pICH41766).	This study
pL2_AtAct2::CYCD3;2MYC	L2 acceptor (pICSL4723) carrying 35S::tGFP-FLAG-3xHA from pL1P1_35S::tGFPFLAGHA in position 1+FAST-R from pL1P2_FASTR in position 2+AtAct2::CYCD3;2-4XMYC from pL1P3_AtAct2::CYCD3;2MYC in position 3 with L1P3 linker (pICH41766).	This study
pL2_AtAct2::CYCD3;3MYC	L2 acceptor (pICSL4723) carrying 35S::tGFP-FLAG-3xHA from pL1P1_35S::tGFPFLAGHA in position 1+FAST-R from pL1P2_FASTR in position 2+AtAct2::CYCD3;3-4XMYC from pL1P3_AtAct2::CYCD3;3MYC in position 3 with L1P3 linker (pICH41766).	This study
pL2_AtAct2::CYCD4;1MYC	L2 acceptor (pICSL4723) carrying 35S::tGFP-FLAG-3xHA from pL1P1_35S::tGFPFLAGHA in position 1+FAST-R from pL1P2_FASTR in position 2+AtAct2::CYCD4;1-4XMYC from pL1P3_AtAct2::CYCD4;1MYC in position 3 with L1P3 linker (pICH41766).	This study
pL2_AtAct2::CYCD4;2MYC	L2 acceptor (pICSL4723) with 35S::tGFP-FLAG-3xHA from pL1P1_35S::tGFPFLAGHA in position 1+FAST-R from pL1P2_FASTR in position 2+AtAct2::CYCD4;2-4XMYC from pL1P3_AtAct2::CYCD4;2MYC in position 3 with L1P3 linker (pICH41766).	This study
pL1P3_AtAct2::CYCD5;1MYC	AtAct2+5'UTR promoter from pICH87644+CYCD5;1 gene from pL0_CYCD5;1, tagged with C-terminally with 4xMYC from pICSL50010+nos terminator from pICH41421 in L1P3 plasmid (pICH47751).	This study
pL2_AtAct2::CYCD6;1MYC	L2 acceptor (pICSL4723) with 35S::tGFP-FLAG-3xHA from pL1P1_35S::tGFPFLAGHA in position 1+FAST-R from pL1P2_FASTR in position 2+AtAct2::CYCD6;1-4XMYC from pL1P3_AtAct2::CYCD6;1MYC in position 3 with L1P3 linker (pICH41766).	This study

Table 2: Cont.

Name	Description	Source
pL2_AtAct2::CYCD7;1MYC	L2 acceptor (pICSL4723) with 35S::tGFP-FLAG-3xHA from pL1P1_35S::tGFPFLAGHA in position 1+ FAST-R from pL1P2_FASTR in position 2+AtAct2::CYCD7;1-4XMYC from pL1P3_AtAct2::CYCD7;1MYC in position 3 with L1P3 linker (pICH41766).	This study
pL2_35SCDKB1;1FLAGHA_AtAct2::CYCD1;1MY(	L2 acceptor (pICSL4723) with 35S::CDKB1;1-FLAG-3xHA from pL1P1_35S::CDKB1;1FLAGHA in position 1+ FAST-R from pL1P2_FASTR in position 2+AtAct2::CYCD1;1-4XMYC from pL1P3_AtAct2::CYCD1;1MYC in position 3 with L1P3 linker	This study
pL2_35SCDKB1;1FLAGHA_AtAct2::CYCD2;1MY(	L2 acceptor (pICSL4723) with 35S::CDKB1;1-FLAG-3xHA from pL1P1_35S::CDKB1;1FLAGHA in position 1+ FAST-R from pL1P2_FASTR in position 2+AtAct2::CYCD2;1-4XMYC from pL1P3_AtAct2::CYCD2;1MYC in position 3 with L1P3 linker	This study
pL2_35SCDKB1;2FLAGHA_AtAct2::CYCD1;1MY(	L2 acceptor (pICSL4723) with 35S::CDKB1;2-FLAG-3xHA from pL1P1_35S::CDKB1;2FLAGHA in position 1+ FAST-R from pL1P2_FASTR in position 2+AtAct2::CYCD1;1-4XMYC from pL1P3_AtAct2::CYCD1;1MYC in position 3 with L1P3 linker	This study
pGEM-T constructs		
pGEMT	pGEM®-T Vector, blue/white selection, ampicillin resistance	Promega
pGEMT_FASTR	pGEMT backbone containing FAST-R cassette with *PmeI* overhangs	This study
pGEMT_pCDKA;1::CDKA;1	pGEMT backbone containing native *CDKA;1* promoter+*CDKA;1* with RsrII and BamHI overhangs	This study
pGEMT_pCDKB1;1::CDKB1;1	pGEMT backbone containing native *CDKB1;1* promoter+*CDKB1;1* with RsrII and BamHI overhangs	This study
pGEMT_pCDKB1;2::CDKB1;2	pGEMT backbone containing native *CDKB1;2* promoter+*CDKB1;2* with RsrII and BamHI overhangs	This study
pGEMT_pCDKB2;1::CDKB2;1	pGEMT backbone containing native *CDKB2;1* promoter+*CDKB2;1* with RsrII and BamHI overhangs	This study
pGEMT_pCDKB2;2::CDKB2;2	pGEMT backbone containing native *CDKB2;2* promoter+*CDKB2;2* with RsrII and BamHI overhangs	This study
pGEMT_pCYCD1;1::CYCD1;1	pGEMT backbone containing native *CYCD1;1* promoter+*CYCD1;1* with RsrII and BamHI overhangs	This study
pGEMT_pCYCD2;1::CYCD2;1	pGEMT backbone containing native *CYCD2;1* promoter+*CYCD2;1* with RsrII and BamHI overhangs	This study
pGEMT_pCYCD5;1::CYCD5;1	pGEMT backbone containing native *CYCD5;1* promoter+*CYCD5;1* with RsrII and BamHI overhangs	This study
pGEMT_pCYCD6;1::CYCD6;1	pGEMT backbone containing native *CYCD6;1* promoter+*CYCD6;1* with RsrII and BamHI overhangs	This study
Fluorescent reporter lines		
pHG151_FAST-R	pHG151 plasmid (pHG151::pUBQ::mVenus::FAST-R) containing FAST-R cascade	This study
pHG141_FAST-R	pHG141 plasmid (pHG141::p35S::mTQ::FAST-R) containing FAST-R cascade	This study
pHG123_FAST-R	pHG123 plasmid (pHG123::p35S::TagRFP::FAST-R) containing FAST-R cascade	This study
pHG151_FASTR_pCDKB1;1:CDKB1;1mVenus	pUBQ of pHG151 plasmid was replaced with native CDKB1;1 promoter+ CDKB1;1 (At full length genomic)	This study
pHG151_FASTR_pCDKB2;1:CDKB2;1mVenus	pUBQ of pHG151 plasmid was replaced with native CDKB2;1 promoter+ CDKB2;1 (At full length genomic)	This study
pHG151_FASTR_pCDKB2;2:CDKB2;2mVenus	pUBQ of pHG151 plasmid was replaced with native CDKB2;2 promoter+ CDKB2;2 (At full length genomic)	This study

2.2.1.2 Transformation of chemically competent *Escherichia coli* cells

Chemically competent *Escherichia coli* (*E. coli)* DH5α cells were prepared according to the Rubidium chloride method (based on Hanahan, 1983) and stored at -80°C. On the transformation day, cells were thawed on ice. 5-10 µL of the ligation mix was added to 50 µL of competent cells and mixed by flicking. The mixture was incubated on ice for 25 min, then heat-shocked for 1 min at 42°C and afterwards kept on ice for 2 min. 250 µL sterile lysogeny broth (LB) media (10 g tryptone, 5 g yeast extract, 10 g NaCl, set pH to 7.5 with 1 M NaOH, up to 1 L with ddH_2O) was added to the cells and incubated at 37°C for 1.5 h. The cells were spread on LB-agar (LB + 1.5% (w/v) agar-agar). For the selection of the colonies containing L0 plasmids, the plates were supplemented with 50 µg/mL spectinomycin, and for blue-white selection, 40 µL 5-bromo-4-chloro-3-indolyl-beta-D-galactopyranoside (X-Gal, stock solution: 20 mg/mL X-Gal in DMSO) and 4 µL isopropyl thiogalactoside (IPTG, stock solution: 200 mg/mL in ddH_2O) per plate. For L1 plasmid selection, plates containing 100 µg/mL ampicillin, 40 µL X-Gal, 4 µL IPTG were used. For L2 plasmid selection, plates were supplemented with 50 µg/mL kanamycin only. Plates were incubated at 37°C overnight. On the next day, white colonies were picked using a sterile toothpick and first transferred to a fresh LB plate (including antibiotic) as a master plate and then to a PCR tube with 19.9 µL ddH_2O for colony PCR. PCR reaction mix was as follows: 19.9 µL ddH_2O with a colony, 2.5 µL 10x buffer A (Taq PCR kit, Kapa Biosystems, cat. # KK1015), 0.5 µL 10 mM dNTPs, 1 µL 10 mM forward primer, 1 µL 10 mM reverse primer (See Table S1 for the primers) and 0.1 µL KAPA Taq DNA polymerase (Taq PCR kit, Kapa Biosystems, cat. # KK1015). Thermal profile: 3 min at 95°C, 35 cycles of [30 s at 95°C, 30 s at 57°C, X min at 72°C], 5 min at 72°C (X: elongation time varies depending on the length of the fragment, 1 min for 1 kb). The presence of the right sized PCR fragments was confirmed with 1.2% agarose gel. A liquid culture of a transformed colony was prepared in 5 mL LB media with corresponding antibiotics. The cultures were incubated at 37°C overnight with 180 rpm shaking. On the next morning, the plasmids were isolated by using the NucleoSpin Plasmid mini kit for plasmid DNA (Marchery-Nagel, cat. # 740588.250) according to the manufacturer's protocol. The correct assembly of the plasmids were checked by sequencing (seq) the isolated plasmid, using Microsynth Seqlab GmbH and LGC Genomics GmbH sequencing services (See Table S1 for the primers).

2.2.1.3 Transformation of *A. tumefaciens*

2.2.1.3.1 Preparation of competent *A. tumefaciens* cells

One colony of *A. tumefaciens* GV3101 was grown in 2x 5 mL LB media supplemented with 25 µg/mL gentamicin (Gent25) and 50 µg/mL rifampicin (Rif50) overnight at 28°C with shaking. Next day, 5 mL of the over-night culture were inoculated into 120 mL LB media containing Gent25 and Rif50. After mixing, the cultures were split into two equal portions and incubated for approximately 6 h at 28°C with shaking until cultures reached an OD_{600} of 0.8. Then the flasks were chilled on ice and the cultures

were split into 4x 50 mL Falcon tubes. Cells were centrifuged at 4°C and 3,200 g for 15 min and the supernatants were removed. The pellets were resuspended in 2 mL sterile pre-cooled 20 mM $CaCl_2$ solution. Subsequently, the bacterial suspensions were aliquoted into 1.5 mL Eppendorf tubes, flash-frozen and stored at -80°C for further use.

2.2.1.3.2 Transformation of competent *A. tumefaciens* cells using the freeze-thaw method

Approximately 500 ng of a plasmid were added to 50 µL competent *A. tumefaciens* GV3101 cells and mixed by tapping. The mixture was then incubated on ice for 5 min, followed by a transfer into liquid nitrogen for 5 min and then to 37°C for 5 min. After the incubation, 250 µL LB media were added and cells were kept at 28°C for 1.5 h at 180 rounds per minute (rpm) shaking. For L1 plasmid transformation, the recovered cells were spread onto LB-agar plates containing Gent25, Rif50 and Carb50, while for L2 transformations, bacteria were spread onto LB-agar plates with Rif50, Kan50, Gent25. Plates were then incubated at 28°C for two days, which was followed by colony PCR to identified successfully transformed colonies (Section 2.2.1.2 for reaction protocol). Positive colonies were inoculated into 5 mL LB media with the corresponding antibiotics and incubated overnight at 28°C with shaking. Bacterial suspensions were spun down at 11,000 g for 5 min at 4°C and approximately 4 mL of supernatant were discarded. The remaining pellets were resuspended and 500 µL of bacteria were mixed with 500 µL of sterile 50% glycerol solution. The cells were frozen in liquid nitrogen and stored at -80°C for further use.

2.2.1.4 *A. tumefaciens*-mediated transformation of *A. thaliana*

A. thaliana Col-0 plants were grown as described in Section 2.1. The first occurring bolts were clipped. Plants were ready for transformation, when secondary bolts reached a size of 1-5 cm (approximately 4-6 days after clipping of the first bolt). 5 mL *A. tumefaciens* cultures were prepared in 50 mL Falcon tubes and incubated overnight at 28°C with shaking. On the day of transformation, the soil in the plant pots was supposed to be moist but plants should not be standing in water. Overnight cultures were centrifuged at 3,000 g for 10 min at 4°C and the supernatants were resuspended in 7 mL infiltration buffer (5% (w/v) sucrose, 0.02% (v/v) Silwet L-77 in dH_2O, prepared freshly). The bacterial suspensions were applied generously to buds and inner rosettes of the plants with a paintbrush. Pots were covered with cling film to increase humidity. After 3 days, the cling film was removed and plants were grown until the harvest of T_1 seeds.

2.2.1.4.1 Confirmation of transformation by gDNA extraction and PCR

To determine whether the *A. thaliana* transformation was successful, genomic DNA was extracted from leaves of T_1 plants, followed by PCR to detect the presence of L2 T-DNAs. Leaves from 3-weeks-old *A. thaliana* plants, which were grown in soil, were used for gDNA extraction. 2 medium sized leaves were harvested into 2 mL Eppendorf tubes containing two metal beads and frozen in liquid nitrogen.

Frozen leaves were ground using a BeadBugTM microtube homogenizer (3x 6 sec at 2,600 rpm). 500 µL fresh gDNA extraction buffer (200 mM Tris-HCL (pH: 7.5), 250 mM NaCl, 25 mM EDTA, 0.5% (v/v) SDS in dH_2O) were added to tubes and mixed. Samples were incubated for 10 min on a shaker at room temperature. After the incubation, 500 µL chloroform were added to each sample and samples were incubated on a shaker for 5 more min. Incubation was followed by centrifugation at 18,000 g for 10 min at room temperature. The supernatants were transferred into new tubes containing 500 µL isopropanol and the samples were vortexed thoroughly. gDNA was precipitated at -20°C overnight. The following day, the samples were centrifuged for 10 min at 18,000 g and the supernatants were discarded. The pellets were washed with 500 µL 70% ethanol and centrifuged for 5 min at 18,000 g. After the ethanol was removed, the pellets were dried completely at 37°C. Finally, the pellets were dissolved in 20-50 µL H_2O, depending on the sizes of pellets. The concentrations were measured using a NanoDrop. For genotyping PCR, KAPA Taq DNA polymerase with primers pGY1-fwd and FASTR_int_rev (See Section 2.2.1.2 for reaction protocol) was used. As a template 200 ng/µL gDNA was pipetted. Elongation time was set to 3 min. The presence of the right sized PCR fragments was confirmed with 1.2% agarose gel.

2.2.1.5 Propagation of homozygous lines

L2 expression cassettes used for *A. thaliana* transformation contained the red fluorescing FAST-R selection marker that allowed selection of successfully transformed T_1 seeds using a fluorescence stereo microscope. Seeds showing red fluorescence were picked with thin tweezers. Transformed T_1 seeds were propagated (Section 2.1) and T_2 seeds were harvested. In the T_2 generation, a segregation rate of 1:2:1 of non-fluorescent to mildly fluorescent to strongly fluorescent seeds indicates a single insertion of the transgene. The brightly fluorescing seeds of the lines showing a 1:2:1 segregation ratio were propagated (Section 2.1). After the determination of the homozygous T_3 lines on the basis of 100% fluorescent seeds, the overexpression of the corresponding genes and the presence of the tagged proteins were confirmed by RT-qPCR (Section 2.7) and Western blot (Section 2.8.1), respectively.

2.2.2 Generation of fluorescent reporter lines

2.2.2.1 COLORFUL-Circuit System

Since BpiI and BsaI restriction enzyme recognition sites are highly abundant in the promoters of CDKs and CYCDs, it was not possible to use Golden Gate Cloning to generate translational fusions with fluorescing protein genes under the control of their native promoters for CDKBs and CYCDs. Instead, the "COLORFUL-Circuit system" was used (Ghareeb et al., 2016). Full sequences of the genes of interest including promoter regions corresponding to approximately 1,000 bp upstream from the transcriptional start sites were obtained by using PlantGenIE ((Sundell et al., 2015);

https://plantgenie.org/). In case of an overlap with another gene or the presence of a restriction enzyme recognition sites intended for the use in the cloning process, the promoter regions were shortened as needed. Genomic DNA (gDNA) was amplified from Col-0 gDNA pool using gene-specific primers with RsrII (forward primer) and BamHI (reverse primer) recognition site overhangs, respectively. FAST-R cascade was amplified with Pme1 restriction enzyme overhangs. The stop codons were removed to allow in-frame fusion with the coding sequence of a fluorescent protein gene (See Table S1 for the primers). For PCR amplification of the gene fragments, Q5 High-Fidelity DNA polymerase was used with the protocol as in Section 2.2.1.1 with minor changes: 3.5 µL of 14 ng/µL gDNA template, primer annealing at 59°C and 2 min extension time. After confirmation of the PCR amplification via 1.2% agarose gel electrophoresis (5 µL of the PCR products were loaded onto the agarose gel), an A-tailing reaction was carried out as follows: 2 µL of 2 mM dNTPs and 0.4 µL DCS Polymerase (DNA Cloning Service, cat. #DPT-500) were directly added to the remaining PCR products and incubated at 72°C for 20 min. The whole PCR reaction mix was then subjected to gel electrophoresis on a 1.2% agarose gel and bands of the correct size were cut out with a clean scalpel blade. The PCR products were extracted from the gel by using the Wizard® SV Gel and PCR Clean-Up System (Promega) according to the manufacturer's protocol.

The extracted PCR products were cloned into the pGEM®-T cloning vector by using pGEM®-T Vector Systems (Promega). As backbone, pHG151, pHG141 and pHG123 were used. For non- invasive and easier selection, *BASTA* gene of the backbones were replaced with FAST-R cascade with help of Pme1 restriction enzyme. CDKBs were intended to clone into pHG151 and CYCDs were aimed to clone into pHG141. The ligation reaction mix was as follows: 10 µL 2x T4 ligation buffer, 1 µL pGEM®-T vector (50 ng), 8 µL PCR product, 1 µl T4 DNA ligase (3 Weiss units/µl). The reaction took place at 4°C overnight. The ligation product was transformed into competent *E. coli* DH5α cells (Section 2.2.1.2). Colony PCR was carried out to determine the presence of the constructs, which was followed by plasmid extraction and sequencing.

2.3 Treatment of *A. thaliana* plants with immunity elicitors flg22 or Pep1

10 mM stock solutions of flg22 (EZBiolab; peptide sequence: QRLSTGSRINSAKDDAAGLQIA) and Pep1 (EZBiolab; peptide sequence: ATKVKAKQRGKEKVSSGRPGQHN) were prepared in sterile ddH_2O and stored at -20°C. For the assays, Col-0 plants or *A. thaliana* overexpressor lines were grown on ATS plates according to Section 2.1. After some days (age varied depending on experiment), seedlings were treated with flg22 or Pep1 solution (concentration varied depending on experiment; 100 nM or 1 µM) under sterile conditions. Control plants were treated with sterile ddH_2O (mock).

2.4 Root growth inhibition assay

For RGI assays, seeds were germinated and grown on respective media plates (Section 2.1). After 10 days, the root tips were marked with a permanent marker. 10-day-old plants were treated with flg22, Pep1 solution (100 nM or 1µM) or ddH_2O under sterile conditions (Section 2.3). 1 mL of the solution was pipetted evenly on the surface of the growth media and distributed throughout the plate by shaking. The treated plates were air dried with open lids and returned to the growth conditions. To measure the root growth increments, root tips were marked every day. After 4 days, the plates were scanned and root lengths were measured using the ImageJ/Fiji software (Schindelin et al., 2012).

2.5 ROS measurement

Roots of 14-day-old plants were cut into small pieces using a sharp razor blade. Around 5 mg of root material per well were transferred into a white 96-well microplate containing 100 µl of water, and incubated overnight to reduce wounding effects. For ROS measurement, 30 µl ml^{-1} horseradish peroxidase (Sigma-Aldrich, 150 U/ml) and 300 µM luminol (Carl Roth) were mixed. 100 µl of the mix were added to each well containing root material in 100 µl water. After. After 10 min , flg22 or Pep1 solutions were added to the wells to reach a final concentration of 1 µM. Luminescence was immediately measured for 40 minutes in an Infinite M Plex plate reader (Tecan) with 1,000 ms integration time.

2.6 Confocal laser-scanning microscopy and fluorescence quantification

14-day-old *pPER5*:: *NLS-3xmVENUS* and *pMYB51*:: *NLS-3xmVENUS* (Poncini et al., 2017) plants were treated with 1 µM flg22, Pep1 or mock. 6 and 24 h after treatment, whole plants were fixed in 4% paraformaldehyde in 1x PBS for 1 h with gentle agitation after vacuum infiltration (3 times 5 min). Roots were washed twice in 1x PBS and transferred to ClearSee solution (Ursache et al., 2018). Samples were kept at RT in the dark. On the day of microscopic examination, the cell walls of the fixed roots were stained with 0.2% Direct Red 23 (Sigma-Aldrich) in ClearSee solution (Ursache et al., 2018). Images were taken with a confocal laser-scanning microscope (Leica SP8). mVENUS fluorescence was excited at 514 nm and detected between 525 and 555 nm. Direct Red 23 was excited with a 561 nm laser line and detected between 580 and 615 nm. Leica Application Suite X was used for image processing and fluorescence quantifications was performed with the ImageJ/Fiji software (Schindelin et al., 2012).

2.7 Quantification of gene expression

2.7.1 Preparation of plant material

To examine PTI marker gene induction and investigate changes in the expression of cell cycle regulators in *A. thaliana*, Col-0 wild type seedlings were grown on ATS media or ½ MS media (Section 2.1). After 12 days, seedlings were treated with 100 nm flg22 or with sterile ddH_2O (mock) (Section 2.3). Root material was harvested and frozen in liquid nitrogen at 4, 24 and 48 h after treatment (hat). For the confirmation the stable overexpression of cell cycle regulators in *A. thaliana* (Section 2.2.1), seeds of transgenic lines as well as Col-0 wild type were sterilized using the chlorine gas method (Section 2.1) and sowed and grow on ATS plates. Approximately 2 weeks later, roots were harvested and transferred into 2 mL Eppendorf tubes with 2 metal beads, which was followed by freezing in liquid nitrogen.

To test induction of PTI marker genes in *N. benthamiana* after flg22 treatment, plant material was prepared according to Section 2.8.2.1 and 2.8.2.2.

2.7.2 Total RNA extraction

Frozen root material or leaf discs were ground using a BeadBugTM microtube homogenizer (3x 6 sec at 2,600 rpm). 1 mL TRI Reagent® (Invitrogen™) was added to each tube and tubes were vortexed thoroughly. Then 200 µL chloroform was added and samples were vortexed for 15 sec, which was followed by 3 min incubation on ice. Samples were centrifuged at full speed for 30 min at 4°C. Supernatants were carefully transferred into RNase-free 1.5 mL Eppendorf tubes without gDNA contamination from the interphase. Subsequently, 500 µL isopropanol was added to samples and RNA was allowed to precipitate at -20°C overnight. The following day samples were centrifuged at full speed for 50 min at 4°C. Supernatants were discarded and pellets were washed with 1 mL ice cold 75% ethanol (prepared with RNase-free water). Pellets were dried and resuspended in 15-30 µL RNase/DNase free H_2O. RNA concentrations were measured with a NanoDrop spectrophotometer.

2.7.3 DNase digest and cDNA synthesis

DNase digest was performed to remove residual gDNA from samples. The reaction per sample was as follows: 2 µg total RNA, 2 µL 10x reaction buffer, 2 µL DNase I (Thermo Scientific, cat. # EN0521), 0.5 µL RiboLock RNase inhibitor (Thermo Scientific, cat. # EO0381), topped up to a total volume of 20 µL with nuclease-free water. The reaction mix was incubated at 37°C for 30 min in a thermal cycler. Afterwards, 2 µL of 50 mM EDTA (Thermo Scientific) was added and samples were incubated at 65°C for 10 min to stop the DNase reaction. RNA concentrations were re-measured before proceeding with cDNA synthesis using the qScript™ cDNA Synthesis Kit (Quanta Biosciences, cat. # 95047-100). The reaction mix was as follows: 1 µg RNA, 4 µL 5x qScript™ reaction mix, 1 µL qScript™ reverse transcriptase, topped up to a total volume of 20 µL with nuclease free water. Thermo cycler program:

5 min at 25°C, 30 min at 42°C, 4 min at 85°C, then held at 8°C. The cDNA samples were diluted to 5 ng/µl by adding ddH_2O.

2.7.4 Quantitative real-time PCR (qRT-PCR)

Standard curves were generated for each primer pair designed in this study to ensure that they bind and amplify their targets precisely. For this purpose, serially diluted cDNA pools from different CDK- or CYC-overexpressing lines were generated (5 ng/µL, 1 ng/µL, 0.2 ng/µL, 0.04 ng/µL). Reaction mixes for the standard curve: 4 µL SYBR® Green JumpStart™Taq ReadyMix (Sigma-Aldrich, cat. # S9194), 0.2 µL 10 µM forward primer, 0.2 µL 10 µM reverse primer, 0.6 µL H_2O and 5 µL cDNA. QuantStudio 5 Real-Time PCR Systems (Thermo Fisher Scientific) was used for amplification using the following thermoprofile: 5 min at 95°C, 40 cycles of [15 s at 95°C, 30 s at 60°C, 30 s at 72°C]. The PCR amplification was followed by a melting curve to confirm single PCR product amplification. For gene expression quantification, qRT-PCR reaction mix was as follows: 4 µL SYBR® Green JumpStart™Taq ReadyMix, 0.2 µL 10 µM forward primer, 0.2 µL 10 µM reverse primer (Supplementary Table 1 for primers), 4.6 µL H_2O and 1 µL of 5 ng/µL cDNA. The thermoprofile was the same as above. Each sample was run in triplicates, and *A. thaliana* samples were normalised against the average *C*T values of house-keeping genes *UBIQUITIN 5* (*AtUBQ5*) and *elongation factor 1 alpha* (*AtEF1α*) for *A. thaliana*, whereas *N. benthamiana* samples were normalised against *NbEF1α*. Absolute expression and/or relative expression were calculated according to the $2^{-\Delta Ct}$ and $2^{-\Delta\Delta Ct}$ methods, respectively (Schmittgen & Livak, 2008).

2.8 Analysis of protein expression levels

2.8.1 Detection of tagged cell cycle proteins in stably transformed *A. thaliana* transgenic lines by Western blot

2.8.1.1 Preparation of plant material and MG132 treatment

In order to confirm the presence of tagged CDKB and CYCD proteins in stably transformed *A. thaliana* lines, plants of each line were grown on ATS plates (2 plates per line with approximately 50 seeds per plate). Although, CDKBs proteins could be detected easily, CYCDs couldn't be detected. Therefore, MG132 treatment was performed with CYCDs overexpressing plants, but not with CDKBs overexpressing lines. 2–3-week-old CYCDs overexpressing plants were treated with the proteosome inhibitor MG132 (Z-Leu-Leu-Leu-CHO, Santa Cruz Biotehnology, cat. # sc-201270, stock 10 mM in DMSO). 50 µM MG132 solution in dH_2O was prepared and 1 mL was applied per plate and spread evenly. Approximately 3 h later, root or whole seedlings were harvested and frozen in liquid nitrogen. The frozen seedlings were stored at -80 C until further use.

2.8.1.2 Nuclear protein extraction from *A. thaliana* roots or whole seedlings

Frozen root samples were ground using a BeadBugTM microtube homogenizer (3x 6 sec at 2,600 rpm), whereas whole seedlings were ground to powder using a pre-chilled pestle and mortar. Ground frozen root or seedling samples were mixed with 1:1 and 1:2 (weight tissue : volume buffer) of protein extraction buffer, respectively (protein extraction buffer: 150 mM Tris-HCL, pH: 7.5, 5 mM EDTA and 150 mM NaCl stored at 4°C and on the day of use supplemented with 10% glycerol, 5 mM dithiothreitol (DTT), 1% plant protease inhibitor cocktail (PIC, Sigma-Aldrich), 1 mM phenylmethylsulfonyl fluoride (PMSF, Sigma-Aldrich), 1% IGEPAL® CA-630 (Sigma-Aldrich, cat. # I3021)). Samples were incubated on ice for 3-5 min and then centrifuged at 20,000 g for 15 min at 4°C. The supernatants were transferred into new tubes. If necessary, centrifugation and transfer steps were repeated several times.

2.8.1.3 Quantification of protein concentrations

An assay using Bradford reagent (Sigma-Aldrich, cat. # B6916) was performed to measure and equalize the protein concentrations in whole-seedling samples. For a standard curve a serial dilution of bovine serum albumin (BSA, 0.0, 0.1, 0.2, 0.4, 0.6, 0.8, 1.0, 1.2, 1.4 mg/mL) was prepared, and 5 µL of each concentration were mixed with 250 µL Bradford reagent in triplicates in a transparent 96-well plate. The protein extracts (Section 2.8.1.2) were diluted with water (1:5) and just like the BSA samples, 5 µL of diluted protein extracts were mixed with 250 µL Bradford reagent in triplicates. Air bubbles were removed, and the plate was gently mixed and incubated for 10 min at room temperature. Using an Infinite M Plex plate reader (Tecan), the absorbance at 595 nm was measured. A linear standard curve was generated by using BSA absorbance values. Based on this and taking the dilution factor into account, the concentrations of protein extracts were calculated.

2.8.1.4 Sodium dodecyl sulfate-polyacrylamide gel electrophoresis (SDS-PAGE)

The Mini-Protean® tetra hand cast system (Bio-Rad Laboratories) was used for gel preparation and electrophoresis. After glass plates (1 mm spacer plates and short plates) were cleaned with 30% SDS and 70% ethanol, the casting stand was aligned. For two gels, a 12% resolution gel was prepared with 4 mL 30% acrylamide/bis solution (Serva), 3.4 mL H_2O, 2.5 mL of 4x resolution buffer (1.5 M Tris base, pH: 8.8 adjusted with 4 M HCl, store at 4°C), 100 µL of 10% SDS), 100 µL 0.1g/mL ammonium persulfate (APS, Sigma-Aldrich), 7.5 µL tetramethylethylenediamine (TEMED, Sigma-Aldrich)). After the resolution gel was polymerized, a stacking gel was prepared with 1 mL 30% acrylamide/bis solution, 3.6 mL H_2O, 600 µL stacking buffer (1 M Tris base, pH: 6.8 adjusted with 4 M HCl, store at 4°C), 50 µL of 10% SDS, 50 µL 0.1g/mL APS, 7.5 µL TEMED and a 10-well comb was inserted into the gel. After complete polymerization, the gels were assembled into the running module and the tank was filled with 1x running buffer (for 1 L: 2.5 mM tris base, 19.2 mM glycine, 1 g SDS pellets, pH:8.3). 4 µl 5x loading buffer (0.25 M Tris-HCl (pH: 6.8), 0.5 M DTT, 10% SDS, 50% glycerol, 0.5% bromophenol blue)

were added to 30 µg of protein sample (calculated according to Section 2.8.1.3), and the mix was topped up to a total volume of 20 µl with H_20. Protein samples were denatured for 10 min at 95°C. 8 µL PageRuler™ Prestained Protein Ladder (ThermoFischer Scientific, cat. # 26616) as size marker was loaded onto the gels. The gel was run at 80 V through the stacking gel and 100 V through the resolution gel at room temperature until the samples reached the bottom of the gel.

2.8.1.5 Membrane transfer, immunoblotting and detection

After separation by electrophoresis, proteins were transferred from the polyacrylamide gel to a polyvinylidene difluoride (PVDF) membrane using a Trans-Blot Turbo Transfer System semi-dry blotting instrument (Bio-Rad Laboratories). A standard sandwich system was employed: 4 layers of Whatman paper soaked in 1x Torbin buffer (25 mM Tris base, 19.2 mM glycine, pH 8.6 with HCl, 20% (v/v) methanol)), activated membrane (Transfer membran ROTI®PVDF 0.45, cat. # T830.1 - activation in methanol for 30 secs and rinsed with 1 x Torbin buffer), polyacrylamide gel, 4 layers of Whatman paper (soaked in 1x Torbin buffer). The following program was used for transfer: >Bio-rad> 2 mini or 1 midi gel> Standard (25 V, 1.0 A, for 30 min).

After the protein transfer, membranes were blocked for 1 h with gentle shaking in 5% milk-TBST buffer (for 10x TBS: 1 M Tris base, 1.5 M NaCl, pH:7.5-8.0 with HCl, for TBST: 1x TBS with 0.1% Tween20 and 5% powdered milk (Carl-Roth, cat. # T 145.2)). Blocking was followed by antibody incubation with 5% milk-TBST with respective antibodies (Table 3) at 4°C overnight.

On the next day, membranes were washed 4 times with TBST for 10 min each with gentle shaking. Finally, membranes were treated with a chemiluminescent substrate (Amersham™ ECL™ Prime Western Blotting Detection System, Cytiva cat. # RPN2232; 300 µl solution A + 300 µl solution B) for 5 min. Chemiluminescence was visualised by a ChemiDoc detection system (Bio-Rad Laboratories).

For loading control, membranes were stained with Coomassie Brilliant Blue (CBB, 50% methanol + 0.1% R-250 Coomassie Brilliant Blue, Serva), and destained in 10% acetic acid + 40% methanol (2x, 5 min). After air-drying of the membranes, membranes were scanned. If necessary, Western blot band intensities were quantified using ImageJ (Fiji) software. Band intensities were normalized against total protein levels, as visualized by CBB-stained membranes.

Table 3: Antibodies used in this study

Antibody name	Working concentration (in 5% TBST-milk)	Source	Cat. #
c-myc antibody-horseradish peroxidase (α-MYC-HRP)	1:10000	Miltenyi Biotec	30-092-113
α-HA-Peroxidase	1:4000	Roche	12013819001

2.8.2 Analysis of tagged protein expression in *N. benthamiana* and assessing protein levels after PTI induction

2.8.2.1 *Agrobacterium* infiltration of *N. benthamiana* leaves for transient protein expression

4-5-weeks-old *N. benthamiana* plants were used for transient transformation by *Agrobacterium* infiltration. 10 mL *A. tumefaciens* cultures containing *CDK* or *CYC* expression constructs (Section 2.2.1.1) were grown at 28°C over night. On the next day, cultures were centrifuged at 3,000 g for 8 min and pellets were resuspended in 5 mL infiltration buffer (19 mM MES pH: 5.6, 10 mM $MgCl_2$, 100 µM 3',5'-dimethoxy-4'-hydroxy-acetophenone (acetosyringone; Sigma-Aldrich, cat. # D134406)). The OD_{600} was measured and each *CDK*- or *CYC*-containing culture were mixed with infiltration buffer to give an OD_{600} of 0.5 and for the P19 culture an OD_{600} of 0.4 in 5 mL each. Equal volumes of each *CDK*- or *CYC*-containing culture and P19 culture were mixed and 1/3 of 3-4 leaves of *N. benthamiana* plants were infiltrated via the abaxial side with infiltration mix using a needle-less 1 mL syringe. Plants were returned to growth conditions.

2.8.2.2 Treatment of *N. benthamiana* leaf discs with immunity elicitor flg22

Two days after *Agrobacterium*-infiltration, 12 leaf discs per condition (0.33 cm diameter) were collected carefully from *A. tumefaciens* infiltrated leaf areas using a biopsy punch. The collected leaf discs were placed singly and with their adaxial side facing upwards into the wells of a 96-well plate each containing 100 µl of ddH_2O. In order to reduce wounding effects, leaf discs were incubated overnight at the growth conditions. On the next day, leaf discs were treated with 1 µM flg22 (final concentration: 1 µM) or with ddH_2O (mock). After 6 and 24 hat, leaf discs were collected into 2 mL Eppendorf tubes, which contained 2 glass beads. Flash frozen leaf discs were stored at -80 C until further use.

2.8.2.3 Protein extraction and detection in *N. benthamiana*

Flash frozen *N. benthamiana* leaf discs were ground using a tissue lyser (TissueLyser II, QIAGEN) at 30 s^{-1} for 2x 15 sec. 300 µL of 2x loading buffer (Section 2.8.1.5 for the loading buffer) was added to ground samples. After incubation on ice for 2-5 min, the samples were vortexed thoroughly and centrifuged at 20,000 g for 15 min at 4°C. 30 µL of the supernatant was transferred into new tubes and protein samples were denaturated at 95°C for 10 min. 18 µL of the samples was loaded onto and SDS polyacrylamide gel and detection of protein expression by Western blot was done as described above (Sections 2.8.1.4-5).

2.9 Statistical analysis

All data are acquired from at least three independent biological experiments if not specified otherwise. All the Statistical analysis was performed using GraphPad Prism version 10. Normality of the data was assessed using Shapiro-Wilk normality test. For comparisons between two groups, an

unpaired two-sided Student´s t-test significant was employed. For multiple group comparisons, one-way ANOVA followed by Tukey´s Honest Significant Difference test was used for normally distributed data. In case of non-normal distribution, the Kruskal-Wallis test followed by Dunn`s multiple test was applied. Statistical comparisons were visualized using asterisks ($p < 0.001$ (***), $p < 0.01$ (**), $p < 0.05$ (*), ns: not significantly different) or a compact letter display, where different letters indicate differences ($p<0.05$).

3 Results

3.1 The effect of growth media on PTI activation levels

3.1.1 Outline of the chapter

ATS and MES-buffered ½ MS media are the most used growth media for PTI studies (Lincoln et al., 1990; Murashige & Skoog, 1962). However, previously in the Schäfer lab, it was observed that flg22-induced RGI was more pronounced in ATS-grown plants when compared to those grown on ½ MS (Rich-Griffin et al., 2020). In this work, I examined immunity outputs such as RGI, ROS burst and upregulation of immunity marker genes in roots of plants grown on ATS or ½ MS media. The aim of the section was to show the importance of growth media choice in determining the immune response of plant roots in a qualitative and quantitative manner.

3.1.2 Plants grown on ATS medium show stronger flg22-induced RGI than plants grown on ½ MS medium, and this is independent of gelling agent or pH buffering

In previous experiments, it had been observed that upon flg22 or Pep1 treatment, immunity reporter lines *pMYB51::NLS-3xmVENUS* and *pPER5::NLS-3xmVENUS* showed more pronounced RGI when grown on ATS medium compared to plants grown on ½ MS medium (Rich-Griffin et al., 2020). In the present work, it should be examined whether the observed phenotype was specific to the reporter lines or if plants grown on ATS medium in general exhibited stronger PTI responses. To investigate this, wild-type Col-0 plants were grown on solid ATS or ½ MS media prepared after standard protocols (Lincoln et al., 1990; Murashige & Skoog, 1962) and treated the roots with 1 µM flg22 or Pep1 solution. With an average length of 73 mm, roots of mock treated seedlings grown during 14 days on ATS medium were much longer than those of seedlings grown on ½ MS (average root length 50 mm; Figure 4A). flg22-treated seedlings grown on ATS medium showed a significant reduction in primary root length and retained a growth of only approximately 65% relative to mock treated seedlings. In contrast, root lengths of flg22-treated plants grown on ½ MS still showed around 92% of the growth when compared to mock treated plants. However, Pep1 treatment resulted in strong decrease in root lengths of both ATS- and ½ MS-grown plants of about 53% and 61%, respectively (Figure 4B). These results indicate that ATS medium supports growth of *A. thaliana* roots better than ½ MS medium, and RGI induced by flg22 but not by Pep1 is impaired in plants grown on ½ MS compared to those grown on ATS medium.

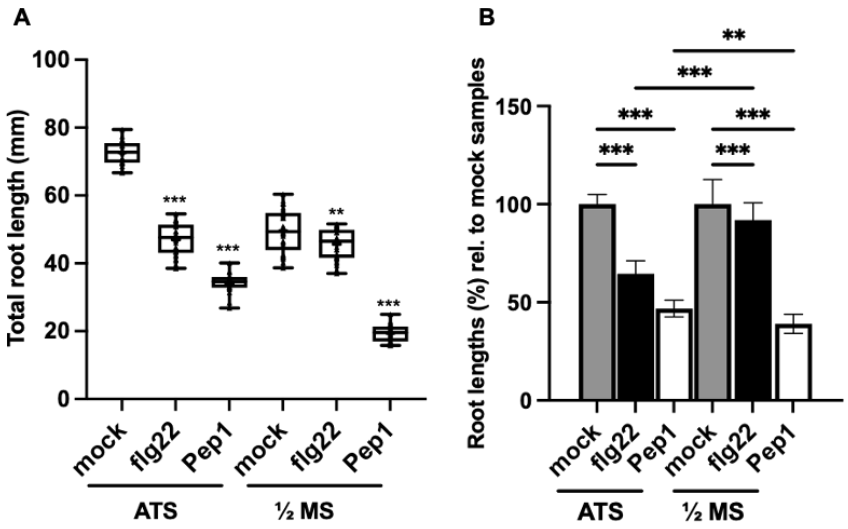

Figure 4: Root growth and flg22-induced RGI is significantly reduced in plants grown on ½ MS medium compared to ATS grown plants: Roots of 10-day-old Col-0 wild-type plants, grown on ½ MS or ATS media plates were treated with 1 µM flg22, 1 µM Pep1 or water (mock). **(A)** Total primary root lengths were measured after 4 days**. (B)** Primary root lengths relative to mock treatment. At least 20 roots were counted per condition. Columns and error bars represent mean values ± SD. The experiment was repeated three times with similar results. Asterisks indicate significant differences with respect to the mock according to ANOVA followed by Tukey´s honest significance test. $p < 0.001$ (***), $p < 0.01$ (**), $p < 0.05$ (*), ns: not significantly different.

Next, I investigated whether the choice of gelling agent has an influence on RGI after activation of root immunity. Phyto agar is a high strength agar selected for plant tissue culture and is commonly used for solidifying MS medium. ATS medium is often solidified with Gelrite™, which is a gelling polysaccharide produced by microbial fermentation (Shungu et al., 1983). Therefore, I used both gelling agents in both types of media and compared flg22- or Pep1-mediated RGI (Figure S1A). When examining the overall growth of plant roots, the use of ATS medium with phyto agar (average root length 58 mm) negatively affected the root lengths compared to the use of ATS medium with Gelrite™ (average root length 71 mm). On the other hand, using ½ MS medium with phyto agar or Gelrite™ had no significant effect on the root lengths: in both conditions the average root length was about 47 mm (Figure S1A). When I analysed flg22- or Pep1-treated plants, phyto agar as a solidifying agent for ATS medium had no significant effect on the severity of RGI induced by either MAMP when compared to Gelrite™-containing ATS medium. Root growth was reduced by about 65% in flg22-treated plants grown on ATS medium with Gelrite™ and 66% in flg22-treated plants grown on ATS medium with phyto agar. In Pep1 treated plants, the reduction was 50% on and 40%, respectively (Figure S1A). In contrast to that, plants grown on ½ MS supplemented with Gelrite™ showed a statistically significant but slightly stronger RGI upon flg22 treatment compared to those grown on ½ MS phyto agar. The reduction was around 73% and 82%, respectively. In Pep1 treated plants, I did not observe a significant difference in RGI, the reduction was about 41% in both conditions (Figure S1A).

Recent studies have indicated that the environmental or extracellular pH has a crucial role in PTI signalling pathways and immune responses (Liu et al., 2022; Yu et al., 2019a). For instance, the extracellular alkalinization plays an important role in promoting PTI in roots (Liu et al., 2022). Furthermore, root-associated bacteria could suppress local root immune responses by lowering the environmental pH in *A. thaliana* seedlings (Yu et al., 2019a). The pH of ½ MS medium is frequently set to around 5.7-5.8, whereas ATS medium is slightly basic (pH around 6.75). Furthermore, the MES-buffer system is commonly employed in ½ MS medium (e.g. Kagenishi et al., 2016)), whereas ATS is usually prepared without buffering (Rich-Griffin et al., 2020). Therefore, I wondered if the reduced RGI could be attributed to the buffering of the media. Col-0 plants were grown on buffered or non-buffered ATS or ½ MS media and treated with flg22 or Pep1. Buffering of ATS did not affect root growth in general or their sensitivity to flg22- or Pep1-induced RGI. Plants grown on non-buffered ½ MS medium grew slightly better, but the buffering of the media had no major effect on RGI levels (Figure S1B). Taken together, plants grown on ATS medium exhibited stronger flg22-induced RGI compared to those grown on ½ MS medium, regardless of gelling agent or pH buffering.

3.1.3 flg22 or Pep1-induced ROS burst is stronger in roots of plants grown on ATS medium when compared to plants grown on ½ MS

The striking difference in RGI intensity between plants grown on ATS or ½ MS media led me to test other hallmark PTI responses. ROS generation is one of the earliest responses of plant cells to flg22 or Pep1 treatment (Poncini et al., 2017). Therefore, I compared ROS burst intensities in ATS- or ½ MS-grown *A. thaliana* roots after treatment with 1 µM flg22 or Pep1 by employing a luminol-based assay (Gómez-Gómez et al., 1999; Jacobs et al., 2011; Poncini et al., 2017). Roots of Col-0 plants grown on ½ MS medium responded with a fast and transient production of ROS to flg22 treatment (Figure 5A and Figure S2). However, plants grown on solid ATS medium produced more than twice the amount of ROS after flg22 treatment compared to plants grown on solid ½ MS medium (Figure 5A). Although the production of ROS in plant roots after Pep1 treatment was generally lower than after flg22 treatment, ROS production in roots of plants grown on ½ MS was considerably lower than that in roots of ATS-grown plants after Pep1 treatment (Figure 5B and Figure S3). These findings indicate that the intensity of flg22- or Pep1-triggered ROS burst varies depending on the growth media used for plant growth and is generally lower in roots of plants grown on ½ MS medium.

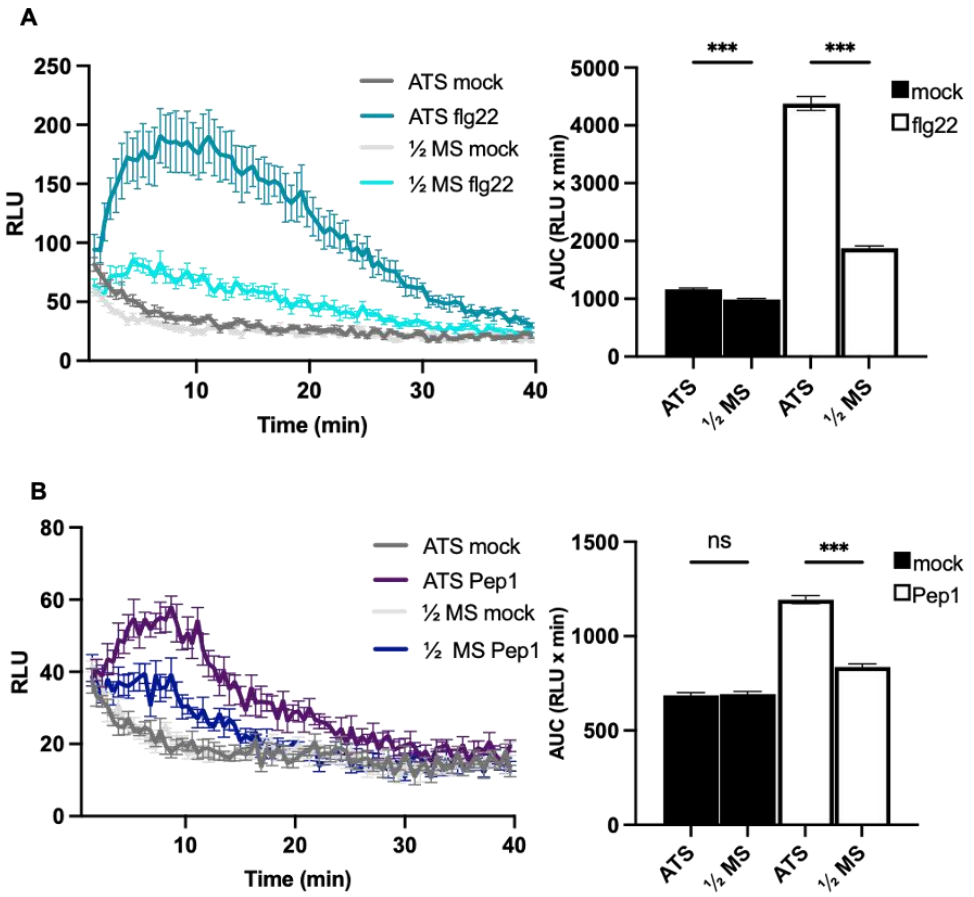

Figure 5: flg22- or Pep1-induced ROS burst is less strong in roots of plants grown on ½ MS medium when compared to ATS medium: 14-day-old Col-0 wild-type plants were grown on ATS or ½ MS and roots were treated with 1 µM flg22, 1 µM Pep1 or water (mock). **(A-B),** Luminol-based detection of ROS production after flg22 or Pep1 treatment, respectively. The graphs show mean values of 6 technical replicates ± SE. The experiments were repeated three times with similar results. RLU: relative luminescence units, AUC: area under curve. Asterisks indicate significant differences according to ANOVA followed by Tukey´s honest significance test. $p < 0.001$ (***), $p < 0.01$ (**), $p < 0.05$ (*), ns: not significantly different.

3.1.4 flg22- or Pep1-induced PTI reporter gene expression is stronger in roots of plants grown on ATS compared to ½ MS-grown plant

I then asked whether the expression of PTI-related marker genes is also affected by the type of plant growth media. I selected a set of defence marker genes: *CALMODULIN-BINDING PROTEIN 60g (CBP60g),* is involved in MAMP-triggered salicylic acid production (Wang et al., 2009), *FLG22-INDUCED RECEPTOR-LIKE KINASE 1* (*FRK1*) is a flg22-responsive receptor-like-kinase (Asai et al., 2002), and *WRKY22* encodes a transcription factor, which activates early MAMP genes (Asai et al., 2002). Col-0 WT plants were grown on either ATS or ½ MS media for 10 days and then treated with 1 µM flg22 or Pep1, or with H_2O as control (mock). 2 h after treatment, whole roots were harvested and total RNA extracted. Transcriptional analysis via qRT-PCR demonstrated that 2 hours after treatment with either immune elicitor, all tested reporter genes showed an induced expression, whereby flg22 always elicited a stronger response than Pep1 irrespective of the media used for plant growth. Importantly,

all tested genes showed a stronger induction in the roots of plants that were grown on ATS medium compared to ½ MS-grown plants in response to both, flg22 or Pep1 treatment (Figure 6 and Figure S4).

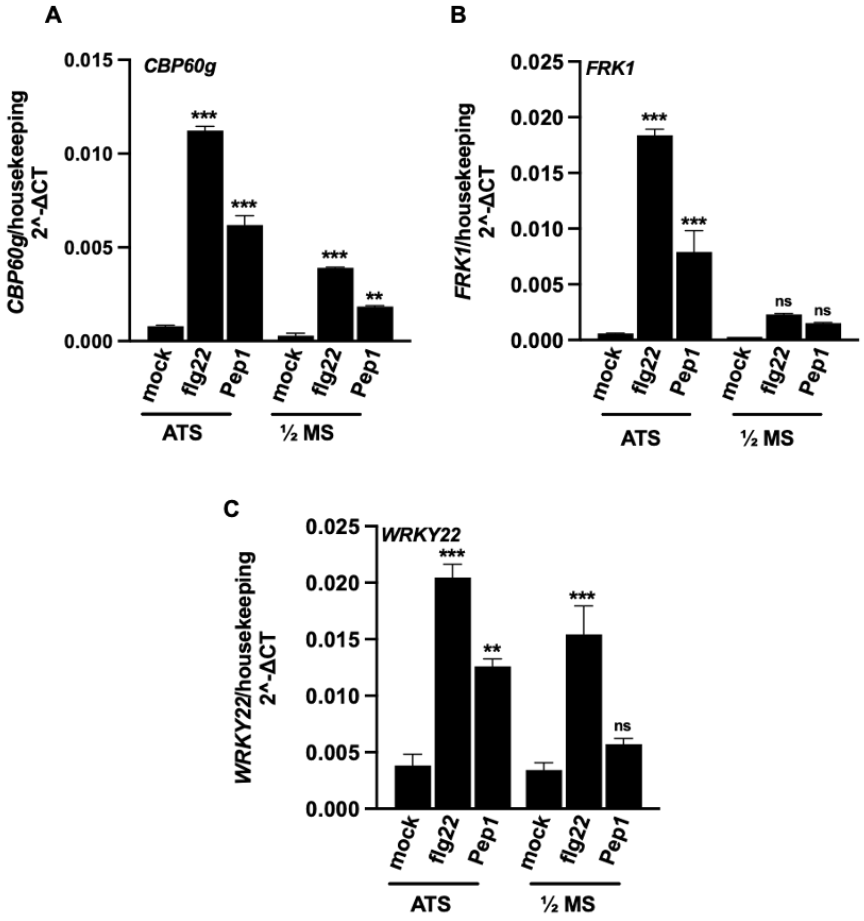

Figure 6: The expression of flg22- or Pep1-induced PTI reporter genes is suppressed in roots of plants grown on ½ MS medium compared to ATS grown plants: 10-day-old Col-0 wild-type plants were grown on solid ATS or ½ MS medium and roots were treated with 1 µM flg22, 1 µM Pep1 or water. Roots were harvested 2 hours after treatment and gene expression was analysed by qRT-PCR. **(A-C),** Expression of the marker genes *CBP60g*, *FRK1*, and *WRKY22***,** respectively. Columns and bars represent mean values ± SE from one representative experiment. The experiment was repeated three times with similar results. Asterisks indicate significant differences with respect to the mock samples according to ANOVA followed by Tukey´s honest significance test. $p < 0.001$ (***), $p < 0.01$ (**), $p < 0.05$ (*), ns: not significantly different.

3.1.5 The media used for plant growth has an influence on the strength and location of flg22-induced expression of PTI reporters in *A. thaliana* roots

I also wanted to analyse whether different growth media have an influence on activation of PTI in different root developmental zones. The oxidative stress-related gene *PEROXIDASE 5* (*PER5*) and *MYB DOMAIN PROTEIN 51* (*MYB51*), a gene involved in the regulation of glucosinolate biosynthesis, are widely used as early PTI response genes (Zhou et al., 2020). In the PTI reporter lines *pPER5::NLS-3xmVENUS* and *pMYB51::NLS-3xmVENUS*, the expression of a nuclear-targeted triple mVENUS fluorophore is driven by the promotor of *PER5* or *MYB51*, respectively. These marker lines can be used to visualize activated root immunity on a cellular level (Poncini et al., 2017; Zhou et al., 2020). To study the spatial activation of PTI in a growth media-dependent way, reporter plants were grown on ATS or ½ MS media for 14 days and then treated with 1 µM flg22, Pep1 or water (mock). After 6 and 24 hours, reporter gene expression was analysed in different root zones via confocal laser-scanning microscopy. In both immunity marker lines, flg22-induced reporter gene expression was strongly induced in the RAM at both time points when plants were grown on ATS medium (Figure 7,8 and Figure S5,6). Marker lines grown on ½ MS showed hardly any fluorescence signal in the RAM at 6 h after flg22 treatment. At 24 hat, there was an increased reporter gene activity in the RAM after flg22 treatment, but this was significantly lower than that induced in the RAM of ATS-grown plants (Figure 7,8).

The Pep1-induced fluorescence signal in the RAM of plants of the *pMYB51::NLS-3xmVENUS* marker line was generally weaker than that induced by flg22 in ATS-grown plants (Figure 7 and Figure S5). There was a significantly stronger signal in ½ MS-grown plants at 6 h after Pep1 treatment, but there was no consistent significant difference between ATS- and ½ MS-grown plants at the later time point across both experiments. In the *pPER5::NLS-3xmVENUS* line, the Pep1-induced fluorescence signal was generally lower than that induced by flg22 in ATS-grown plants at both 6 and 24 hat. In addition, unlike in flg22-treated roots, the fluorescence signal was hardly detectable in the outermost cell layer of the RAM when roots had been treated with Pep1. Instead, it was much stronger in the cells of the stele. After Pep1 treatment, there was no quantitative difference in the fluorescence intensities in the RAM between plants grown on different growth media (Figure 8).

In the differentiation zone (DZ), both elicitors induced reporter gene expression at both time points. At 6 h after flg22 treatment, a fluorescence signal could be detected in epidermis and cortex cells of *pMYB51::NLS-3xmVENUS* roots and the signal intensities were not statistically different between plants grown on ATS or grown on ½ MS media. At 24 hat, there was no difference in the signal intensities. In the Pep1-treated plants, the fluorescence signal intensities were higher at both time points than those in flg22-treated plants and more pronounced in the stele. There was no significant

difference in fluorescence intensities when I compared ATS- with ½ MS-grown plants after Pep1 treatment at 6 or 24 hat in the DZ (Figure 7 and Figure S5).

In the *pPER5::NLS-3xmVENUS* line, fluorescence signals in the RAM were significantly higher in ATS-grown plants at both timepoints after flg22. However, flg22 treatment induced significantly stronger fluorescence signals in the DZ of ½ MS-grown plants compared to ATS-grown plants at 6 hat. However, at 24 hat there was no more significant difference in fluorescence intensities between ATS- and ½ MS-grown plants after flg22 treatment in the DZ. The growth medium did not seem to have a significant effect on the Pep1-induced *pPER5::NLS-3xmVENUS* signal in both RAM and DZ. Like in the RAM, flg22 mostly induced the fluorescence signal in the outermost cell layers of the roots, whereas Pep1 prompted a reporter signal in the stele in the DZ of *pPER5::NLS-3xmVENUS* plants (Figure 8 and Figure S6). It can be concluded that the type of plant growth media used can lead to major differences in elicitor-induced PTI-marker expression, especially in the RAM.

Taken together, these analyses show that there are qualitative and quantitative differences in the spatio-temporal induction of root immune responses to various immune elicitors, and these can be affected by the kind of medium used for plant growth.

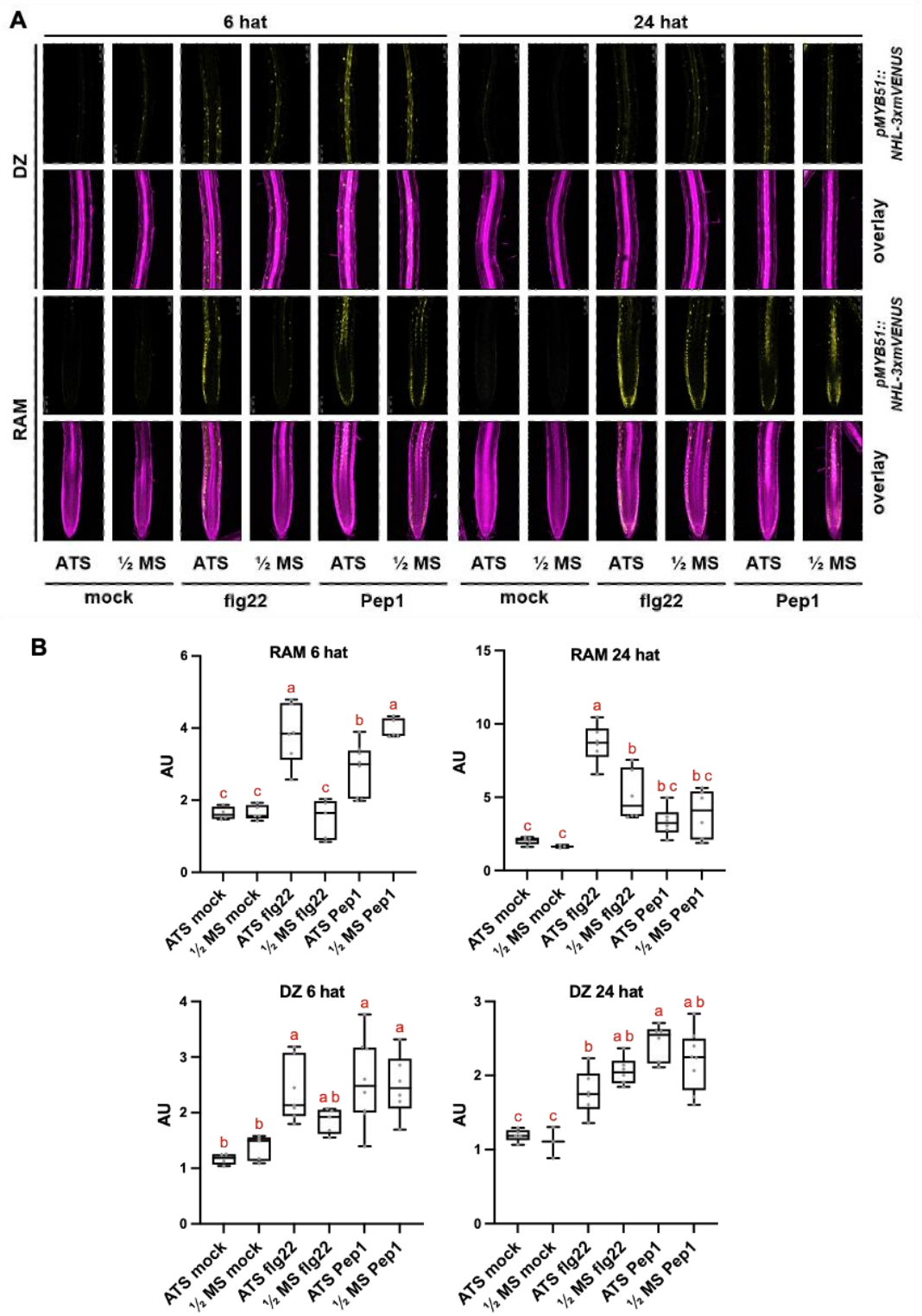

Figure 7: flg22 induces stronger PTI reporter gene expression in the meristematic zone of plant roots grown on ATS media: *pMYB51::NLS-3xmVENUS* plants were grown on solid ATS or ½ MS media and roots were treated with 1 µM flg22, 1 µM Pep1 or water. Roots were harvested 6 or 24 hours after treatment (hat). **(A)** mVENUS expression (yellow) in the root apical meristem (RAM) and differentiation zone (DZ). Root cell walls were stained with Direct Red 23 (magenta). **(B)** Quantification of mVENUS signals in the respective root areas. AU: arbitrary unit. Columns and bars represent mean values ± SD of one representative. Different letters indicate significant differences according to ANOVA test followed by Tukey´s honest significance test. The experiment was repeated two times with similar results.

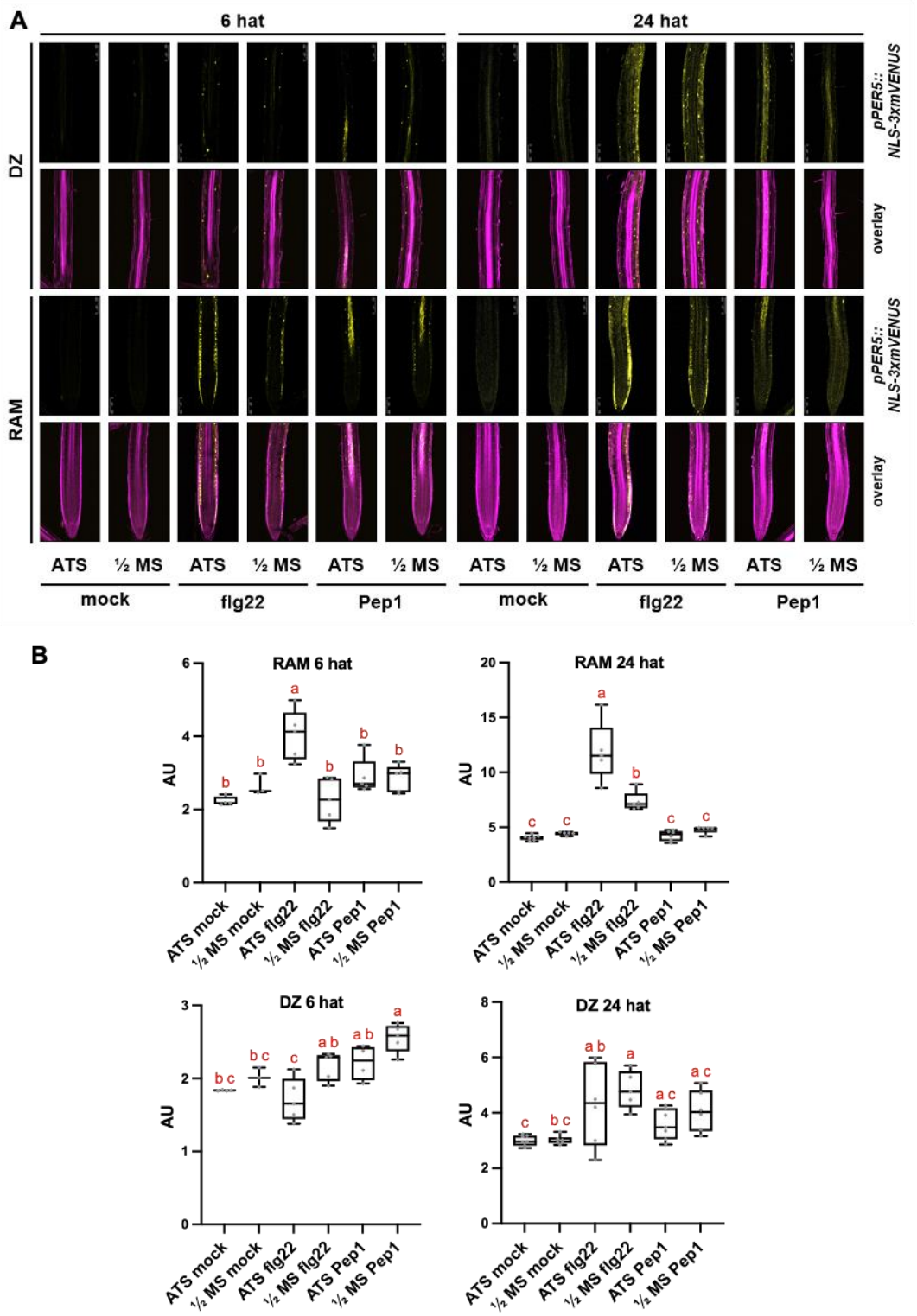

Figure 8: flg22 induces stronger PTI reporter gene expression in meristematic zone of plants grown on ATS plates: 14-day-old *pPER-5::NLS-3xmVENUS* plants were grown on solid ATS or ½ MS and roots were treated with 1µM flg22, Pep1 or water. Roots were harvested 6 hours after treatment (hat) **(A)** mVENUS expression (yellow) in the root apical meristem (RAM) and differentiation zone (DZ). Root cell walls were stained with Direct Red 23 (magenta). **(B)** Quantification of mVENUS signals in the respective root areas. AU: arbitrary unit. Columns and bars represent mean values ± SD of one representative. Different letters indicate significant differences according to ANOVA test followed by Tukey´s honest significance test. The experiment was repeated two times with similar results.

3.2 An overview of *A. thaliana* B-type CDKs and D-type CYCs

3.2.1 Outline of the chapter

This chapter includes computational analyses of *A. thaliana* CDKB and CYCD gene and protein sequences, focusing on understanding their genomic organization and structural features. This includes gene models, protein sequence alignments, phylogenetic trees, analysis of protein domains and common motifs of the proteins of interest, their predicted subcellular localization and their stability. The aim of the chapter was to gain insight into the (predicted) functional nature of CDKBs and CYCDs and to provide a guide to experimental research in the following chapters.

3.2.2 *In silico* analysis of *A. thaliana* B-type CDKs and D-type CYCs

In the *A. thaliana* genome, there are 4 genes coding for B-type CDKs (*CDKB1;1*, *CDKB1;2, CDKB2;1, CDKB2;2*), and 10 genes for D-type CYCs (*CYCD1;1*, *CYCD2;1, CYCD3;1, CYCD3;2, CYCD3;3, CYCD4;1, CYCD4;2, CYCD5;1, CYCD6;1, CYCD7;1*) (Oakenfull et al., 2002). The genes encoding *CDKB2;1*, *CDKB2;2*, *CYCD1;1* are located on chromosome 1, *CDKB1;2* and *CYCD2;1* are found on chromosome 2, *CDKB1;1* and *CYCD3;3* are situated on chromosome 3, *CYCD3;1*, *CYCD5;1* and *CYCD6;1* are found on chromosome 4, and *CYCD3;2*, *CYCD4;1*, *CYCD4;2* and *CYCD7;1* are located on chromosome 5. The gene models were obtained from The Arabidopsis Information Resource (TAIR) and visualized using http://wormweb.org/exonintron (Berardini et al., 2015; Bhatla, 2012) (Figure S7). TAIR proposes one gene model for *CDKB1;1*, *CDKB2;1*, *CDKB2;2*, *CYCD1;1*, *CYCD3;1*, and *CYCD3;3*, two for *CYCD2;1*, *CYCD3;2*, *CYCD4;2*, *CYCD6;1* and *CYCD7;1*, three for *CYCD5;1*, and four gene models for *CDKB1;2* and *CYCD4;1*.

The canonical protein sequences of AtCDKBs and *At*CYCDs were obtained from the UniProt database (https://www.uniprot.org/) and were aligned using the Clustal Omega multiple sequence alignment tool (https://www.ebi.ac.uk/jdispatcher/msa/clustalo) with the default settings and depicted using Jalview 2. Conserved amino acids were highlighted in blue (Figure S8 and S9) (Madeira et al., 2024; Waterhouse et al., 2009). In addition, phylogenetic trees were generated using the Clustal Omega multiple sequence alignment tool. According to the phylogenetic tree, CDKB1;1 and CDKB1;2 likely diverged from a common ancestor as they shared the same node, while CDKB2;1 and CDKB2;2 formed another clade. The sequence alignment revealed that there was a high homology between CDKB1;1-CDKB1;2 (88.75% identical) and CDKB2;1-CDKB2;2 (87.58% identical), respectively (Figure S10).

For the *A. thaliana* D-type CYCs the protein sequence alignment showed a much higher diversity. The closest homologs of CYCD1;1 were likely CYCD2;1, CYCD4;1 and CYCD4;2 (35.09%, 36.16% and 33.66% identical with CYCD1;1, respectively). CYCD3;1, CYCD3;3, CYCD3;2 and CYCD5;1 formed a separate. CYCD6;1 and CYCD7;1 were more distantly related to the other CYCs. The distribution of CYCD proteins

in different clades and the low level of sequence conversation indicated that they have likely evolved independently from one another and may have slightly different structures and functions (Figure S11). To have a better understanding of potential functional features of the protein of interests, protein structures were analyzed *in silico* (Figure 9 and 10). According to InterPro analysis (https://www.ebi.ac.uk/interpro/), all of the CDKBs have a protein kinase domain (Pkinase), as expected. The hallmark amino acid sequence motif of the CDKB1 family is PPTALRE, whereas the CDKB2 family has a P(S/P)TTLRE motif (Vandepoele et al., 2002). In line with this, the PPTALRE motif was identified in the N-terminus of CDKB1;1 and CDKB1;2, while PSPTTLRE and PPTTLRE motifs could be located in the N-terminus of CDKB2;1 and CDKB2;2, respectively (Figure S8). Data from the UniProt (UniProt Consortium, 2018) protein database indicated that all CDKB proteins are localized to the nucleus.

It is thought that polypeptide sequences enriched in proline, glutamic acid, serine and threonine (PEST) serve as proteolytic degradation signals by typically the ubiquitin-proteasome system. Therefore, the presence of PEST motifs may indicate short protein half-lifes (Rechsteiner & Rogers, 1996). To gain more insights into the stability of CDKBs and CYCDs, potential PEST motifs within the protein sequences were analyzed by using the bioinformatic tool "ePestfind" (https://emboss.bioinformatics.nl/cgi-bin/emboss/epestfind). A PEST score above 5 was considered as a real biological interest. According to this, CDKB1;1, CDKB2;1 and CDKB2;2 were predicted to have one PEST motif within their protein sequences. This might indicate that the proteins mentioned above could be susceptible to rapid protein degradation. In addition to the PEST motif analysis, the instability index (I.I) of the proteins was calculated by using the ProtParam tool (https://web.expasy.org/protparam/) (Gasteiger et al., 2005). If I.I is greater than 40, the protein is expected to be unstable *in vitro*. The instability indices of CDKB1;1, CDKB1;2, CDKB2;1, CDKB2;2 were calculated as being 29.33, 32.06, 31.99, and 29.63, respectively. These values indicate that the proteins of interest could be relatively stable *in vitro* (Figure 9).

CYCD protein sequences were examined for the features described above as well. It is important to highlight that those analysis were conducted on CYCD variants that were successfully cloned (Figure 10) (Section 3.4.2). UniPortKB accession numbers of the isoforms analysed can be found in Figure 10. CYCs have a conserved region, which is called cyclin core (Nugent et al., 1991). The cyclin core may contain the Cyclin_N and the Cyclin_C domains. The former is highly conserved and contains the CDK-binding site, which is known as cyclin box. The latter is less conserved (Buendía-Monreal et al., 2011). According to the data obtained from InterPro, all of the CYCDs, except CYCD5;1 and CYCD7;1, have the Cyclin_N and the Cyclin_C_2 domain in the N-terminus and C-terminus, respectively. CYCD5;1 and CYCD7;1 have Cyclin_N domain as well, whereas they contain CYCLIN_ATCycD-like_rpt2 and Cyclin_C

domains, which are slightly different than the Cyclin_C_2 domain. It is known that many *A. thaliana* CYCDs have a LxCxE motif, which functions as plant retinoblastoma-related protein (pRBR)-binding sequence (Buendía-Monreal et al., 2011). All CYCDs, except CYCD4;2, CYCD5;1 and CYCD6;1 contain a LxCxE motif in their protein sequences, which is in line with Strzalka et al. (Figure S9) (Strzalka et al., 2015). Similar to CDKBs, all CYCDs were predicted to localized to the nucleus (UniProt). All members of the CYCD family, pose at least one PEST motif, which might indicate that they are prone to proteolysis. In addition, I.I values for all CYCD1;1, CYCD2;1, CYCD3;1, CYCD3;2, CYCD3;3, CYCD4;1, CYCD4;2, CYCD5;1, CYCD6;1 and CYCD7;1 were calculated greater than 40, which may suggest that CYCDs are rather unstable proteins (Figure 10).

Protein	Domain	Hallmark motif	NL	PEST motif	I.I
CDKB1;1 (P25859)	Pkinase	PPTALRE	+	+	29.33
CDKB1;2 (Q2V419)	Pkinase	PPTALRE	+	-	32.06
CDKB2;1 (Q8LF80)	Pkinase	PSTTLRE	+	+	31.99
CDKB2;2 (Q8LG64)	Pkinase	PPTTLRE	+	+	29.63

Figure 9: Protein features of the CDKBs of *A. thaliana*: The UniProt accession numbers of the isoforms used in this study are given in the parentheses in the first columns. Domain information was taken from InterPro analysis. NL: nuclear protein localization according to data from UniPort. The presence of a PEST motif was predicted by "ePestfind". I.I: protein instability index, I.I>40 means protein is predicted to be instable *in vitro.* I.I scores were calculated by the ProtParam tool. Pkinase: protein kinase domain.

Protein	Domains	LxCxE motif	NLS	PEST motif	I.I
CYCD1;1 (P42751)	Cyclin_N Cyclin_C_2	+	+	+	52
CYCD2;1 (F4IJJ3)	Cyclin_N Cyclin_C_2	+	+	+	55.26
CYCD3;1 (P42753)	Cyclin_N Cyclin_C_2	+	+	+	63.79
CYCD3;2 (Q9FGQ7)	Cyclin_N Cyclin_C_2	+	+	+	53.54
CYCD3;3 (Q9SN11)	Cyclin_N Cyclin_C_2	+	+	+	63.66
CYCD4;1 (F4KHY3)	Cyclin_N Cyclin_C_2	+	-	+	53.47
CYCD4;2 (Q0WQN9)	Cyclin_N Cyclin_C_2	-	-	+	45.04
CYCD5;1 (Q2V3B2-1)	Cyclin_N ATcycD_like	-	+	+	60.03
CYCD6;1 (Q9ZR04)	Cyclin_N Cyclin_C_2	-	+	+	46.61
CYCD7;1 (Q9LZM0)	Cyclin_N Cyclin_C	+	+	+	40.79

Figure 10: Protein features of the CYCDs of *A. thaliana*: The UniProt accession numbers of the isoforms used in this study are given in the parentheses in the first columns. Domain information was taken from InterPro analysis. LxCxE motif: conserved amino acid sequence, where L is leucine, C is cysteine, E is glutamic acid, and x is any amino acid (See Figure S9). NL: nuclear protein localization according to data from UniPort. The presence of a PEST motif was predicted by "ePestfind". I.I: protein instability index, I.I>40 means protein is predicted to be instable *in vitro.* I.I scores were calculated by the ProtParam tool. Cyclin_N: Cyclin, N-terminal domain, Cyclin_C_2: Cyclin, C-terminal domain, ATcycD_like: second cyclin box found in plant cyclin-delta family, Cyclin_C: C-terminal domain, slightly different than Cyclin_C_2.

3.3 The effect of immunity activation on cell cycle regulators

3.3.1 Outline of the chapter

As it was mentioned in Section 1.5.3, Eichmann et al. showed that PTI may lead to RGI by inhibiting the cell cycle, and thus cell division in *A. thaliana* roots. This raises the question whether PTI activation influences cell cycle regulators at the transcriptional or protein level. In this chapter, the expression patterns of *CDKB*s and *CYCD*s in roots were analyzed *in silico*. Then it was investigated whether flg22-induced PTI alters the expression patterns of the above-mentioned genes in *A. thaliana* root tissues. In the second part, I analyzed the impact of activated PTI on the protein accumulation of CDKBs and CYCDs. Together, this chapter was aimed at elucidating the involvement of cell cycle regulators in the growth-immunity antagonism.

3.3.2 The effect of immunity activation on the transcript accumulation of cell cycle regulators

3.3.2.1 Expression pattern of *CDKBs* and *CYCDs* in *A. thaliana* roots

Before investigating the effects of flg22 treatment on the expression of *CDKB*s and *CYCDs*, it should be explored whether these genes are expressed in roots and if so in which root tissues and at what levels. To answer these questions, the expression profile maps found at the Bio-Analytic Resource for Plant Biology (BAR) ePlant tool were analyzed (https://bar.utoronto.ca/eplant/) (Fucile et al., 2011). The maps at the BAR ePlant tool were generated based on gene expression data from Brady et al (Brady et al., 2007). In this study, GFP-marked cells of 5-7-day-old *A. thaliana* roots were sorted according to their cell types by using fluorescence-activated cell sorting (FACS) and the sorted cells were subjected to microarray analysis to generate spatiotemporal expression maps (Brady et al., 2007). The acquired expression maps can be seen in Figure S12.

In order to make comparisons, the expression profiles of *CHLOROPHYLL A/B PROTEIN 140* (*AB140*, AT1G29930) and *ACTIN 2* (*ACT2*, AT3G18780) were also included. It is known that *AB140* encodes a protein, which plays a role in photosynthesis in leaves (Sun & Tobin, 1990), and is not expressed in roots. On the other hand, *ACT2* is constitutively expressed in roots (An et al., 1996). As expected, *AB140* was not expressed in the root at all and *ACT2* was expressed strongly in the meristematic zone and in the elongation zone, the expression was relatively low in the maturation zone according to the BAR ePlant expression maps. The expression patterns of *CDKB1;1*, *CDKB1;2*, *CDKB2;1* and *CDKB2;2* were very similar: They were all expressed relatively strongly in the root meristem, but virtually not expressed in the elongation or maturation zones (Figure S12). According to the BAR ePlant, *CYCD* genes seemed to be expressed at relatively low levels in roots and did not follow a general pattern. Only four genes have marked expression in the root meristem (*CYCD2;1*, *CYCD3;2*, *CYCD4;1* and *CYCD5;1*). *CYCD2;1*, *CYCD3;1*, *CYCD4;1* and *CYCD5;1* also seemed to be expressed to some extent in the elongation and maturation zone (Figure S12). *CYCD6;1* seemed hardly expressed in the root at all,

and there was no information available for the expression of *CYCD7;1* in the Brady dataset. The latter was supported by the data set from Klepikova et al., who performed RNA-seq profiling of *A. thaliana*, which can also be found in the BAR ePlant (Klepikova et al., 2016). In summary, the data retrieved from the BAR ePlant showed that *A. thaliana CDKB*s are mainly expressed in the root meristem. Some *CYCDs* can clearly be detected in the meristematic zone, where cell division takes place.

To gain more insights into expression profiles of *CDKB*s and *CYCD*s in different developmental root zones, Xuesong Wang (Institute of Phytopathology, Justus-Liebig Universtität Gießen) has generated a heatmap for the expression of selected genes with a potential role in the cell cycle by using a single cell RNA-seq dataset from Shahan et al., 2022 (Shahan et al., 2022) (Figure 11). As references, the house-keeping genes, *AtUBQ5* and *AtEF1α* were included in the heatmap. In addition to *CDKBs* and *CYCDs*, the heatmap also showed the expression of other cell cycle regulators such as *CDKA*, *CDC10-DEPENDENT TRANSCRIPT 1* (*CDT1a*), *PROLIFERATING CELL NUCLEAR ANTIGEN 1* (*PCNA1*), *CYCB1;1*, *KNOLLE*, which are expressed in different phases of the cell cycle (Echevarría et al., 2021). *CDKB*s exhibited the strongest expression in meristem cells and hardly any in cells in the upper developmental zones. Among the *CDKB*s, *CDKB1;2* showed the lowest expression and it had no expression in the elongation and maturation zones. For *CYCD1;1,* a very weak expression in the meristem could be observed, which increased in the elongation and the maturation zones. *CYCD2;1* and *CYCD3;2* had relatively high expression levels in cells of all three root zones. *CYCD3;1* expression was mostly limited to cells in the meristem. The expression levels of *CYCD3;3*, *CYCD4;1* and *CYCD5;1* were generally rather low, but highest in the meristem. *CYCD4;2* was very weakly expressed in cells of each part of the root. *CYCD6;1* and *CYCD7;1* were virtually not expressed in the analyzed cells at all.

The expression maps that were obtained from the BAR ePlant tool and the single cell RNA-seq data gave similar information about the expression patterns of *CDKBs* and *CYCDs* in the developmental zones of roots. Although some genes such as *CYCD1;1*, *CYCD4;2* or *CYCD6;1* were only weakly expressed in root cells, and especially in the root meristem, the vast majority were expressed in moderate amounts. In addition, the expression of these genes was not necessarily limited to meristematic cells, they can be expressed in the elongation and maturation zones as well.

In this chapter, the main aim was to analyze *CDKB* and *CYCD* expressions upon PTI activation. To meet this purpose, it was crucial to know whether the genes of interest are expressed in roots. Except for *CYCD7;1* and maybe *CYCD6;1*, all genes seemed to be expressed in *A. thaliana* root cells. Another concern was whether the expression is limited to the meristematic zone (root tips), where cell division takes place, and would therefore be hard to measure in whole root tissue. However, the dataset showed that some of the cell cycle regulators analyzed here exhibited expression in the elongation

and maturation zones, as well. Overall, these results indicate that it should be feasible to study whole roots for PTI-dependently altered gene expression.

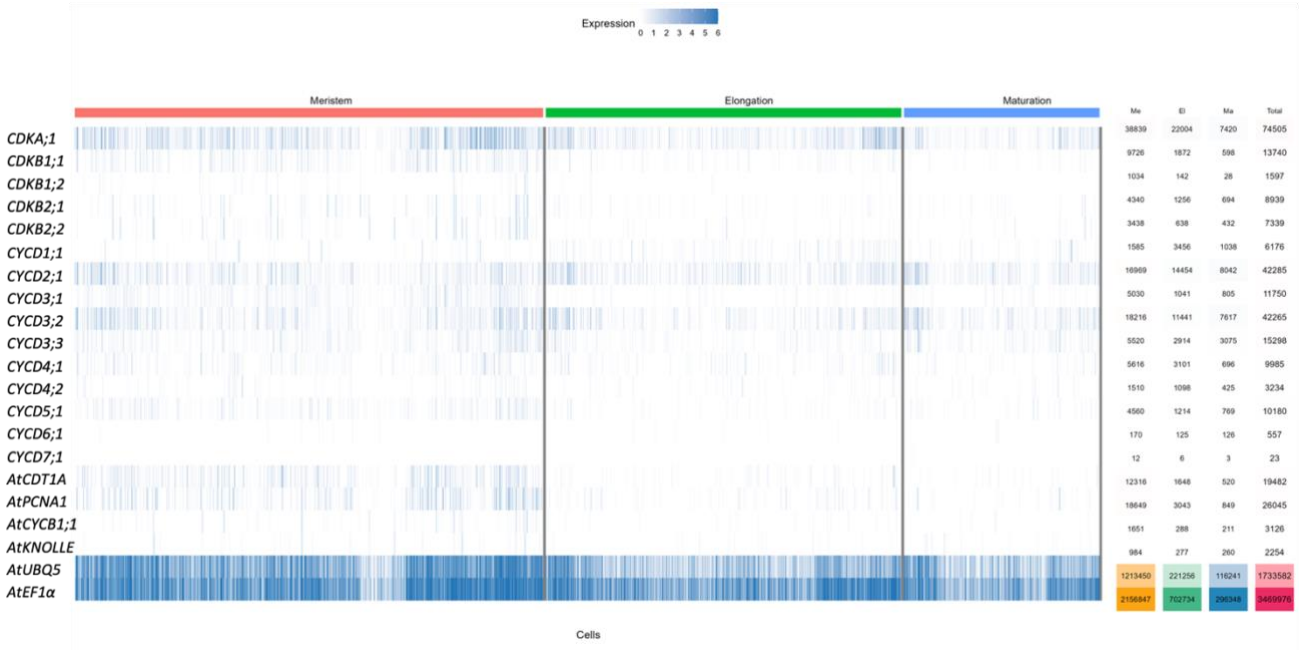

Figure 11: Heatmap of single-cell RNA-seq read counts of *CDKBs*, *CYCDs* and other cell cycle-related genes in different root zones: The heatmap shows the gene expression profiles of individual cells. Each row represents the expression levels of the genes of interest, and each column shows an individual cell. The colour intensity depicts the gene expression levels in read counts per cell. Numbers at the end of each row represent the read counts in all cells (total) or cells in the different developmental zones of the root. Housekeeping genes *AtUBQ5* and *AtEF1α* serve as reference. The heatmap was generated by Xuesong Wang by using single cell RNA-seq data from Shahan et al., 2020.

3.3.2.2 Expression analysis of cell cycle regulator genes in whole roots after PTI elicitation

In order to understand the role of cell cycle regulators in PTI-induced RGI, potential changes in their expression were investigated.

To determine whether flg22-induced PTI influences the expression of *CDKB*s and *CYCD*s, 12-day-old-*A. thaliana* wild-type seedlings were treated with 100 nM flg22 or mock (water) and the whole roots were harvested at 4, 24 or 48 hours after treatment. Total RNA was extracted and reverse transcribed into cDNA, which was followed by qRT-PCR. First, it was verified whether PTI was successfully activated by flg22. For this purpose, expression of PTI marker genes *CBP60g* and *WRKY22* were quantified from two biological replicates (Figure S13). Upon flg22 treatment, expression of *CBP60g* and *WRKY22* were strongly induced at all time points when compared to the mock samples. These results show that immunity was activated by flg22 treatment.

After proving that flg22 treatment had elicited detectable PTI responses in the roots, the expression of *A. thaliana CDKB* and *CYCD* genes was measured (Figure 12 and 13). In Rep 1, at 4 hours after flg22 treatment, the expression of *CDKB1;1, CDKB1;2, CDKB2;1* and *CDKB2;2* significantly decreased to 0.53-fold, 0.72-fold, 0.64-fold and 0.67-fold, respectively, of that in the mock treated samples. At 24 hat,

CDKB1;1, *CDKB1;2*, *CDKB2;1* and *CDKB2;2* were still down regulated (0.47-fold, 0.76-fold, 0.57 fold and 0.52-fold of the expression in the mock samples, respectively). At 48 hat, the expression of *CDKB1;1*, *CDKB2;1* and *CDKB2;2* in the flg22-treated samples was still significantly suppressed to 78%, 76% and 80% of that in the mock samples, while *CDKB1;2* expression had gone back to the level of the mock treated sample (Figure 12). In Rep 2, the expression of all of the *CDKB* genes was either slightly upregulated or not significantly different from levels in mock treated samples at 4 and 24 hat. However, *CDKB1;2*, CDKB2;1 and *CDKB2;2* were significantly down regulated at 48 h after flg22 treatment (0.85-fold, 0.68-fold, 0.75-fold) (Figure S14).

It is important to note that in the qRT-PCR analyses, no signal was detected for *CYCD7;1.* Therefore, *CYCD7;1* was excluded from the analyses (Figure 13 and Figure S15). In Rep 1, at 4 hat, the expression of all *CYCD* genes was significantly downregulated, except for *CYCD2;1*, which remained at the level of the mock treated sample (*CYCD1;1*: 81%, *CYCD3;1*: 66%, *CYCD3;2*: 72%*, CYCD3;3*: 66%, *CYCD4;1*: 67%, *CYCD4;2*: 69%, *CYCD5;1*: 73% and *CYCD6;1*: 64% less of the mock samples*)*. At 24 hat, all the *CYCD* genes were still slightly down regulated except for *CYCD3;3*, whose expression had gone back to the level of the mock sample. At 48 hat, the expression of *CYCD2;1*, *CYCD3;1*, *CYCD3;2*, *CYCD4;1*, *CYCD5;1* and *CYCD6;1* was restored to the level observed in the mock sample, while the expression of CYCD1;1, *CYCD3;3* and *CYCD4;2* in the flg22-treated samples remained significantly suppressed to 53%, 65% and 83% of that in the mock samples, respectively (Figure 13). In Rep 2, at 4 hat, the expression of *CYCD1;1* was significantly increased to 2.31-fold of mock treated samples and the expression of *CYCD2;1*, *CYCD3;2*, *CYCD3;3*, *CYCD4;2* and *CYCD6;1* was slightly upregulated. flg22 treatment did not significantly change the expression of *CYCD3;1*, *CYCD4;1* and *CYCD5;1* at 4 hat. At 24 hat, the expression of *CYCD1;1*, *CYCD4;1* and *CYCD5;1,* was significantly suppressed. At 48 hat, the expression of all the *CYCD* genes was either slightly downregulated or not significantly different from levels in mock treated samples with the exception of *CYCD3;3*, which was slightly upregulated (1.25-fold) (Figure S15).

Taken together, compared to the mock treated samples, an overall trend of downregulation was observed in the expression of various *CDKB* and *CYCD* genes after flg22 treatment. Notably, in both of the biological replicates, the expression of *CYCD1;1* and *CYCD5;1* significantly decreased 24 h after flg22 treatment, while the decline in *CYCD1;1* persisted through 48 hat. Furthermore, by 48 hours, the expression of *CDKB2;1*, *CDKB2;2*, and *CYCD4;2* also showed a consistent decrease in both replicates. These results indicate that flg22-induced PTI may reduce the expression of cell cycle regulator genes.

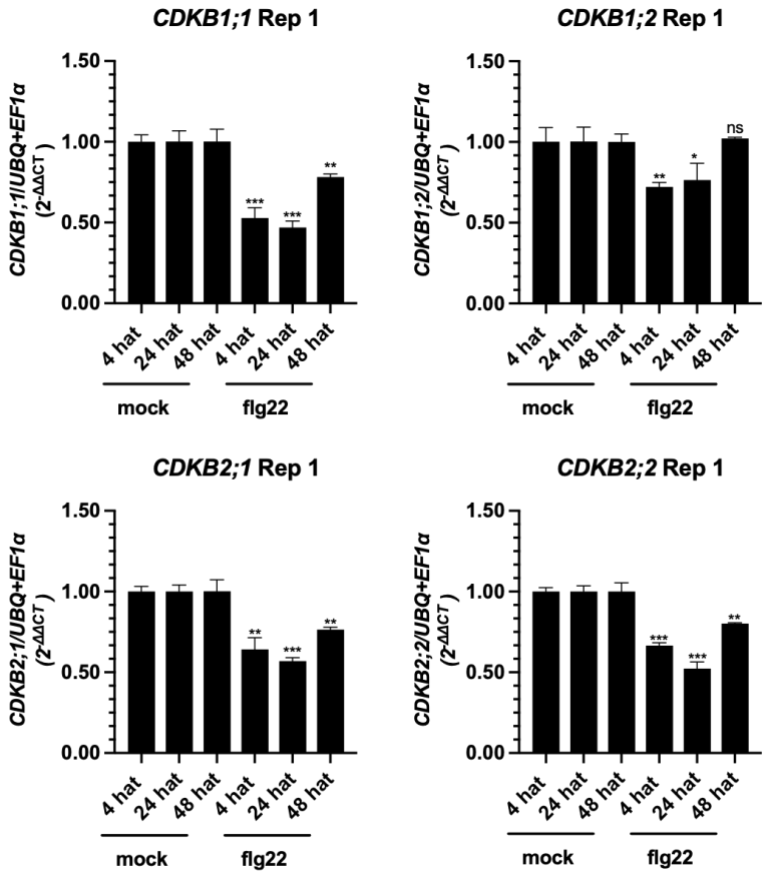

Figure 12: Expression of *CDKB* genes in *A. thaliana* roots after flg22 treatment: 12-day-old Col-0 seedlings were treated with 100 nM flg22 or with water (mock). Whole roots were harvested at 4, 24 and 48 hours after treatment (hat). Total RNA was extracted, reverse transcribed into cDNA and qRT-PCR was performed. The columns represent normalized mean values relative to the mock treated samples ($2^{-\Delta\Delta Ct}$). Housekeeping genes *AtUBQ5* and *AtEF1α* were used to normalize data. Error bars show SE of the mean. Asterisks indicate significant differences between mock and flg22 treated samples according to unpaired two-sided Student´s *t* test. $p < 0.001$ (***), $p < 0.01$ (**), $p < 0.05$ (*), ns: not significantly different.

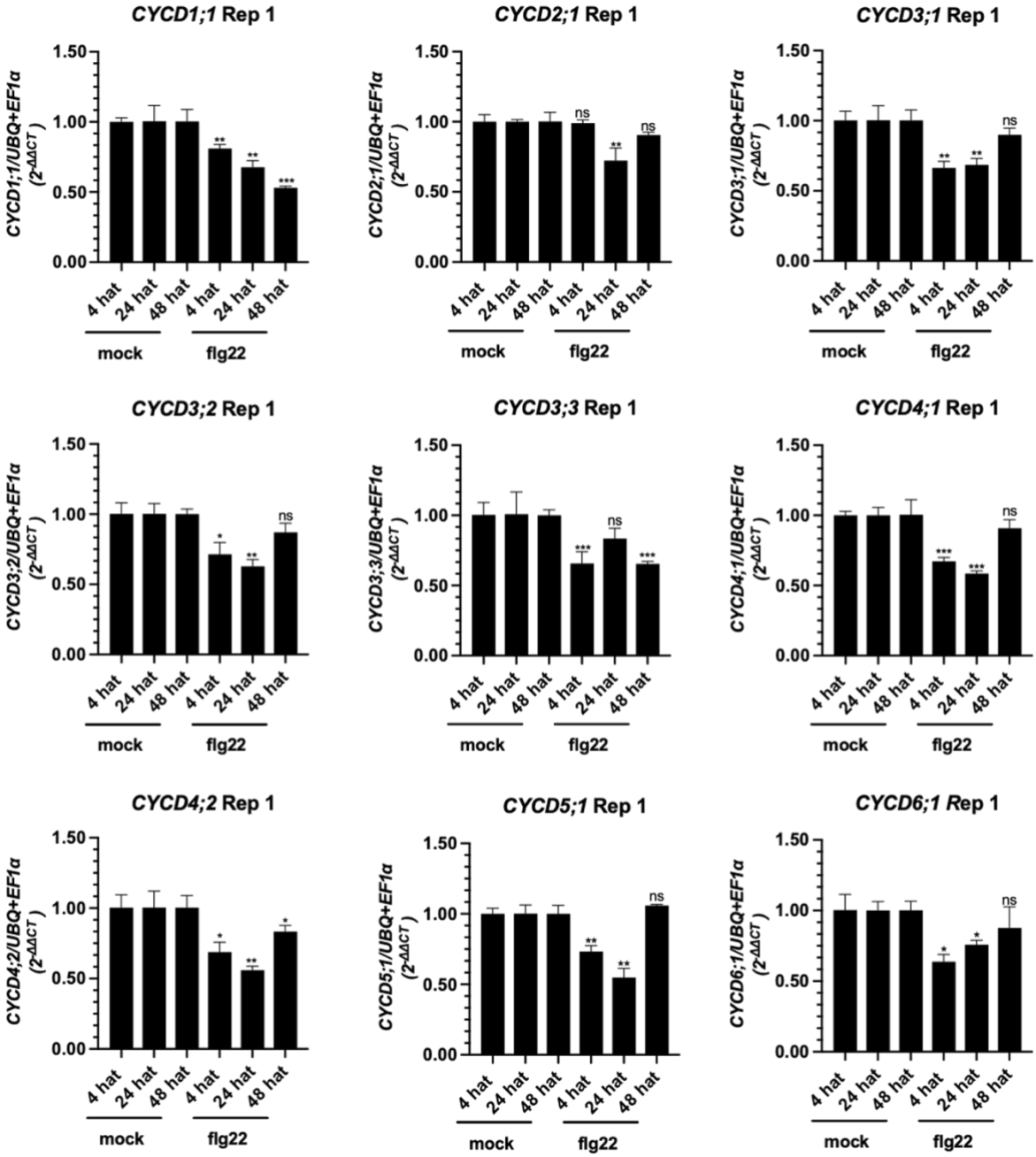

Figure 13: Expression of *CYCD* genes in *A. thaliana* roots after flg22 treatment: 12-day-old Col-0 seedlings were treated with 100 nM flg22 or with water (mock). Whole roots were harvested at 4, 24 and 48 hours after treatment (hat). Total RNA was extracted, reverse transcribed into cDNA and qRT-PCR was performed. The columns represent normalized mean values relative to the mock treated samples ($2^{-\Delta\Delta Ct}$). Housekeeping genes *AtUBQ5* and *AtEF1α* were used to normalize data. Error bars show SE of the mean. Asterisks indicate significant differences between mock and flg22 treated samples according to unpaired two-sided Student´s *t* test. $p < 0.001$ (***), $p < 0.01$ (**), $p < 0.05$ (*), ns: not significantly different.

3.3.3 The effect of immunity activation on protein abundance of cell cycle regulators

The previous section focused on the impact of immunity on the expression of plant cell cycle regulators (*CDKBs* and *CYCDs*). However, transcriptional quantification by qRT-PCR may not necessarily reflect actual protein levels in a sample. *In silico* analyses in the Section 3.2 indicated that *A. thaliana* CYCDs may be regulated by post-translational modifications, such as ubiquitination, which may lead to protein degradation. Therefore, the question arised if plant immunity activation may influence the protein abundance of cell cycle regulators. In this section, this question was addressed by transiently overexpressing *A. thaliana* CDKBs and CYCDs in *N. benthamiana* in the presence or absence of flg22-treatment, and subsequent measurement of the protein levels by Western blot.

3.3.3.1 Transient overexpression of *A. thaliana* CDKBs and CYCDs in *N. benthamiana*

3.3.3.1.1 Generating expression plasmids and confirmation of protein expression

To test for any potential alterations in CDKB and CYCD protein levels after PTI activation, first it was crucial to have a system that enables the detection of the proteins of interest efficiently. In order to generate plant expression constructs, Golden Gate Cloning was employed. Golden Gate Cloning is a molecular cloning method, which enables the assembly of modular DNA fragments avoiding inefficient and time-consuming steps of traditional molecular cloning (Engler et al., 2014). Golden Gate Cloning relies on the Type IIS restriction enzymes and does not require overlapping flanking sequences or recombination sites. As Golden Gate Cloning is a hierarchical and modular cloning system, one can easily assemble multiple DNA fragments with a small number of reactions (Weber et al., 2011). The basic units required for gene expression, such as promoter, coding sequence (of reporter genes), selection marker cassette, protein tags and terminators can be found in L0 acceptor plasmids (standard parts) supplied in the Golden Gate Plant Parts Kit or MoClo Plant Tool Kit (Engler et al., 2014). Genes of interest can easily be cloned into L0 acceptors vectors as well. Then, selected level zero parts are assembled into L1 acceptor plasmids to generate the transcriptional units (expression cassette). Moreover, it is possible to generate multi gene expression constructs by assembling several L1 expression cassettes into L2 acceptor plasmids. Importantly, all the L1 and L2 acceptor vectors are binary vectors with left and right borders for the transfer into plants cells through *A. tumefaciens* (Engler et al., 2014). For overexpression of *A. thaliana* CDKBs in *N. benthamiana*, the following parts were assembled into level 1 plasmids (pL1P3): 35S + 5´ UTRΩ promoter, CDKB or CYCD coding sequence (see Figure 9 and Figure 10 for the cloned isoforms of the proteins), C-terminal tag (3xHA-FLAG for CDKBs or 4xMYC for CYCDs, 3´ UTR + NOS terminator. In addition, C-terminally 3xHA-FLAG-tagged or C-terminally 4x MYC-tagged turbo GFP (tGFP*)* was cloned into pL1P3 under 35S + 5´ UTRΩ promoter as controls. After the transformation of *A. tumefaciens* with the generated constructs, *N. benthamiana* leaves were infiltrated with the bacteria containing *tGFP-3xHA-FLAG* or *tGFP-4xMYC*

plasmid to validate the expression of the proteins in *N. benthamiana* by fluorescence microscopy and to determine the time point when the expression was the strongest. It is important to note that *A. tumefaciens* carrying the tGFP expression constructs were co-infiltrated with *A. tumefaciens* carrying a construct for the expression of the p19 protein, which is a suppressor of post-transcriptional gene silencing (Das, 2020; Kontra et al., 2016; Lakatos et al., 2004), in order to enhance protein detection levels. tGFP accumulation was checked under a fluorescence microscope at 1 day after infiltration (dai), 2 dai and 3 dai (Figure S16). At 1 dai, a very weak tGFP signal was observed in the leaf discs which were infiltrated with tGFP-3xHA-FLAG or tGFP-4MYC. A limited number of cells showed tGFP accumulation. The intensity and the number of the cells expressing tGFP increased at 2 dai and reached the highest level at 3 dai. Therefore, for the future assays, the 3 dai timepoint was chosen. Interestingly, expression of tGFP-4xMYC resulted in a stronger tGFP signal than tGFP-3xHA-FLAG. Quantification of the fluorescence intensity performed using ImageJ also confirmed these observations. At 1 dai, there was no difference in tGFP intensities between tGFP-3xHA-FLAG and tGFP-4xMYC. At 2 dai, the intensity of tGFP-4xMYC was 10 times higher than that of tGFP-3xHA-FLAG, and at 3 dai, it was still more than 4 times higher (Figure S16B).

3.3.3.1.2 Detection of 3xHA-FLAG-tagged CDKB- and 3xMYC-tagged CYCD proteins

To verify that CDKBs-3xHA-FLAG and CYCDs-4xMYC were expressed in *N. benthamiana* and that the proteins could be detected by Western blot, *N. benthamiana* leaves were co-infiltrated with *A. tumefaciens* carrying one of the *CDKB* or *CYC* expression plasmids and *A. tumefaciens* carrying p19. Based on the finding that tGFP was most strongly expressed at 3 dai, the infiltrated leaf discs were also collected at 3 dai. The crude protein extracts were subjected to Western blot. All CDKB proteins could successfully be detected at the expected sizes (Figure 14). However, CYCDs were more difficult to detect. It was necessary to load samples with a higher concentration and use a longer exposure time during imaging (Figure 14). CYCD3;3 could not be detected at all, and was excluded from further analysis. Importantly, the CYCD3;1 protein band ran at a higher size than calculated. This could be due incomplete denaturation or post-translational modifications.

Construct	Molecular mass (kDa)
35S::tGFP-3xHA-FLAG	31.13
35S::CDKB1;1-3xHA-FLAG	40.45
35S::CDKB1;2-3xHA-FLAG	40.71
35S::CDKB2;1-3xHA-FLAG	40.72
35S::CDKB2;2-3xHA-FLAG	40.97

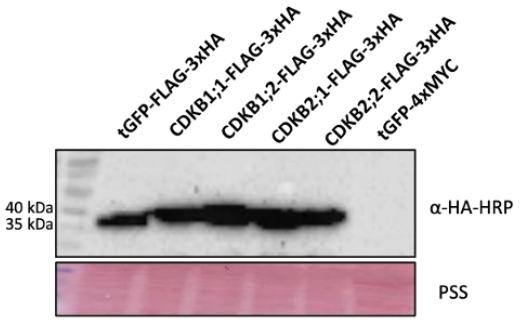

Construct	Molecular mass (kDa)
35S::tGFP-4xMYC	30.96
35S::CYCD1;1-4xMYC	43.09
35S::CYCD2;1-4xMYC	45.53
35S::CYCD3;1-4xMYC	47.52
35S::CYCD3;2-4xMYC	47.17
35S::CYCD3;3-4xMYC	46.56

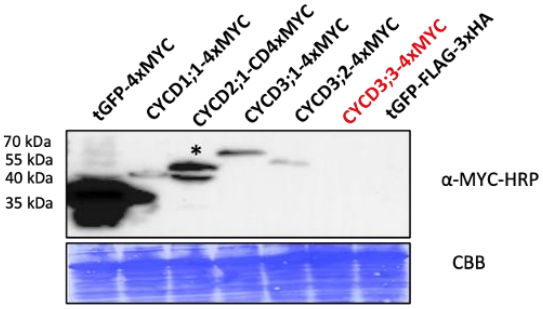

Construct	Molecular mass (kDa)
35S::tGFP-4xMYC	30.96
35S::CYCD4;1-4xMYC	40.73
35S::CYCD4;2-4xMYC	38.60
35S::CYCD5;1-4xMYC	41.99
35S::CYCD6;1-4xMYC	39.49
35S::CYCD7;1-4xMYC	44.73

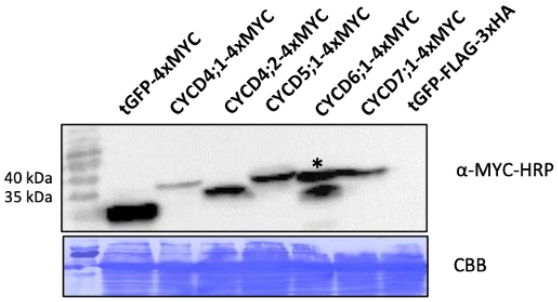

Figure 14: Western blot detection of 3xHA-FLAG-tagged *A. thaliana* CDKB proteins and 4xMYC-tagged *A. thaliana* CYCD proteins in cell lysates from transiently transformed *N. benthamiana* leaves: 4-5-week-old *N. benthamiana* leaves were co-infiltrated with *A. tumefaciens* carrying either one of the *pL1P3_35S::CDKBs-3xHA-FLAG* or *pL1P3_35S::CYCDs-4xMYC* plasmids together with *A. tumefaciens carrying an* expression construct for the p19 silencing suppressor. 3 days after infiltration (dai), leaf discs were collected and total proteins extracted. Western blot analysis was performed with antibodies against HA- or MYC-tags. As loading control, membranes were stained with either Ponceau S staining (PSS) or Coomassie brilliant blue (CBB). The calculated molecular weights of the tagged proteins are indicated in the tables on the left.

3.3.3.2 Eliciting PTI in *N. benthamiana* by applying flg22

To investigate the effect of PTI on cell cycle regulator protein levels in *N. benthamiana*, the most effective way to apply flg22 to *N. benthamiana* was tested. There were two possible treatment methods to activate PTI in *N. benthamiana* leaves. The first one was direct infiltration of a flg22 solution into the leaves with a needle-less syringe, which is similar to *Agrobacterium* infiltration. The second one was to float leaf discs in flg22 solution. Another issue that needed to be tested was whether *A. tumefaciens* would have an effect on flg22-induced PTI. According to the literature, *A. tumefaciens* infiltration rewires cellular processes and may induce plant immunity responses in the host plant (Beritza et al., 2024; Grosse-Holz et al., 2018). On the other hand, *A. tumefaciens* may hijack elements of the immune machinery and could lower plant immune responses in *A. thaliana* (Shi et al., 2014; Tiwari et al., 2022). This would be undesirable because the aim here was to observe the effect of immunity on the protein accumulation of cell cycle regulators.

To test whether flg22 infiltration or floating is better and whether *A. tumefaciens* has any impact on PTI levels, the following experimental setup was established: For the flg22 floating method, *N. benthamiana* leaves were infiltrated with *A. tumefaciens* containing the plasmid for *tGFP-MYC* expression or infiltration buffer only (control) on day 0. Two days later, leaf discs were collected from a batch of plants and transferred into 96-well plates containing water. To reduce the effects of wounding, the harvested leaf discs were incubated at growth conditions overnight. On the next day, 1 µM flg22 or mock (water) was applied to the leaf discs. For the flg22 infiltration method, 1 µM flg22 solution or water was directly infiltrated into the leaves of another batch of plants two days after *A. tumefaciens* infiltration. 2 hours after transfer to flg22 solution or flg22 infiltration, leaf discs were collected and RNA was extracted. qRT-PCR analysis of the PTI marker gene *NbCYP71D20* (Heese et al., 2007; Segonzac et al., 2011*)* was performed. In the absence of flg22, *Agrobacterium* infiltration on its own could induces PTI marker gene expression to some extent. Importantly, floating in flg22 solution induced PTI gene expression much more strongly than flg22 infiltration. Prior infiltration with *A. tumefaciens* resulted in a slightly higher PTI marker gene upregulation in the flg22-treated samples (Figure S17). Together, these results show, that floating *N. benthamiana* leaf discs on flg22 solution strongly induced PTI marker gene expression, and that *Agrobacterium* infiltration did not impair this.

After finding an efficient flg22 treatment method, the best timepoint for the activation of PTI genes should be identified, again in the presence and absence of *A. tumefaciens*. The experimental set-up was that described above for the floating method. Samples were harvested 2, 6 and 24 h after flg22 treatment. The expression of two PTI marker genes, *NbCyp71D20* and *AVR9/CF-9 RAPIDLY ELICITED 31* (*NbACRE31)* (Heese et al., 2007; Segonzac et al., 2011) were studied. Expression of the both marker genes, *NbCyp71D20* and *NbACRE31* showed a significant increase following flg22 treatment, with or

without *A. tumefaciens* across all measured time points but the highest expression levels were observed at 2 hat (Figure 15). These results show that at all tested time points, it is possible to observe PTI marker gene activities.

In conclusion, *A. tumefaciens* does not affect the induction of PTI marker gene expression, and floating in flg22 solution is a better way of treatment than infiltration. Furthermore, PTI is still active at 6 and 24 hat. This shows that the designed experiment is feasible under these conditions.

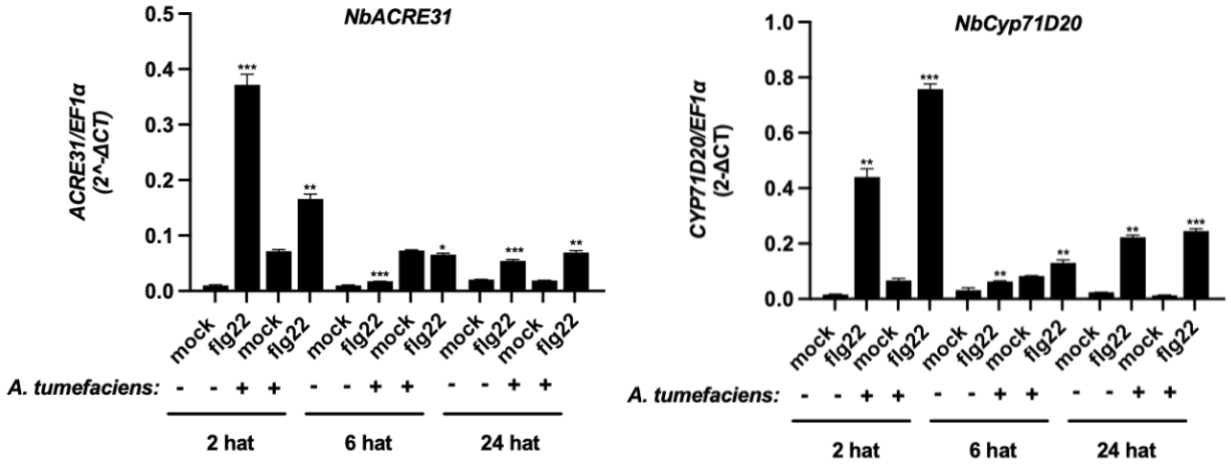

Figure 15: Upregulation of immunity marker genes in *N. benthamiana* leaf discs after flg22 treatment: 4-week-old *N. benthamiana* leaves were infiltrated with *A. tumefaciens* or infiltration buffer (control). 2 dai, leaf discs were collected, and a day later treated with 1 µM flg22 solution or water. 2, 6 and 24 hours after treatment (hat), samples were collected, total RNA extracted and reverse transcribed into cDNA, and qRT-PCR was performed to analyze the expression of the immunity marker genes *NbACRE31* and *NbCyp71D20*. The columns represent mean gene expression values ($2^{-\Delta Ct}$), normalised against the house keeping gene, *NbEF1α*. Error bars show standard errors. Asterisks indicate significant differences between mock and flg22-treated samples according to unpaired two-sided Student´s *t* test. $p < 0.001$ (***), $p < 0.01$ (**), $p < 0.05$ (*), ns: not significantly different.

3.3.3.3 Analysis of the accumulation of *A. thaliana* CDKB and CYCD proteins in *N. benthamiana* leaves after elicitation of PTI

After successfully establishing the experimental set-up, protein levels of ectopically overexpressed *A. thaliana* CDKBs and CYCDs were investigated in *N. benthamiana* leaves after in the presence and absence of flg22-induced PTI. In summary the following experimental procedure was designed (Figure 16): On day 0, leaves of *N. benthamiana* were co-infiltrated with *A. tumefaciens* containing *CDKB* or *CYCD* expression constructs, together with *A. tumefaciens* containing a plasmid for the expression of the silencing suppressor p19. 2 dai, leaf discs were collected and transferred into 96-well plates containing water. To reduce the effects of wounding, the leaf discs were incubated at growth conditions overnight. On the next day, 1 µM flg22 or water (mock treatment) was applied to the discs. The discs were harvested at 6 and 24 hat, which was followed by protein extraction and the detection of proteins by Western blot. The results showed that CDKB levels were not affected by flg22 treatment at 6 hat or 24 hat (Figure 16B). CYCD2;1-4x MYC levels were lower at 24 h after flg22-treatment in two

independent experiments (Figure 17, Figure S18). CYCD2;1 protein band intensities were quantified using ImageJ/Fiji software, and the quantification confirmed the decrease in CYCD2;1 protein levels observed 24 hours after flg22 treatment in both biological replicates (Figure S19). All other CYCDs showed similar protein levels irrespective of the treatment. Together, this indicates that flg22-induced PTI may reduce CYCD2;1 protein accumulation.

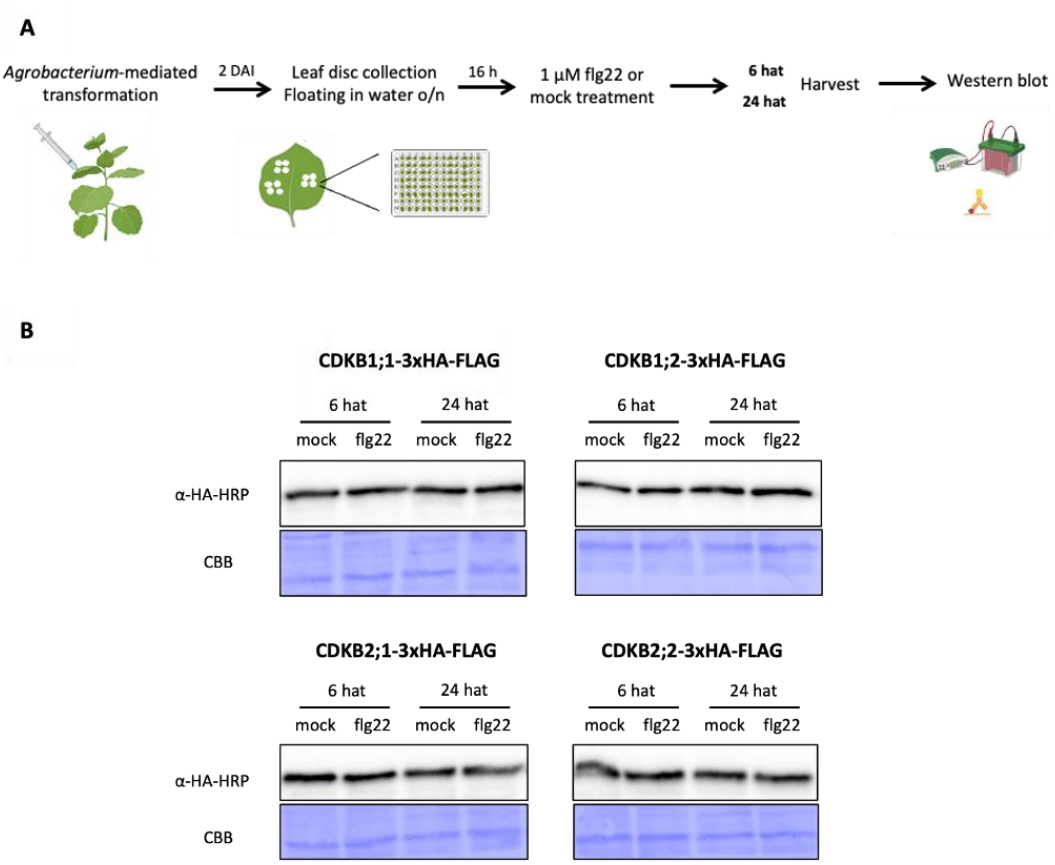

Figure 16: AtCDKB protein levels in *N. benthamiana* leaf discs after flg22 treatment: (A) Experimental set-up: 4-week-old *N. benthamiana* leaves were co-infiltrated with *A. tumefaciens* carrying the plasmids for *AtCDKBs-3xHA-FLAG* expression and expression of the p19 silencing suppressor. 2 dai, leaf discs were collected and transferred into a 96-well plate containing water. On the next morning, leaf discs were treated with 1 µM flg22 solution or water. At 6 and 24 hours after treatment (hat), samples were harvested and proteins extracted. **(B)** Western blot was performed with antibodies against HA- or MYC-tags. As loading control, membranes were stained with Coomassie brilliant blue (CBB). (A) created with biorender.com

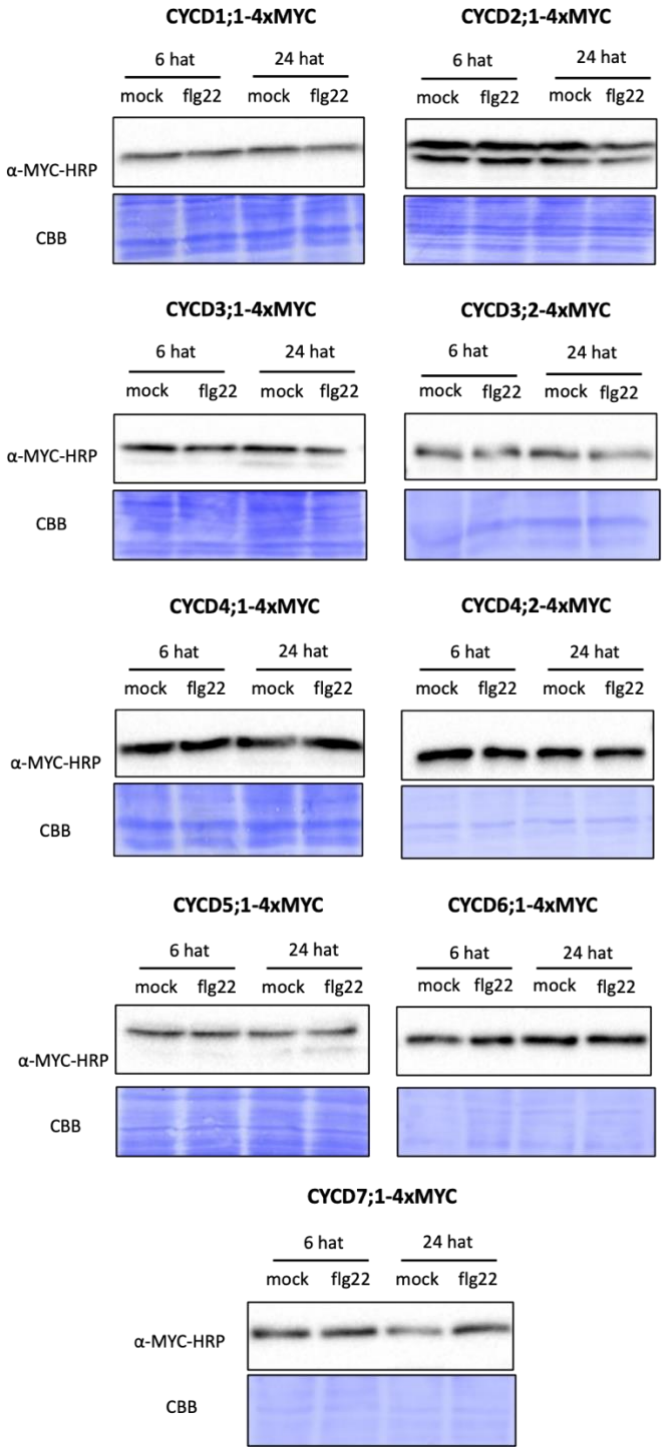

Figure 17: AtCYCD protein levels in *N. benthamiana* leaf discs after flg22 treatment: Experimental set-up: 4-week-old *N. benthamiana* leaves were co-infiltrated with *A. tumefaciens* carrying the plasmids for *AtCYCDs-4xMYC* expression and expression of the p19 silencing suppressor. 2 dai, leaf discs were collected and transferred into a 96-well plate containing water. On the next morning, leaf discs were treated with 1 µM flg22 solution or water. At 6 and 24 hours after treatment (hat), samples were harvested and proteins extracted. Western blot was performed with antibodies against HA- or MYC-tags. As loading control, membranes were stained with Coomassie brilliant blue (CBB).

3.4 Overcoming the growth immunity antagonism by supporting cell cycle regulators

3.4.1 Outline of the chapter

As explained in Section 1.5.3, it might be possible to uncouple negative growth-immunity cross-talk by supporting specific cell cycle regulators without disturbing defense signaling. According to Eichmann et al. and Finch (Eichmann et al., unpublished; Finch, 2019), CDKB1;1 and CYCD1;1 might be among the proteins that could uncouple the growth-immunity cross-talk. *A. thaliana* plants overexpressing *CDKB1;1* or *CYCD1;1* were less sensitive to flg22-induced RGI. However, above mentioned studies did not test all 4 B-type CDKs and 10 members of the D-type CYCs. It is thought that D-type CYCs may play major roles in linking environmental changes, both biotic and abiotic, to cell division (De Veylder, 2019). Therefore, it would be highly relevant to test all CYCDs. To this end, a major part of this project was to generate *CDKB* and *CYCD* overexpressing *A. thaliana* plants. These transgenic plants were supposed to be phenotyped for altered RGI after flg22 treatment. In addition, given the fact that CYCDs are activating subunits of CDKs, it could be hypothesized that they work together with CDKBs to control root growth under immunity. To investigate this, CDKB/CYCD double overexpresser plants were generated, as well.

3.4.2 Generating plant expression plasmids

To generate plant expression constructs with multiple gene expression cassettes, Golden Gate Cloning was employed. In this study, the CDS of *CDKB*s and *CYCD*s without stop codons (See Table 1 for the CDS) were cloned into L0 acceptor plasmids (Table 2). Some of the L0 plasmids were already cloned by J. Finch. In order to easily detect proteins and to perform co-immunoprecipitation assays (Co-IPs), it was aimed to tag CDKBs with 3xHA-FLAG and CYCDs with 4xMYC. As control, tGFP was tagged with 3xHA-FLAG or 4xMYC. For the protein detection in *N. benthamiana* (Section 3.3.3.3), all of the tagged *CDKB*s and *CYCD*s had already been cloned into a L1 plasmid (*CDKB*s into L1P1 and CYCDs into L1P3) with 0.4 kb *CaMV35S* promoter and *nos* terminator. For double overexpression in *A. thaliana*, an alternative promoter for the expression of the *CYCD*s was used to avoid potential silencing of gene expression due to the use of multiple *CaMV35S* promoters. Therefore, level 1 plasmids with *CYCDs-4xMYC* were generated under control of the *AtACT2* promoter (Figure 18).

Level 2 plasmids, which contain 3 gene expression cassettes (*CDKB* overexpression cassette/selection marker expression cassette/*CYCD* overexpression cassette), were produced for the stable transformation of *A. thaliana* plants via *A. tumefaciens*. In the second position, all L2 plasmids contain the expression cassette for the selection of the transformed seeds, FAST-R. The FAST-R selection expression cassette includes the promoter, terminator and CDS of At*OLE1* fused to TagRFP. At*OLE1* encodes *OLEOSIN 1*, a gene that is exclusively expressed in oil bodies in *A. thaliana* seeds (Shimada et al., 2010). The selection marker allows the direct identification of transformed seeds after harvesting

the transformed plants. In this way, it is possible to avoid using antibiotic or herbicide selection, which imposes considerable stress to the plants. In addition, FAST-R selection is efficient and not time-consuming. For the *CDKB* single overexpression plasmids, position 1 was filled with one of the *35S::CDKB-3xHA-FLAG* expression cassettes derived from pL1P1, and position 3 was filled with the *AtAct2::tGFP-4xMYC* expression cassette derived from pL1P3. For the *CYCD* single overexpression plasmids, position 1 was filled with the *pL1P1 35S::tGFP-3xHA-FLAG* expression cassette, and position 3 was filled with one of the *pL1P3 AtAct2::CYCD-4xMYC* expression cassettes. To test the hypothesis that CDKB1;1 and CYCD1;1 work together to alleviate the growth-immunity cross-talk, the double overexpression plasmid was generated that includes the pL1P1 *35S::CDKB1;1-3xHA-FLAG* expression cassette and the *pL1P3 AtAct2::CYCD1;1-4xMYC* expression cassette. As mentioned in Section 3.2.2, CDKB1;2 and CYCD2;1 might be the closest homologs of CDKB1;1 and CYCD1;1, respectively. Therefore, the double overexpression plasmids containing *pL1P1 35S::CDKB1;2-3xHA-FLAG* plus *pL1P3 AtAct2::CYCD1;1-4xMYC* and *pL1P1 35S::CDKB1;1-3xHA-FLAG* plus *pL1P3 AtAct2::CYCD2;1-4xMYC* were produced, as well (Figure 18). See Materials and Methods for full details of plasmids used and generated in this work.

A

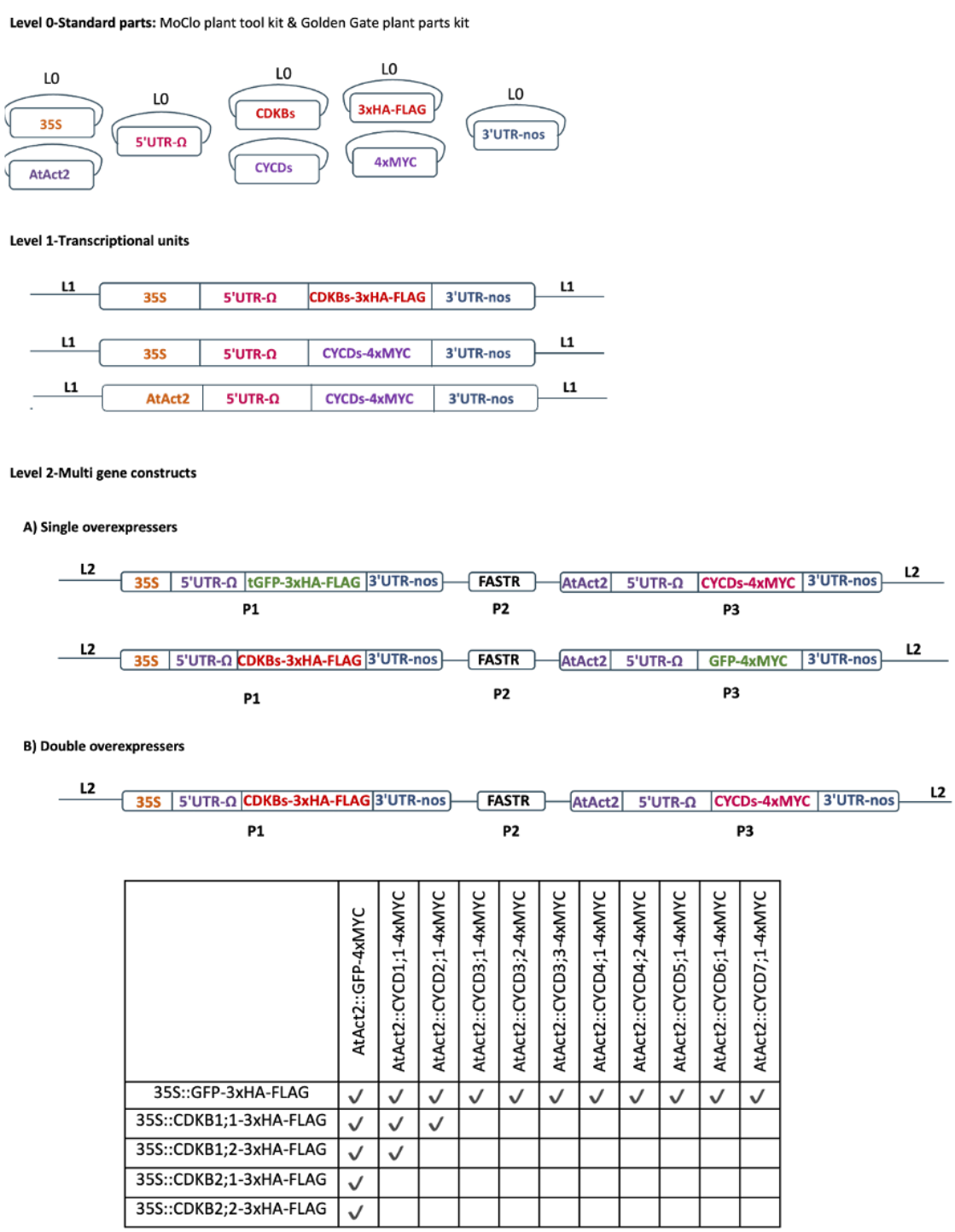

B

	AtAct2::GFP-4xMYC	AtAct2::CYCD1;1-4xMYC	AtAct2::CYCD2;1-4xMYC	AtAct2::CYCD3;1-4xMYC	AtAct2::CYCD3;2-4xMYC	AtAct2::CYCD3;3-4xMYC	AtAct2::CYCD4;1-4xMYC	AtAct2::CYCD4;2-4xMYC	AtAct2::CYCD5;1-4xMYC	AtAct2::CYCD6;1-4xMYC	AtAct2::CYCD7;1-4xMYC
35S::GFP-3xHA-FLAG	✓	✓	✓	✓	✓	✓	✓	✓	✓	✓	✓
35S::CDKB1;1-3xHA-FLAG	✓	✓	✓								
35S::CDKB1;2-3xHA-FLAG	✓	✓									
35S::CDKB2;1-3xHA-FLAG	✓										
35S::CDKB2;2-3xHA-FLAG	✓										

Figure 18: *CDKB* and *CYCD* expression constructs generated using Golden Gate Cloning: (A) L0-standard parts were taken from the MoClo plant tool kit or the Golden Gate plant parts kit (Engler et al. 2014). CDKB and CYCD parts were generated by J. Finch or cloned in the present study. For this, the coding sequences (CDS) of *CDKB*s and *CYCD*s without stop codon were cloned into a L0 acceptor plasmid. L0 parts were assembled into L1 acceptor plasmids. *CDKB*s were tagged with a 3xHA-FLAG tag and cloned into L1 position 1 under transcriptional control of the *35S* promoter and with a nopaline synthase (*nos*) terminator. *CYCD*s were tagged with a 4xMYC tag and cloned into L1 position 3 either under transcriptional control of the *35S* promoter (for transient overexpression in *N. benthamiana*) or of the *AtAct2* promoter (for stable overexpression in *A. thaliana*), and with a *nos* terminator. In L2 multigene constructs, the second position was filled with the FAST-R selection maker, position 1 was filled with either *35S::GFP-3xHA-FLAG* (as control) or with *35S::CDKBs-3xHA-FLAG*. *AtAct2::CYCD-4xMYCs* or *AtAct2::tGFP-4xMYCs* were cloned into the third position. In the case of double overexpressers, the expression cassettes of interest replaced the respective *tGFP* expression cassettes. **(B)** Combinations of *CDKB* (*tGFP*) and *CYCD* (*tGFP*) expression constructs in L2 vectors. L0: level 0, L1: level 1, L2: level 2, P1: position 1, P2: position 2, P3: position 3

3.4.3 Generating transgenic *A. thaliana* lines for stable overexpression of *CDKB*s or *CYCD*s

The successfully assembled L2 plasmids (See Section 3.4.2 and Table 2 for the plasmids generated and used in this study) were transformed by *Agrobacterium*-mediated transformation into Col-0 plants (T0 plants). Thanks to the FAST-R selection marker, it was possible to identify and pick the transformed T1 seeds based on their red fluorescence. The selected seeds were grown for propagation. From the leaves of the T1 plants, genomic DNA was extracted for an independent confirmation of the presence of the transgene by PCR. The progenies of T1 plants represent a segregating population, which means the seeds are a mixture of homozygous (for the presence of the transgene), heterozygous and wild-type-like seeds. Based on the strength of fluorescence of the FAST-R selection marker, it was possible to determine the segregation ratio. The ratio of strongly fluorescing T2 seeds to fluorescing seeds to non-fluorescing seeds of 1:2:1 indicates a single T-DNA insertion. The very brightly fluorescing red seeds supposedly indicating homozygosity for the T-DNA were picked and propagated. It has to be noted that in most of the lines, the above-mentioned ratio was not observed, which may indicate multiple T-DNA insertions. T3 seeds were harvested from T2 plants and used for further experiments. In order to confirm the overexpression of the genes of interest, T3 seeds were grown on ATS plates, roots were harvested and RNA was extracted. Gene expression was determined by qRT-PCR (Figures 19 to 34). As proteins of interest could be subject to post-translational modifications and targeted for protein degradation, the presence of the proteins was also confirmed via Western blot (Figures 19 to 34). Although detection of *CDKB* overexpression by qRT-PCR or Western blot in root samples was easy, the detection of *CYCD* expression was challenging. In order to reduce potential degradation through the ubiquitination pathway, *CYCD* overexpressing seedlings were treated with MG132 before harvesting. MG132 is a synthetic peptide aldehyde that binds to the 26S core particle of the proteasome. As a result, ubiquitinated proteins within the cells cannot be degraded (Lee & Goldberg, 1998). As roots contain less protein than leaves and less sample could be obtained from roots, the whole seedlings of CYCD transgenic lines were used to confirm protein accumulation via Western blot. Except for CYCD3;3-4xMYC, all CYCD proteins could be detected. Figures 19-34 (Figure S20-S39) summarize the results obtained for *CDKB* and *CYCD* single and double overexpression lines in terms of root growth and sensitivity to flg22-induced RGI. They also contain the results of qRT-PCR and Western blot used to confirm transgene expression.

It is also important to mention some phenotypes of the T2 transgenic plants. Overexpression of *CDKB2;1* seemed to have a strong negative impact on plant growth, as only a few seedlings were viable and the ones that survived had a stunted growth, shorter floral stalk, and produced very few seeds (data not shown). Although, the overexpression of *CDKB2;1* led to impaired development and growth, two independent *CDKB2;1* overexpresser lines could be generated. Interestingly, when the transgenic

lines were grown on ATS media plates, the plants exhibited better growth and longer primary root lengths compared to wild-type plants (Figure 21). Overexpression of *CYCD3;1* also resulted in severely impaired plant development and growth retardation, with shorter floral stalks, and fewer flowers (data not shown) (also observed by Dewitte et al., 2003). To gain a better understanding of the root phenotypes of the transgenic lines, primary root lengths of the transgenic *CDKB* and *CYCD* lines were compared to the root length of control plant lines carrying a *35S::tGFP-3xHA-FLAG* and *AtAct2::tGFP-4xMYC* expression cassette. For this purpose, plants used in the RGI assay were grown (Section 3.4.4), and the root lengths of 10-day-old seedlings were measured prior to flg22 treatment (Figure 19C-34C). The primary roots of the following lines were significantly shorter than that of control plant lines: *35S::CDKB1;1-3xHA-FLAG* line #1 and #2, *35S::CDKB1;2-3xHA-FLAG* line #1, *35S::CDKB2;2-3xHA-FLAG* line #1, *AtAct2::CYCD1;1-4xMYC* line #1, *AtAct2::CYCD3;1-4xMYC* line #1 and #2, *AtAct2::CYCD3;2-4xMYC* line #2, *AtAct2::CYCD4;1-4xMYC* line #2, *AtAct2::CYCD4;2-4xMYC* line #1 and the double overexpresser line *35S::CDKB1;1-3xHA-FLAG* plus *AtAct2:CYCD1;1-4xMYC* line #1. In contrast, the following plants lines had longer roots than the control lines: *35S::CDKB2;1-3xHA-FLAG* line #1 and #2, *AtAct2::CYCD1;1-4xMYC* line #2, *AtAct2::CYCD6;1-4xMYC* line #1 and *AtAct2::CYCD7;1-4xMYC* line #2.

3.4.4 Root growth inhibition assays of transgenic *A. thaliana* lines overexpressing *CDKB*s or *CYCD*s

In order to determine whether the *CDKB* and *CYCD* overexpression lines show an altered root growth inhibition upon flg22 treatment, RGI assays were conducted. At least two independent transgenic *A. thaliana* lines per construct, and as control plant line carrying a *35S::tGFP-3xHA-FLAG*, and *AtAct2::tGFP-4xMYC* (hereafter, *tGFP*) expression cassette were employed, and grown on solid ATS growth media plates. 10-day-old seedlings were treated with 100 nM flg22 or water (mock), and four days after treatment, primary root lengths were measured: Data are depicted as percentage of the mean total length of mock treated roots (Figures 19D-34D and Figure S20D-39D).

4 days after treatment, the flg22 treated roots of the control plants were generally around 15%-20% shorter than mock treated plants. In all two independent *35S::CDKB1;1-3xHA-FLAG* lines tested, there was around 30% reduction in root lengths after flg22 treatment as compared to the mock treated *35S::CDKB1;1-3xHA-FLAG* plants (Figure 19D and Figure S24). Thus, the overexpression of *CDKB1;1* did not abolish root growth inhibition in the transgenic lines in the experiments conducted here. *35S:CDKB1;2-3xHA-FLAG* line #1 plants were more sensitive to flg22 treatment when compared to the flg22 treated *tGFP* plants in one out of three experiments. The root lengths of *35S::CDKB1;2-3xHA-FLAG* line #1 plants were around 35% shorter than mock treated *35S::CDKB1;2-3xHA-FLAG* line #1 plants, which indicated a more severe RGI compared to the flg22 treated control plants. The level of root growth inhibition of the line *35S::CDKB1;2-3xHA-FLAG* #2 was more sensitive in one out of two replicates (Figure 20D and Figure S25). In *35S::CDKB2;1-3xHA-FLAG* lines, RGI after flg22 treatment

varied across replicates, and lines. While some replicates showed significantly less inhibition compared to flg22-treated *tGFP* plants, this phenotype was not consistently observed in Rep 2, and Rep 3. Overall, the results were inconclusive, with sensitivity to flg22 sometimes being reduced or unchanged across different lines, and replicates (Figure 21D and Figure S26). In Rep 1, and Rep 3, *35S::CDKB2;2-3xHA-FLAG* line #1 plants were slightly less sensitive to flg22 treatment compared to the *tGFP* plants, on the other hand, this effect was not observed in Rep 2 and in the *35S::CDKB2;2-3xHA-FLAG* line #2 plants (Figure 22D and Figure S27).

Most *CYCD* overexpresser lines showed *tGFP* (control) like root growth inhibition in response to flg22 treatment, except for *CYCD3;2* partially *CYCD1;1* overexpresser lines, which had a reduced sensitivity to flg22 treatment in terms of reduced root length. *AtAct2::CYCD3;2-4xMYC* line #1 plants were slightly less sensitive to flg22 treatment compared to *tGFP* plants, although this trend was not always statistically significantly between biological replicates (Figure 26D and Figure S31). While flg22-treated *AtAct2::CYCD1;1-4xMYC* line #1 plants were as sensitive as flg22-treated *tGFP* plants, *AtAct2::CYCD1;1-4xMYC* line #2 plants showed reduced sensitivity to flg22-induced RGI. In Rep 1, only a 8% root length reduction was observed in flg22-treated *AtAct2::CYCD1;1-4xMYC* line #2 plants, which was not significantly different from that of mock treated plants. In Rep 2, the reduction was slightly higher with 16%. This indicated that in *AtAct2::CYCD1;1-4xMYC* line #2 plants, flg22 induced root growth inhibition was abolished (Figure 23D and Figure S28).

These results indicate, although it was not always significantly different and consistent, overexpression of *CDKB2;1*, *CYCD1;1,* and *CYCD3;2* may completely or partially abolish flg22-triggered RGI.

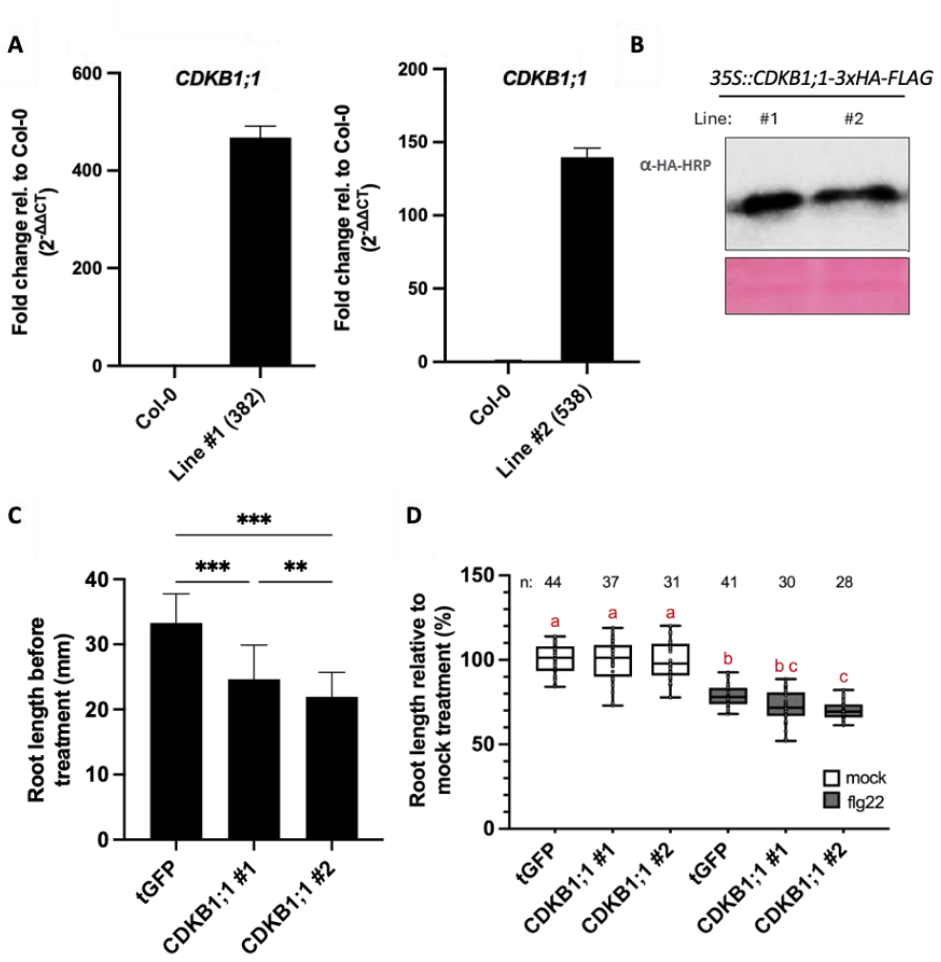

Figure 19: Root growth inhibition assay of *CDKB1;1*-overexpressing *A. thaliana* plants: Two independent *35S::CDKB1;1-3xHA-FLAG::FASTR::AtAct2::tGFP-4xMYC (CDKB1;1)* lines were selected. Col-0 wildtype or *35S::tGFP-3xHA-FLAG::FASTR::AtAct2::tGFP-4xMYC* (tGFP) plants served as controls **(A)** Confirmation of *CDKB1;1* overexpression. Plants were grown on ATS plates. Roots were harvested and total RNA was extracted followed by reverse transcription into cDNA and gene expression analysis using qRT-PCR. The graphs show the fold change ($2^{-\Delta\Delta Ct}$) of *CDKB1;1* expression in transgenic lines compared to Col-0 plants. Normalization was done against the housekeeping genes, *UBQ5* and *EF1α*. The numbers in parentheses on the x-axis are internal lines identifiers. **(B)** Confirmation of protein abundance in the *CDKB1;1* overexpresser lines. Plants were grown on ATS plates. After protein extraction, proteins were subjected to Western blot analysis with anti-HA antibodies. **(C)** The primary root lengths of transgenic plant grown on ATS for 10 days. Columns represent mean values of at least 50 plants ± SD. Asterisks indicate significant differences according to ANOVA followed by Tukey´s honest significance test. $p < 0.001$ (***), $p < 0.01$ (**), $p < 0.05$ (*). **(D)** 10-day-old seedlings were treated with 100 nM flg22 or mock (water). After 4 days, primary root lengths were measured. Box and whisker plots show mean primary root lengths in % relative to mock treated roots. n: samples size. The letters above bars indicate significant differences as determined by ANOVA followed by Tukey´s honest significance test, or Kruskal-Wallis test followed by Dunn's multiple comparison test in case of non-normal distribution. Compact letter display was used for grouping statistical comparisons, where different letters denote significant difference ($p<0.05$) (performed using GraphPad). C,D The experiment was repeated at least three times.

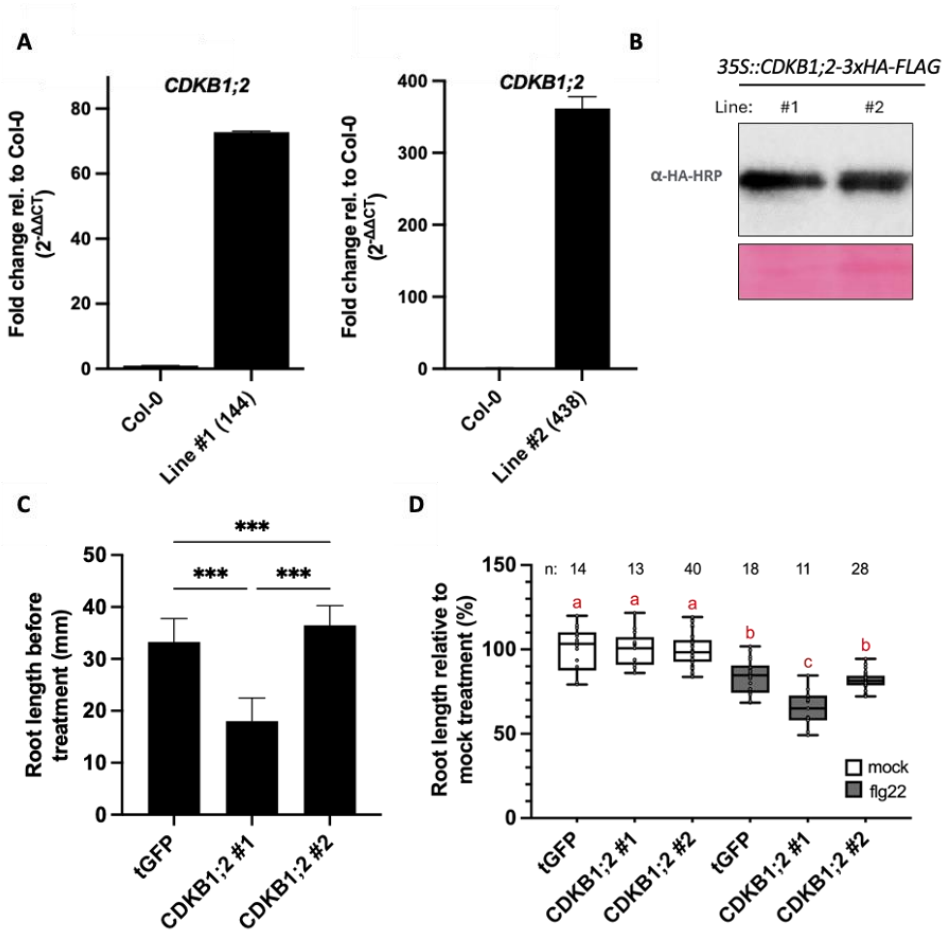

Figure 20: Root growth inhibition assay of *CDKB1;2*-overexpressing *A. thaliana* plants: Two independent *35S::CDKB1;2-3xHA-FLAG::FASTR::AtAct2::tGFP-4xMYC (CDKB1;2)* lines were selected. Col-0 wildtype or *35S::tGFP-3xHA-FLAG::FASTR::AtAct2::tGFP-4xMYC* (tGFP) plants served as controls **(A)** Confirmation of *CDKB1;2* overexpression. Plants were grown on ATS plates. Roots were harvested and total RNA was extracted followed by reverse transcription into cDNA and gene expression analysis using qRT-PCR. The graphs show the fold change ($2^{-\Delta\Delta Ct}$) of *CDKB1;2* expression in transgenic lines compared to Col-0 plants. Normalization was done against the housekeeping genes, *UBQ5* and *EF1α.* The numbers in parentheses on the x-axis are internal lines identifiers. **(B)** Confirmation of protein abundance in the *CDKB1;2* overexpresser lines. Plants were grown on ATS plates. After protein extraction, proteins were subjected to Western blot analysis with anti-HA antibodies. **(C)** The primary root lengths of transgenic plant grown on ATS for 10 days. Columns represent mean values of at least 50 plants ± SD. Asterisks indicate significant differences according to ANOVA followed by Tukey´s honest significance test. $p < 0.001$ (***), $p < 0.01$ (**), $p < 0.05$ (*). **(D)** 10-day-old seedlings were treated with 100 nM flg22 or mock (water). After 4 days, primary root lengths were measured. Box and whisker plots show mean primary root lengths in % relative to mock treated roots. n: samples size. The letters above bars indicate significant differences as determined by ANOVA followed by Tukey´s honest significance test, or Kruskal-Wallis test followed by Dunn's multiple comparison test in case of non-normal distribution. Compact letter display was used for grouping statistical comparisons, where different letters denote significant difference (p<0.05) (performed using GraphPad). C,D The experiment was repeated at least two times.

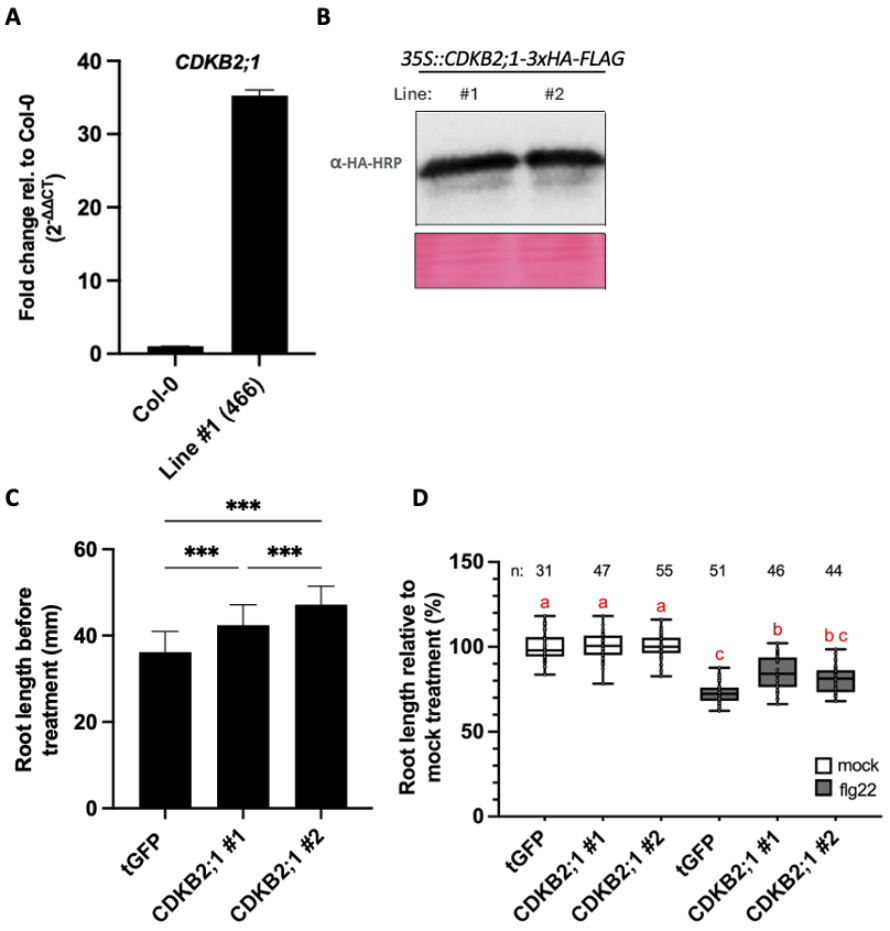

Figure 21: Root growth inhibition assay of *CDKB2;1*-overexpressing *A. thaliana* plants: Two independent *35S::CDKB2;1-3xHA-FLAG::FASTR::AtAct2::tGFP-4xMYC (CDKB2;1)* lines were selected. Col-0 wildtype or *35S::tGFP-3xHA-FLAG::FASTR::AtAct2::tGFP-4xMYC* (tGFP) plants served as controls **(A)** Confirmation of *CDKB2;1* overexpression. Plants were grown on ATS plates. Roots were harvested and total RNA was extracted followed by reverse transcription into cDNA and gene expression analysis using qRT-PCR. The graphs show the fold change ($2^{-\Delta\Delta Ct}$) of *CDKB2;1* expression in transgenic lines compared to Col-0 plants. Normalization was done against the housekeeping genes, *UBQ5* and *EF1α*. The numbers in parentheses on the x-axis are internal lines identifiers. **(B)** Confirmation of protein abundance in the *CDKB2;1* overexpresser lines. Plants were grown on ATS plates. After protein extraction, proteins were subjected to Western blot analysis with anti-HA antibodies. **(C)** The primary root lengths of transgenic plant grown on ATS for 10 days. Columns represent mean values of at least 50 plants ± SD. Asterisks indicate significant differences according to ANOVA followed by Tukey´s honest significance test. $p < 0.001$ (***), $p < 0.01$ (**), $p < 0.05$ (*). **(D)** 10-day-old seedlings were treated with 100 nM flg22 or mock (water). After 4 days, primary root lengths were measured. Box and whisker plots show mean primary root lengths in % relative to mock treated roots. n: samples size. The letters above bars indicate significant differences as determined by ANOVA followed by Tukey´s honest significance test, or Kruskal-Wallis test followed by Dunn's multiple comparison test in case of non-normal distribution. Compact letter display was used for grouping statistical comparisons, where different letters denote significant difference (p<0.05) (performed using GraphPad). C,D The experiment was repeated at least three times.

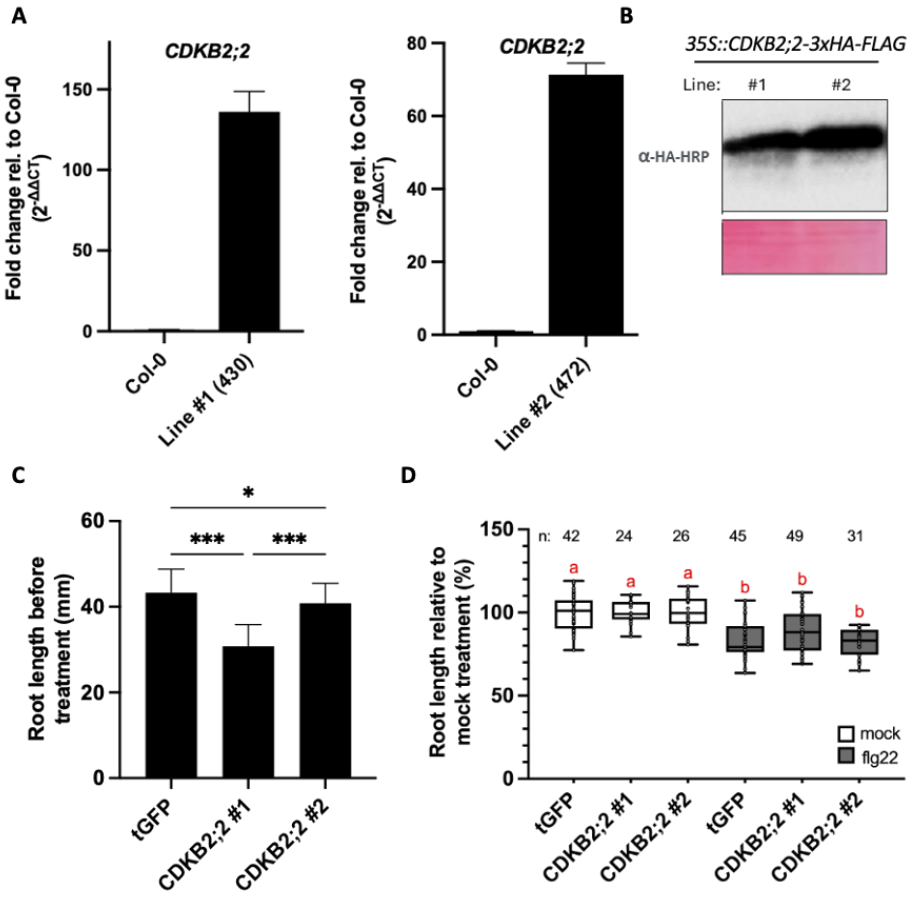

Figure 22: Root growth inhibition assay of *CDKB2;2*-overexpressing *A. thaliana* plants: Two independent *35S::CDKB2;2-3xHA-FLAG::FASTR::AtAct2::tGFP-4xMYC (CDKB2;2)* lines were selected. Col-0 wildtype or *35S::tGFP-3xHA-FLAG::FASTR::AtAct2::tGFP-4xMYC* (tGFP) plants served as controls **(A)** Confirmation of *CDKB2;2* overexpression. Plants were grown on ATS plates. Roots were harvested and total RNA was extracted followed by reverse transcription into cDNA and gene expression analysis using qRT-PCR. The graphs show the fold change ($2^{-\Delta\Delta Ct}$) of *CDKB2;2* expression in transgenic lines compared to Col-0 plants. Normalization was done against the housekeeping genes, *UBQ5* and *EF1α*. The numbers in parentheses on the x-axis are internal lines identifiers. **(B)** Confirmation of protein abundance in the *CDKB2;2* overexpresser lines. Plants were grown on ATS plates. After protein extraction, proteins were subjected to Western blot analysis with anti-HA antibodies. (**C)** The primary root lengths of transgenic plant grown on ATS for 10 days. Columns represent mean values of at least 50 plants ± SD. Asterisks indicate significant differences according to ANOVA followed by Tukey´s honest significance test. $p < 0.001$ (***), $p < 0.01$ (**), $p < 0.05$ (*). **(D)** 10-day-old seedlings were treated with 100 nM flg22 or mock (water). After 4 days, primary root lengths were measured. Box and whisker plots show mean primary root lengths in % relative to mock treated roots. n: samples size. The letters above bars indicate significant differences as determined by ANOVA followed by Tukey´s honest significance test, or Kruskal-Wallis test followed by Dunn's multiple comparison test in case of non-normal distribution. Compact letter display was used for grouping statistical comparisons, where different letters denote significant difference (p<0.05) (performed using GraphPad). C,D The experiment was repeated at least three times.

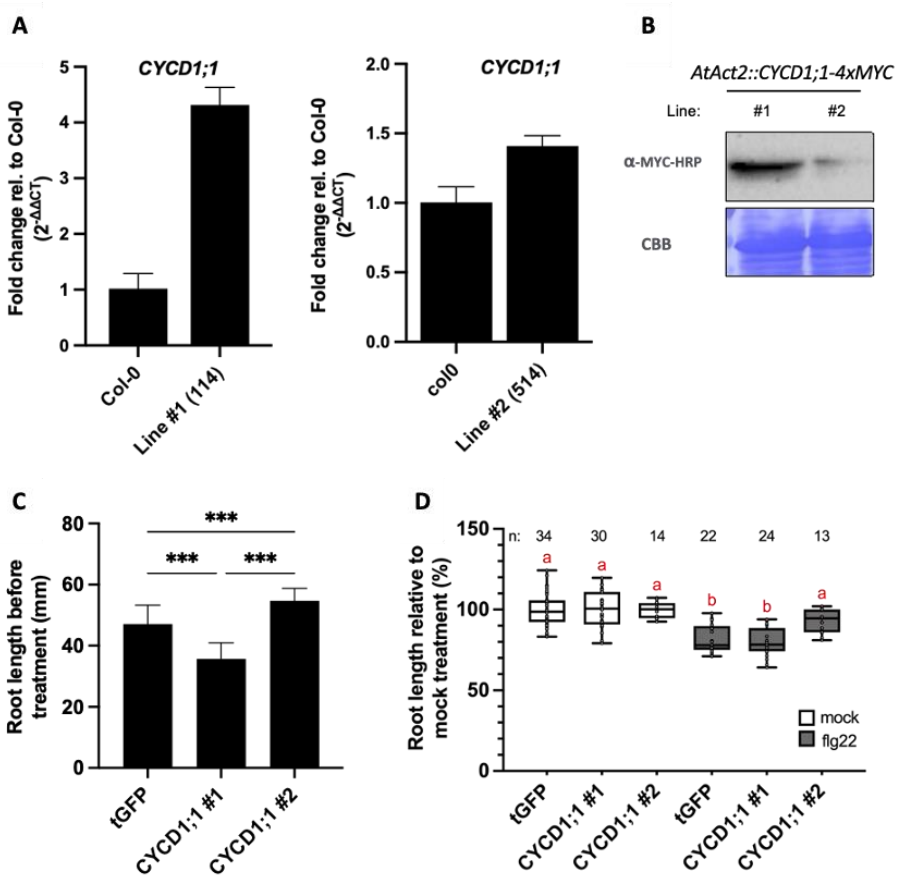

Figure 23: Root growth inhibition assay of *CYCD1;1*-overexpressing *A. thaliana* plants: Two independent *35S::tGFP-3xHA-FLAG::FASTR::AtAct2::CYCD1;1-4xMYC (CYCD1;1)* lines were selected. Col-0 wildtype or *35S::tGFP-3xHA-FLAG::FASTR::AtAct2::tGFP-4xMYC* (tGFP) plants served as controls **(A)** Confirmation of *CYCD1;1* overexpression. Plants were grown on ATS plates. Roots were harvested and total RNA was extracted followed by reverse transcription into cDNA and gene expression analysis using qRT-PCR. The graphs show the fold change ($2^{-\Delta\Delta Ct}$) of *CYCD1;1* expression in transgenic lines compared to Col-0 plants. Normalization was done against the housekeeping genes, *UBQ5* and *EF1α*. The numbers in parentheses on the x-axis are internal lines identifiers. **(B)** Confirmation of protein abundance in the *CYCD1;1* overexpresser lines. Plants were grown on ATS plates. After protein extraction, proteins were subjected to Western blot analysis with anti-MYC antibodies. **(C)** The primary root lengths of transgenic plant grown on ATS for 10 days. Columns represent mean values of at least 50 plants ± SD. Asterisks indicate significant differences according to ANOVA followed by Tukey´s honest significance test. $p < 0.001$ (***), $p < 0.01$ (**), $p < 0.05$ (*). **(D)** 10-day-old seedlings were treated with 100 nM flg22 or mock (water). After 4 days, primary root lengths were measured. Box and whisker plots show mean primary root lengths in % relative to mock treated roots. n: samples size. The letters above bars indicate significant differences as determined by ANOVA followed by Tukey´s honest significance test, or Kruskal-Wallis test followed by Dunn's multiple comparison test in case of non-normal distribution. Compact letter display was used for grouping statistical comparisons, where different letters denote significant difference ($p<0.05$) (performed using GraphPad). C,D The experiment was repeated at least three times.

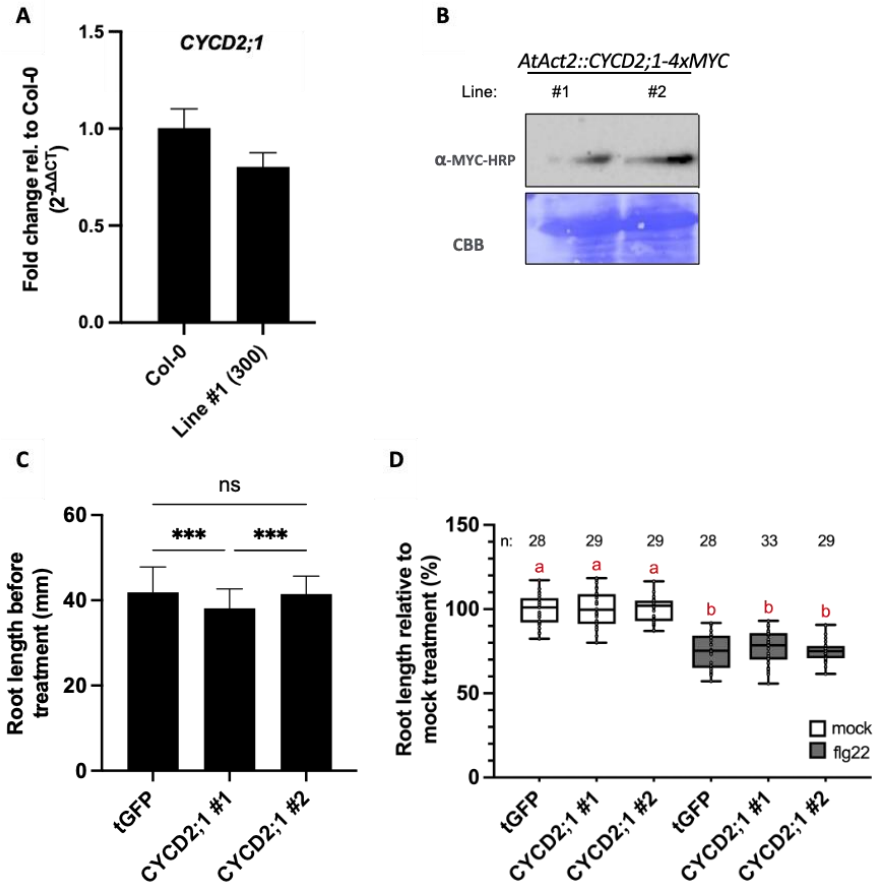

Figure 24: Root growth inhibition assay of *CYCD2;1*-overexpressing *A. thaliana* plants: Two independent *35S::tGFP-3xHA-FLAG::FASTR::AtAct2::CYCD2;1-4xMYC (CYCD2;1)* lines were selected. Col-0 wildtype or *35S::tGFP-3xHA-FLAG::FASTR::AtAct2::tGFP-4xMYC* (tGFP) plants served as controls **(A)** Confirmation of *CYCD2;1* overexpression. Plants were grown on ATS plates. Roots were harvested and total RNA was extracted followed by reverse transcription into cDNA and gene expression analysis using qRT-PCR. The graphs show the fold change ($2^{-\Delta\Delta Ct}$) of *CYCD2;1* expression in transgenic lines compared to Col-0 plants. Normalization was done against the housekeeping genes, *UBQ5* and *EF1α*. The numbers in parentheses on the x-axis are internal lines identifiers. **(B)** Confirmation of protein abundance in the *CYCD2;1* overexpresser lines. Plants were grown on ATS plates. After protein extraction, proteins were subjected to Western blot analysis with anti-MYC antibodies. **(C)** The primary root lengths of transgenic plant grown on ATS for 10 days. Columns represent mean values of at least 50 plants ± SD. Asterisks indicate significant differences according to ANOVA followed by Tukey´s honest significance test. $p < 0.001$ (***), $p < 0.01$ (**), $p < 0.05$ (*). **(D)** 10-day-old seedlings were treated with 100 nM flg22 or mock (water). After 4 days, primary root lengths were measured. Box and whisker plots show mean primary root lengths in % relative to mock treated roots. n: samples size. The letters above bars indicate significant differences as determined by ANOVA followed by Tukey´s honest significance test, or Kruskal-Wallis test followed by Dunn's multiple comparison test in case of non-normal distribution. Compact letter display was used for grouping statistical comparisons, where different letters denote significant difference ($p<0.05$) (performed using GraphPad). C,D The experiment was repeated at least two times.

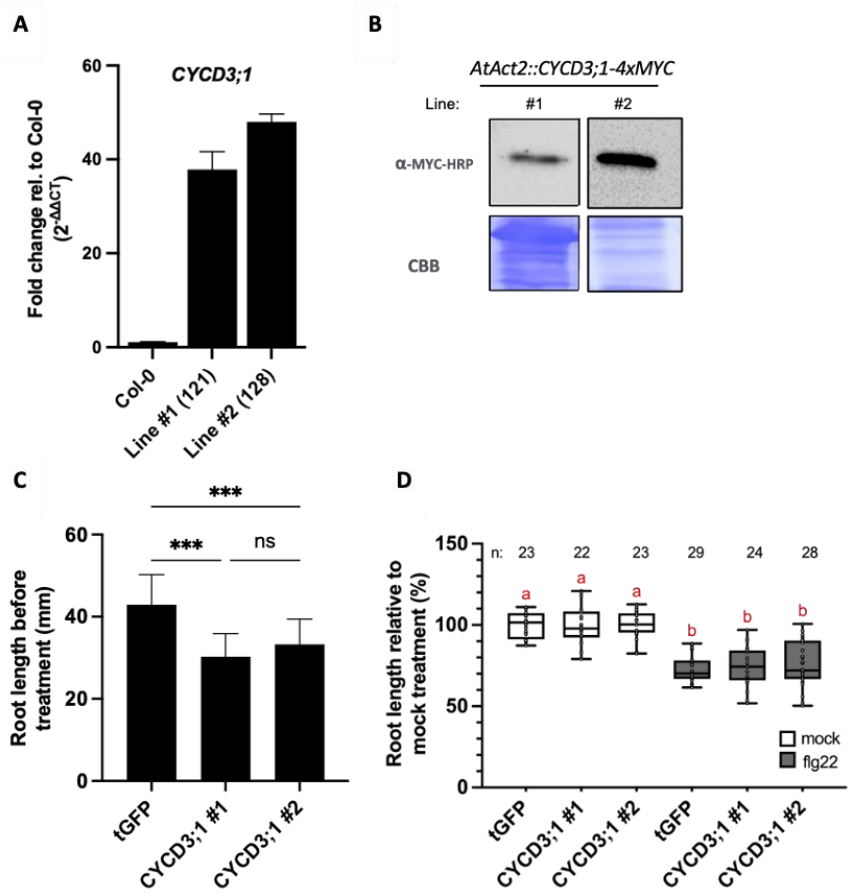

Figure 25: Root growth inhibition assay of *CYCD3;1*-overexpressing *A. thaliana* plants: Two independent *35S::tGFP-3xHA-FLAG::FASTR::AtAct2::CYCD3;1-4xMYC (CYCD3;1)* lines were selected. Col-0 wildtype or *35S::tGFP-3xHA-FLAG::FASTR::AtAct2::tGFP-4xMYC* (tGFP) plants served as controls **(A)** Confirmation of *CYCD3;1* overexpression. Plants were grown on ATS plates. Roots were harvested and total RNA was extracted followed by reverse transcription into cDNA and gene expression analysis using qRT-PCR. The graphs show the fold change ($2^{-\Delta\Delta Ct}$) of *CYCD3;1* expression in transgenic lines compared to Col-0 plants. Normalization was done against the housekeeping genes, *UBQ5* and *EF1α*. The numbers in parentheses on the x-axis are internal lines identifiers. **(B)** Confirmation of protein abundance in the *CYCD3;1* overexpresser lines. Plants were grown on ATS plates. After protein extraction, proteins were subjected to Western blot analysis with anti-MYC antibodies. **(C)** The primary root lengths of transgenic plant grown on ATS for 10 days. Columns represent mean values of at least 50 plants ± SD. Asterisks indicate significant differences according to ANOVA followed by Tukey´s honest significance test. $p < 0.001$ (***), $p < 0.01$ (**), $p < 0.05$ (*). **(D)** 10-day-old seedlings were treated with 100 nM flg22 or mock (water). After 4 days, primary root lengths were measured. Box and whisker plots show mean primary root lengths in % relative to mock treated roots. n: samples size. The letters above bars indicate significant differences as determined by ANOVA followed by Tukey´s honest significance test, or Kruskal-Wallis test followed by Dunn's multiple comparison test in case of non-normal distribution. Compact letter display was used for grouping statistical comparisons, where different letters denote significant difference ($p<0.05$) (performed using GraphPad). C,D The experiment was repeated at least three times.

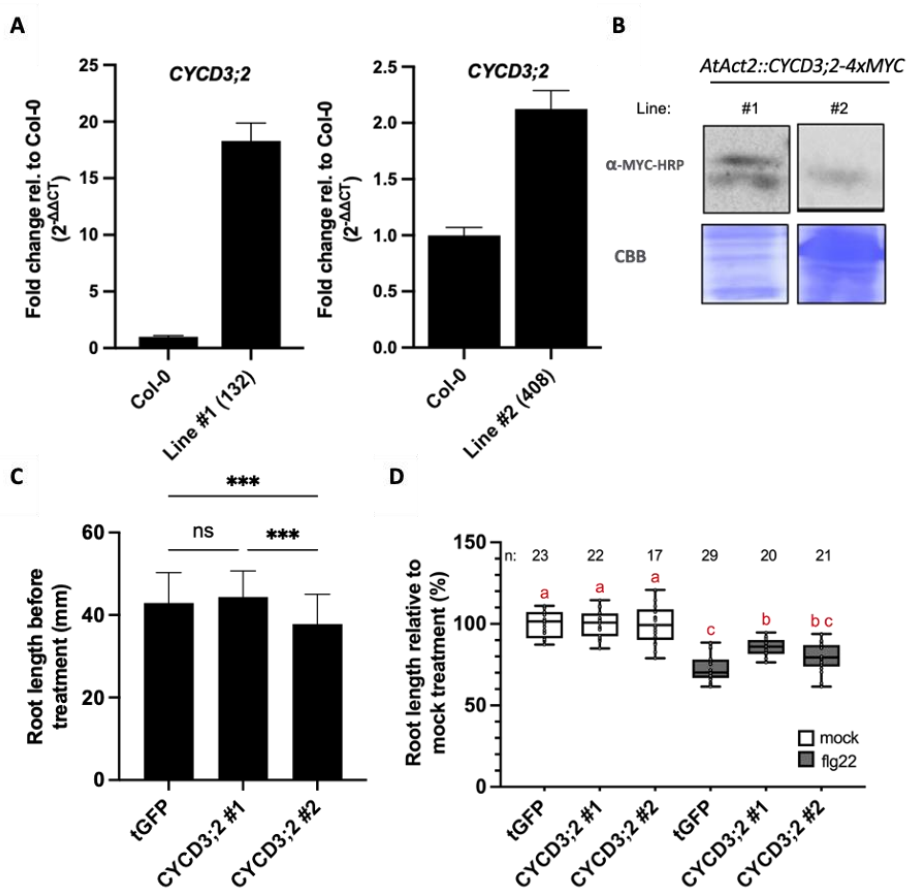

Figure 26: Root growth inhibition assay of *CYCD3;2*-overexpressing *A. thaliana* plants: Two independent *35S::tGFP-3xHA-FLAG::FASTR::AtAct2::CYCD3;2-4xMYC (CYCD3;2)* lines were selected. Col-0 wildtype or *35S::tGFP-3xHA-FLAG::FASTR::AtAct2::tGFP-4xMYC* (tGFP) plants served as controls **(A)** Confirmation of *CYCD3;2* overexpression. Plants were grown on ATS plates. Roots were harvested and total RNA was extracted followed by reverse transcription into cDNA and gene expression analysis using qRT-PCR. The graphs show the fold change ($2^{-\Delta\Delta Ct}$) of *CYCD3;2* expression in transgenic lines compared to Col-0 plants. Normalization was done against the housekeeping genes, *UBQ5* and *EF1α*. The numbers in parentheses on the x-axis are internal lines identifiers. **(B)** Confirmation of protein abundance in the *CYCD3;2* overexpresser lines. Plants were grown on ATS plates. After protein extraction, proteins were subjected to Western blot analysis with anti-MYC antibodies. **(C)** The primary root lengths of transgenic plant grown on ATS for 10 days. Columns represent mean values of at least 50 plants ± SD. Asterisks indicate significant differences according to ANOVA followed by Tukey´s honest significance test. $p < 0.001$ (***), $p < 0.01$ (**), $p < 0.05$ (*). **(D)** 10-day-old seedlings were treated with 100 nM flg22 or mock (water). After 4 days, primary root lengths were measured. Box and whisker plots show mean primary root lengths in % relative to mock treated roots. n: samples size. The letters above bars indicate significant differences as determined by ANOVA followed by Tukey´s honest significance test, or Kruskal-Wallis test followed by Dunn's multiple comparison test in case of non-normal distribution. Compact letter display was used for grouping statistical comparisons, where different letters denote significant difference (p<0.05) (performed using GraphPad). C,D The experiment was repeated at least four times.

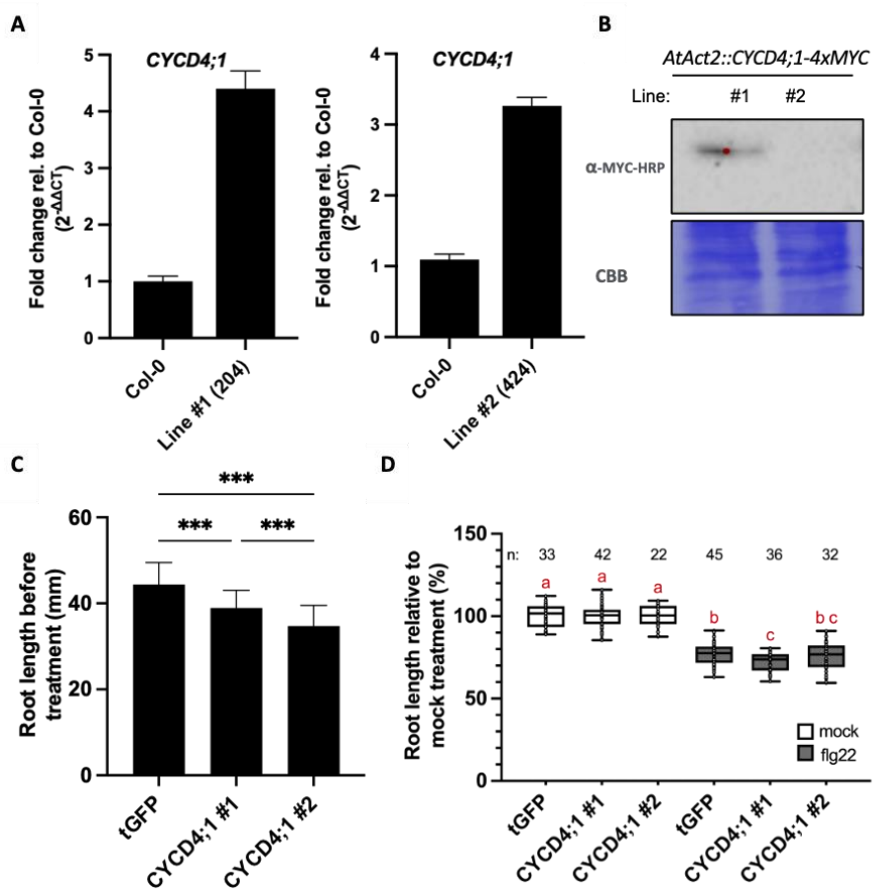

Figure 27: Root growth inhibition assay of *CYCD4;1*-overexpressing *A. thaliana* plants: Two independent *35S::tGFP-3xHA-FLAG::FASTR::AtAct2::CYCD4;1-4xMYC (CYCD4;1)* lines were selected. Col-0 wildtype or *35S::tGFP-3xHA-FLAG::FASTR::AtAct2::tGFP-4xMYC* (tGFP) plants served as controls **(A)** Confirmation of *CYCD4;1* overexpression. Plants were grown on ATS plates. Roots were harvested and total RNA was extracted followed by reverse transcription into cDNA and gene expression analysis using qRT-PCR. The graphs show the fold change ($2^{-\Delta\Delta Ct}$) of *CYCD4;1* expression in transgenic lines compared to Col-0 plants. Normalization was done against the housekeeping genes, *UBQ5* and *EF1α*. The numbers in parentheses on the x-axis are internal lines identifiers. **(B)** Confirmation of protein abundance in the *CYCD4;1* overexpresser lines. Plants were grown on ATS plates. After protein extraction, proteins were subjected to Western blot analysis with anti-MYC antibodies. **(C)** The primary root lengths of transgenic plant grown on ATS for 10 days. Columns represent mean values of at least 50 plants ± SD. Asterisks indicate significant differences according to ANOVA followed by Tukey´s honest significance test. $p < 0.001$ (***), $p < 0.01$ (**), $p < 0.05$ (*). **(D)** 10-day-old seedlings were treated with 100 nM flg22 or mock (water). After 4 days, primary root lengths were measured. Box and whisker plots show mean primary root lengths in % relative to mock treated roots. n: samples size. The letters above bars indicate significant differences as determined by ANOVA followed by Tukey´s honest significance test, or Kruskal-Wallis test followed by Dunn's multiple comparison test in case of non-normal distribution. Compact letter display was used for grouping statistical comparisons, where different letters denote significant difference (p<0.05) (performed using GraphPad). C,D The experiment was repeated at least two times.

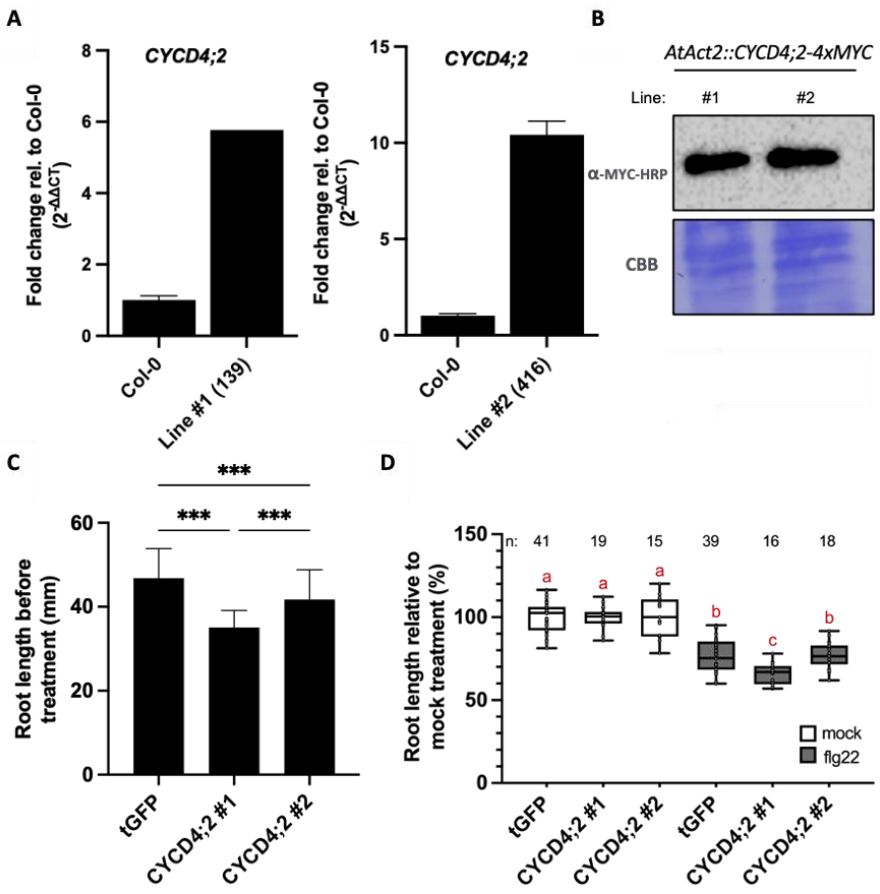

Figure 28: Root growth inhibition assay of *CYCD4;2*-overexpressing *A. thaliana* plants: Two independent *35S::tGFP-3xHA-FLAG::FASTR::AtAct2::CYCD4;2-4xMYC (CYCD4;2)* lines were selected. Col-0 wildtype or *35S::tGFP-3xHA-FLAG::FASTR::AtAct2::tGFP-4xMYC* (tGFP) plants served as controls **(A)** Confirmation of *CYCD4;2* overexpression. Plants were grown on ATS plates. Roots were harvested and total RNA was extracted followed by reverse transcription into cDNA and gene expression analysis using qRT-PCR. The graphs show the fold change ($2^{-\Delta\Delta Ct}$) of *CYCD4;2* expression in transgenic lines compared to Col-0 plants. Normalization was done against the housekeeping genes, *UBQ5* and *EF1α*. The numbers in parentheses on the x-axis are internal lines identifiers. **(B)** Confirmation of protein abundance in the *CYCD4;2* overexpresser lines. Plants were grown on ATS plates. After protein extraction, proteins were subjected to Western blot analysis with anti-MYC antibodies. **(C)** The primary root lengths of transgenic plant grown on ATS for 10 days. Columns represent mean values of at least 50 plants ± SD. Asterisks indicate significant differences according to ANOVA followed by Tukey´s honest significance test. $p < 0.001$ (***), $p < 0.01$ (**), $p < 0.05$ (*). **(D)** 10-day-old seedlings were treated with 100 nM flg22 or mock (water). After 4 days, primary root lengths were measured. Box and whisker plots show mean primary root lengths in % relative to mock treated roots. n: samples size. The letters above bars indicate significant differences as determined by ANOVA followed by Tukey´s honest significance test, or Kruskal-Wallis test followed by Dunn's multiple comparison test in case of non-normal distribution. Compact letter display was used for grouping statistical comparisons, where different letters denote significant difference ($p<0.05$) (performed using GraphPad). C,D The experiment was repeated at least three times.

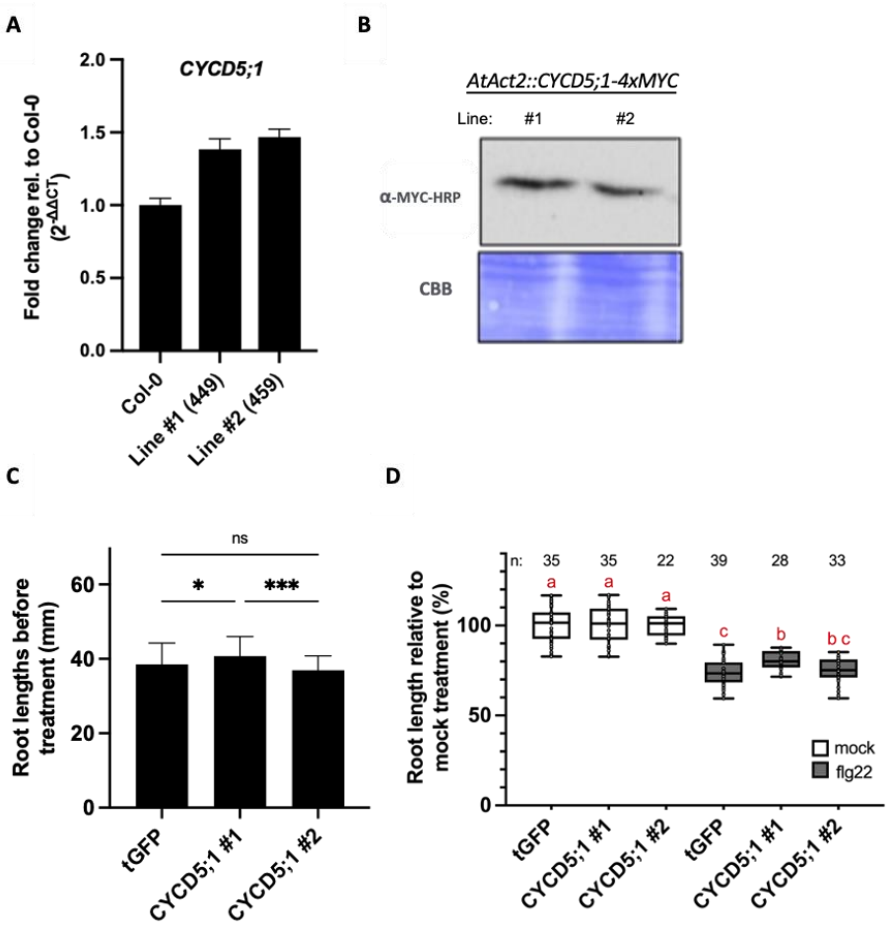

Figure 29: Root growth inhibition assay of *CYCD5;1*-overexpressing *A. thaliana* plants: Two independent *35S::tGFP-3xHA-FLAG::FASTR::AtAct2::CYCD5;1-4xMYC (CYCD5;1)* lines were selected. Col-0 wildtype or *35S::tGFP-3xHA-FLAG::FASTR::AtAct2::tGFP-4xMYC* (tGFP) plants served as controls **(A)** Confirmation of *CYCD5;1* overexpression. Plants were grown on ATS plates. Roots were harvested and total RNA was extracted followed by reverse transcription into cDNA and gene expression analysis using qRT-PCR. The graphs show the fold change ($2^{-\Delta\Delta Ct}$) of *CYCD5;1* expression in transgenic lines compared to Col-0 plants. Normalization was done against the housekeeping genes, *UBQ5* and *EF1α*. The numbers in parentheses on the x-axis are internal lines identifiers. **(B)** Confirmation of protein abundance in the *CYCD5;1* overexpresser lines. Plants were grown on ATS plates. After protein extraction, proteins were subjected to Western blot analysis with anti-MYC antibodies. **(C)** The primary root lengths of transgenic plant grown on ATS for 10 days. Columns represent mean values of at least 50 plants ± SD. Asterisks indicate significant differences according to ANOVA followed by Tukey´s honest significance test. $p < 0.001$ (***), $p < 0.01$ (**), $p < 0.05$ (*). **(D)** 10-day-old seedlings were treated with 100 nM flg22 or mock (water). After 4 days, primary root lengths were measured. Box and whisker plots show mean primary root lengths in % relative to mock treated roots. n: samples size. The letters above bars indicate significant differences as determined by ANOVA followed by Tukey´s honest significance test, or Kruskal-Wallis test followed by Dunn's multiple comparison test in case of non-normal distribution. Compact letter display was used for grouping statistical comparisons, where different letters denote significant difference ($p<0.05$) (performed using GraphPad). C,D The experiment was repeated at least two times.

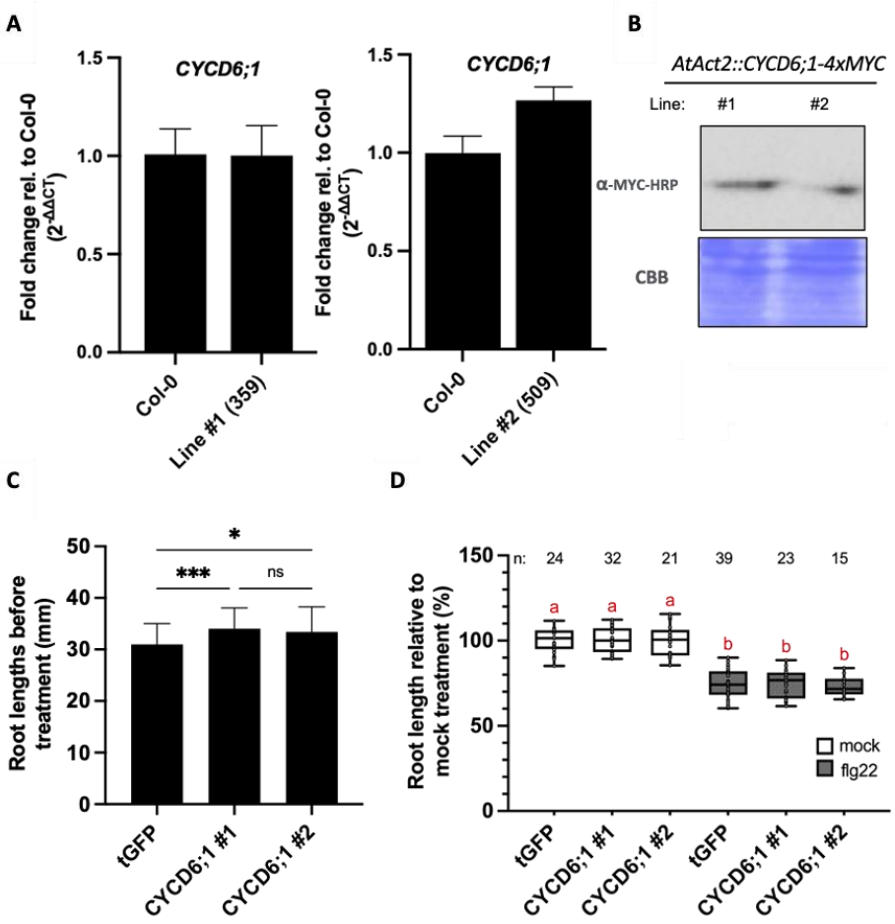

Figure 30: Root growth inhibition assay of *CYCD6;1*-overexpressing *A. thaliana* plants: Two independent *35S::tGFP-3xHA-FLAG::FASTR::AtAct2::CYCD6;1-4xMYC (CYCD6;1)* lines were selected. Col-0 wildtype or *35S::tGFP-3xHA-FLAG::FASTR::AtAct2::tGFP-4xMYC* (tGFP) plants served as controls **(A)** Confirmation of *CYCD6;1* overexpression. Plants were grown on ATS plates. Roots were harvested and total RNA was extracted followed by reverse transcription into cDNA and gene expression analysis using qRT-PCR. The graphs show the fold change ($2^{-\Delta\Delta Ct}$) of *CYCD6;1* expression in transgenic lines compared to Col-0 plants. Normalization was done against the housekeeping genes, *UBQ5* and *EF1α*. The numbers in parentheses on the x-axis are internal lines identifiers. **(B)** Confirmation of protein abundance in the *CYCD6;1* overexpresser lines. Plants were grown on ATS plates. After protein extraction, proteins were subjected to Western blot analysis with anti-MYC antibodies. **(C)** The primary root lengths of transgenic plant grown on ATS for 10 days. Columns represent mean values of at least 50 plants ± SD. Asterisks indicate significant differences according to ANOVA followed by Tukey´s honest significance test. $p < 0.001$ (***), $p < 0.01$ (**), $p < 0.05$ (*). **(D)** 10-day-old seedlings were treated with 100 nM flg22 or mock (water). After 4 days, primary root lengths were measured. Box and whisker plots show mean primary root lengths in % relative to mock treated roots. n: samples size. The letters above bars indicate significant differences as determined by ANOVA followed by Tukey´s honest significance test, or Kruskal-Wallis test followed by Dunn's multiple comparison test in case of non-normal distribution. Compact letter display was used for grouping statistical comparisons, where different letters denote significant difference ($p<0.05$) (performed using GraphPad). C,D The experiment was repeated at least two times.

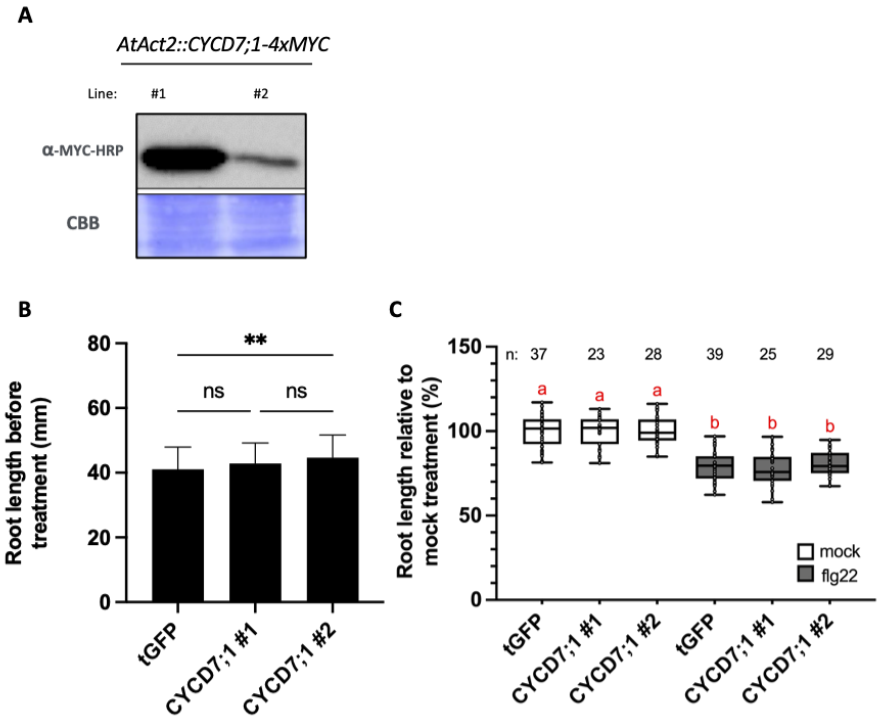

Figure 31: Root growth inhibition assay of *CYCD7;1*-overexpressing *A. thaliana* plants: Two independent *35S::tGFP-3xHA-FLAG::FASTR::AtAct2::CYCD7;1-4xMYC (CYCD7;1)* lines were selected. Col-0 wildtype or *35S::tGFP-3xHA-FLAG::FASTR::AtAct2::tGFP-4xMYC* (tGFP) plants served as controls **(A)** Confirmation of protein abundance in the *CYCD7;1* overexpresser lines. Plants were grown on ATS plates. After protein extraction, proteins were subjected to Western blot analysis with anti-MYC antibodies. **(B)** The primary root lengths of transgenic plant grown on ATS for 10 days. Columns represent mean values of at least 50 plants ± SD. Asterisks indicate significant differences according to ANOVA followed by Tukey´s honest significance test. $p < 0.001$ (***), $p < 0.01$ (**), $p < 0.05$ (*). **(C)** 10-day-old seedlings were treated with 100 nM flg22 or mock (water). After 4 days, primary root lengths were measured. Box and whisker plots show mean primary root lengths in % relative to mock treated roots. n: samples size. The letters above bars indicate significant differences as determined by ANOVA followed by Tukey´s honest significance test, or Kruskal-Wallis test followed by Dunn's multiple comparison test in case of non-normal distribution. Compact letter display was used for grouping statistical comparisons, where different letters denote significant difference ($p<0.05$) (performed using GraphPad). C,D The experiment was repeated at least two times.

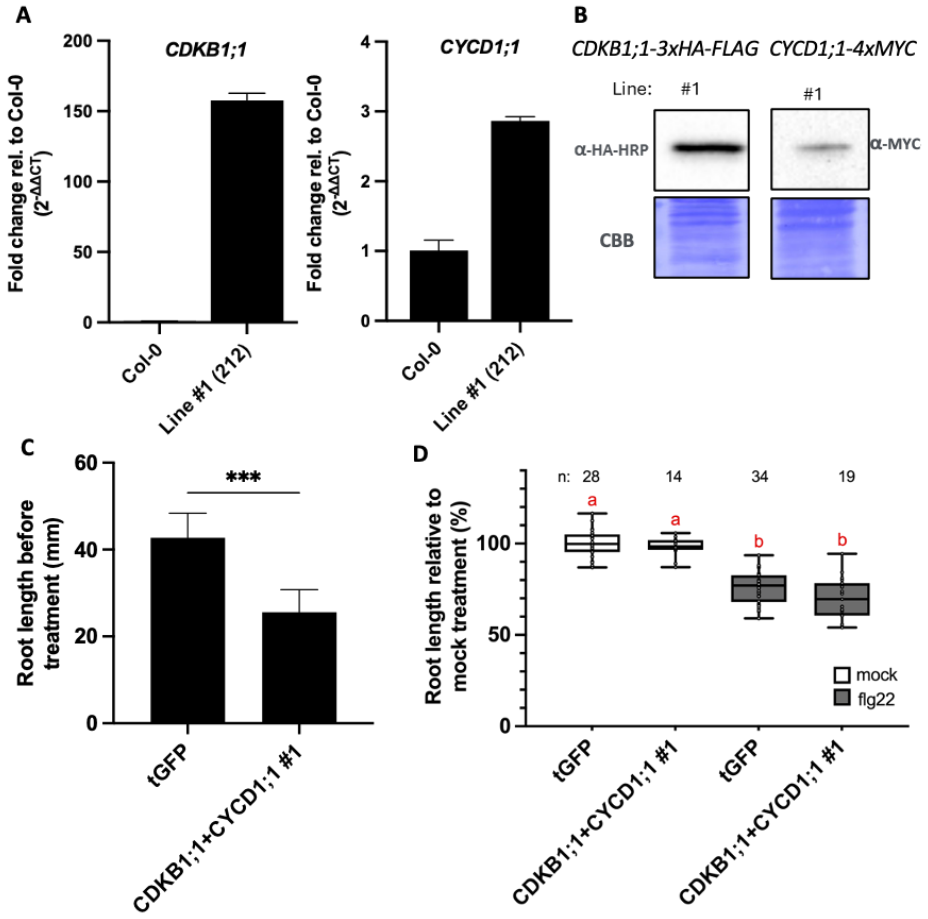

Figure 32: Root growth inhibition assay of *CDKB1;1* and *CYCD1;1*-overexpressing *A. thaliana* plants: Two independent *35S::CDKB1;1-3xHA-FLAG::FASTR::AtAct2::CYCD1;1-4xMYC (CDKB1;1+CYCD1;1)* lines were selected. Col-0 wildtype or *35S::tGFP-3xHA-FLAG::FASTR::AtAct2::tGFP-4xMYC* (tGFP) plants served as controls **(A)** Confirmation of the overexpression. Plants were grown on ATS plates. Roots were harvested and total RNA was extracted followed by reverse transcription into cDNA and gene expression analysis using qRT-PCR. The graphs show the fold change ($2^{-\Delta\Delta Ct}$) of the expression in transgenic lines compared to Col-0 plants. Normalization was done against the housekeeping genes, *UBQ5* and *EF1α*. The numbers in parentheses on the x-axis are internal lines identifiers. **(B)** Confirmation of protein abundance in the overexpresser lines. Plants were grown on ATS plates. After protein extraction, proteins were subjected to Western blot analysis with anti-HA and anti-MYC antibodies. **(C)** The primary root lengths of transgenic plant grown on ATS for 10 days. Columns represent mean values of at least 50 plants ± SD. Asterisks indicate significant differences according to ANOVA followed by Tukey´s honest significance test. $p < 0.001$ (***), $p < 0.01$ (**), $p < 0.05$ (*). **(D)** 10-day-old seedlings were treated with 100 nM flg22 or mock (water). After 4 days, primary root lengths were measured. Box and whisker plots show mean primary root lengths in % relative to mock treated roots. n: samples size. The letters above bars indicate significant differences as determined by ANOVA followed by Tukey´s honest significance test, or Kruskal-Wallis test followed by Dunn's multiple comparison test in case of non-normal distribution. Compact letter display was used for grouping statistical comparisons, where different letters denote significant difference (p<0.05) (performed using GraphPad). C,D The experiment was repeated at least two times.

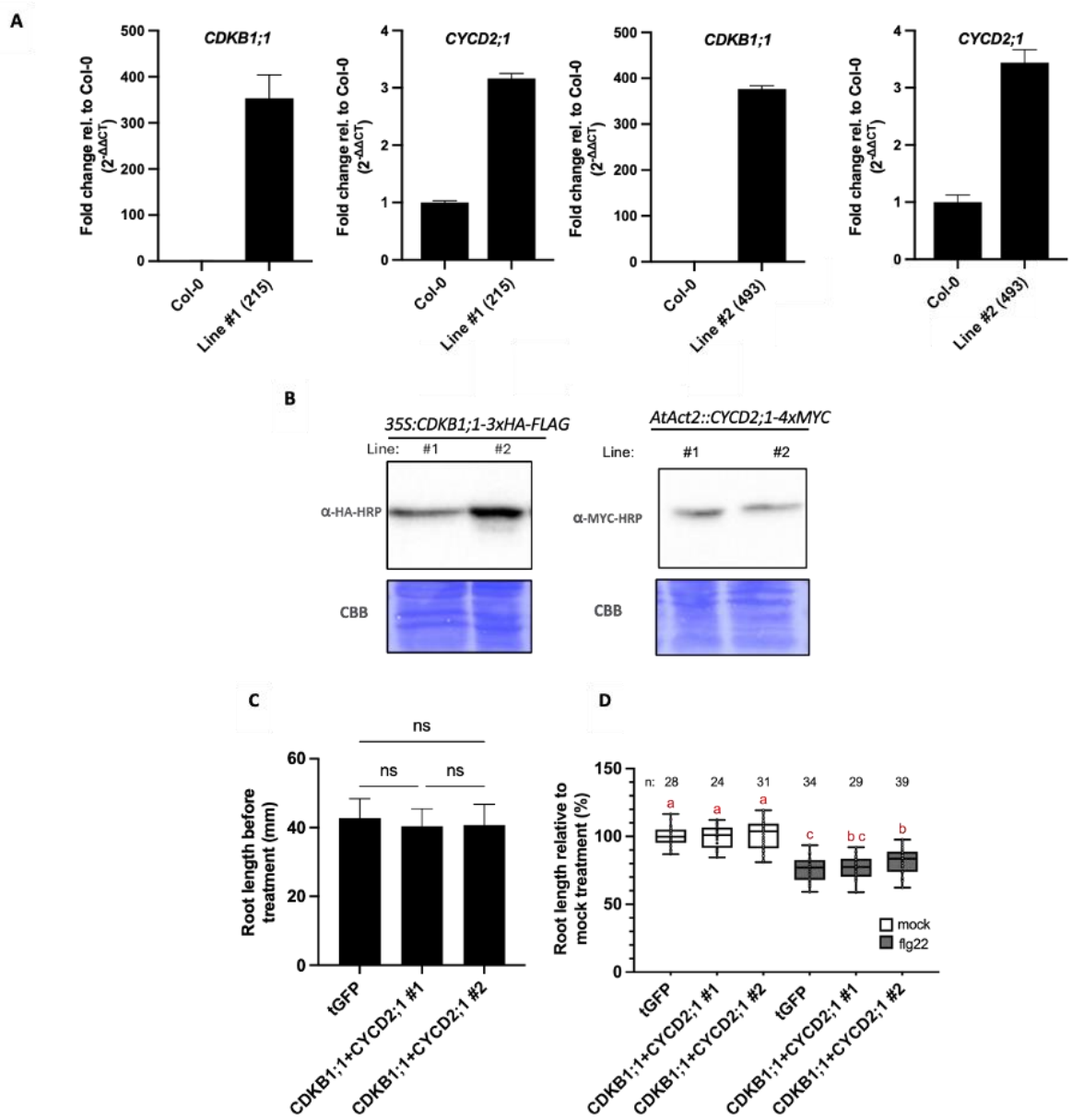

Figure 33: Root growth inhibition assay of *CDKB1;1* and *CYCD2;1*-overexpressing *A. thaliana* plants: Two independent *35S::CDKB1;1-3xHA-FLAG::FASTR::AtAct2::CYCD2;1-4xMYC* (CDKB1;1+CYCD2;1) lines were selected. Col-0 wildtype or *35S::tGFP-3xHA-FLAG::FASTR::AtAct2::tGFP-4xMYC* (tGFP) plants served as controls **(A)** Confirmation of the overexpression. Plants were grown on ATS plates. Roots were harvested and total RNA was extracted followed by reverse transcription into cDNA and gene expression analysis using qRT-PCR. The graphs show the fold change ($2^{-\Delta\Delta Ct}$) of the expression in transgenic lines compared to Col-0 plants. Normalization was done against the housekeeping genes, *UBQ5* and *EF1α*. The numbers in parentheses on the x-axis are internal lines identifiers. **(B)** Confirmation of protein abundance in the overexpresser lines. Plants were grown on ATS plates. After protein extraction, proteins were subjected to Western blot analysis with anti-HA and anti-MYC antibodies. **(C)** The primary root lengths of transgenic plant grown on ATS for 10 days. Columns represent mean values of at least 50 plants ± SD. Asterisks indicate significant differences according to ANOVA followed by Tukey´s honest significance test. $p < 0.001$ (***), $p < 0.01$ (**), $p < 0.05$ (*). **(D)** 10-day-old seedlings were treated with 100 nM flg22 or mock (water). After 4 days, primary root lengths were measured. Box and whisker plots show mean primary root lengths in % relative to mock treated roots. n: samples size. The letters above bars indicate significant differences as determined by ANOVA followed by Tukey´s honest significance test, or Kruskal-Wallis test followed by Dunn's multiple comparison test in case of non-normal distribution. Compact letter display was used for grouping statistical comparisons, where different letters denote significant difference ($p<0.05$) (performed using GraphPad). C,D The experiment was repeated at least two times.

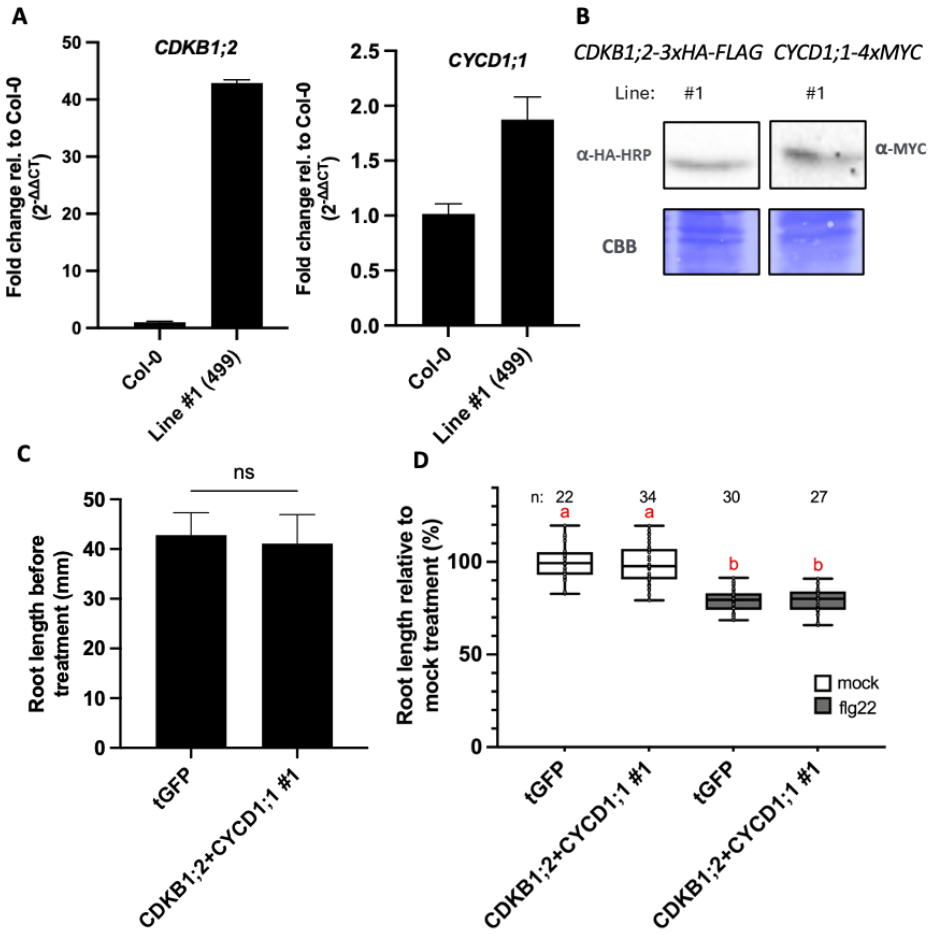

Figure 34: Root growth inhibition assay of *CDKB1;2* and *CYCD1;1*-overexpressing *A. thaliana* plants: Two independent *35S::CDKB1;2-3xHA-FLAG::FASTR::AtAct2::CYCD1;1-4xMYC (CDKB1;2+CYCD1;1)* lines were selected. Col-0 wildtype or *35S::tGFP-3xHA-FLAG::FASTR::AtAct2::tGFP-4xMYC* (tGFP) plants served as controls **(A)** Confirmation of the overexpression. Plants were grown on ATS plates. Roots were harvested and total RNA was extracted followed by reverse transcription into cDNA and gene expression analysis using qRT-PCR. The graphs show the fold change ($2^{-\Delta\Delta Ct}$) of the expression in transgenic lines compared to Col-0 plants. Normalization was done against the housekeeping genes, *UBQ5* and *EF1α*. The numbers in parentheses on the x-axis are internal lines identifiers. **(B)** Confirmation of protein abundance in the overexpresser lines. Plants were grown on ATS plates. After protein extraction, proteins were subjected to Western blot analysis with anti-HA and anti-MYC antibodies. **(C)** The primary root lengths of transgenic plant grown on ATS for 10 days. Columns represent mean values of at least 50 plants ± SD. Asterisks indicate significant differences according to ANOVA followed by Tukey´s honest significance test. $p < 0.001$ (***), $p < 0.01$ (**), $p < 0.05$ (*). **(D)** 10-day-old seedlings were treated with 100 nM flg22 or mock (water). After 4 days, primary root lengths were measured. Box and whisker plots show mean primary root lengths in % relative to mock treated roots. n: samples size. The letters above bars indicate significant differences as determined by ANOVA followed by Tukey´s honest significance test, or Kruskal-Wallis test followed by Dunn's multiple comparison test in case of non-normal distribution. Compact letter display was used for grouping statistical comparisons, where different letters denote significant difference ($p<0.05$) (performed using GraphPad). C,D The experiment was repeated at least two times.

4 Discussion

Roots play essential roles in water and nutrient uptake, anchorage, and interactions with the soil environment (Taiz & Zeiger, 1991). Root growth is determined by cell proliferation and cell elongation. RAM is the primary site of cell division in roots, which is responsible for continuous root growth and it serves as a reservoir of undifferentiated cells (Perilli et al., 2012). In RAM, rarely dividing quiescent centre cells are surrounded by stem cells, which undergo asymmetric cell division and produce self-renewing daughter cells. After dividing several times, cells reach the elongation/differentiation zone, in which they exit cell cycle and differentiate to form root architecture (Perilli et al., 2012; Strotmann & Stahl, 2021). Root growth is influenced by a wide range of internal (e.g. hormonal regulation) and external factors, such as the availability of macro (e.g. nitrogen, phosphorus, and potassium) and micronutrients (e.g. zinc, manganese), texture of soil, pH of soil, temperature etc. In addition, biotic factors can influence root growth (Taiz & Zeiger, 1991). The impact of biotic factors can be growth-promoting (mutualists) or detrimental (soil-borne pathogens) (Raaijmakers et al., 2009). Soil-borne pathogens can target plant roots and may cause devastating plant diseases, posing a major threat to global crop production. Alarmingly, it is expected that in the future, climate change will exacerbate crop losses by leading to the emergence of new pathogens and increasing the severity of existing plant diseases (Delgado-Baquerizo et al., 2020). Therefore, understanding the molecular basis of plant immunity is crucial to develop new strategies to control devastating plant diseases.

4.1. Plant growth media may affect PTI activation levels

Studies over the last decades have made significant contributions to our understanding of plant immunity. The implementation of cutting-edge technologies such as cell sorting and single-cell transcriptomics have enabled researchers to reveal transcriptional networks in plant responses to pathogens at the tissue and even single-cell level (Nobori & Ecker, 2023). However, many questions remain unanswered regarding how individual cells respond to pathogen attacks. To answer those questions, it is vital to have potent experimental systems. The inhibition of seedling or root growth is a common side effect of flg22 or Pep1-induced PTI and can be used as a measure for PTI activity (Jacobs et al., 2011; Poncini et al., 2017). In the past, experiments carried out by the Schäfer group have shown that the extent of RGI varied depending on the media used for plant growth (Rich-Griffin et al., 2020). In this thesis, I demonstrated that plant growth, as well as activation and strength of various PTI responses could strongly depend on the growth media used in the experiments. Recent studies on the spatial analysis of PTI activity in roots have shown that in some tissues PTI responses were low or totally absent. However, in those studies ½ MS was used as the growth medium. Since PTI activation levels may generally be low on this kind of medium, the results might be misleading (Emonet et al., 2021; Zhou et al., 2020). MES-buffered ½ MS medium, which contains macronutrients,

micronutrients, vitamins and organic nutrients is widely used as growth medium for plant studies (Murashige & Skoog, 1962). An alternative plant growth medium is ATS, which contains macro and micronutrients (Haughn & Somerville, 1986; Lincoln et al., 1990). When I compared plant growth on the two media types, I observed that seedlings grown on ATS media had longer roots and an overall better growth compared to the seedlings grown on ½ MS media (see also Rich-Griffin et al., 2020). When I examined root PTI responses other than RGI, e.g. ROS burst, or up-regulation of PTI marker genes, I noticed that both ROS production and PTI-gene induction were much stronger in *A. thaliana* seedlings grown on ATS media as compared to plants grown on ½ MS media upon flg22 or Pep1 treatment. Furthermore, the ATS-grown PTI-reporter lines *pMYB51::NLS-3xmVENUS* and *pPER5::NLS-3xmVENUS* showed strong fluorescence signal induction in the RAM after flg22 treatment. In contrast, the reporter lines which were grown on ½ MS media had barely any fluorescence signal in the RAM at 6 h after flg22 treatment, and at 24 hat, the expression of the fluorescence reporter genes was slightly increased but it was still significantly lower than those in ATS plants. In the Pep1 treated roots, I did not observe a significant difference in the fluorescent signal intensities among the plants grown on ATS or ½ MS (Figure 7,8 and Figure S5. S6). While the flg22 treatment of plants grown in both types of media induced signals in the epidermis cells, Pep1 treatment induced signals in the stele. The observed difference in the fluorescence signal patterns of the flg22- or Pep1 treated plants can be attributed to the fact that different PTI elicitors activate immunity networks in a cell type-specific manner (Rich-Griffin et al., 2020). Recent studies have shown that different cell types launch different immune responses and the developmental identity and the age of the root play a key role in cell type-specific immunity (reviewed in Üstüner et al., 2022). For instance, cell type-specific transcriptome analyses in *A. thaliana* roots after flg22 or Pep1 treatment revealed that different defense programs were activated in epidermis, cortex and pericycle after flg22 or Pep1 treatment (Rich-Griffin et al., 2020). Translating ribosome affinity purification (TRAP)-seq analysis demonstrated that upon infection with mutualistic or pathogenic microbes, different root layers responded differently (Fröschel et al., 2021). In this context, it was not surprising to see that the reporter gene activity varied in the RAM and DZ, and flg22 or Pep1 induce the reporter gene expression in cortex-epidermis and stele, respectively. Interestingly, elicitor treatment affected the PTI reporter signal in a growth media-dependent manner in the RAM, but not the DZ. Whether this may be attributed to the age and/or the degree of cell differentiation is currently unknown.

The two growth media used in the present study were prepared using common recipes. ½ MS media is often prepared using phyto agar as solidifying agent, while ATS media is often supplemented with Gelrite™. Phyto agar is a purified form of agar-agar, supposedly reduced in contaminants that may affect plant growth (https://goldbio.com/product/1742/phyto-agar). Gelrite™ (also known as

Phytagel or gellan gum) is a polysaccharide produced by microbial fermentation of glucuronic acid, rhamnose and glucose. Gelrite™ may be free from toxic contaminants, such as phenolic compounds, and, unlike agar-agar, is considered to have a consistent quality (https://www.duchefa-biochemie.com/; Huang et al., 1995). Furthermore, to solidify media, a lower amount of Gelrite™ is necessary compared to phyto agar (Huang et al., 1995), and media that are supplemented with Gelrite™ are more rigid (depending on the salt composition), which could enable plants to have a better root penetration, thus a better growth. In the literature it has been shown that the choice of the gelling agent might affect experimental results. For instance, it has been shown that gellan gum is more suitable than phyto agar for reproducibility of *A. thaliana* morphometric experiments (Jacques et al., 2020). In a similar way, Kikuchi et al., demonstrated that depending on the polyploidy level of *A. thaliana*, agar and gellan gum could differently affect root growth, which might be due to the amount of aluminum in gellan gum (Kikuchi et al., 2023). In the model moss *Physcomitrella patens*, the choice of the gelling agent can affect cytokinin sensitivity by an unexplained mechanism (Hadeler et al., 1995). In the present study, root growth was significantly reduced in the Col-0 plants grown on ATS containing phyto agar compared to ATS containing Gelrite™. However, in ½ MS growth media, the gelling agent did not have any significant effect on the root growth in general. After flg22 treatment I did not observe a significant difference in RGI intensity in the plants grown on ATS Gelrite™ or ATS phyto agar. However, the gelling agent slightly affected the RGI intensities in plants grown on ½ MS media: on ½ MS containing Gelrite™, plants were slightly more sensitive to flg22-induced RGI than on ½ MS containing phyto agar. I therefore conclude that the gelling agent might have some effect on RGI levels but does not explain the differences between ATS media and ½ MS media in full (Figure S1).

Root-associated bacteria can suppress local root immune responses by reducing the environmental pH in *A. thaliana* seedlings, and PTI alkalinizes the extracellular pH in the root meristem, which promotes binding of Pep1 to its receptors on plant cell membrane (Yu et al., 2019a; Liu et al., 2022). Although these findings indicate the importance of pH in PTI, I showed that MES-based buffer of growth media had no effect on flg22 or Pep1 induced RGI (Figure S1).

ATS and ½ MS are slightly different in terms of macro/micronutrient composition. Recent findings showed that there might be a cross-talk between nutrient signaling pathways and plant immunity (Val-Torregrosa et al., 2021). For example, phosphate stress can lead to a repression of defense-related genes in *A. thaliana* (Castrillo et al., 2017). In addition, C-TERMINALLY ENCODED PEPTIDES (CEPs) are phytocytokines in *A. thaliana,* which regulate root development and growth (Chapman et al., 2019). Recently, Rzemieniewski et al. showed that CEPs and their receptors mediate molecular cross-talk between plant nutrition and immunity. Accordingly, high nitrogen levels can make plants less sensitive

to flg22 treatment in CEP-dependent manner (Rzemieniewski et al., 2024). There are some differences in the salt compositions of ATS and ½ MS medium, e.g. ATS contains 505 mg l^{-1} KNO_3 and 739 mg l^{-1} $MgSO_4$, whereas ½ MS contains 950 mg/L KNO_3 and 90.5 mg/L $MgSO_4$. Further studies will be needed to test for potential effects of individual micro- or macro-elements in plant growth media on the variance in PTI activation levels.

This study highlights that the choice of growth media has a very strong influence on the qualitative and quantitative levels of PTI activity that can be observed in *A. thaliana* in response to various immune elicitors. This information is critical for the scientific community to accurately interpret results of immunity-related experiments. Further experiments will be required to see if the observed media-dependent effects on PTI levels are also visible in other plant organs or tissue types, and whether they affect plant species other than *A. thaliana* as well.

4.2 flg22-triggered PTI may interfere with the expression of *CDKB* and *CYCD* cell cycle regulator genes

In response to abiotic and biotic stress factors, plants can adjust their cell cycle machinery so that they can achieve developmental plasticity, which enables them to survive under challenging environments. Like other organisms, plants must preserve their genomic integrity, and ensure accurate transmission of the genome to the next generations. However, stress can cause DNA damage (Nisa et al., 2019). Plants should prevent the replication of cells with damaged DNA. By slowing down or arresting the cell cycle, cells can allocate time for DNA repair mechanisms to restore genome integrity (Carneiro et al., 2021; Shimotohno et al., 2021). In this context, CDKs and their activating subunits, CYCs are believed to play major roles in regulating cell division rates, under environmental stress. It is believed that environmental stress response signaling cascades can affect directly or indirectly the expression and activity of *CDK* and *CYC* genes and proteins. This can lead to cell cycle delay or cell cycle arrest at G_1/S or G_2/M phase transitions, and thus impaired growth (Carneiro et al., 2021; Shimotohno et al., 2021). There are many examples in the literature showing the effects of stress on the expression of cell cycle regulators. For instance, in *A. thaliana* root tip cells, in which the cell cycle was synchronized via hydroxyurea (HU) treatment, ultraviolet-B (UV-B) irradiation changed the expression patterns of cell cycle regulatory genes (e.g *CDKA;1*, *CDKB1;1*) and the delay in the expression of *CYCD3;1* suggested that UV-B irradiation may cause G_1/S arrest. Consistent with this, in *A. thaliana,* DNA damage could alter the expression of key *CDK* and *CYC* genes, which could delay cell cycle progression at the G_2/M or late S/G_2 phase (Jia et al., 2016). In response to cabbage leaf curl virus infection, microarray analysis of the *A. thaliana* transcriptome showed that expression of cell cycle regulator genes was altered (Ascencio-Ibáñez et al., 2008). I hypothesized therefore that the activation of flg22-

induced PTI may directly or indirectly alter the expression of *CDKB* and *CYCD* genes during *A. thaliana* RGI.

BAR ePlant expression profile maps (Figure S12) and publicly available single cell RNA-seq data (Figure 11) indicated that under non-stress conditions, *CDKB* genes are expressed in meristem cells and hardly in cells of the maturation zone, which is in agreement with previously published experimental data (Adachi et al., 2006; Andersen et al., 2008; Martinez et al., 1992; Okushima et al., 2014). It is not surprising that *CDKB* genes, which regulate the G_2/M transition in dividing cells, are not strongly expressed in the upper parts of roots, as the cells in the maturation zone exit the cell cycle and enter endoreplication (Hayashi et al., 2013). According to the BAR ePlant expression maps (Figure S12) and publicly available single cell RNA-seq data (Figure 11), the expression of some *CYCD* genes is observed only in meristem cells (e.g., *CYCD3;1*), while some others show expression in cells of the elongation and maturation zone (e.g., *CYCD1;1*, *CYCD2;1*, *CYCD3;2*), which may reflect a role of CYCD protein beyond regulation of cell division. Examples for such roles include the regulation of cell differentiation (e.g. control of the balance cell division and cell differentiation in vascular tissue development by CYCD3 proteins, Collins et al., 2015), organ formation in response to hormones (e.g. lateral root formation in pericycle and the control, De Veylder et al., 2007; Sanz et al., 2011), and balancing cell division and endoreplication (Dewitte et al., 2007; Magyar et al., 2012).

In order to determine whether flg22-induced PTI influences cell cycle in *A.thaliana* roots, I analyzed *CDKB* and *CYCD* gene expression kinetics in wild-type *A. thaliana* roots after flg22 treatment (Figure 12,13 and Figure S14, S15). In both of the biological replicates, compared to the mock treated samples, the expression of *CYCD1;1* and *CYCD5;1* significantly decreased 24 h after flg22 treatment, and the decline in the expression of *CYCD1;1* continued at 48 h after treatment. Furthermore, at 48 hat, the expression of *CDKB2;1*, *CDKB2;2*, and *CYCD4;2* decreased in both of the biological replicates. In the other tested genes, an overall trend towards down regulation was observed, although the timepoint for downregulation of the genes varied between biological experiments. Several reasons make expression analyses of cell cycle regulators in roots difficult: Only a small number of the overall root cells undergo cell division, and the cell cycle in these cells is not synchronised. This leads to a heterogenous population of dividing cells which may undergo different cell cycle phases at any given time. Chemical agents such as HU are widely used to synchronise plant cell cultures (Cools et al., 2010; Planchais et al., 2000). HU treatment can be applied to *A. thaliana* seedlings to achieve synchronization of root tips, as well (Cools et al., 2010; Jiang et al., 2011). However, this approach would not have been suitable for the present study as HU treatment could lead to DNA damage, induction of stress-related genes, changes in overall cellular metabolism and even cell death (Winnicki et al., 2013). HU-induced stress responses could therefore interfere with the flg22 induced immune

signalling pathway. In addition, most *CDKB* and *CYCD* genes are not very strongly expressed in *A. thaliana* roots and their expression decrease in the elongation and differentiation zones, where cells become non-cycling. This could dilute *CDKB* and *CYCD* transcripts and mask the effects of flg22 treatment on *CDKB* or *CYC* expression. According to the BAR ePlant expression maps (Figure S12) and single cell RNA-seq data (Figure 11), besides in the RAM, some *CYCD* genes (e.g. *CYCD2;1* and *CYCD4;1*) are expressed in the elongation and differentiation zone, where cells exit cell cycle and enter endoreplication. Changes in expression of these genes after flg22 treatment would be difficult to interpret in the context of a potential effect of immunity on cell cycle regulation.

The data presented here indicate that PTI induction may lead to a reduction in expression of *CDKB* genes, which are believed to regulate G_2/M transition. That PTI activity interferes with cell division in G_2/M phase is supported by the observation that flg22 treatment reduced the number of dividing cells that express the G2/M transition maker *pCYCB1;1::CYCB1;1-GFP* (Eichmann et al. unpublished). However, it cannot be excluded that the downregulation of *CDKB* genes was the result of an impairment in the upstream signalling pathways that regulate cell cycle or that PTI could delay or arrest earlier cell cycle phases such as G_1 and S. In that case any negative effects of PTI on G_1/S phases would negatively affect the activation of later cell cycle phases as well (Inzé & De Veylder, 2006). It might be difficult to directly determine which phase of the cell cycle is affected by immunity using the transcriptional data from *CDKB* and *CYCD* genes. The expression of cell cycle regulator genes may start before their protein activity peaks (e.g. *CDKB1;1* expression starts in S phase and the protein activity peaks at G_2/M phase (Dewitte & Murray, 2003)). On the other hand, expression of some cell cycle regulator genes is constant throughout the cell cycle and/or regulated by environmental factors. For instance, in *N. tabacum* Bright Yellow-2 cells, *CYCD3;1* transcript accumulation was constant throughout the cell cycle, but decreased under depleting sugar levels in the culture medium (Dewitte & Murray, 2003; Riou-Khamlichi et al., 2000; Sorrell et al., 1999). Employing phase-specific fluorescing cell cycle markers, which have a well-defined expression pattern, would help to understand which cell cycle phase is affected by PTI. For instance, “Plant Cell Cycle Indicator” (PlaCCI) is a recently developed fluorescent reporter system, which employs cell cycle phase-specific fluorescent markers. PlaCCI integrates three fluorescent markers, which are fused to specific protein associated with distinct cell cycle (CHROMATIN LICENSING AND DNA REPLICATION FACTOR-CFP for G_1-phase, HISTONE H3.1-mCherry for S-phase, and CYCB1;1-YFP for G_2-phase). It allows to monitor cell cycle in real-time using live imaging (Desvoyes et al., 2020). Using PlaCCI reporter lines, it would be interesting to monitor cell cycle and endocycle after flg22 treatment.

4.3 flg22-triggered PTI may interfere with CYCD2;1 protein accumulation

Although many studies focused primarily on the genetic and transcriptional aspects of plant immunity, it does not fully reflect the complete regulatory processes. Accumulating evidence suggests that post-translational modifications (PTMs) such as ubiquitination and phosphorylation, which enable rapid and dynamic changes in protein abundance and activity are essential for defense-related signaling events at almost all stages of immunity (Withers & Dong, 2017). PTMs play roles in the activation of PTI, signal amplification, regulation of the activity of transcription factors, which control defense-related genes, ETI responses and deactivation of immunity (Bigeard et al., 2015; Chung et al., 2014; Liu et al., 2011; Sarris et al., 2015; Y. Wang et al., 2014; Withers & Dong, 2017). Moreover, recent studies have indicated that PTMs are also involved in the regulation of growth-immunity trade-offs (Gough & Sadanandom, 2021; Withers & Dong, 2017). For instance, the protein kinase complexes SUCROSE NON-FERMENTING 1-RELATED PROTEIN KINASE1 (SnRK1) and TARGET OF RAPAMYCIN (TOR) are key regulators of stress responses, growth and plant metabolism. Under favorable conditions, TOR promotes growth, while under biotic stress SnRK1 inhibits TOR through phosphorylation and thus promotes disease resistance at the expense of growth (Margalha et al., 2019). The regulation of SnRKI1 activity itself depends on SUMOylation, e.g. the enzymatic conjugation of Small Ubiquitin-like Modifier (SUMO) proteins, which results in its ubiquitination and proteasomal degradation to prevent over-activation of plant stress responses and growth inhibition (Crozet et al., 2016). In addition, it is thought that plant growth repressors DELLA proteins (Section 1.3.2) are less ubiquitinated during biotic stress, which makes them more stable. This suggests that the inhibition of DELLA degradation is crucial for maintaining the balance between growth and defense (Gough & Sadanandom, 2021; Navarro et al., 2008; Sun, 2010).

I hypothesized that under flg22-induced immunity, the levels of cell cycle regulator protein can decrease to slow down or arrest the cell cycle, which can contribute to RGI. To test whether PTI has any effect on protein levels of cell cycle regulators, 3xHA-FLAG- or 4xMYC-tagged versions of AtCDKB and AtCYCD proteins were transiently over-expressed in *N. benthamiana* leaves, which was followed by flg22 treatment. According to the Western blot analyses of the samples, AtCYCD2;1 protein levels slightly decreased 24 hours after flg22 treatment (Figure 17 and Figure S18, S19). Since in the experimental system, the At*CYCD2;1* gene was strongly and constitutively expressed under the control of the CaMV 35S promoter, reduced protein levels were unlikely due to reduced *AtCYCD2;1* transcription. More likely, the reduction in protein levels might be due to increased protein degradation following PTMs. All CYCD proteins have a PEST motif (Figure 10), which may function in proteolytic degradation typically by the ubiquitin proteasome system (Rechsteiner & Rogers, 1996). In addition, as has been observed for many other CYCDs, treating plant samples with the proteasome

inhibitor MG132 (inhibits the 26S proteasome) resulted in higher levels of CYCD2;1 compared to untreated samples (Sanz et al., 2011). This was confirmed in this thesis: MG132 treatment of *A. thaliana* seedlings that overexpress CYCD2;1-4xMYC resulted in higher protein levels in roots compared to water treated samples (data not shown). This supports that CYCD2;1 is regulated through the ubiquitin-proteasome system. Taken together, one could speculate that flg22 treatment directly or indirectly promotes ubiquitination of CYCD2;2 and increases its degradation.

It is known that CYCD2;1 is involved in cell cycle stimulation in root meristems (Sanz et al., 2011). Overexpression of *A. thaliana CYCD2;1* resulted in enhanced cell division in the RAM without changing the overall root growth rate (Qi & John, 2007) and in *N. tabacum roots*, overexpression of *A. thaliana CYCD2;1* led to a reduction in the length of G_1 phase and a faster cell cycle (Cockcroft et al., 2000). Furthermore, CYCD2;1 is thought to regulate the G_1/S transition with CDKA;1 (Boniotti & Gutierrez, 2001). It is conceivable that during RGI, PTI may influence CYCD2;1 protein levels and that this could result in an arrest of the cell cycle at G_1 followed by reduced growth. To support this hypothesis, it is crucial to test weather CYCD2;1 accumulation in *A. thaliana* roots is affected by flg22 treatment as well. Furthermore, it would be interesting to investigate how flg22-induced PTI alters PTM, especially ubiquitination of the CYCD2;1 protein. In the same experimental setup, one could also apply MG132 to stop proteasomal degradation and investigate whether this would affect the flg22-triggered reduction in CYCD2;1 levels as well. In addition, a ubiquitination assay could be performed under flg22-induced PTI conditions.

Although Western blot is a valuable method for detecting the presence of proteins, it might not be very sensitive to detect low abundance proteins and to quantify small changes in protein levels. Since it is a semi-quantitative method, it can only give a rough estimation but cannot provide precise or absolute values. For the quantification of the accumulation of native CDKB and CYCD proteins in the presence or absence of PTI activation, more sensitive quantitate techniques such as mass spectrometry could be an option (Zhang et al., 2010). In addition, in this study (Section 2.2.2.1), *A. thaliana* lines were generated that express mVENUS-tagged CDKB1;1, CDKB2;1 and CDKB2;2 under control of their native promotors. In future analyses, these lines could reveal how immunity affects the abundance and distribution of fluorescently-labelled CDKB proteins in root meristems.

Together, the generated tagged *CDKB* and *CYCD* overexpression constructs, along with the optimization and detection of CDKB and the highly unstable CYCD proteins by Western blot in this study, will be highly valuable for future experiments.

4.4 Overexpression of *CDKB* and *CYCD* genes could abolish flg22-induced RGI

Previous findings of the Schäfer lab indicated that overexpression of *CDKB1;1* and potentially *CYCD1;1* could abolish flg22-induced RGI in *A. thaliana* plants (Eichmann et al., unpublished; Finch,2019). In the present work, new 3xHA-FLAG-tagged overexpresser *A. thaliana* lines were generated for all members of the B-type *CDKs*. In the present work, flg22-induced RGI was not observed in *35S::CDKB1;1-3xHA-FLAG* plants as it was observed before (Eichmann et al., unpublished) for a *35S::CDKB1;1* line (Boudolf et al., 2004a). In the study by Eichmann et al., *35S::CDKB1;1* plants generally exhibited much longer roots compared to the wild-type plants, which indicated that overexpression of *CDKB1;1* supported cell cycle and cell growth in that line. However, in the *35S::CDKB1;1-3xHA-FLAG* lines generated in this study, I observed much shorter roots compared to the control plants. The shorter roots may have made the plants more sensitive to flg22 treatment, which may be the reason why I was unable to observe abolished RGI in the *35S::CDKB1;1-3xHA-FLA* plants (Figure 19 and Figure S24). The reasons for these differences in the phenotypes can be attributed to factors such as off-target effects of T-DNA insertions, different activities of the 35S promoter fragments used, functional inhibition through protein tagging, or differences in growth conditions, and seed viability. However, RGI assays using the novel transgenic lines indicated that overexpression of *CDKB2;1* may partially overcome flg22-induced RGI, as well (Figure 21 and Figure S26). It is thought that *CDKB2;1* is expressed specifically at G_2/M and that it regulates the G_2/M phase transition (Polyn et al., 2015). In contrast to the previous observation that *35S::CDKB2;1* plants were indistinguishable from wild-type plants in terms of root growth (Andersen et al., 2008), I observed that the *CDKB2;1* overexpressing plants had slightly longer roots compared to wild-type *A. thaliana* plants. The longer roots might be an indicator of accelerated cell division due to *CDKB2;1* overexpression and this could potentially also partially overcome the negative effect of PTI on root growth.

CYCD proteins, which link environmental factors to the cell cycle machinery and act as activating subunits of CDK proteins, may also serve as mediators of the growth-immunity cross-talk. Similar to overexpression of *CDKB1;1* and *CDKB2;1*, the overexpression of *CYCD1;1* and *CYCD3;2* partially overcame flg22-induced RGI in *A. thaliana* plants (Figure 21, 23, 26 and Figure S26, S28 and S31, Finch, 2019). However, the phenotypes were observed only in one line for both genes. To draw firm conclusions, it will be necessary to test more lines. It is important to note that overexpressing core cell cycle genes such as *CDKB*s and *CYCD*s may have deleterious effects, as they have vital roles in plant growth and development and are usually tightly regulated. Therefore, it is conceivable that transgenic lines that strongly overexpress *CDKB*s and *CYCD*s may not have survived. In *AtAct2::tGFP-4xMYC* lines, *AtAct2* promoter led thousands-folds higher expression of the expression in the control samples (data not shown), whereas in *AtAct2::CYCD* lines, the AtAct2 promoter led only 2 to 40-fold of the expression

in the control samples. As a result, we may underestimate measured phenotypes in "weaker" overexpressers. To overcome negative effects of constitutive overexpression on plant growth, one could employ chemically inducible promoters such as an estrogen receptor-based trans-activator XVE system (Zuo et al., 2000).

If the effects of *CDKB/CYC* overexpression could be confirmed in future experiments, it will be necessary to examine whether PTI signalling would still be functioning in the overexpressing lines to rule out the possibility that reduced flg22-induced RGI resulted from impaired PTI signalling. To this end, wild-type and the transgenic lines could be treated with flg22 and it could be checked whether the PTI hallmark responses, such as ROS burst, induction of defence gene expression, or MAPK phosphorylation would still be activated. Furthermore, it would be important to examine if the transgenic lines would be resistant against pathogens (e.g. *P. syringae* pv. *tomato* DC3000) after PTI activation. If PTI would not be impaired and the transgenic plants would be less sensitive to PTI-activated RGI, this will show that one can potentially uncouple the negative growth-immunity cross-talk.

The similar phenotypes regarding reduced sensitivity observed after flg22 treatment of the *CDKB1;1*, *CDKB2;1* and *CYCD1;1* and *CYCD3;2* overexpression lines suggest that these proteins might be working together in regulating growth-immunity cross-talk. To test this hypothesis physical protein-protein interactions could be investigated. There is previous evidence that some CDKBs and CYCDs physically interact. These findings have been mapped in a protein-protein interactome network, which was generated using yeast two-hybrid and bi-fluorescence complementation assays and, in another study, *in vitro* co-immunoprecipitation was employed (Boruc et al., 2010; Kono et al., 2003; Veylder et al., 1997). According to the protein-protein interactome network generated by Boruc et al., CDKB1;1 interacts with CDKB2;1, CYCD1;1, CYCD3;2, furthermore CDKB2;1 interacts with CYCD3;2 (Boruc et al., 2010). In addition, Kono showed that CDKB2;1 and CYCD1;1 interact using *in vitro* pull-down assay (Kono et al., 2003). In the present study, plasmids containing the *3xHA-FLAG*- and *4xMYC*-tagged versions of *CDKB*s and *CYCD*s were generated. These plasmids were successfully used for transient expressing of *CDKB*s and *CYCD*s in *N. benthamiana* via *Agrobacterium*-mediated transformation, and the expressed proteins were detected with Western blot (Figure 14). Using this established system, in future experiments, co-expression of interesting CDKB and CYCD pairs can be carried out in *N. benthamiana*, followed by co-immunoprecipitation to confirm protein-protein interactions *in planta*. Given the reduction in *CDKB2;1* expression after flg22 treatment (Section 3.3.2.2) and the reduced RGI in *35S::CDKB2;1-3xHA-FLAG*, *AtAct2::CYCD1;1-4xMYC,* and *AtAct2::CYCD3;2-4xMYC* plants, CDKB2;1, CYCD1;1, and CYCD3;2 may work together to mediate immunity and cell cycle signalling. *CDKB2;1* transcript level and activity peak during G_2/M phase, whereas, *CYCD1;1* expression is not phase-

dependent (Menges et al., 2003; Polyn et al., 2015). In addition to CYCD1;1, CYCD4;1 may play role in immunity-cell cycle cross-talk. Kono et al showed that like *CYCD1;1*, *CYCD4;1* is expressed throughout the cell cycle and the authors suggested that CDKB2;1 and CYCD4;1 form an active kinase complex, which may control G_2/M transition (Kono et al., 2003). When PTI is triggered, it could be argued that the CDKB2;1-CYCD kinase complexes disassociate, thereby blocking G_2/M transition and leading to arrested cell cycle and growth inhibition. After confirming the interaction partners of CDKBs, one could investigate whether these interactions are altered by flg22-induced PTI by using the experimental system developed in Section 3.3.3.2. In this study, although the overexpression of the CDKB1;1 protein did not cause any changes in RGI phenotype, investigating whether PTI affects the physical interaction between CDKB1;1 and CYCD proteins could provide valuable insights.

4.5 Multifaceted roles of CDKB and CYCD proteins in growth- and stress-related process

The results of this work indicate potential effects of flg22-induced PTI on CDKB and CYCD proteins during RGI. Root growth is dependent on cell division, cell growth (elongation) and undisturbed root patterning (Heidstra & Sabatini, 2014; Sablowski & Carnier Dornelas, 2014). Although, the primary role of CDKB and CYCD proteins is cell cycle regulation, as it was mentioned in Section 4.2, some of these proteins have been shown to be involved in other cellular processes, which could also play roles in the growth-immunity cross-talk.

CDKBs and CYCDs are known to play a role in the maintenance of both shoot and root meristem organization, root patterning and root architecture. Knockdown or overexpression of *CDKB2;1* and *CDKB2;2* led to disturbed shoot meristem and overall growth inhibition. However, this phenotype was not observed in the RAM, although a reduction in the number of lateral roots was observed (Andersen et al., 2008). WUSCHEL-RELATED HOMEOBOX 5 (WOX5) is a transcription factor that is required for QC function and maintenance of columella stem cell (Haecker et al., 2004; Sarkar et al., 2007). WOX5 suppresses *CYCD* expression to restrict cell division in the QC. Specifically, WOX5 interacts with the promoter of *CYCD3;3* to repress its expression. Ectopic expression of *CYCD3;3* is sufficient to trigger cell division in the QC. On the other hand, WOX5, CYCD1;1 and CYCD3;3 promote cell division in the columella (Forzani et al., 2014). SCARECROW(SCR) and SHORTROOT(SHR) are two transcription factors that control patterning of the root ground tissues. The SCR/SHR complex controls the expression of *CYCD6;1* in cortex-endodermis initials and cortex-endodermis initial daughter cells. The expression is critical for promoting asymmetric stem cell division, which is essential for correct patterning of root tissue (Cruz-Ramírez et al., 2012; Long et al., 2015; Xie et al., 2023). The examples mentioned above, along with many other findings, show that CDKB and CYCD proteins are important in tissue patterning and proper root development. The reduction in the expression of certain *CDKB* and *CYCD* genes after flg22-induced PTI activation and reduced RGI in the overexpression plants raise the question of

whether PTI disrupts stem cell niche organization and root patterning in the RAM. However, previous results by the Schäfer lab showed that flg22 treatment did not affect the number of QC cells or the expression of *pWOX5::GFP*. Furthermore, the expression pattern of GFP-tagged versions of various stem cell markers, such as *SHR*, *SCR* was not affected by flg22 treatment. The results indicate that root stem cell niche organization and root pattering were not significantly affected by PTI activation (Eichmann et al., unpublished).

Another cellular activity in which CDK and CYC proteins play a role is the endocycle. During endocycle, cells multiply the genomic material without dividing, which leads to polyploidy (Breuer et al., 2014). In principle, the activity of certain CDK-CYC complexes should be downregulated to exit mitotic cell division and enter the endocycle (Breuer et al., 2014). Endocycle and cell cycle share many regulatory proteins. For instance, CDKB1;1 together with CYCA2;3 promotes cell division and inhibits endoreduplication in *A. thaliana*. To enter the endocycle, CELL CYCLE SWITCH 52A1 was shown to activate an E3 ubiquitin ligase to degrade CYCA3;2 (Boudolf et al., 2009). A recent study showed that CDKB1;1 and CDKG2 function in a common pathway to control endoreduplication and cell growth in *A. thaliana* (Jiang et al., 2022). In addition, Dewitte et al. found that the CYCD3 group is required for promoting mitotic cell cycle and inhibit endocycle in shoots of *A. thaliana*, which is crucial for determining cell number and size in organ development (Dewitte et al., 2007). It is also known that stress conditions such as heat, drought, salinity, or DNA damage could increase endoreplication and potentially ploidy levels in roots (Bhosale et al., 2018; Hase et al., 2006; Lang & Schnittger, 2020; Matsuda et al., 2018; Monjardino et al., 2006). Furthermore, upon beneficial or pathogenic infections, e.g. during colonization of the *Medicago truncatula* root cortex by arbuscular mycorrhizal fungi, in symbiosis between legumes and nitrogen-fixing rhizobia, in powdery mildew-infected *A. thaliana* leaves, or in epidermal cells of rosette leaves infected by the cabbage leaf curl virus, endocycle induction was observed in the vicinity of infection sites (Ascencio-Ibáñez et al., 2008; Carotenuto et al., 2019; Cebolla et al., 1999; Chandran et al., 2010; Fan et al., 2022). It is important to mention that in *A. thaliana* roots, endoreduplication takes place before rapid cell expansion and it is believed that there is a correlation between ploidy levels and cell size, including elongation (Hayashi et al., 2013; Sugimoto-Shirasu & Roberts, 2003). As the root growth rate is determined by cell division and cell elongation (Beemster & Baskin, 1998), it would be interesting to investigate in the future whether PTI influences the endocycle, and whether this contributes to RGI as well.

It is thought that CDKB proteins also play role in the DNA damage responses (DDR). Being sessile organisms, plants are exposed to DNA damage from internal (e.g. replication errors, ROS production due to cellular metabolism) and external factors (e.g. UV light, heat stress). DNA damage can threaten genome integrity, which can cause developmental defects, lethality and impaired transmission of

genetic information to the next generations (Nisa et al., 2019; Szurman-Zubrzycka et al., 2023). To maintain genomic stability, it is essential to sense DNA damage and have repair mechanisms. Like in animals, ATAXIA TELANGIECTASIA MUTATED (ATM) and ATM and RAD3-RELATED (ATR) are two protein kinases, which regulate DDR activation. DNA double strand breaks (DSB) are primarily detected by ATM, while single strand breaks (SSB) activate ATR (Nisa et al., 2019). Suppressor Of Gamma Radiation 1 (SOG1) is considered as a downstream element of ATR and ATM (Yoshiyama et al., 2009; Yoshiyama et al., 2013). SOG1 is believed to be the main regulator of the DDR network and it controls the expression of DNA repair genes and cell cycle regulators (Nisa et al., 2019). Another important kinase in DDR pathways is WEE1, which is activated by both ATR and ATM (Cools et al., 2011; De Schutter et al., 2007). Upon DNA damage detection, cell division seems to be arrested to allow sufficient time for DNA repair and thus to maintain genome integrity. CDK-CYCLIN complexes are among the key targets for cells cycle arrest (Caneiro et al., 2021). For instance, it has been shown that upon DNA damage, SOG1 downregulats the expression of *CDKB2;1* (Yoshiyama et al., 2009). In addition, in case of DSB, the ATR-SOG1 pathway controls proteasome-dependent degradation of CDKB2;1 (Adachi et al., 2011). A recent study showed that in *A. thaliana*, WEE1 led to ubiquitination and degradation of PLEIOTROPIC REGULATORY LOCUS 1 (PRL1) in response to replication stress. It was suggested that loss of PRL1 causes an alteration in RNA splicing of *CYCD1;1* and *CYCD3;1* genes, resulting in downregulation of their expression, which may contribute to cell cycle arrest (Wang et al., 2021b). Although DNA damage could inhibit CDK activity, counter-intuitively, CDKB1s are known to be activated (both at the transcriptional and posttranslational level) after DNA damage presumably in order to play a role in a DNA repair mechanism. RADIATION SENSITIVE 51 (RAD51) is an important mediator of homology-dependent repair. Weimer et al showed that a CDKB1-CYCB1 complex could phosphorylate RAD51 to mediate homology-dependent repair in *A. thaliana* (Weimer et al., 2016). Unlike *AtCDKB2;1* in *A. thaliana*, *Oryza sativa* (*Os*) *CDKB2;1* transcription was not downregulated during the DNA damage response induced by X-ray in rice. Moreover, rice *cdkb2;1* knockdown plants exhibited increased sensitivity to DNA damage, suggesting that OsCDKB2;1 could directly play a role in DNA repair through an unknown mechanism (Endo et al., 2012). Considering the roles of CDKs and CYCDs in DDR and the results of this work, which indicates a downregulation of various *CDK*s and *CYCD*s after flg22 treatment, one may speculate that flg22-induced PTI induces a DNA damage response, which inhibits root growth. Song and Bent showed that several bacteria, fungi and oomycetes could cause DSBs in host plant DNA in *A. thaliana* (Song & Bent, 2014). A ROS burst is one of the earliest responses of PTI, and ROS production can be genotoxic (Dutta et al., 2018; Gilroy et al., 2014). It is known that in animals, infection-induced ROS production can lead to DNA damage in host cells (Chakraborty et al., 2011). However, it has been shown that in *A. thaliana* plants deficient in ROS

production , *P. syringae* infection-induced DSB formation still occurred (Song & Bent, 2014). Therefore, how infection leads to DNA damage remains unknown. Interestingly, DNA repair mutants and DDR signaling mutants are more susceptible to *P. syringae* (Nisa et al., 2019). In addition, SOG1 controls the expression of some defense-related genes (Bourbousse et al., 2018; Ogita et al., 2018). This indicates that DDR activation and plant immunity are indeed linked.

Taken together, CDK and CYC proteins are not only involved in cell cycle regulation, but are also important components of many other cellular growth-related processes. It will be interesting to investigate whether PTI affects their roles in orchestrating cellular functions beyond cell cycle regulation, such as their involvement in root development and DDR.

Final remarks and future perspective

Having a better understanding of the molecular basis of the growth-immunity antagonism, which can be observed under both lab and field conditions, will support the breeding efforts to generate disease resistance in crops without trading-off growth. Impaired growth under immunity may be the result of imperfect energy and resource allocation (Brown, 2002; Herms & Mattson, 1992; Huot et al., 2014; Monson et al., 2022). However, accumulating evidence suggests that immunity-induced growth inhibition could also be due to (multiple) conflicting immunity and growth-related signalling pathways (Eichmann & Schäfer, 2015; Kliebenstein, 2016; Reitz et al., 2015). If this is the case, there is a chance that immunity and growth could be genetically uncoupled via supporting the shared intersecting compounds of immunity and growth (See Section 1.3.3).

Growing evidence indicates that hormones play a vital role in orchestrating immunity and growth (Denancé et al., 2013; Spoel & Dong, 2008). One could argue that under favourable conditions hormones promote cell proliferation and upon biotic stress, stress hormone signalling could be redirected to immunity. Although, we begin to have a better understanding about how hormones coordinate immunity and growth (Reitz et al., 2015), it remains elusive how immune signalling is connected to the mitotic cell cycle and/or the endocycle. In the present thesis the effects of immunity on cell cycle regulators were investigated, with a focus on CDKBs and CYCDs. The reason for my focus on this protein families was based on previous results in the Schäfer lab (Section 1.5.3) and the potential roles of CYCD proteins in connecting environmental cues into the cell cycle machinery. Indeed, the present work supports that flg22-induced PTI can alter the transcription of *CDKB*s and *CYCD*s and maybe protein levels. Furthermore, reduction in flg22-induced RGI via overexpression of *CDKB1;1*, *CDKB2;1*, *CYCD1;1* and maybe *CYCD3;2* strengthen the hypothesis that PTI interferes with cell cycle regulation through an unknown pathway. To gain a better understanding of the molecular mechanism behind this, a first step might be to analyse protein-protein interactions between CDKBs and CYCDs under immunity by using the system established in this work. Investigating hormone signalling in these processes might be interesting as it is known that cell cycle regulators are heavily regulated by hormones at both mRNA and protein levels. For instance, auxin seems to support both CDKB2;1 transcript and protein levels in the *A. thaliana* root meristem (Okushima et al., 2014). It is also known that auxin can mediate the balance between growth and defence (Kazan & Manners, 2009).

The present work focused on the impact of PTI activation on younger root cells in the root meristem, which still undergo cell cycle. However, scientists are beginning to focus on the understanding of development-related aspects of immunity in differentiated cells in older root tissues (Üstüner et al., 2022). Growth is maintained by cell elongation in the older tissues as well. In this respect, it would be

important to investigate the relationship between cell elongation and endoreduplication with a focus on cell cycle regulators, which are involved in endoreduplication and are affected by PTI. In addition, different root cell types and tissues can exhibit different immune responses quantitatively and qualitatively (Chuberre et al., 2018; Fröschel et al., 2021; Poncini et al., 2017; Rich-Griffin et al., 2020; Üstüner et al., 2022; Zhou et al., 2020). It seems that several mechanisms regulate growth-defence trade-offs and these might be interconnected (Huot et al., 2014; Reitz et al., 2015). Having a better understanding of the interference of immune signalling and growth regulatory processes and cell type-specific immune responses would potentially help us in breeding processes towards highly resistant crops without impaired growth.

References

Achard, P., Gusti, A., Cheminant, S., Alioua, M., Dhondt, S., Coppens, F., Beemster, G. T. S., & Genschik, P. (2009). Gibberellin signaling controls cell proliferation rate in Arabidopsis. Current Biology: CB, 19(14), 1188–1193.

Adachi, S., Minamisawa, K., Okushima, Y., Inagaki, S., Yoshiyama, K., Kondou, Y., Kaminuma, E., Kawashima, M., Toyoda, T., Matsui, M., Kurihara, D., Matsunaga, S., & Umeda, M. (2011). Programmed induction of endoreduplication by DNA double-strand breaks in Arabidopsis. Proceedings of the National Academy of Sciences of the United States of America, 108(24), 10004–10009.

Adachi, S., Uchimiya, H., & Umeda, M. (2006). Expression of B2-type cyclin-dependent kinase is controlled by protein degradation in *Arabidopsis thaliana*. *Plant and Cell Physiology, 47*(12), 1683–1686.

Aichinger, E., Kornet, N., Friedrich, T., & Laux, T. (2012). Plant stem cell niches. Annual Review of Plant Biology, 63, 615–636.

Albert, I., Böhm, H., Albert, M., Feiler, C. E., Imkampe, J., Wallmeroth, N., Brancato, C., Raaymakers, T. M., Oome, S., Zhang, H., Krol, E., Grefen, C., Gust, A. A., Chai, J., Hedrich, R., Van den Ackerveken, G., & Nürnberger, T. (2015). An RLP23-SOBIR1-BAK1 complex mediates NLP-triggered immunity. Nature Plants, 1, 15140.

Albert, M., & Felix, G. (2010). Chimeric receptors of the Arabidopsis thaliana pattern recognition receptors EFR and FLS2. Plant Signaling & Behavior, 5(11), 1430–1432.

An, Y. Q., McDowell, J. M., Huang, S., McKinney, E. C., Chambliss, S., & Meagher, R. B. (1996). Strong, constitutive expression of the Arabidopsis ACT2/ACT8 actin subclass in vegetative tissues. The Plant Journal: For Cell and Molecular Biology, 10(1), 107–121.

Andersen, S. U., Buechel, S., Zhao, Z., Ljung, K., Novák, O., Busch, W., Schuster, C., & Lohmann, J. U. (2008). Requirement of B2-type cyclin-dependent kinases for meristem integrity in Arabidopsis thaliana. The Plant Cell, 20(1), 88–100.

Andolfo, G., & Ercolano, M. R. (2015). Plant Innate Immunity Multicomponent Model. Frontiers in Plant Science, 6, 987.

Asai, T., Tena, G., Plotnikova, J., Willmann, M. R., Chiu, W.-L., Gomez-Gomez, L., Boller, T., Ausubel, F. M., & Sheen, J. (2002). MAP kinase signalling cascade in Arabidopsis innate immunity. Nature, 415(6875), 977–983.

Ascencio-Ibáñez, J. T., Sozzani, R., Lee, T.-J., Chu, T.-M., Wolfinger, R. D., Cella, R., & Hanley-Bowdoin, L. (2008). Global analysis of Arabidopsis gene expression uncovers a complex array of changes impacting pathogen response and cell cycle during geminivirus infection. Plant Physiology, 148(1), 436–454.

Banda, J., Bellande, K., von Wangenheim, D., Goh, T., Guyomarc'h, S., Laplaze, L., & Bennett, M. J. (2019). Lateral Root Formation in Arabidopsis: A Well-Ordered LRexit. Trends in Plant Science, 24(9), 826–839.

Barberon, M., & Geldner, N. (2014). Radial transport of nutrients: The plant root as a polarized epithelium. Plant Physiology, 166(2), 528–537.
Bartels, S., Lori, M., Mbengue, M., van Verk, M., Klauser, D., Hander, T., Böni, R., Robatzek, S., & Boller, T. (2013). The family of Peps and their precursors in Arabidopsis: Differential expression and localization but similar induction of pattern-triggered immune responses. Journal of Experimental Botany, 64(17), 5309–5321.

Beck, M., Wyrsch, I., Strutt, J., Wimalasekera, R., Webb, A., Boller, T., & Robatzek, S. (2014). Expression patterns of flagellin sensing 2 map to bacterial entry sites in plant shoots and roots. Journal of Experimental Botany, 65(22), 6487–6498.

Beeckman, T., & De Smet, I. (2014). Pericycle. Current Biology: CB, 24(10), R378-379.

Beemster, G. T., & Baskin, T. I. (1998). Analysis of cell division and elongation underlying the developmental acceleration of root growth in Arabidopsis thaliana. Plant Physiology, 116(4), 1515–1526.

Benfey, P. N., & Scheres, B. (2000). Root development. Current Biology: CB, 10(22), R813-815.

Berardini, T. Z., Reiser, L., Li, D., Mezheritsky, Y., Muller, R., Strait, E., & Huala, E. (2015). The Arabidopsis information resource: Making and mining the "gold standard" annotated reference plant genome. *Genesis (New York, N.Y. : 2000)*, *53*(8), 474–485.

Beritza, K., Watts, E. C., & van der Hoorn, R. A. L. (2024). Improving transient protein expression in agroinfiltrated Nicotiana benthamiana. The New Phytologist, 243(3), 846–850.

Betsuyaku, S., Katou, S., Takebayashi, Y., Sakakibara, H., Nomura, N., & Fukuda, H. (2018). Salicylic Acid and Jasmonic Acid Pathways are Activated in Spatially Different Domains Around the Infection Site During Effector-Triggered Immunity in Arabidopsis thaliana. Plant & Cell Physiology, 59(2), 439.

Bhatla, N. (2012). Exon-Intron Graphic Maker. http://wormweb.org/exonintron

Bhosale, R., Boudolf, V., Cuevas, F., Lu, R., Eekhout, T., Hu, Z., Van Isterdael, G., Lambert, G. M., Xu, F., Nowack, M. K., Smith, R. S., Vercauteren, I., De Rycke, R., Storme, V., Beeckman, T., Larkin, J. C., Kremer, A., Höfte, H., Galbraith, D. W., … De Veylder, L. (2018). A Spatiotemporal DNA Endoploidy Map of the Arabidopsis Root Reveals Roles for the Endocycle in Root Development and Stress Adaptation. The Plant Cell, 30(10), 2330–2351.

Bigeard, J., Colcombet, J., & Hirt, H. (2015). Signaling mechanisms in pattern-triggered immunity (PTI). Molecular Plant, 8(4), 521–539.

Birkenbihl, R. P., Liu, S., & Somssich, I. E. (2017). Transcriptional events defining plant immune responses. Current Opinion in Plant Biology, 38, 1–9.

Birnbaum, K. D. (2016). How many ways are there to make a root? Current Opinion in Plant Biology, 34, 61–67.

Birnbaum, K., Shasha, D. E., Wang, J. Y., Jung, J. W., Lambert, G. M., Galbraith, D. W., & Benfey, P. N. (2003). A gene expression map of the Arabidopsis root. Science (New York, N.Y.), 302(5652), 1956–1960.

Bjornson, M., & Zipfel, C. (2021). Plant immunity: Crosstalk between plant immune receptors. Current Biology: CB, 31(12), R796–R798.

Böhm, H., Albert, I., Oome, S., Raaymakers, T. M., Van den Ackerveken, G., & Nürnberger, T. (2014). A conserved peptide pattern from a widespread microbial virulence factor triggers pattern-induced immunity in Arabidopsis. PLoS Pathogens, 10(11), e1004491.

Boller, T., & Felix, G. (2009). A renaissance of elicitors: Perception of microbe-associated molecular patterns and danger signals by pattern-recognition receptors. Annual Review of Plant Biology, 60, 379–406.

Boniotti, M. B., & Gutierrez, C. (2001). A cell-cycle-regulated kinase activity phosphorylates plant retinoblastoma protein and contains, in Arabidopsis, a CDKA/cyclin D complex. The Plant Journal: For Cell and Molecular Biology, 28(3), 341–350.

Boruc, J., Van den Daele, H., Hollunder, J., Rombauts, S., Mylle, E., Hilson, P., Inzé, D., De Veylder, L., & Russinova, E. (2010). Functional modules in the Arabidopsis core cell cycle binary protein-protein interaction network. The Plant Cell, 22(4), 1264–1280.

Boudolf, V., Barrôco, R., Engler, J. de A., Verkest, A., Beeckman, T., Naudts, M., Inzé, D., & De Veylder, L. (2004a). B1-type cyclin-dependent kinases are essential for the formation of stomatal complexes in Arabidopsis thaliana. The Plant Cell, 16(4), 945–955.

Boudolf, V., Lammens, T., Boruc, J., Van Leene, J., Van Den Daele, H., Maes, S., Van Isterdael, G., Russinova, E., Kondorosi, E., Witters, E., De Jaeger, G., Inzé, D., & De Veylder, L. (2009). CDKB1;1 forms a functional complex with CYCA2;3 to suppress endocycle onset. Plant Physiology, 150(3), 1482–1493.

Boudolf, V., Vlieghe, K., Beemster, G. T. S., Magyar, Z., Torres Acosta, J. A., Maes, S., Van Der Schueren, E., Inzé, D., & De Veylder, L. (2004b). The plant-specific cyclin-dependent kinase CDKB1;1 and transcription factor E2Fa-DPa control the balance of mitotically dividing and endoreduplicating cells in Arabidopsis. The Plant Cell, 16(10), 2683–2692.

Boudsocq, M., Willmann, M. R., McCormack, M., Lee, H., Shan, L., He, P., Bush, J., Cheng, S.-H., & Sheen, J. (2010). Differential innate immune signalling via Ca(2+) sensor protein kinases. Nature, 464(7287), 418–422.

Bourbousse, C., Vegesna, N., & Law, J. A. (2018). SOG1 activator and MYB3R repressors regulate a complex DNA damage network in Arabidopsis. Proceedings of the National Academy of Sciences of the United States of America, 115(52), E12453–E12462.

Brady, S. M., Orlando, D. A., Lee, J.-Y., Wang, J. Y., Koch, J., Dinneny, J. R., Mace, D., Ohler, U., & Benfey, P. N. (2007). A high-resolution root spatiotemporal map reveals dominant expression patterns. Science (New York, N.Y.), 318(5851), 801–806.

Breuer, C., Braidwood, L., & Sugimoto, K. (2014). Endocycling in the path of plant development. Current Opinion in Plant Biology, 17, 78–85.

Brown, J. K. M. (2002). Yield penalties of disease resistance in crops. Current Opinion in Plant Biology, 5(4), 339–344.

Buendía-Monreal, M., Rentería-Canett, I., Guerrero-Andrade, O., Bravo-Alberto, C. E., Martínez-Castilla, L. P., García, E., & Vázquez-Ramos, J. M. (2011). The family of maize D-type cyclins: Genomic organization, phylogeny and expression patterns. Physiologia Plantarum, 143(3), 297–308.

Camejo, D., Guzmán-Cedeño, Á., & Moreno, A. (2016). Reactive oxygen species, essential molecules, during plant-pathogen interactions. Plant Physiology and Biochemistry: PPB, 103, 10–23.

Campos, M. L., Yoshida, Y., Major, I. T., de Oliveira Ferreira, D., Weraduwage, S. M., Froehlich, J. E., Johnson, B. F., Kramer, D. M., Jander, G., Sharkey, T. D., & Howe, G. A. (2016). Rewiring of jasmonate and phytochrome B signalling uncouples plant growth-defense tradeoffs. Nature Communications, 7, 12570.

Carneiro, A. K., Montessoro, P. da F., Fusaro, A. F., Araújo, B. G., & Hemerly, A. S. (2021). Plant CDKs-Driving the Cell Cycle through Climate Change. Plants (Basel, Switzerland), 10(9), 1804.

Carotenuto, G., Volpe, V., Russo, G., Politi, M., Sciascia, I., de Almeida-Engler, J., & Genre, A. (2019). Local endoreduplication as a feature of intracellular fungal accommodation in arbuscular mycorrhizas. The New Phytologist, 223(1), 430–446.

Castrillo, G., Teixeira, P. J. P. L., Paredes, S. H., Law, T. F., de Lorenzo, L., Feltcher, M. E., Finkel, O. M., Breakfield, N. W., Mieczkowski, P., Jones, C. D., Paz-Ares, J., & Dangl, J. L. (2017). Root microbiota drive direct integration of phosphate stress and immunity. Nature, 543(7646), 513–518.

Cebolla, A., Vinardell, J. M., Kiss, E., Oláh, B., Roudier, F., Kondorosi, A., & Kondorosi, E. (1999). The mitotic inhibitor ccs52 is required for endoreduplication and ploidy-dependent cell enlargement in plants. The EMBO Journal, 18(16), 4476–4484.

Chakraborty, S. P., Kar Mahapatra, S., Sahu, S. K., Das, S., Tripathy, S., Dash, S., Pramanik, P., & Roy, S. (2011). Internalization of Staphylococcus aureus in lymphocytes induces oxidative stress and DNA fragmentation: Possible ameliorative role of nanoconjugated vancomycin. Oxidative Medicine and Cellular Longevity, 2011, 942123.

Chandran, D., Inada, N., Hather, G., Kleindt, C. K., & Wildermuth, M. C. (2010). Laser microdissection of Arabidopsis cells at the powdery mildew infection site reveals site-specific processes and regulators. Proceedings of the National Academy of Sciences of the United States of America, 107(1), 460–465.

Chapman, K., Taleski, M., Ogilvie, H. A., Imin, N., & Djordjevic, M. A. (2019). CEP-CEPR1 signalling inhibits the sucrose-dependent enhancement of lateral root growth. Journal of Experimental Botany, 70(15), 3955–3967.

Chen, Q., Sun, J., Zhai, Q., Zhou, W., Qi, L., Xu, L., Wang, B., Chen, R., Jiang, H., Qi, J., Li, X., Palme, K., & Li, C. (2011). The basic helix-loop-helix transcription factor MYC2 directly represses PLETHORA expression during jasmonate-mediated modulation of the root stem cell niche in Arabidopsis. The Plant Cell, 23(9), 3335–3352.

Chinchilla, D., Zipfel, C., Robatzek, S., Kemmerling, B., Nürnberger, T., Jones, J. D. G., Felix, G., & Boller, T. (2007). A flagellin-induced complex of the receptor FLS2 and BAK1 initiates plant defence. Nature, 448(7152), 497–500.

Chuberre, C., Plancot, B., Driouich, A., Moore, J. P., Bardor, M., Gügi, B., & Vicré, M. (2018). Plant Immunity Is Compartmentalized and Specialized in Roots. Frontiers in Plant Science, 9, 1692.

Chung, E.-H., El-Kasmi, F., He, Y., Loehr, A., & Dangl, J. L. (2014). A plant phosphoswitch platform repeatedly targeted by type III effector proteins regulates the output of both tiers of plant immune receptors. Cell Host & Microbe, 16(4), 484–494.

Churchman, M. L., Brown, M. L., Kato, N., Kirik, V., Hülskamp, M., Inzé, D., De Veylder, L., Walker, J. D., Zheng, Z., Oppenheimer, D. G., Gwin, T., Churchman, J., & Larkin, J. C. (2006). SIAMESE, a plant-specific cell cycle regulator, controls endoreplication onset in Arabidopsis thaliana. The Plant Cell, 18(11), 3145–3157.

Clowes, F. (1953). The cytogenerative centre in roots with broad columellas. The New Phytologist, 52(1), 48–57.

Cockcroft, C. E., den Boer, B. G., Healy, J. M., & Murray, J. A. (2000). Cyclin D control of growth rate in plants. Nature, 405(6786), 575–579.

Collins, C., Dewitte, W., & Murray, J. A. H. (2012). D-type cyclins control cell division and developmental rate during Arabidopsis seed development. Journal of Experimental Botany, 63(10), 3571–3586.

Collins, C., Maruthi, N. M., & Jahn, C. E. (2015). CYCD3 D-type cyclins regulate cambial cell proliferation and secondary growth in Arabidopsis. Journal of Experimental Botany, 66(15), 4595–4606.

Cools, T., Iantcheva, A., Maes, S., Van den Daele, H., & De Veylder, L. (2010). A replication stress-induced synchronization method for Arabidopsis thaliana root meristems. The Plant Journal: For Cell and Molecular Biology, 64(4), 705–714.

Cools, T., Iantcheva, A., Weimer, A. K., Boens, S., Takahashi, N., Maes, S., Van den Daele, H., Van Isterdael, G., Schnittger, A., & De Veylder, L. (2011). The Arabidopsis thaliana checkpoint kinase WEE1 protects against premature vascular differentiation during replication stress. The Plant Cell, 23(4), 1435–1448.

Couto, D., & Zipfel, C. (2016). Regulation of pattern recognition receptor signalling in plants. Nature Reviews. Immunology, 16(9), 537–552.

Crozet, P., Margalha, L., Butowt, R., Fernandes, N., Elias, C. A., Orosa, B., Tomanov, K., Teige, M., Bachmair, A., Sadanandom, A., & Baena-González, E. (2016). SUMOylation represses SnRK1 signaling in Arabidopsis. The Plant Journal: For Cell and Molecular Biology, 85(1), 120–133.

Cruz-Ramírez, A., Díaz-Triviño, S., Blilou, I., Grieneisen, V. A., Sozzani, R., Zamioudis, C., Miskolczi, P., Nieuwland, J., Benjamins, R., Dhonukshe, P., Caballero-Pérez, J., Horvath, B., Long, Y., Mähönen, A. P., Zhang, H., Xu, J., Murray, J. A. H., Benfey, P. N., Bako, L., Marée A., Scheres, B. (2012). A bistable circuit involving SCARECROW-RETINOBLASTOMA integrates cues to inform asymmetric stem cell division. Cell, 150(5), 1002–1015.

Cui, H., Tsuda, K., & Parker, J. E. (2015). Effector-triggered immunity: From pathogen perception to robust defense. Annual Review of Plant Biology, 66, 487–511.

Das, A. (2020). P19 to the Rescue: How to Increase Protein Expression in Agroinfiltration. https://bitesizebio.com/29964/p19-increase-expression-agroinfiltration/

Datta, S., Kim, C. M., Pernas, M., Pires, N. D., Proust, H., Tam, T., Vijayakumar, P., & Dolan, L. (2011). Root hairs: Development, growth and evolution at the plant-soil interface. Plant and Soil, 346, 1–14.

de Luis Balaguer, M. A., Fisher, A. P., Clark, N. M., Fernandez-Espinosa, M. G., Möller, B. K., Weijers, D., Lohmann, J. U., Williams, C., Lorenzo, O., & Sozzani, R. (2017). Predicting gene regulatory networks by combining spatial and temporal gene expression data in Arabidopsis root stem cells. Proceedings of the National Academy of Sciences of the United States of America, 114(36), E7632–E7640.

De Schutter, K., Joubès, J., Cools, T., Verkest, A., Corellou, F., Babiychuk, E., Van Der Schueren, E., Beeckman, T., Kushnir, S., Inzé, D., & De Veylder, L. (2007). Arabidopsis WEE1 kinase controls cell cycle arrest in response to activation of the DNA integrity checkpoint. The Plant Cell, 19(1), 211–225.

De Veylder, L. (2019). The Discovery of Plant D-Type Cyclins. The Plant Cell, 31(6), 1194–1195.

De Veylder, L., Beeckman, T., & Inzé, D. (2007). The ins and outs of the plant cell cycle. Nature Reviews. Molecular Cell Biology, 8(8), 655–665.

Delgado-Baquerizo, M., Guerra, C. A., Cano-Díaz, C., Egidi, E., Wang, J.-T., Eisenhauer, N., Singh, B. K., & Maestre, F. T. (2020). The proportion of soil-borne pathogens increases with warming at the global scale. Nature Climate Change, 10(6), 550–554.

Denancé, N., Sánchez-Vallet, A., Goffner, D., & Molina, A. (2013). Disease resistance or growth: The role of plant hormones in balancing immune responses and fitness costs. Frontiers in Plant Science, 4, 155.

Deng, Y., Zhai, K., Xie, Z., Yang, D., Zhu, X., Liu, J., Wang, X., Qin, P., Yang, Y., Zhang, G., Li, Q., Zhang, J., Wu, S., Milazzo, J., Mao, B., Wang, E., Xie, H., Tharreau, D., & He, Z. (2017). Epigenetic regulation of antagonistic receptors confers rice blast resistance with yield balance. Science (New York, N.Y.), 355(6328), 962–965.

Deslandes, L., & Rivas, S. (2012). Catch me if you can: Bacterial effectors and plant targets. Trends in Plant Science, 17(11), 644–655.

Desvoyes, B., Arana-Echarri, A., Barea, M. D., & Gutierrez, C. (2020). A comprehensive fluorescent sensor for spatiotemporal cell cycle analysis in Arabidopsis. Nature Plants, 6(11), 1330–1334.

Dewitte, W., & Murray, J. A. H. (2003). The plant cell cycle. Annual Review of Plant Biology, 54, 235–264.

Dewitte, W., Riou-Khamlichi, C., Scofield, S., Healy, J. M. S., Jacqmard, A., Kilby, N. J., & Murray, J. A. H. (2003). Altered cell cycle distribution, hyperplasia, and inhibited differentiation in Arabidopsis caused by the D-type cyclin CYCD3. The Plant Cell, 15(1), 79–92.

Dewitte, W., Scofield, S., Alcasabas, A. A., Maughan, S. C., Menges, M., Braun, N., Collins, C., Nieuwland, J., Prinsen, E., Sundaresan, V., & Murray, J. A. H. (2007). Arabidopsis CYCD3 D-type cyclins link cell proliferation and endocycles and are rate-limiting for cytokinin responses. Proceedings of the National Academy of Sciences of the United States of America, 104(36), 14537–14542.

Dietrich, D., Pang, L., Kobayashi, A., Fozard, J. A., Boudolf, V., Bhosale, R., Antoni, R., Nguyen, T., Hiratsuka, S., Fujii, N., Miyazawa, Y., Bae, T.-W., Wells, D. M., Owen, M. R., Band, L. R., Dyson, R. J.,

Jensen, O. E., King, J. R., Tracy, S. R., … Bennett, M. J. (2017). Root hydrotropism is controlled via a cortex-specific growth mechanism. Nature Plants, 3, 17057.

Dinneny, J. R., & Benfey, P. N. (2008). Plant stem cell niches: Standing the test of time. Cell, 132(4), 553–557.

Dodds, P. N., & Rathjen, J. P. (2010). Plant immunity: Towards an integrated view of plant-pathogen interactions. Nature Reviews. Genetics, 11(8), 539–548.

Dolan, L., Janmaat, K., Willemsen, V., Linstead, P., Poethig, S., Roberts, K., & Scheres, B. (1993). Cellular organisation of the Arabidopsis thaliana root. Development (Cambridge, England), 119(1), 71–84.

Dutta, S., Mitra, M., Agarwal, P., Mahapatra, K., De, S., Sett, U., & Roy, S. (2018). Oxidative and genotoxic damages in plants in response to heavy metal stress and maintenance of genome stability. Plant Signaling & Behavior, 13(8), e1460048.

Dwivedi, S. L., Reynolds, M. P., & Ortiz, R. (2021). Mitigating tradeoffs in plant breeding. iScience, 24(9), 102965.

Echevarría, C., Gutierrez, C., & Desvoyes, B. (2021). Tools for Assessing Cell-Cycle Progression in Plants. Plant & Cell Physiology, 62(8), 1231–1238.

Edgar, B. A., Zielke, N., & Gutierrez, C. (2014). Endocycles: A recurrent evolutionary innovation for post-mitotic cell growth. Nature Reviews. Molecular Cell Biology, 15(3), 197–210.

Eichmann, R., Finch, J., Reitz, M. U., & Schäfer, P. (unpublished). Root growth inhibition induced by the immune elicitor flg22 is mediated by cell cycle arrest.

Eichmann, R., & Schäfer, P. (2015). Growth versus immunity—A redirection of the cell cycle? Current Opinion in Plant Biology, 26, 106–112.

Emonet, A., Zhou, F., Vacheron, J., Heiman, C. M., Dénervaud Tendon, V., Ma, K.-W., Schulze-Lefert, P., Keel, C., & Geldner, N. (2021). Spatially Restricted Immune Responses Are Required for Maintaining Root Meristematic Activity upon Detection of Bacteria. Current Biology: CB, 31(5), 1012-1028.e7.

Endo, M., Nakayama, S., Umeda-Hara, C., Ohtsuki, N., Saika, H., Umeda, M., & Toki, S. (2012). CDKB2 is involved in mitosis and DNA damage response in rice. The Plant Journal: For Cell and Molecular Biology, 69(6), 967–977.

Engler, C., Youles, M., Gruetzner, R., Ehnert, T.-M., Werner, S., Jones, J. D. G., Patron, N. J., & Marillonnet, S. (2014). A golden gate modular cloning toolbox for plants. ACS Synthetic Biology, 3(11), 839–843.

Fan, M., Bai, M.-Y., Kim, J.-G., Wang, T., Oh, E., Chen, L., Park, C. H., Son, S.-H., Kim, S.-K., Mudgett, M. B., & Wang, Z.-Y. (2014). The bHLH transcription factor HBI1 mediates the trade-off between growth and pathogen-associated molecular pattern-triggered immunity in Arabidopsis. The Plant Cell, 26(2), 828–841.

Fan, W., Xia, C., Wang, S., Liu, J., Deng, L., Sun, S., & Wang, X. (2022). Rhizobial infection of 4C cells triggers their endoreduplication during symbiotic nodule development in soybean. The New Phytologist, 234(3), 1018–1030.

Finch, J. (2019). He role of cell cycle regulation in immunity-induced root growth inhibition in Arabidopsis thaliana. University of Warwick.

Forzani, C., Aichinger, E., Sornay, E., Willemsen, V., Laux, T., Dewitte, W., & Murray, J. A. H. (2014). WOX5 suppresses CYCLIN D activity to establish quiescence at the center of the root stem cell niche. Current Biology: CB, 24(16), 1939–1944.

Fröschel, C., Komorek, J., Attard, A., Marsell, A., Lopez-Arboleda, W. A., Le Berre, J., Wolf, E., Geldner, N., Waller, F., Korte, A., & Dröge-Laser, W. (2021). Plant roots employ cell-layer-specific programs to respond to pathogenic and beneficial microbes. Cell Host & Microbe, 29(2), 299-310.e7.

Fucile, G., Di Biase, D., Nahal, H., La, G., Khodabandeh, S., Chen, Y., Easley, K., Christendat, D., Kelley, L., & Provart, N. J. (2011). ePlant and the 3D data display initiative: Integrative systems biology on the world wide web. PloS One, 6(1), e15237.

Gao, M., He, Y., Yin, X., Zhong, X., Yan, B., Wu, Y., Chen, J., Li, X., Zhai, K., Huang, Y., Gong, X., Chang, H., Xie, S., Liu, J., Yue, J., Xu, J., Zhang, G., Deng, Y., Wang, E., … He, Z. (2021). Ca2+ sensor-mediated ROS scavenging suppresses rice immunity and is exploited by a fungal effector. Cell, 184(21), 5391-5404.e17.

Gasteiger, E., Hoogland, C., Gattiker, A., Duvaud, S., Wilkins, M. R., Appel, R. D., & Bairoch, A. (2005). Protein Identification and Analysis Tools on the ExPASy Server. In J. M. Walker (Ed.), The Proteomics Protocols Handbook (pp. 571–607). Humana Press. https://doi.org/10.1385/1-59259-890-0:571

Geldner, N. (2013). The endodermis. Annual Review of Plant Biology, 64, 531–558.

Geng, Y., Wu, R., Wee, C. W., Xie, F., Wei, X., Chan, P. M. Y., Tham, C., Duan, L., & Dinneny, J. R. (2013). A spatio-temporal understanding of growth regulation during the salt stress response in Arabidopsis. The Plant Cell, 25(6), 2132–2154.

Ghareeb, H., Laukamm, S., & Lipka, V. (2016). COLORFUL-Circuit: A Platform for Rapid Multigene Assembly, Delivery, and Expression in Plants. Frontiers in Plant Science, 7, 246.

Gilroy, S., Suzuki, N., Miller, G., Choi, W.-G., Toyota, M., Devireddy, A. R., & Mittler, R. (2014). A tidal wave of signals: Calcium and ROS at the forefront of rapid systemic signaling. Trends in Plant Science, 19(10), 623–630.

Gómez-Gómez, L., Bauer, Z., & Boller, T. (2001). Both the extracellular leucine-rich repeat domain and the kinase activity of FSL2 are required for flagellin binding and signaling in Arabidopsis. The Plant Cell, 13(5), 1155–1163.

Gómez-Gómez, L., & Boller, T. (2000). FLS2: An LRR Receptor–like Kinase Involved in the Perception of the Bacterial Elicitor Flagellin in Arabidopsis. Molecular Cell, 5(6), 1003–1011.

Gómez-Gómez, L., Felix, G., & Boller, T. (1999). A single locus determines sensitivity to bacterial flagellin in Arabidopsis thaliana. The Plant Journal: For Cell and Molecular Biology, 18(3), 277–284.

Goto, S., Sasakura-Shimoda, F., Suetsugu, M., Selvaraj, M. G., Hayashi, N., Yamazaki, M., Ishitani, M., Shimono, M., Sugano, S., Matsushita, A., Tanabata, T., & Takatsuji, H. (2015). Development of disease-resistant rice by optimized expression of WRKY45. Plant Biotechnology Journal, 13(6), 753–765.
Gough, C., & Sadanandom, A. (2021). Understanding and Exploiting Post-Translational Modifications for Plant Disease Resistance. Biomolecules, 11(8), 1122.

Grosse-Holz, F., Kelly, S., Blaskowski, S., Kaschani, F., Kaiser, M., & van der Hoorn, R. A. L. (2018). The transcriptome, extracellular proteome and active secretome of agroinfiltrated Nicotiana benthamiana uncover a large, diverse protease repertoire. Plant Biotechnology Journal, 16(5), 1068–1084.

Guo, Q., Major, I. T., & Howe, G. A. (2018). Resolution of growth-defense conflict: Mechanistic insights from jasmonate signaling. Current Opinion in Plant Biology, 44, 72–81.

Gust, A. A., Biswas, R., Lenz, H. D., Rauhut, T., Ranf, S., Kemmerling, B., Götz, F., Glawischnig, E., Lee, J., Felix, G., & Nürnberger, T. (2007). Bacteria-derived peptidoglycans constitute pathogen-associated molecular patterns triggering innate immunity in Arabidopsis. The Journal of Biological Chemistry, 282(44), 32338–32348.

Hadeler, B., Scholz, S., & Reski, R. (1995). Gelrite and Agar Differently Influence Cytokinin-Sensitivity of a Moss. Journal of Plant Physiology, 146(3), 369–371.

Haecker, A., Gross-Hardt, R., Geiges, B., Sarkar, A., Breuninger, H., Herrmann, M., & Laux, T. (2004). Expression dynamics of WOX genes mark cell fate decisions during early embryonic patterning in Arabidopsis thaliana. Development (Cambridge, England), 131(3), 657–668.

Han, S.-K., Qi, X., Sugihara, K., Dang, J. H., Endo, T. A., Miller, K. L., Kim, E.-D., Miura, T., & Torii, K. U. (2018). MUTE Directly Orchestrates Cell-State Switch and the Single Symmetric Division to Create Stomata. Developmental Cell, 45(3), 303-315.e5.

Hanahan, D. (1983). Studies on transformation of Escherichia coli with plasmids. Journal of Molecular Biology, 166(4), 557–580.

Haruta, M., Sabat, G., Stecker, K., Minkoff, B. B., & Sussman, M. R. (2014). A peptide hormone and its receptor protein kinase regulate plant cell expansion. Science (New York, N.Y.), 343(6169), 408–411.

Hase, Y., Trung, K. H., Matsunaga, T., & Tanaka, A. (2006). A mutation in the uvi4 gene promotes progression of endo-reduplication and confers increased tolerance towards ultraviolet B light. The Plant Journal: For Cell and Molecular Biology, 46(2), 317–326.

Haughn, G. W., & Somerville, C. (1986). Sulfonylurea-resistant mutants of Arabidopsis thaliana. Molecular and General Genetics MGG, 204, 430–434.

Hayashi, K., Hasegawa, J., & Matsunaga, S. (2013). The boundary of the meristematic and elongation zones in roots: Endoreduplication precedes rapid cell expansion. Scientific Reports, 3, 2723.

He, Z., Webster, S., & He, S. Y. (2022). Growth-defense trade-offs in plants. Current Biology: CB, 32(12), R634–R639.

Healy, J. M., Menges, M., Doonan, J. H., & Murray, J. A. (2001). The Arabidopsis D-type cyclins CycD2 and CycD3 both interact in vivo with the PSTAIRE cyclin-dependent kinase Cdc2a but are differentially controlled. The Journal of Biological Chemistry, 276(10), 7041–7047.

Heese, A., Hann, D. R., Gimenez-Ibanez, S., Jones, A. M. E., He, K., Li, J., Schroeder, J. I., Peck, S. C., & Rathjen, J. P. (2007). The receptor-like kinase SERK3/BAK1 is a central regulator of innate immunity in plants. Proceedings of the National Academy of Sciences of the United States of America, 104(29), 12217–12222.

Heidstra, R., & Sabatini, S. (2014). Plant and animal stem cells: Similar yet different. Nature Reviews. Molecular Cell Biology, 15(5), 301–312.

Herms, D. A., & Mattson, W. J. (1992). The Dilemma of Plants: To Grow or Defend. The Quarterly Review of Biology, 67(3), 283–335.

Heyman, J., & De Veylder, L. (2012). The anaphase-promoting complex/cyclosome in control of plant development. Molecular Plant, 5(6), 1182–1194.

Huang, L.-C., Curtis Kohashi, Richard Vangundy, & Murashige, T. (1995). Effects of Common Components on Hardness of Culture Media Prepared with GelriteTM. In Vitro Cellular & Developmental Biology. Plant, 31(2), 84–89.

Huffaker, A., Pearce, G., & Ryan, C. A. (2006). An endogenous peptide signal in Arabidopsis activates components of the innate immune response. Proceedings of the National Academy of Sciences of the United States of America, 103(26), 10098–10103.

Huot, B., Yao, J., Montgomery, B. L., & He, S. Y. (2014). Growth-defense tradeoffs in plants: A balancing act to optimize fitness. Molecular Plant, 7(8), 1267–1287.

Iijima, M., Morita, S., & Barlow, P. W. (2008). Structure and function of the root cap. Plant Production Science, 11(1), 17–27.

Inzé, D., & De Veylder, L. (2006). Cell cycle regulation in plant development. Annual Review of Genetics, 40, 77–105.

Iwakawa, H., Shinmyo, A., & Sekine, M. (2006). Arabidopsis CDKA;1, a cdc2 homologue, controls proliferation of generative cells in male gametogenesis. The Plant Journal: For Cell and Molecular Biology, 45(5), 819–831.

Jacobs, S., Zechmann, B., Molitor, A., Trujillo, M., Petutschnig, E., Lipka, V., Kogel, K.-H., & Schäfer, P. (2011). Broad-spectrum suppression of innate immunity is required for colonization of Arabidopsis roots by the fungus Piriformospora indica. Plant Physiology, 156(2), 726–740.

Jacques, C. N., Hulbert, A. K., Westenskow, S., & Neff, M. M. (2020). Production location of the gelling agent Phytagel has a significant impact on Arabidopsis thaliana seedling phenotypic analysis. PLoS ONE, 15(5), e0228515.

Jehle, A. K., Lipschis, M., Albert, M., Fallahzadeh-Mamaghani, V., Fürst, U., Mueller, K., & Felix, G. (2013). The receptor-like protein ReMAX of Arabidopsis detects the microbe-associated molecular pattern eMax from Xanthomonas. The Plant Cell, 25(6), 2330–2340.

Jeworutzki, E., Roelfsema, M. R. G., Anschütz, U., Krol, E., Elzenga, J. T. M., Felix, G., Boller, T., Hedrich, R., & Becker, D. (2010). Early signaling through the Arabidopsis pattern recognition receptors FLS2 and

EFR involves Ca-associated opening of plasma membrane anion channels. The Plant Journal: For Cell and Molecular Biology, 62(3), 367–378.

Jia, N., Liu, X., & Gao, H. (2016). A DNA2 Homolog Is Required for DNA Damage Repair, Cell Cycle Regulation, and Meristem Maintenance in Plants. Plant Physiology, 171(1), 318–333.

Jiang, L., Wang, Y., Björn, L. O., & Li, S. (2011). UV-B-induced DNA damage mediates expression changes of cell cycle regulatory genes in Arabidopsis root tips. Planta, 233(4), 831–841.

Jiang, S., Wei, J., Li, N., Wang, Z., Zhang, Y., Xu, R., Zhou, L., Huang, X., Wang, L., Guo, S., Wang, Y., Song, C.-P., Qian, W., & Li, Y. (2022). The UBP14-CDKB1;1-CDKG2 cascade controls endoreduplication and cell growth in Arabidopsis. The Plant Cell, 34(4), 1308–1325.

Jones, J. D. G., & Dangl, J. L. (2006). The plant immune system. Nature, 444(7117), 323–329.

Jørgensen, I. H. (1992). Discovery, characterization and exploitation of Mlo powdery mildew resistance in barley. Euphytica, 63(1), 141–152.

Kagenishi, T., Yokawa, K., & Baluška, F. (2016). MES Buffer Affects Arabidopsis Root Apex Zonation and Root Growth by Suppressing Superoxide Generation in Root Apex. Frontiers in Plant Science, 7, 79.

Kaku, H., Nishizawa, Y., Ishii-Minami, N., Akimoto-Tomiyama, C., Dohmae, N., Takio, K., Minami, E., & Shibuya, N. (2006). Plant cells recognize chitin fragments for defense signaling through a plasma membrane receptor. Proceedings of the National Academy of Sciences of the United States of America, 103(29), 11086–11091.

Kanno, S., Arrighi, J.-F., Chiarenza, S., Bayle, V., Berthomé, R., Péret, B., Javot, H., Delannoy, E., Marin, E., Nakanishi, T. M., Thibaud, M.-C., & Nussaume, L. (2016). A novel role for the root cap in phosphate uptake and homeostasis. eLife, 5, e14577.

Kawamura, K., Murray, J. A. H., Shinmyo, A., & Sekine, M. (2006). Cell cycle regulated D3-type cyclins form active complexes with plant-specific B-type cyclin-dependent kinase in vitro. Plant Molecular Biology, 61(1–2), 311–327.

Kazan, K., & Manners, J. M. (2009). Linking development to defense: Auxin in plant-pathogen interactions. Trends in Plant Science, 14(7), 373–382.

Kikuchi, S., Horiuchi, A., Nishimoto, Y., & Iwamoto, A. (2023). Different effects of gellan gum and agar on change in root elongation in Arabidopsis thaliana by polyploidization: The key role of aluminum. Journal of Plant Research, 136(2), 253–263.

Klepikova, A. V., Kasianov, A. S., Gerasimov, E. S., Logacheva, M. D., & Penin, A. A. (2016). A high resolution map of the Arabidopsis thaliana developmental transcriptome based on RNA-seq profiling. The Plant Journal: For Cell and Molecular Biology, 88(6), 1058–1070.

Kliebenstein, D. J. (2016). False idolatry of the mythical growth versus immunity tradeoff in molecular systems plant pathology. The U.S.-Japan Scientific Seminar: Molecular Contact Points in Host-Pathogen Co-Evolution, 95, 55–59.

Kono, A., Umeda-Hara, C., Adachi, S., Nagata, N., Konomi, M., Nakagawa, T., Uchimiya, H., & Umeda, M. (2007). The Arabidopsis D-type cyclin CYCD4 controls cell division in the stomatal lineage of the hypocotyl epidermis. The Plant Cell, 19(4), 1265–1277.

Kono, A., Umeda-Hara, C., Lee, J., Ito, M., Uchimiya, H., & Umeda, M. (2003). Arabidopsis D-type cyclin CYCD4;1 is a novel cyclin partner of B2-type cyclin-dependent kinase. Plant Physiology, 132(3), 1315–1321.

Kontra, L., Csorba, T., Tavazza, M., Lucioli, A., Tavazza, R., Moxon, S., Tisza, V., Medzihradszky, A., Turina, M., & Burgyán, J. (2016). Distinct Effects of p19 RNA Silencing Suppressor on Small RNA Mediated Pathways in Plants. PLoS Pathogens, 12(10), e1005935.

Krol, E., Mentzel, T., Chinchilla, D., Boller, T., Felix, G., Kemmerling, B., Postel, S., Arents, M., Jeworutzki, E., Al-Rasheid, K. A. S., Becker, D., & Hedrich, R. (2010). Perception of the Arabidopsis danger signal peptide 1 involves the pattern recognition receptor AtPEPR1 and its close homologue AtPEPR2. The Journal of Biological Chemistry, 285(18), 13471–13479.

Kumar, H., & Asino, G. O. (1994). Grain yield losses in maize (Zea mays L.) genotypes in relation to their resistance against Chilo partellus (Swinhoe) infestation at anthesis. Crop Protection, 13(2), 136–140.

Kumpf, R. P., & Nowack, M. K. (2015). The root cap: A short story of life and death. Journal of Experimental Botany, 66(19), 5651–5662.

Kunze, G., Zipfel, C., Robatzek, S., Niehaus, K., Boller, T., & Felix, G. (2004). The N terminus of bacterial elongation factor Tu elicits innate immunity in Arabidopsis plants. The Plant Cell, 16(12), 3496–3507.

Lakatos, L., Szittya, G., Silhavy, D., & Burgyán, J. (2004). Molecular mechanism of RNA silencing suppression mediated by p19 protein of tombusviruses. The EMBO Journal, 23(4), 876–884.

Lang, L., & Schnittger, A. (2020). Endoreplication—A means to an end in cell growth and stress response. Current Opinion in Plant Biology, 54, 85–92.

Laskowski, M., & Ten Tusscher, K. H. (2017). Periodic Lateral Root Priming: What Makes It Tick? The Plant Cell, 29(3), 432–444. H

Lee, D. H., & Goldberg, A. L. (1998). Proteasome inhibitors: Valuable new tools for cell biologists. Trends in Cell Biology, 8(10), 397–403.

Li, S., Lin, D., Zhang, Y., Deng, M., Chen, Y., Lv, B., Li, B., Lei, Y., Wang, Y., Zhao, L., Liang, Y., Liu, J., Chen, K., Liu, Z., Xiao, J., Qiu, J.-L., & Gao, C. (2022). Genome-edited powdery mildew resistance in wheat without growth penalties. Nature, 602(7897), 455–460.

Lin, W., Lu, D., Gao, X., Jiang, S., Ma, X., Wang, Z., Mengiste, T., He, P., & Shan, L. (2013). Inverse modulation of plant immune and brassinosteroid signaling pathways by the receptor-like cytoplasmic kinase BIK1. Proceedings of the National Academy of Sciences of the United States of America, 110(29), 12114–12119.

Lincoln, C., Britton, J. H., & Estelle, M. (1990). Growth and development of the axr1 mutants of Arabidopsis. The Plant Cell, 2(11), 1071–1080.

Liu, J., Elmore, J. M., Lin, Z.-J. D., & Coaker, G. (2011). A receptor-like cytoplasmic kinase phosphorylates the host target RIN4, leading to the activation of a plant innate immune receptor. Cell Host & Microbe, 9(2), 137–146.

Liu, L., Song, W., Huang, S., Jiang, K., Moriwaki, Y., Wang, Y., Men, Y., Zhang, D., Wen, X., Han, Z., Chai, J., & Guo, H. (2022). Extracellular pH sensing by plant cell-surface peptide-receptor complexes. Cell, 185(18), 3341-3355.e13.

Liu, M., Shi, Z., Zhang, X., Wang, M., Zhang, L., Zheng, K., Liu, J., Hu, X., Di, C., Qian, Q., He, Z., & Yang, D.-L. (2019). Inducible overexpression of Ideal Plant Architecture1 improves both yield and disease resistance in rice. Nature Plants, 5(4), 389–400.

Long, Y., Smet, W., Cruz-Ramírez, A., Castelijns, B., de Jonge, W., Mähönen, A. P., Bouchet, B. P., Perez, G. S., Akhmanova, A., Scheres, B., & Blilou, I. (2015). Arabidopsis BIRD Zinc Finger Proteins Jointly Stabilize Tissue Boundaries by Confining the Cell Fate Regulator SHORT-ROOT and Contributing to Fate Specification. The Plant Cell, 27(4), 1185–1199.

Lozano-Durán, R., Macho, A. P., Boutrot, F., Segonzac, C., Somssich, I. E., & Zipfel, C. (2013). The transcriptional regulator BZR1 mediates trade-off between plant innate immunity and growth. eLife, 2, e00983.

Lozano-Durán, R., & Zipfel, C. (2015). Trade-off between growth and immunity: Role of brassinosteroids. Trends in Plant Science, 20(1), 12–19.

Mabuchi, K., Maki, H., Itaya, T., Suzuki, T., Nomoto, M., Sakaoka, S., Morikami, A., Higashiyama, T., Tada, Y., Busch, W., & Tsukagoshi, H. (2018). MYB30 links ROS signaling, root cell elongation, and plant immune responses. Proceedings of the National Academy of Sciences of the United States of America, 115(20), E4710–E4719.

Madeira, F., Madhusoodanan, N., Lee, J., Eusebi, A., Niewielska, A., Tivey, A. R. N., Lopez, R., & Butcher, S. (2024). The EMBL-EBI Job Dispatcher sequence analysis tools framework in 2024. Nucleic Acids Research, 52(W1), W521–W525.

Magyar, Z., Horváth, B., Khan, S., Mohammed, B., Henriques, R., De Veylder, L., Bakó, L., Scheres, B., & Bögre, L. (2012). Arabidopsis E2FA stimulates proliferation and endocycle separately through RBR-bound and RBR-free complexes. The EMBO Journal, 31(6), 1480–1493.

Margalha, L., Confraria, A., & Baena-González, E. (2019). SnRK1 and TOR: Modulating growth-defense trade-offs in plant stress responses. Journal of Experimental Botany, 70(8), 2261–2274.

Martinez, M. C., Jørgensen, J. E., Lawton, M. A., Lamb, C. J., & Doerner, P. W. (1992). Spatial pattern of cdc2 expression in relation to meristem activity and cell proliferation during plant development. Proceedings of the National Academy of Sciences of the United States of America, 89(16), 7360–7364.

Mase, K., & Tsukagoshi, H. (2021). Reactive Oxygen Species Link Gene Regulatory Networks During Arabidopsis Root Development. Frontiers in Plant Science, 12, 660274.

Matsuda, M., Iwata, Y., Koizumi, N., & Mishiba, K.-I. (2018). DNA double-strand breaks promote endoreduplication in radish cotyledon. Plant Cell Reports, 37(6), 913–921.

Menges, M., Hennig, L., Gruissem, W., & Murray, J. A. H. (2003). Genome-wide gene expression in an Arabidopsis cell suspension. Plant Molecular Biology, 53(4), 423–442.

Millet, Y. A., Danna, C. H., Clay, N. K., Songnuan, W., Simon, M. D., Werck-Reichhart, D., & Ausubel, F. M. (2010). Innate immune responses activated in Arabidopsis roots by microbe-associated molecular patterns. The Plant Cell, 22(3), 973–990.

Mitchell-Olds, T., & Bradley, D. (1996). GENETICS OF BRASSICA RAPA. 3. COSTS OF DISEASE RESISTANCE TO THREE FUNGAL PATHOGENS. Evolution; International Journal of Organic Evolution, 50(5), 1859–1865.

Monjardino, P., Smith, A. G., & Jones, R. J. (2006). Zein Transcription and Endoreduplication in Maize Endosperm are Differentially Affected by Heat Stress. Crop Science, 46(6), 2581–2589.

Monson, R. K., Trowbridge, A. M., Lindroth, R. L., & Lerdau, M. T. (2022). Coordinated resource allocation to plant growth-defense tradeoffs. The New Phytologist, 233(3), 1051–1066.

Morris, J. L., Puttick, M. N., Clark, J. W., Edwards, D., Kenrick, P., Pressel, S., Wellman, C. H., Yang, Z., Schneider, H., & Donoghue, P. C. J. (2018). The timescale of early land plant evolution. Proceedings of the National Academy of Sciences of the United States of America, 115(10), E2274–E2283.

Murashige, T., & Skoog, F. (1962). A Revised Medium for Rapid Growth and Bio Assays with Tobacco Tissue Cultures. Physiologia Plantarum, 15(3), 473–497.

Navarro, L., Bari, R., Achard, P., Lisón, P., Nemri, A., Harberd, N. P., & Jones, J. D. G. (2008). DELLAs control plant immune responses by modulating the balance of jasmonic acid and salicylic acid signaling. Current Biology: CB, 18(9), 650–655.

Neilson, E. H., Goodger, J. Q. D., Woodrow, I. E., & Møller, B. L. (2013). Plant chemical defense: At what cost? Trends in Plant Science, 18(5), 250–258.

Neuser, J., Metzen, C. C., Dreyer, B. H., Feulner, C., van Dongen, J. T., Schmidt, R. R., & Schippers, J. H. M. (2019). HBI1 Mediates the Trade-off between Growth and Immunity through Its Impact on Apoplastic ROS Homeostasis. Cell Reports, 28(7), 1670-1678.e3.

Newman, M.-A., Sundelin, T., Nielsen, J. T., & Erbs, G. (2013). MAMP (microbe-associated molecular pattern) triggered immunity in plants. Frontiers in Plant Science, 4, 139.

Ngou, B. P. M., Ahn, H.-K., Ding, P., & Jones, J. D. G. (2021). Mutual potentiation of plant immunity by cell-surface and intracellular receptors. Nature, 592(7852), 110–115.

Ning, Y., Liu, W., & Wang, G.-L. (2017). Balancing Immunity and Yield in Crop Plants. Trends in Plant Science, 22(12), 1069–1079.

Nisa, M.-U., Huang, Y., Benhamed, M., & Raynaud, C. (2019). The Plant DNA Damage Response: Signaling Pathways Leading to Growth Inhibition and Putative Role in Response to Stress Conditions. Frontiers in Plant Science, 10, 653.

Nobori, T., & Ecker, J. R. (2023). Yet uninfected? Resolving cell states of plants under pathogen attack. Cell Reports Methods, 3(7), 100538.

Nugent, J. H., Alfa, C. E., Young, T., & Hyams, J. S. (1991). Conserved structural motifs in cyclins identified by sequence analysis. Journal of Cell Science, 99 (Pt 3), 669–674.

Oakenfull, E. A., Riou-Khamlichi, C., & Murray, J. A. H. (2002). Plant D-type cyclins and the control of G1 progression. Philosophical Transactions of the Royal Society of London. Series B, Biological Sciences, 357(1422), 749–760.

Ogita, N., Okushima, Y., Tokizawa, M., Yamamoto, Y. Y., Tanaka, M., Seki, M., Makita, Y., Matsui, M., Okamoto-Yoshiyama, K., Sakamoto, T., Kurata, T., Hiruma, K., Saijo, Y., Takahashi, N., & Umeda, M. (2018). Identifying the target genes of SUPPRESSOR OF GAMMA RESPONSE 1, a master transcription factor controlling DNA damage response in Arabidopsis. The Plant Journal: For Cell and Molecular Biology, 94(3), 439–453.

Okushima, Y., Shimizu, K., Ishida, T., Sugimoto, K., & Umeda, M. (2014). Differential regulation of B2-type CDK accumulation in Arabidopsis roots. Plant Cell Reports, 33(7), 1033–1040.

Ortega, M. A., Celoy, R. M., Chacon, F., Yuan, Y., Xue, L.-J., Pandey, S. P., Drowns, M. R., Kvitko, B. H., & Tsai, C.-J. (2024). Altering cold-regulated gene expression decouples the salicylic acid-growth trade-off in Arabidopsis. The Plant Cell, 36(10), 4293–4308.

Pardal, R., & Heidstra, R. (2021). Root stem cell niche networks: It's complexed! Insights from Arabidopsis. Journal of Experimental Botany, 72(19), 6727–6738.

Pedroza-Garcia, J. A., Xiang, Y., & De Veylder, L. (2022). Cell cycle checkpoint control in response to DNA damage by environmental stresses. The Plant Journal: For Cell and Molecular Biology, 109(3), 490–507.

Pequeno, D. N. L., Ferreira, T. B., Fernandes, J. M. C., Singh, P. K., Pavan, W., Sonder, K., Robertson, R., Krupnik, T. J., Erenstein, O., & Asseng, S. (2024). Production vulnerability to wheat blast disease under climate change. Nature Climate Change, 14(2), 178–183.

Perilli, S., Di Mambro, R., & Sabatini, S. (2012). Growth and development of the root apical meristem. Current Opinion in Plant Biology, 15(1), 17–23.

Petricka, J. J., Winter, C. M., & Benfey, P. N. (2012). Control of Arabidopsis root development. Annual Review of Plant Biology, 63, 563–590.

Planchais, S., Glab, N., Inzé, D., & Bergounioux, C. (2000). Chemical inhibitors: A tool for plant cell cycle studies. FEBS Letters, 476(1–2), 78–83.

Polyn, S., Willems, A., & De Veylder, L. (2015). Cell cycle entry, maintenance, and exit during plant development. Current Opinion in Plant Biology, 23, 1–7.

Poncini, L., Wyrsch, I., Dénervaud Tendon, V., Vorley, T., Boller, T., Geldner, N., Métraux, J.-P., & Lehmann, S. (2017). In roots of Arabidopsis thaliana, the damage-associated molecular pattern AtPep1 is a stronger elicitor of immune signalling than flg22 or the chitin heptamer. PloS One, 12(10), e0185808.

Pruitt, R. N., Locci, F., Wanke, F., Zhang, L., Saile, S. C., Joe, A., Karelina, D., Hua, C., Fröhlich, K., Wan, W.-L., Hu, M., Rao, S., Stolze, S. C., Harzen, A., Gust, A. A., Harter, K., Joosten, M. H. A. J., Thomma, B.

P. H. J., Zhou, J.-M., … Nürnberger, T. (2021). The EDS1-PAD4-ADR1 node mediates Arabidopsis pattern-triggered immunity. Nature, 598(7881), 495–499.

Qi, F., & Zhang, F. (2019). Cell Cycle Regulation in the Plant Response to Stress. Frontiers in Plant Science, 10, 1765.

Qi, R., & John, P. C. L. (2007). Expression of genomic AtCYCD2;1 in Arabidopsis induces cell division at smaller cell sizes: Implications for the control of plant growth. Plant Physiology, 144(3), 1587–1597.

Raaijmakers, J. M., Paulitz, T. C., Steinberg, C., Alabouvette, C., & Moënne-Loccoz, Y. (2009). The rhizosphere: A playground and battlefield for soilborne pathogens and beneficial microorganisms. Plant and Soil, 321(1), 341–361.

Rechsteiner, M., & Rogers, S. W. (1996). PEST sequences and regulation by proteolysis. Trends in Biochemical Sciences, 21(7), 267–271.

Rehman, M., Saeed, M. S., Fan, X., Salam, A., Munir, R., Yasin, M. U., Khan, A. R., Muhammad, S., Ali, B., Ali, I., Khan, J., & Gan, Y. (2023). The Multifaceted Role of Jasmonic Acid in Plant Stress Mitigation: An Overview. Plants (Basel, Switzerland), 12(23), 3982.

Reitz, M. U., Gifford, M. L., & Schäfer, P. (2015). Hormone activities and the cell cycle machinery in immunity-triggered growth inhibition. Journal of Experimental Botany, 66(8), 2187–2197.

Rich-Griffin, C., Eichmann, R., Reitz, M. U., Hermann, S., Woolley-Allen, K., Brown, P. E., Wiwatdirekkul, K., Esteban, E., Pasha, A., Kogel, K.-H., Provart, N. J., Ott, S., & Schäfer, P. (2020). Regulation of Cell Type-Specific Immunity Networks in Arabidopsis Roots. The Plant Cell, 32(9), 2742–2762.

Riou-Khamlichi, C., Menges, M., Healy, J. M., & Murray, J. A. (2000). Sugar control of the plant cell cycle: Differential regulation of Arabidopsis D-type cyclin gene expression. Molecular and Cellular Biology, 20(13), 4513–4521.

Robbins, N. E., Trontin, C., Duan, L., & Dinneny, J. R. (2014). Beyond the barrier: Communication in the root through the endodermis. Plant Physiology, 166(2), 551–559.

Rymen, B., & Sugimoto, K. (2012). Tuning growth to the environmental demands. Current Opinion in Plant Biology, 15(6), 683–690.

Rzemieniewski, J., Leicher, H., Lee, H. K., Broyart, C., Nayem, S., Wiese, C., Maroschek, J., Camgöz, Z., Olsson Lalun, V., Djordjevic, M. A., Vlot, A. C., Hückelhoven, R., Santiago, J., & Stegmann, M. (2024). CEP signaling coordinates plant immunity with nitrogen status. Nature Communications, 15(1), 10686.

Rzemieniewski, J., & Stegmann, M. (2022). Regulation of pattern-triggered immunity and growth by phytocytokines. Current Opinion in Plant Biology, 68, 102230.

Sablowski, R., & Carnier Dornelas, M. (2014). Interplay between cell growth and cell cycle in plants. Journal of Experimental Botany, 65(10), 2703–2714.

Sablowski, R., & Gutierrez, C. (2022). Cycling in a crowd: Coordination of plant cell division, growth, and cell fate. The Plant Cell, 34(1), 193–208.

Saijo, Y., & Loo, E. P.-I. (2020). Plant immunity in signal integration between biotic and abiotic stress responses. The New Phytologist, 225(1), 87–104.

Salvi, E., Di Mambro, R., & Sabatini, S. (2020). Dissecting mechanisms in root growth from the transition zone perspective. Journal of Experimental Botany, 71(8), 2390–2396.

Sanz, L., Dewitte, W., Forzani, C., Patell, F., Nieuwland, J., Wen, B., Quelhas, P., De Jager, S., Titmus, C., Campilho, A., Ren, H., Estelle, M., Wang, H., & Murray, J. A. H. (2011). The Arabidopsis D-type cyclin CYCD2;1 and the inhibitor ICK2/KRP2 modulate auxin-induced lateral root formation. The Plant Cell, 23(2), 641–660.

Sarkar, A. K., Luijten, M., Miyashima, S., Lenhard, M., Hashimoto, T., Nakajima, K., Scheres, B., Heidstra, R., & Laux, T. (2007). Conserved factors regulate signalling in Arabidopsis thaliana shoot and root stem cell organizers. Nature, 446(7137), 811–814.

Sarris, P. F., Duxbury, Z., Huh, S. U., Ma, Y., Segonzac, C., Sklenar, J., Derbyshire, P., Cevik, V., Rallapalli, G., Saucet, S. B., Wirthmueller, L., Menke, F. L. H., Sohn, K. H., & Jones, J. D. G. (2015). A Plant Immune Receptor Detects Pathogen Effectors that Target WRKY Transcription Factors. Cell, 161(5), 1089–1100.

Schindelin, J., Arganda-Carreras, I., Frise, E., Kaynig, V., Longair, M., Pietzsch, T., Preibisch, S., Rueden, C., Saalfeld, S., Schmid, B., Tinevez, J.-Y., White, D. J., Hartenstein, V., Eliceiri, K., Tomancak, P., & Cardona, A. (2012). Fiji: An open-source platform for biological-image analysis. Nature Methods, 9(7), 676–682.

Schmittgen, T. D., & Livak, K. J. (2008). Analyzing real-time PCR data by the comparative C(T) method. Nature Protocols, 3(6), 1101–1108.

Segonzac, C., Feike, D., Gimenez-Ibanez, S., Hann, D. R., Zipfel, C., & Rathjen, J. P. (2011). Hierarchy and roles of pathogen-associated molecular pattern-induced responses in Nicotiana benthamiana. Plant Physiology, 156(2), 687–699.

Sestari, I., & Campos, M. L. (2022). Into a dilemma of plants: The antagonism between chemical defenses and growth. Plant Molecular Biology, 109(4–5), 469–482.

Shabala, S., White, R. G., Djordjevic, M. A., Ruan, Y.-L., & Mathesius, U. (2016). Root-to-shoot signalling: Integration of diverse molecules, pathways and functions. Functional Plant Biology: FPB, 43(2), 87–104

Shahan, R., Hsu, C.-W., Nolan, T. M., Cole, B. J., Taylor, I. W., Greenstreet, L., Zhang, S., Afanassiev, A., Vlot, A. H. C., Schiebinger, G., Benfey, P. N., & Ohler, U. (2022). A single-cell Arabidopsis root atlas reveals developmental trajectories in wild-type and cell identity mutants. Developmental Cell, 57(4), 543-560.e9.

Shan, L., He, P., Li, J., Heese, A., Peck, S. C., Nürnberger, T., Martin, G. B., & Sheen, J. (2008). Bacterial effectors target the common signaling partner BAK1 to disrupt multiple MAMP receptor-signaling complexes and impede plant immunity. Cell Host & Microbe, 4(1), 17–27.

Sharp, G. L., Martin, J. M., Lanning, S. P., Blake, N. K., Brey, C. W., Sivamani, E., Qu, R., & Talbert, L. E. (2002). Field Evaluation of Transgenic and Classical Sources of Wheat streak mosaic virus Resistance. Crop Science, 42(1), 105–110.

Sherr, C. J. (1995). D-type cyclins. Trends in Biochemical Sciences, 20(5), 187–190.

Shi, H., Shen, Q., Qi, Y., Yan, H., Nie, H., Chen, Y., Zhao, T., Katagiri, F., & Tang, D. (2013). BR-SIGNALING KINASE1 physically associates with FLAGELLIN SENSING2 and regulates plant innate immunity in Arabidopsis. The Plant Cell, 25(3), 1143–1157.

Shi, Y., Lee, L.-Y., & Gelvin, S. B. (2014). Is VIP1 important for Agrobacterium-mediated transformation? The Plant Journal: For Cell and Molecular Biology, 79(5), 848–860.

Shimada, T. L., Shimada, T., & Hara-Nishimura, I. (2010). A rapid and non-destructive screenable marker, FAST, for identifying transformed seeds of Arabidopsis thaliana. The Plant Journal: For Cell and Molecular Biology, 61(3), 519–528.

Shimotohno, A., Aki, S. S., Takahashi, N., & Umeda, M. (2021). Regulation of the Plant Cell Cycle in Response to Hormones and the Environment. Annual Review of Plant Biology, 72, 273–296.

Shungu, D., Valiant, M., Tutlane, V., Weinberg, E., Weissberger, B., Koupal, L., Gadebusch, H., & Stapley, E. (1983). GELRITE as an Agar Substitute in Bacteriological Media. Applied and Environmental Microbiology, 46(4), 840–845.

Simillion, C., Vandepoele, K., Van Montagu, M. C. E., Zabeau, M., & Van de Peer, Y. (2002). The hidden duplication past of Arabidopsis thaliana. Proceedings of the National Academy of Sciences of the United States of America, 99(21), 13627–13632.

Singh, B. K., Delgado-Baquerizo, M., Egidi, E., Guirado, E., Leach, J. E., Liu, H., & Trivedi, P. (2023). Climate change impacts on plant pathogens, food security and paths forward. Nature Reviews. Microbiology, 21(10), 640–656.

Smakowska, E., Kong, J., Busch, W., & Belkhadir, Y. (2016). Organ-specific regulation of growth-defense tradeoffs by plants. Current Opinion in Plant Biology, 29, 129–137.

Smedegaard-Petersen, V., & Tolstrup, K. (1985). The Limiting Effect of Disease Resistance on Yield. Annual Review of Phytopathology, 23(Volume 23,), 475–490.

Song, J., & Bent, A. F. (2014). Microbial pathogens trigger host DNA double-strand breaks whose abundance is reduced by plant defense responses. PLoS Pathogens, 10(4), e1004030.

Sornay, E., Dewitte, W., & Murray, J. a. H. (2016). Seed size plasticity in response to embryonic lethality conferred by ectopic CYCD activation is dependent on plant architecture. Plant Signaling & Behavior, 11(7), e1192741.

Sorrell, D. A., Combettes, B., Chaubet-Gigot, N., Gigot, C., & Murray, J. A. (1999). Distinct cyclin D genes show mitotic accumulation or constant levels of transcripts in tobacco bright yellow-2 cells. Plant Physiology, 119(1), 343–352.

Sozzani, R., Cui, H., Moreno-Risueno, M. A., Busch, W., Van Norman, J. M., Vernoux, T., Brady, S. M., Dewitte, W., Murray, J. a. H., & Benfey, P. N. (2010). Spatiotemporal regulation of cell-cycle genes by SHORTROOT links patterning and growth. Nature, 466(7302), 128–132.

Spoel, S. H., & Dong, X. (2008). Making sense of hormone crosstalk during plant immune responses. Cell Host & Microbe, 3(6), 348–351.

Staswick, P. E., Su, W., & Howell, S. H. (1992). Methyl jasmonate inhibition of root growth and induction of a leaf protein are decreased in an Arabidopsis thaliana mutant. Proceedings of the National Academy of Sciences of the United States of America, 89(15), 6837–6840.

Stegmann, M., Monaghan, J., Smakowska-Luzan, E., Rovenich, H., Lehner, A., Holton, N., Belkhadir, Y., & Zipfel, C. (2017). The receptor kinase FER is a RALF-regulated scaffold controlling plant immune signaling. Science (New York, N.Y.), 355(6322), 287–289.

Stegmann, M., Zecua-Ramirez, P., Ludwig, C., Lee, H.-S., Peterson, B., Nimchuk, Z. L., Belkhadir, Y., & Hückelhoven, R. (2022). RGI-GOLVEN signaling promotes cell surface immune receptor abundance to regulate plant immunity. EMBO Reports, 23(5), e53281.

Strotmann, V. I., & Stahl, Y. (2021). At the root of quiescence: Function and regulation of the quiescent center. Journal of Experimental Botany, 72(19), 6716–6726.

Strzalka, W. K., Aggarwal, C., Krzeszowiec, W., Jakubowska, A., Sztatelman, O., & Banas, A. K. (2015). Arabidopsis PCNAs form complexes with selected D-type cyclins. Frontiers in Plant Science, 6, 516.

Sugimoto-Shirasu, K., & Roberts, K. (2003). 'Big it up': Endoreduplication and cell-size control in plants. Current Opinion in Plant Biology, 6(6), 544–553.

Sun, L., & Tobin, E. M. (1990). Phytochrome-regulated expression of genes encoding light-harvesting chlorophyll a/b-protein in two long hypocotyl mutants and wild type plants of Arabidopsis thaliana. Photochemistry and Photobiology, 52(1), 51–56.

Sun, T. (2010). Gibberellin-GID1-DELLA: A pivotal regulatory module for plant growth and development. Plant Physiology, 154(2), 567–570.

Sun, Y., Li, L., Macho, A. P., Han, Z., Hu, Z., Zipfel, C., Zhou, J.-M., & Chai, J. (2013). Structural basis for flg22-induced activation of the Arabidopsis FLS2-BAK1 immune complex. Science (New York, N.Y.), 342(6158), 624–628

Sundell, D., Mannapperuma, C., Netotea, S., Delhomme, N., Lin, Y.-C., Sjödin, A., Van de Peer, Y., Jansson, S., Hvidsten, T. R., & Street, N. R. (2015). The Plant Genome Integrative Explorer Resource: PlantGenIE.org. New Phytologist, 208(4), 1149–1156.

Szurman-Zubrzycka, M., Jędrzejek, P., & Szarejko, I. (2023). How Do Plants Cope with DNA Damage? A Concise Review on the DDR Pathway in Plants. International Journal of Molecular Sciences, 24(3), 2404.

Taiz, & Zeiger. (1991). Plant Physiology.

Tegeder, M., & Hammes, U. Z. (2018). The way out and in: Phloem loading and unloading of amino acids. Current Opinion in Plant Biology, 43, 16–21.

Tena, G. (2021). PTI and ETI are one. Nature Plants, 7(12), 1527.

Tilman, D., Balzer, C., Hill, J., & Befort, B. L. (2011). Global food demand and the sustainable intensification of agriculture. Proceedings of the National Academy of Sciences, 108(50), 20260–20264.

Tiwari, M., Mishra, A. K., & Chakrabarty, D. (2022). Agrobacterium-mediated gene transfer: Recent advancements and layered immunity in plants. Planta, 256(2), 37.

Tomescu, A. M. F. (2021). The stele—A developmental perspective on the diversity and evolution of primary vascular architecture. Biological Reviews of the Cambridge Philosophical Society, 96(4), 1263–1283.

Topp, C. N., & Benfey, P. N. (2012). Growth control of root architecture. Plant Biotechnology and Agriculture, 373–386.

Umeda, M., Shimotohno, A., & Yamaguchi, M. (2005). Control of cell division and transcription by cyclin-dependent kinase-activating kinases in plants. Plant & Cell Physiology, 46(9), 1437–1442.

UniProt Consortium, T. (2018). UniProt: The universal protein knowledgebase. Nucleic Acids Research, 46(5), 2699.

United Nations. (2019). World Population Prospects 2019: Highlights. Department of Economic and Social Affairs.

Ursache, R., Andersen, T. G., Marhavý, P., & Geldner, N. (2018). A protocol for combining fluorescent proteins with histological stains for diverse cell wall components. The Plant Journal, 93(2), 399–412.

Üstüner, S., Schäfer, P., & Eichmann, R. (2022). Development specifies, diversifies and empowers root immunity. EMBO Reports, 23(12), e55631.

Val-Torregrosa, B., Bundó, M., & San Segundo, B. (2021). Crosstalk between Nutrient Signalling Pathways and Immune Responses in Rice. Agriculture, 11(8).

van den Berg, C., Willemsen, V., Hendriks, G., Weisbeek, P., & Scheres, B. (1997). Short-range control of cell differentiation in the Arabidopsis root meristem. Nature, 390(6657), 287–289.

Van Leene, J., Hollunder, J., Eeckhout, D., Persiau, G., Van De Slijke, E., Stals, H., Van Isterdael, G., Verkest, A., Neirynck, S., Buffel, Y., De Bodt, S., Maere, S., Laukens, K., Pharazyn, A., Ferreira, P. C. G., Eloy, N., Renne, C., Meyer, C., Faure, J.-D., … De Jaeger, G. (2010). Targeted interactomics reveals a complex core cell cycle machinery in Arabidopsis thaliana. Molecular Systems Biology, 6, 397.

van Wersch, R., Li, X., & Zhang, Y. (2016). Mighty Dwarfs: Arabidopsis Autoimmune Mutants and Their Usages in Genetic Dissection of Plant Immunity. Frontiers in Plant Science, 7, 1717.

Vandepoele, K., Raes, J., De Veylder, L., Rouzé, P., Rombauts, S., & Inzé, D. (2002). Genome-wide analysis of core cell cycle genes in Arabidopsis. The Plant Cell, 14(4), 903–916.

Veylder, L. D., Segers, G., Glab, N., Van Montagu, M., & Inzé, D. (1997). Identification of proteins interacting with the Arabidopsis Cdc2aAt protein. Journal of Experimental Botany, 48(12), 2113–2114.

Vyska, M., Cunniffe, N., & Gilligan, C. (2016). Trade-off between disease resistance and crop yield: A landscape-scale mathematical modelling perspective. Journal of the Royal Society, Interface, 13(123), 20160451.

Wang, J., Long, X., Chern, M., & Chen, X. (2021a). Understanding the molecular mechanisms of trade-offs between plant growth and immunity. Science China. Life Sciences, 64(2), 234–241.

Wang, J., Zhou, L., Shi, H., Chern, M., Yu, H., Yi, H., He, M., Yin, J., Zhu, X., Li, Y., Li, W., Liu, J., Wang, J., Chen, X., Qing, H., Wang, Y., Liu, G., Wang, W., Li, P., … Chen, X. (2018). A single transcription factor promotes both yield and immunity in rice. Science (New York, N.Y.), 361(6406), 1026–1028.

Wang, L., Tsuda, K., Sato, M., Cohen, J. D., Katagiri, F., & Glazebrook, J. (2009). Arabidopsis CaM binding protein CBP60g contributes to MAMP-induced SA accumulation and is involved in disease resistance against Pseudomonas syringae. PLoS Pathogens, 5(2), e1000301.

Wang, L., Zhan, L., Zhao, Y., Huang, Y., Wu, C., Pan, T., Qin, Q., Xu, Y., Deng, Z., Li, J., Hu, H., Xue, S., & Yan, S. (2021b). The ATR-WEE1 kinase module inhibits the MAC complex to regulate replication stress response. Nucleic Acids Research, 49(3), 1411–1425.

Wang, Y., Li, J., Hou, S., Wang, X., Li, Y., Ren, D., Chen, S., Tang, X., & Zhou, J.-M. (2010). A Pseudomonas syringae ADP-ribosyltransferase inhibits Arabidopsis mitogen-activated protein kinase kinases. The Plant Cell, 22(6), 2033–2044.

Wang, Y., Li, Z., Liu, D., Xu, J., Wei, X., Yan, L., Yang, C., Lou, Z., & Shui, W. (2014). Assessment of BAK1 activity in different plant receptor-like kinase complexes by quantitative profiling of phosphorylation patterns. Journal of Proteomics, 108, 484–493.

Wasternack, C. (2007). Jasmonates: An update on biosynthesis, signal transduction and action in plant stress response, growth and development. Annals of Botany, 100(4), 681–697.

Waterhouse, A. M., Procter, J. B., Martin, D. M. A., Clamp, M., & Barton, G. J. (2009). Jalview Version 2—A multiple sequence alignment editor and analysis workbench. Bioinformatics (Oxford, England), 25(9), 1189–1191.

Weber, E., Engler, C., Gruetzner, R., Werner, S., & Marillonnet, S. (2011). A modular cloning system for standardized assembly of multigene constructs. PloS One, 6(2), e16765.

Weimer, A. K., Biedermann, S., Harashima, H., Roodbarkelari, F., Takahashi, N., Foreman, J., Guan, Y., Pochon, G., Heese, M., Van Damme, D., Sugimoto, K., Koncz, C., Doerner, P., Umeda, M., & Schnittger, A. (2016). The plant-specific CDKB1-CYCB1 complex mediates homologous recombination repair in Arabidopsis. The EMBO Journal, 35(19), 2068–2086.

Weimer, A. K., Matos, J. L., Sharma, N., Patell, F., Murray, J. A. H., Dewitte, W., & Bergmann, D. C. (2018). Lineage- and stage-specific expressed CYCD7;1 coordinates the single symmetric division that creates stomatal guard cells. Development (Cambridge, England), 145(6), dev160671.

West, G., Inzé, D., & Beemster, G. T. S. (2004). Cell cycle modulation in the response of the primary root of Arabidopsis to salt stress. Plant Physiology, 135(2), 1050–1058.

Winnicki, K., Polit, J. T., & Maszewski, J. (2013). Increased transcription in hydroxyurea-treated root meristem cells of Vicia faba. Protoplasma, 250(1), 251–259.

Withers, J., & Dong, X. (2017). Post-translational regulation of plant immunity. Current Opinion in Plant Biology, 38, 124–132.

World Resources Institute. (2019). Creating a sustainable food future: A menu of solutions to feed nearly 10 billion people by 2050.

Wyrsch, I., Domínguez-Ferreras, A., Geldner, N., & Boller, T. (2015). Tissue-specific FLAGELLIN-SENSING 2 (FLS2) expression in roots restores immune responses in Arabidopsis fls2 mutants. The New Phytologist, 206(2), 774–784.

Xiao, Y., Stegmann, M., Han, Z., DeFalco, T. A., Parys, K., Xu, L., Belkhadir, Y., Zipfel, C., & Chai, J. (2019). Mechanisms of RALF peptide perception by a heterotypic receptor complex. Nature, 572(7768), 270–274.

Xie, C., Li, C., Wang, F., Zhang, F., Liu, J., Wang, J., Zhang, X., Kong, X., & Ding, Z. (2023). NAC1 regulates root ground tissue maturation by coordinating with the SCR/SHR-CYCD6;1 module in Arabidopsis. Molecular Plant, 16(4), 709–725.

Xie, Z., Lee, E., Lucas, J. R., Morohashi, K., Li, D., Murray, J. A. H., Sack, F. D., & Grotewold, E. (2010). Regulation of cell proliferation in the stomatal lineage by the Arabidopsis MYB FOUR LIPS via direct targeting of core cell cycle genes. The Plant Cell, 22(7), 2306–2321.

Yamaguchi, Y., Huffaker, A., Bryan, A. C., Tax, F. E., & Ryan, C. A. (2010). PEPR2 is a second receptor for the Pep1 and Pep2 peptides and contributes to defense responses in Arabidopsis. The Plant Cell, 22(2), 508–522.

Yamaguchi, Y., Pearce, G., & Ryan, C. A. (2006). The cell surface leucine-rich repeat receptor for AtPep1, an endogenous peptide elicitor in Arabidopsis, is functional in transgenic tobacco cells. Proceedings of the National Academy of Sciences of the United States of America, 103(26), 10104–10109.

Yang, K., Wang, H., Xue, S., Qu, X., Zou, J., & Le, J. (2014). Requirement for A-type cyclin-dependent kinase and cyclins for the terminal division in the stomatal lineage of Arabidopsis. Journal of Experimental Botany, 65(9), 2449–2461.

Yi, D., Alvim Kamei, C. L., Cools, T., Vanderauwera, S., Takahashi, N., Okushima, Y., Eekhout, T., Yoshiyama, K. O., Larkin, J., Van den Daele, H., Conklin, P., Britt, A., Umeda, M., & De Veylder, L. (2014). The Arabidopsis SIAMESE-RELATED cyclin-dependent kinase inhibitors SMR5 and SMR7 regulate the DNA damage checkpoint in response to reactive oxygen species. The Plant Cell, 26(1), 296–309.

Yoshiyama, K., Conklin, P. A., Huefner, N. D., & Britt, A. B. (2009). Suppressor of gamma response 1 (SOG1) encodes a putative transcription factor governing multiple responses to DNA damage. Proceedings of the National Academy of Sciences of the United States of America, 106(31), 12843–12848.

Yoshiyama, K. O., Kobayashi, J., Ogita, N., Ueda, M., Kimura, S., Maki, H., & Umeda, M. (2013). ATM-mediated phosphorylation of SOG1 is essential for the DNA damage response in Arabidopsis. EMBO Reports, 14(9), 817–822.

Yu, K., Liu, Y., Tichelaar, R., Savant, N., Lagendijk, E., van Kuijk, S. J. L., Stringlis, I. A., van Dijken, A. J. H., Pieterse, C. M. J., Bakker, P. A. H. M., Haney, C. H., & Berendsen, R. L. (2019a). Rhizosphere-Associated Pseudomonas Suppress Local Root Immune Responses by Gluconic Acid-Mediated Lowering of Environmental pH. Current Biology: CB, 29(22), 3913-3920.e4.

Yu, K., Pieterse, C. M. J., Bakker, P. A. H. M., & Berendsen, R. L. (2019b). Beneficial microbes going underground of root immunity. Plant, Cell & Environment, 42(10), 2860–2870.

Yuan, M., Jiang, Z., Bi, G., Nomura, K., Liu, M., Wang, Y., Cai, B., Zhou, J.-M., He, S. Y., & Xin, X.-F. (2021a). Pattern-recognition receptors are required for NLR-mediated plant immunity. Nature, 592(7852), 105–109.

Yuan, M., Ngou, B. P. M., Ding, P., & Xin, X.-F. (2021b). PTI-ETI crosstalk: An integrative view of plant immunity. Current Opinion in Plant Biology, 62, 102030.

Zhang, G., Ueberheide, B. M., Waldemarson, S., Myung, S., Molloy, K., Eriksson, J., Chait, B. T., Neubert, T. A., & Fenyö, D. (2010). Protein quantitation using mass spectrometry. Methods in Molecular Biology (Clifton, N.J.), 673, 211–222.

Zhang, X., Yang, Z., Wu, D., & Yu, F. (2020). RALF-FERONIA Signaling: Linking Plant Immune Response with Cell Growth. Plant Communications, 1(4), 100084.

Zhou, F., Emonet, A., Dénervaud Tendon, V., Marhavy, P., Wu, D., Lahaye, T., & Geldner, N. (2020). Co-incidence of Damage and Microbial Patterns Controls Localized Immune Responses in Roots. Cell, 180(3), 440-453.e18.

Zhou, J.-M., & Zhang, Y. (2020). Plant Immunity: Danger Perception and Signaling. Cell, 181(5), 978–989.

Zuo, J., Niu, Q. W., & Chua, N. H. (2000). Technical advance: An estrogen receptor-based transactivator XVE mediates highly inducible gene expression in transgenic plants. The Plant Journal: For Cell and Molecular Biology, 24(2), 265–273.

Züst, T., & Agrawal, A. A. (2017). Trade-Offs Between Plant Growth and Defense Against Insect Herbivory: An Emerging Mechanistic Synthesis. Annual Review of Plant Biology, 68, 513–534.

Supplementary Data

Table S1: Primers used in this work

Primer name	Sequence (5`to 3`)	Purpose
tGFP_for_Cter_fw	TTGAAGACAACTCAAATGAGAGGATCTGGATCTGAGTCTG	Golden Gate cloning
tGFP_for_Cter_re	TTGAAGACAACTCGCGAATCCTCACCAGCATCAGCATCAG	Golden Gate cloning
L0_UA_fw	TTACGGTTCCTGCACTCTGTG	Colony PCR L0 UA+ seq
L0_UA_rev	GCTTATGTCCACTGGGTTCGT	Colony PCR L0 UA+seq
GG_L0_f2	GTGAGCGAGGAAGCGGAAG	Colony PCR L0+seq
GG_L0_re	GTCTCATGAGCGGATACATATTTGAATG	Colony PCR L0 +seq
GG_L1_fw	GAACCCTGTGGTTGGCATGCACATAC	Colony PCR L1 +seq
GG_L1_re	CTGGTGGCAGGATATATTGTGGTG	Colony PCR L1 + seq
pGY1-fwd	TGACGCACAATCCCACTAT	Colony PCR
FASTR_int_fwd	CATCTACAACGTCAAGATCAGA	Colony PCR+ seq
FASTR_int_rev	CATCTACAACGTCAAGATCAGA	Colony PCR+ seq
L2_rev_to_linker	CATCTACAACGTCAAGATCAGA	Colony PCR
FASTRfPmeI	GTTTAAACAAGCTTGGAGTTCTAGAATG	Cloning
FASTRrPmeI	GTTTAAACAGCGACTAAATGGAGCAACC	Cloning
AtCDKA,1_pgfwdRsrII	CGGTCCGTCCGTCGGTGTGCTAGTCT	Cloning
AtCDKA,1_pgrevBamHI	GGATCCTCCATTAACAGCATTTTCT	Cloning
AtCDKB1,1_pgfwdRsrII	CGGTCCGGAATTTGTAGCTTTCAAA	Cloning
AtCDKB1,1_pgrevBamHI	GGATCCGAACTGAGACTTGTCAAGG	Cloning
AtCDKB1,2_pgfwdRsrII	CGGTCCGTTTCCCCTTTACATAGAA	Cloning
AtCDKB1,2_pgrevBamHI	GGATCCGAACTGAGATTTGTCAAG	Cloning
AtCDKB2,1_pgfwdRsrII	CGGTCCGAATTCTGGTTCTACTACGAT	Cloning
AtCDKB2,1_pgrevBamHI	GGATCCATCCATCAAGAGATTGTG	Cloning
AtCDKB2,2_pgfwdRsrII	CGGTCCGACATTTAGGGCCTATAGAT	Cloning
AtCDKB2,2_pgrevBamHI	GGATCCGAGAGAGGACTTGTCAGG	Cloning
AtCYCD1,1_pgfwdRsrII	CGGTCCGAACTGATTTATCATACGGTT	Cloning
AtCYCD1,1_pgrevBamHI	GGATCCATTAGAGGTAGATGTTTCA	Cloning
AtCYCD2,1_pgfwdRsrII	CGGTCCGAGAAACATAGCCTTAGCT	Cloning
AtCYCD2,1_pgrevBamHI	GGATCCTTGTTTTCTCCTCCTCT	Cloning
AtCYCD3,1_pgfwdRsrII	CGGTCCGAGCGTTTGGCGTTTAGAA	Cloning
AtCYCD3,1_pgrevBamHI	GGATCCTGGAGTGGCTACGATTGCCCA	Cloning
AtCYCD3,2_pgfwdRsrII	CGGTCCGCTTTCATTTGAATAATAT	Cloning
AtCYCD3,2_pgrevBamHI	GGATCCGCGGCGACGTTCTAGTCGG	Cloning
AtCYCD3,3_pgfwdRsrII	CGGTCCGTTTCCTAGTTAATTATGTT	Cloning
AtCYCD3,3_pgrevBamHI	GGATCCGCGAGGACTACTACTAAG	Cloning
AtCYCD4,1_pgfwdRsrII	CGGTCCGAGATATTGAAATTATTGT	Cloning
AtCYCD4,1_pgrevBamHI	GGATCCAGAAAGATGTGTATAAGA	Cloning
AtCYCD4,2_pgfwdRsrII	CGGTCCGCTAACTAACAACACTAATA	Cloning
AtCYCD4,2_pgrevBamHI	GGATCCAGAAAGAGAAGTGAGGGA	Cloning
AtCYCD5,1_pgfwdRsrII	CGGTCCGTCCTATAAATCTTATCTC	Cloning
AtCYCD5,1_pgrevBamHI	GGATCCTAGCCTACGCATTCTCT	Cloning
AtCYCD6,1_pgfwdRsrII	CGGTCCGTATTTATGAGTAAATGACA	Cloning
AtCYCD6,1_pgrevBamHI	GGATCCGTAACGACGAGTACTA	Cloning
AtCYCD7,1_pgfwdRsrII	CGGTCCGCACCAGTTTCATTGTAATT	Cloning
AtCYCD7,1_pgrevBamHI	GGATCCAATGTAATTTGACATTTCA	Cloning
NbEF1a_fwd *	GTATGCCTGGGTGCTTGAC	qPCR
NbEF1a_rev *	ACAGGGACAGTTCCAATACCA	qPCR
NbCyp71D20_fwd *	CCGCACCATGTCCTTAGAG	qPCR
NbCyp71D20_rev *	CTTGCCCCTTGAGTACTTGC	qPCR

(*): Gimenez-Ibanez et al., 2018

Supplementary table 1 cont.: Primers used in this work

Primer name	Sequence (5`to 3`)	Purpose
NbACRE31_fwd **	CGTCTTCGTCGGATCTTCG	qPCR
NbACRE31_rev **	GGCCATCGTGATCTTGGTC	qPCR
AtUBQ5-4fwd	CCAAGCCGAAGAAGATCAAG	qPCR
AtUBQ5-4rev	ATGACTCGCCATGAAAGTCC	qPCR
AtEF1alphafwd	CTGTTGTAACAAGATGGATGCC	qPCR
AtEF1alpharev	CCCTCGAATCCAGAGATTGG	qPCR
AtCBP60gfwd	AAGAAGAATTGTCCGAGAGGAG	qPCR
AtCBP60grev	GGCGAGTTTATGAAGCACAG	qPCR
AtWRKY22fwd	ATCTCCGACGACCACTATTG	qPCR
AtWRKY22rev	TCATCGCTAACCACCGTATC	qPCR
AtFRK1F	CGGTCAGATTTCAACAGTTGTC	qPCR
AtFRK1F	AATAGCAGGTTGGCCTGTAATC	qPCR
AtCDKB1,1f	CTTCATATCTTCAGGTTGCTAGGA	qPCR
AtCDKB1,1r	TGAGGTGAAAGAGAAGGAACAG	qPCR
AtCDKB1,2fwd	AAGAAGGTATACCACCAACGG	qPCR
AtCDKB1,2rev	AGAGATTGGATTTGGGAGAGTG	qPCR
AtCDKB2,1fwd	CTAAAGAAGACGCGTCTCCA	qPCR
AtCDKB2,1rev	ACCTGACGACGTGAGGA	qPCR
AtCDKB2,2fwd	CAGAAGCTTTCGTCAAGCTG	qPCR
AtCDKB2,2rev	TTGTGAGGCTTAAGATCCCTG	qPCR
AtCYCD1,1fwd	TATGGATCGGTTTCTTTACGCT	qPCR
AtCYCD1,1rev	AAATACTTCACTCCTGCAACCT	qPCR
AtCYCD2,1fwd	CGGATTTACGAACGAGATTGATTAC	qPCR
AtCYCD2,1rev	CACTCAAGGACGATGAAGAAGA	qPCR
AtCYCD3,1fwd	GAAGCTGTTGGTTGGATTCTG	qPCR
AtCYCD3,1rev	CTGAAGCATCCATGGTTTGTC	qPCR
AtCYCD3,2fwd	TATGGGATGACGATGAGATTCTG	qPCR
AtCYCD3,2fwd	ACCTATCGAAGTAGTTCACAGC	qPCR
AtCYCD3,3fwd	AAGAACCGTGTCTTTATGACGA	qPCR
AtCYCD3,3rev	TGAGACATCCATGGCTTATCTG	qPCR
AtCYCD4,1fwd	GTTGGCTGTGGCTTGTTTATC	qPCR
AtCYCD4,1rev	ACAAACTGAGGATCTCCAACC	qPCR
AtCYCD4,2fwd	GAGAGAGACGGATCAAGTTCAAG	qPCR
AtCYCD4,2rev	GAGGAGGAAACAGAAGCAGTAG	qPCR
AtCYCD5,1fwd	TCGATCTCTTGGTGGACTTCTA	qPCR
AtCYCD5,1rev	CGGTGGAGGTGTCATATGTTT	qPCR
AtCYCD6,1fwd	GCCCTGGATTCTTAAGCTCATA	qPCR
AtCYCD6,1rev	AGAGGACTTGAGGCTATGGA	qPCR

(**): Heese et al., 2007

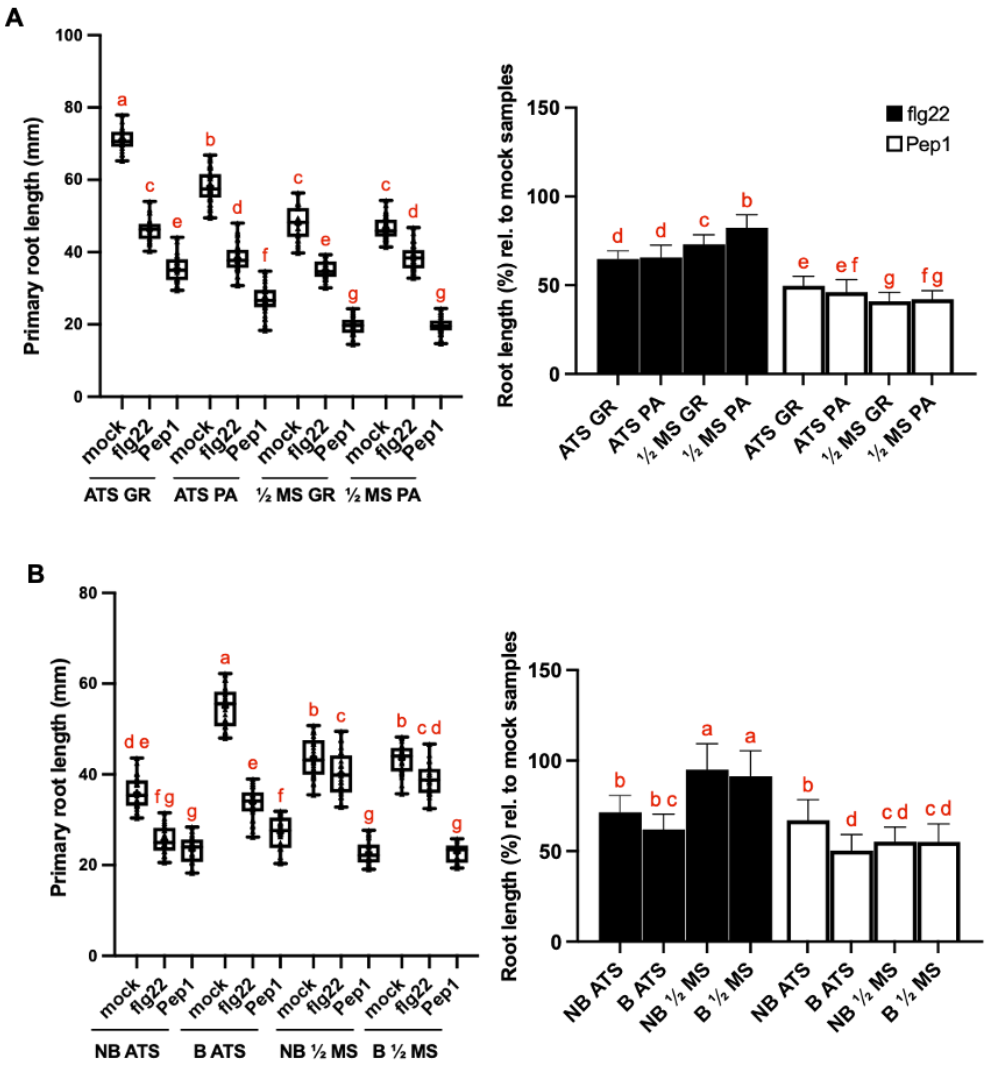

Figure S1: Differences in RGI responses on different growth media are independent of media buffering and the choice of gelling agent: Col-0 wild-type plant were grown for 10 days on **(A),** ATS supplemented with either Gelrite™ (GR) or phyto agar (PA), or **(B),** ATS or or ½ MS media buffered (B) with MES or non-buffered (NB). Plants were then treated with 1 µM flg22, 1 µM Pep1 or water (mock). Total primary root lengths were measured after 4 days and primary root lengths relative to mock treated roots were calculated. Per condition at least 20 roots were counted. Columns and error bars represent mean values ± SD. The experiment was repeated three times with similar results. Statistical comparisons were performed using ANOVA followed by Tukey´s honest significance test. Compact letter display was used for grouping statistical comparisons, where different letters denote significant difference ($p<0.05$).

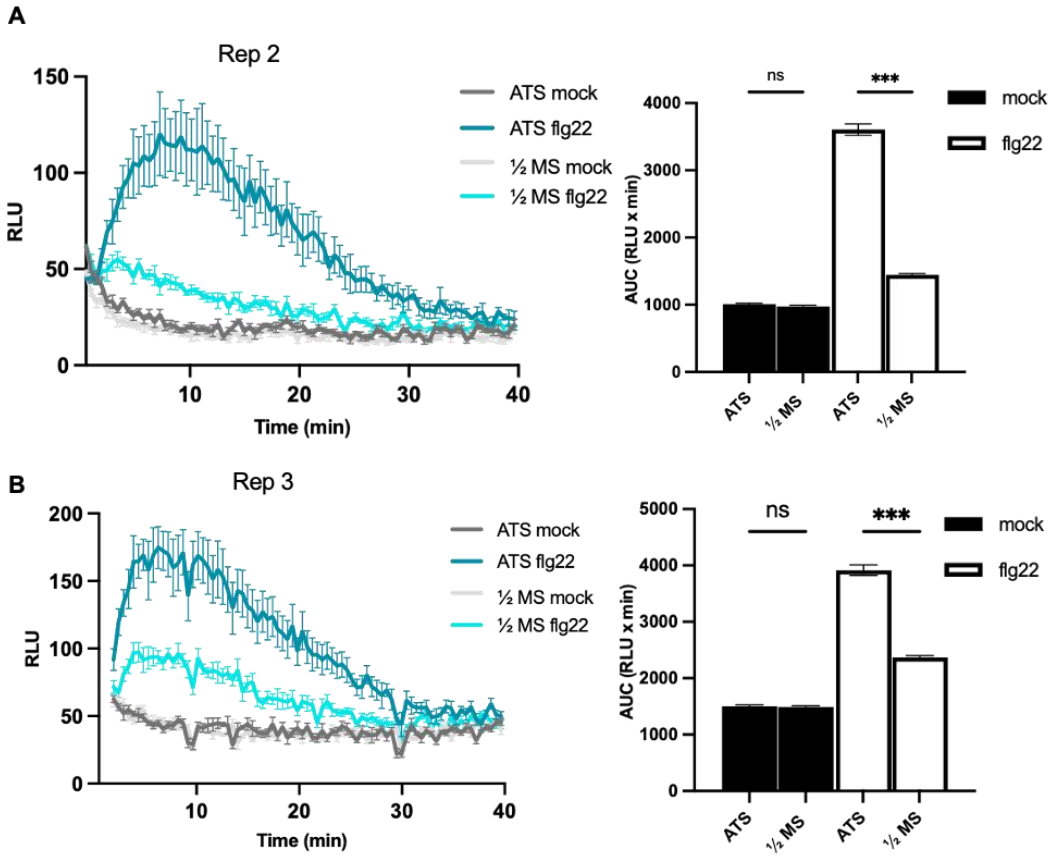

Figure S2: flg22- induced ROS burst is less strong in roots of plants grown on ½ MS medium when compared to ATS medium: 14-day-old Col-0 wild-type plants were grown on ATS or ½ MS and roots were treated with 1 µM flg22, 1 µM Pep1 or water (mock). **(A-B),** Luminol-based detection of ROS production after flg22 or Pep1 treatment, respectively. The graphs show mean values of 6 technical replicates ± SE. The experiments were repeated three times with similar results. RLU: relative luminescence units, AUC: area under curve. Asterisks indicate significant differences according to ANOVA followed by Tukey´s honest significance test. $p < 0.001$ (***), $p < 0.01$ (**), $p < 0.05$ (*), ns: not significantly different.

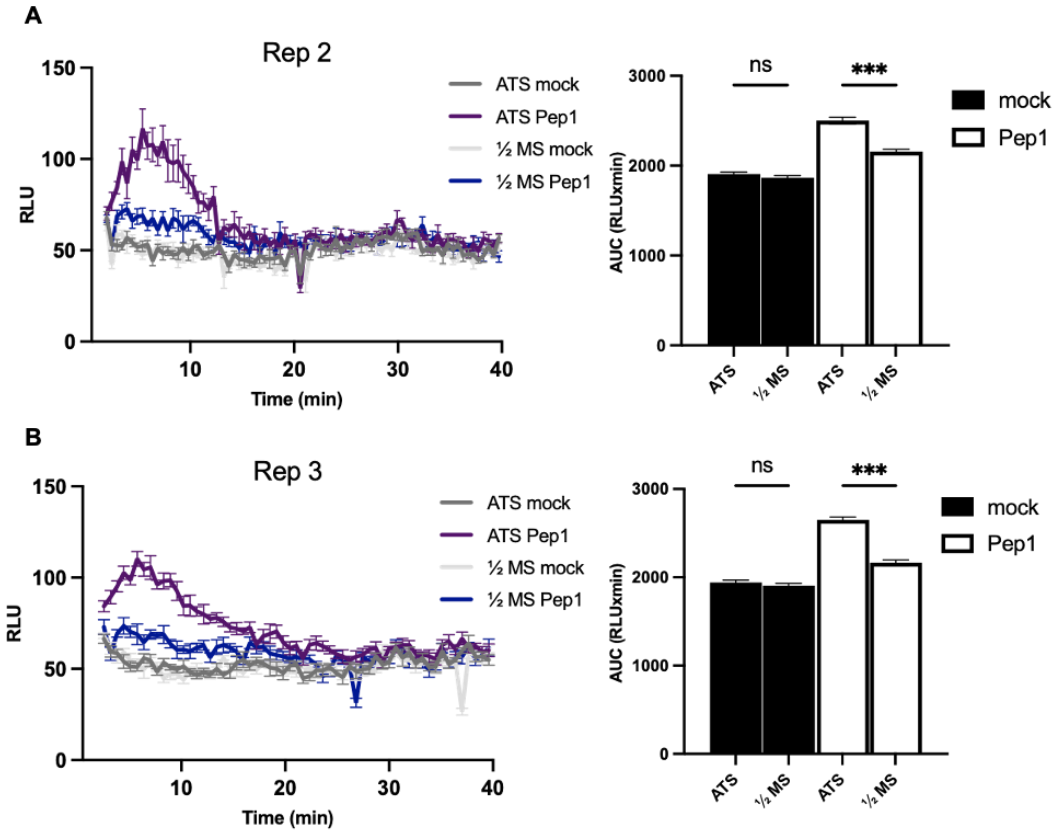

Figure S3: Pep1- induced ROS burst is less strong in roots of plants grown on ½ MS medium when compared to ATS medium: 14-day-old Col-0 wild-type plants were grown on ATS or ½ MS and roots were treated with 1 µM flg22, 1 µM Pep1 or water (mock). **(A-B),** Luminol-based detection of ROS production after flg22 or Pep1 treatment, respectively. The graphs show mean values of 6 technical replicates ± SE. The experiments were repeated three times with similar results. RLU: relative luminescence units, AUC: area under curve. Asterisks indicate significant differences according to ANOVA followed by Tukey´s honest significance test. $p < 0.001$ (***), $p < 0.01$ (**), $p < 0.05$ (*), ns: not significantly different.

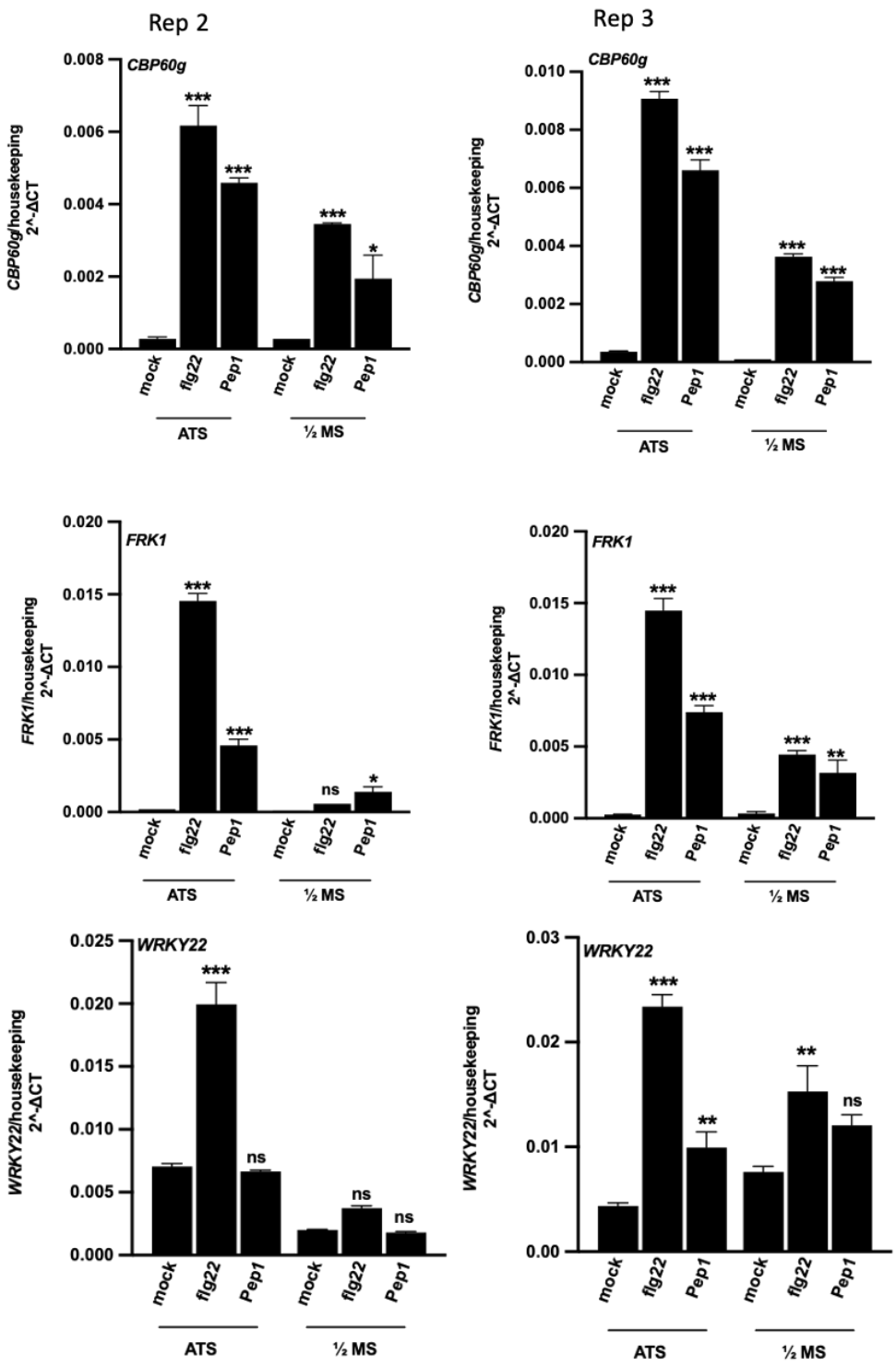

Figure S4: The expression of flg22- or Pep1-induced PTI reporter genes is suppressed in roots of plants grown on ½ MS medium compared to ATS grown plants: 10-day-old Col-0 wild-type plants were grown on solid ATS or ½ MS medium and roots were treated with 1 µM flg22, 1 µM Pep1 or water. Roots were harvested 2 hours after treatment and gene expression was analysed by qRT-PCR. Expression of the marker genes *CBP60g*, *FRK1*, and *WRKY22***,** respectively. Columns and bars represent mean values ± SE from one representative experiment. The experiment was repeated three times with similar results. Asterisks indicate significant differences with respect to the mock samples according to ANOVA followed by Tukey´s honest significance test. $p < 0.001$ (***), $p < 0.01$ (**), $p < 0.05$ (*), ns: not significantly different.

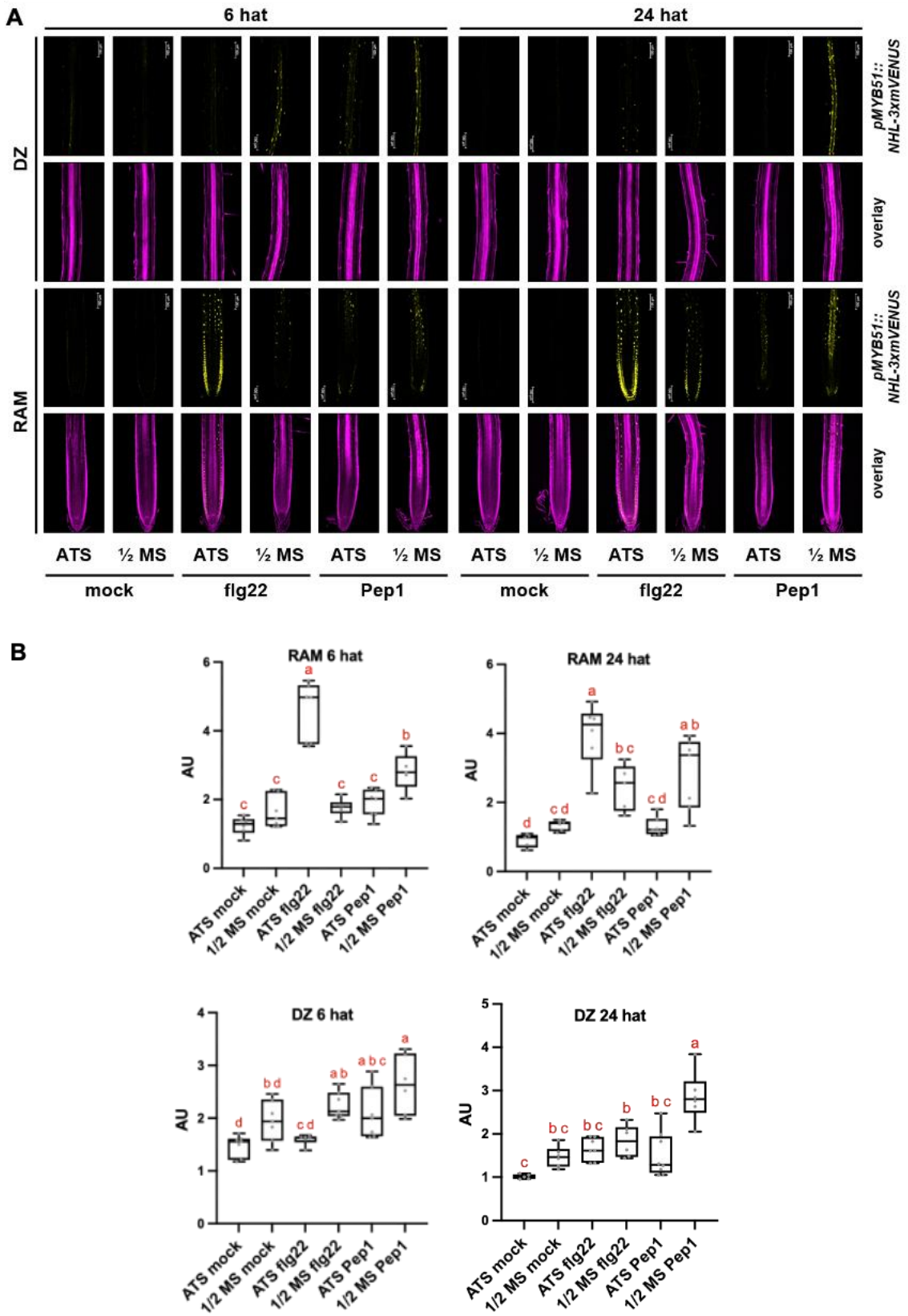

Figure S5: flg22 induces stronger PTI reporter gene expression in the meristematic zone of plant roots grown on ATS media: *pMYB51::NLS-3xmVENUS* plants were grown on solid ATS or ½ MS media and roots were treated with 1 µM flg22, 1 µM Pep1 or water. Roots were harvested 6 or 24 hours after treatment (hat). **(A)** mVENUS expression (yellow) in the root apical meristem (RAM) and differentiation zone (DZ). Root cell walls were stained with Direct Red 23 (magenta). **(B)** Quantification of mVENUS signals in the respective root areas. AU: arbitrary unit. Columns and bars represent mean values ± SD of one representative. Different letters indicate significant differences according to ANOVA test followed by Tukey´s honest significance test. The experiment was repeated two times with similar results.

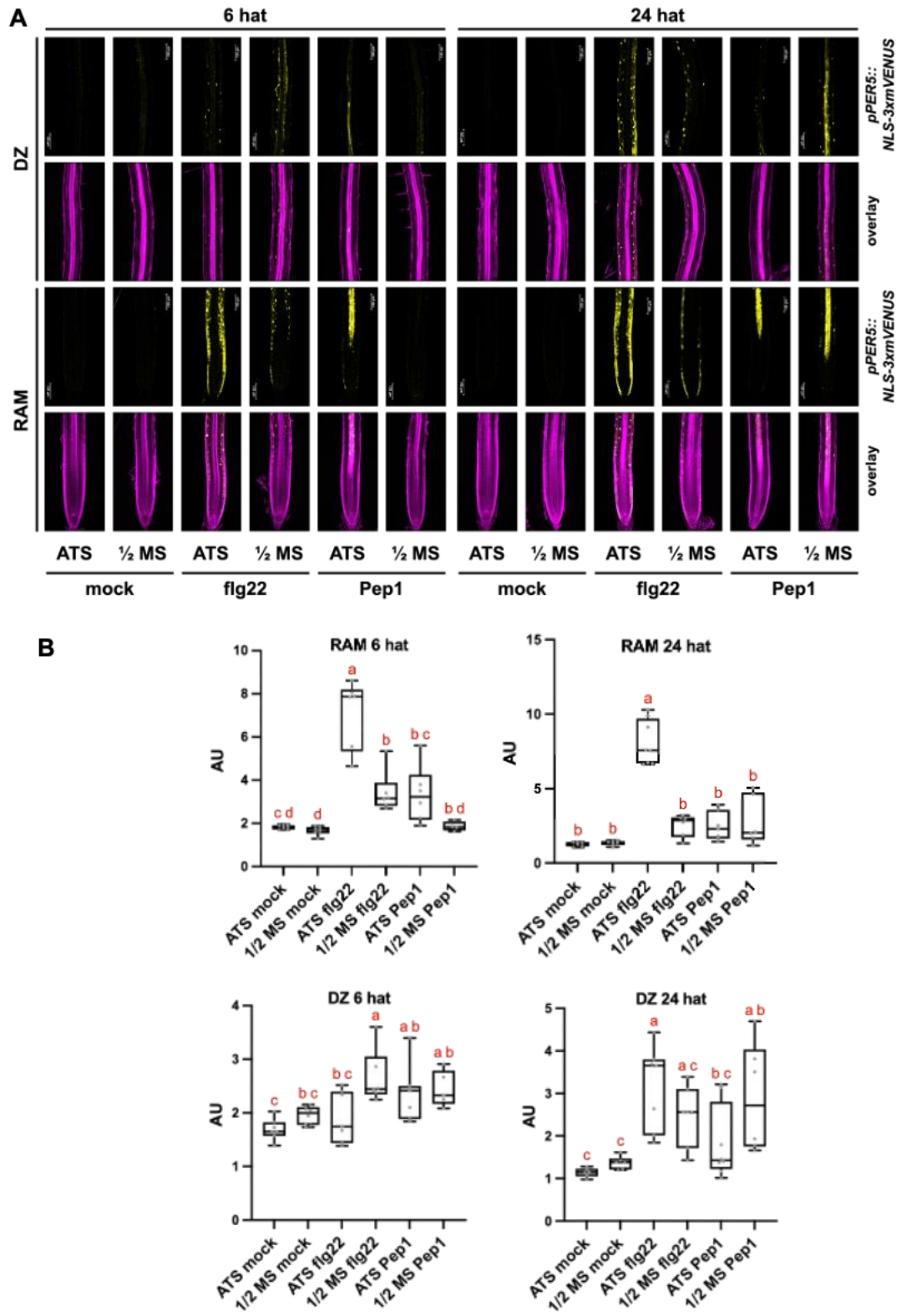

Figure S6: flg22 induces stronger PTI reporter gene expression in meristematic zone of plants grown on ATS plates: 14-day-old *pPER-5::NLS-3xmVENUS* plants were grown on solid ATS or ½ MS and roots were treated with 1µM flg22, Pep1 or water. Roots were harvested 6 hours after treatment (hat) **(A)** mVENUS expression (yellow) in the root apical meristem (RAM) and differentiation zone (DZ). Root cell walls were stained with Direct Red 23 (magenta). **(B)** Quantification of mVENUS signals in the respective root areas. AU: arbitrary unit. Columns and bars represent mean values ± SD of one representative. Different letters indicate significant differences according to ANOVA test followed by Tukey´s honest significance test. The experiment was repeated two times with similar results.

AGI	Gene	Gene model
AT3G54180.1	*CDKB1;1*	
AT2G38620.2	*CDKB1;2*	
AT2G38620.3	*CDKB1;2*	
AT2G38620.4	*CDKB1;2*	
AT1G76540.1	*CDKB2;1*	
AT1G20930.1	*CDKB2;2*	
AT1G70210.1	*CYCD1;1*	
AT2G22490.1	*CYCD2;1*	
AT2G22490.2	*CYCD2;1*	
AT4G34160.1	*CYCD3;1*	
AT5G67260.1	*CYCD3;2*	
AT5G67260.2	*CYCD3;2*	
AT3G50070.1	*CYCD3;3*	
AT5G65420.1	*CYCD4;1*	
AT5G65420.2	*CYCD4;1*	
AT5G65420.3	*CYCD4;1*	
AT5G65420.4	*CYCD4;1*	
AT5G10440.1	*CYCD4;2*	
AT5G10440.2	*CYCD4;2*	
AT4G37630.1	*CYCD5;1*	
AT4G37630.2	*CYCD5;1*	
AT4G37630.3	*CYCD5;1*	
AT4G03270.1	*CYCD6;1*	
AT4G03270.2	*CYCD6;1*	
AT5G02110.1	*CYCD7;1*	
AT5G02110.2	*CYCD7;1*	

Figure S7: Gene models for *CDKB* and *CYCD* genes in *A. thaliana*: Gene models were acquired from TAIR and the representative graphics were generated using the Exon-Intron Graphic Maker (http://wormweb.org/exonintron). Untranslated regions (UTRs) and exons are depicted in white and black bars, respectively. Lines represent introns. When there is more than one predicted gene model, the one that was used for further analyses is highlighted in red.

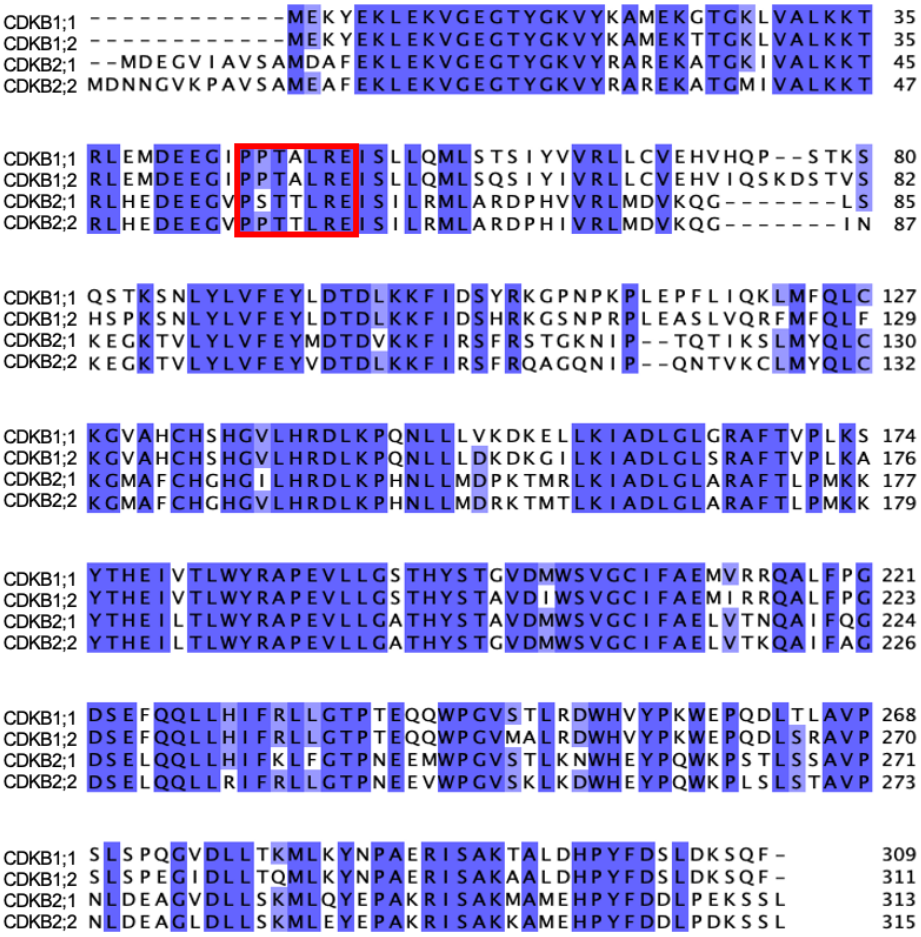

Figure S8: Protein sequence alignments of the B-type CDK family of *A. thaliana*: Canonical protein sequences of CDKBs were obtained form UniPort. The multiple sequence alignments were generated by Clustal Omega. The figure was generated by using Jalview 2. Percentage identity threshold was set to 60%. The red frame shows the conserved PPTALRE and P(S/P)TTLRE motifs.

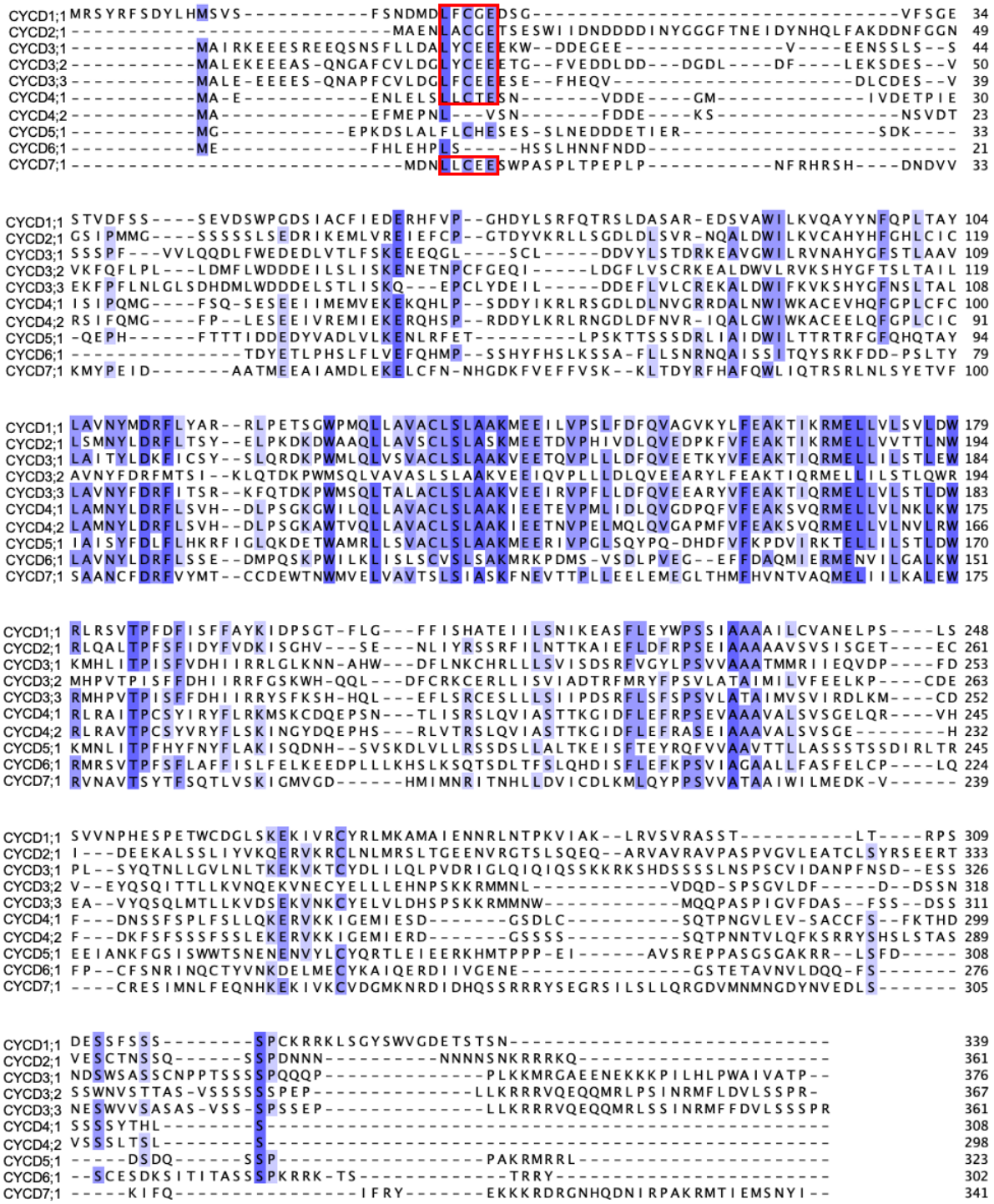

Figure S9: Protein sequence alignments of the D-type CYC family of *A. thaliana*: Canonical protein sequences of CYCDs were obtained form UniPort. The multiple sequence alignments were generated by Clustal Omega. The figure was generated by using Jalview 2. Percentage identity threshold was set to 60%. The red frame shows the conserved LxCxE motif.

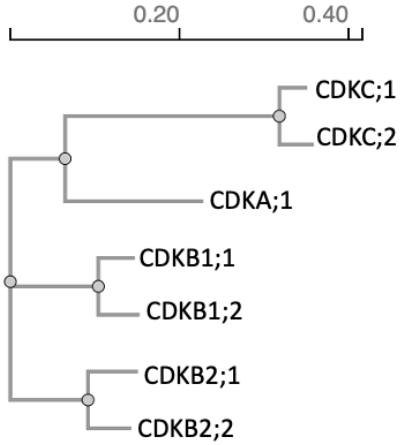

Figure S10: Unrooted phylogenetic tree of the B-type CDK family of *A. thaliana*: Protein sequences were obtained from UniPort. The phylogenetic tree was generated after Multiple Sequence Alignment using Clustal Omega, with the default settings. For reference, *A. thaliana* C-type CDKs (CDKC;1 and CDKC;2) and A-type CDK (CDKA;1) were included.

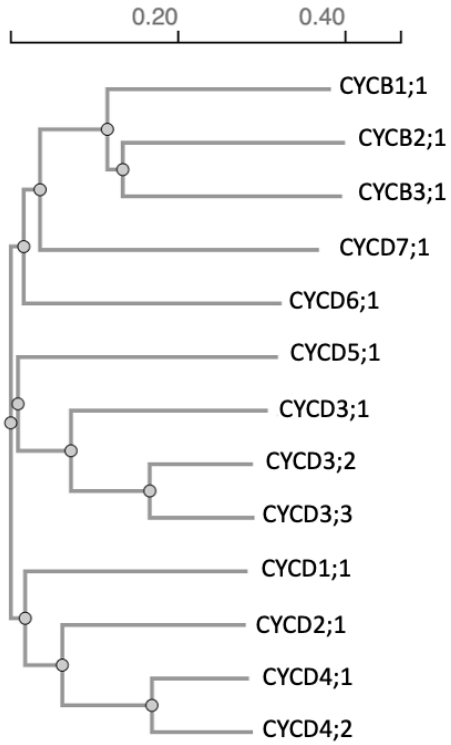

Figure S11: Unrooted phylogenetic tree of the D-type CYC family of *A. thaliana*: Canonical protein sequences were obtained form UniPort. The phylogenetic tree was generated after Multiple Sequence Alignment using Clustal Omega, with the default settings. For reference, *A. thaliana* B-type CYCs (CYCB1;1, CYCB2;1 and CYCB3;1) were included.

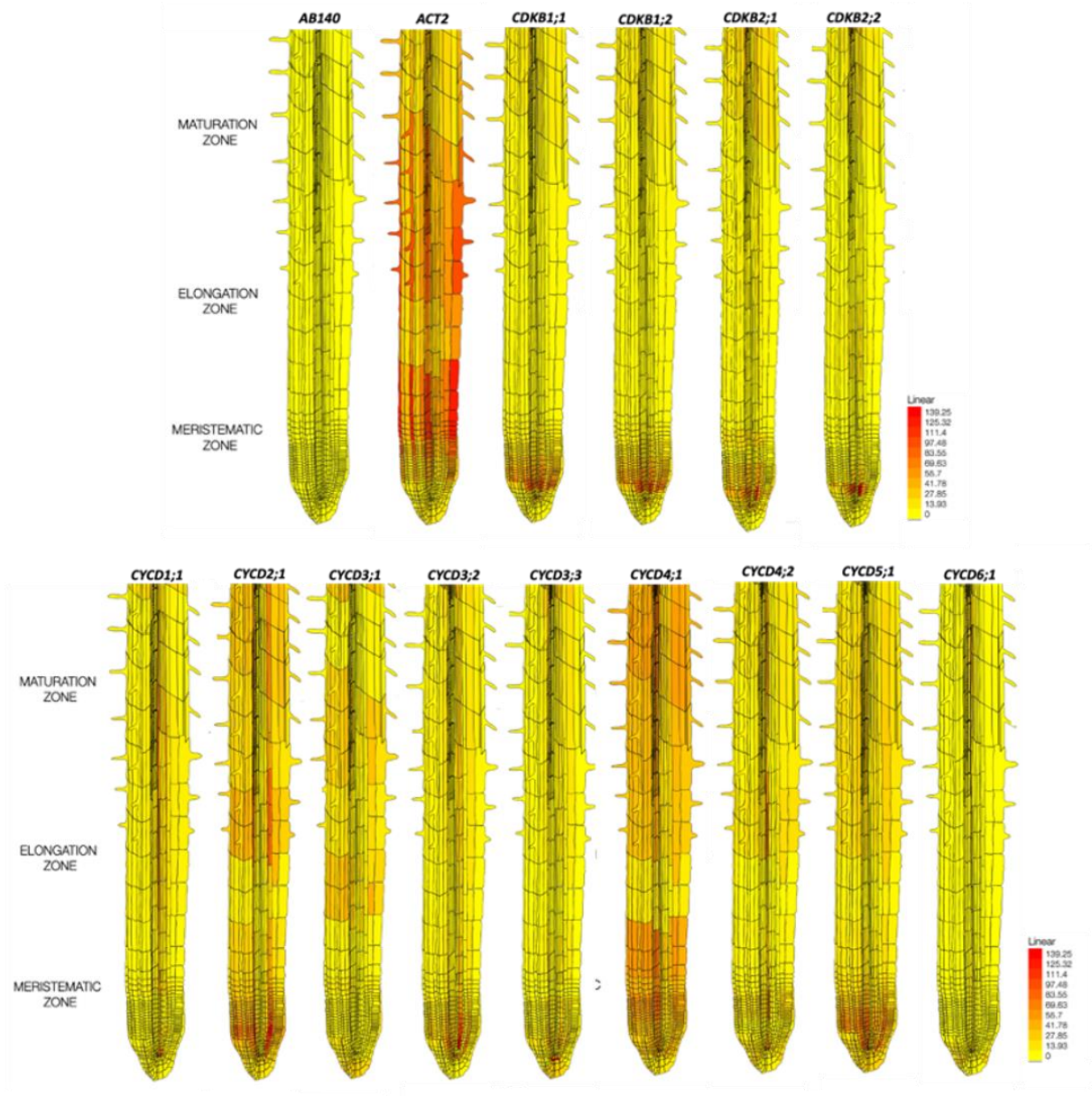

Figure S12: Expression maps showing cell type-specific expression patterns of *CDKB*s and *CYCD*s in *A. thaliana* roots: Data were retrieved from the BAR Arabidopsis BAR ePlant (https://bar.utoronto.ca/eplant/). Expression maps for *AB140* and *ACT2* were used as negative and positive control for expression in root tissues. Intensity of expression in different cell types and developmental zones are shown in colour range from yellow (no expression) to dark red (highest expression).

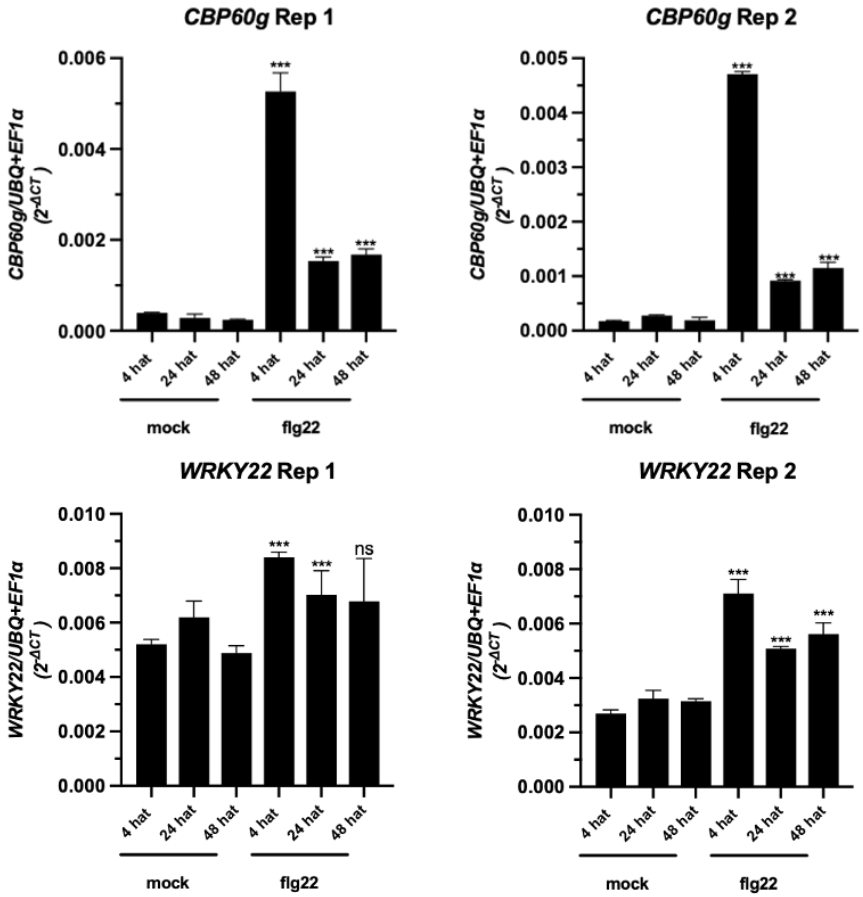

Figure S13: Expression of PTI marker genes in *A. thaliana* roots after flg22 treatment: 12-day-old Col-0 seedlings were treated with 100 nM flg22 or with water (mock). Whole roots were harvested at 4, 24 and 48 hours after treatment (hat). Total RNA was extracted, reverse transcribed into cDNA and qRT-PCR was performed. The columns represent normalized mean values relative to the mock treated samples ($2^{-\Delta\Delta Ct}$). Housekeeping genes *AtUBQ5* and *AtEF1α* were used to normalize data. Error bars show SE of the mean. Asterisks indicate significant differences between mock and flg22 treated samples according to unpaired two-sided Student´s *t* test. $p < 0.001$ (***), $p < 0.01$ (**), $p < 0.05$ (*), ns: not significantly different.

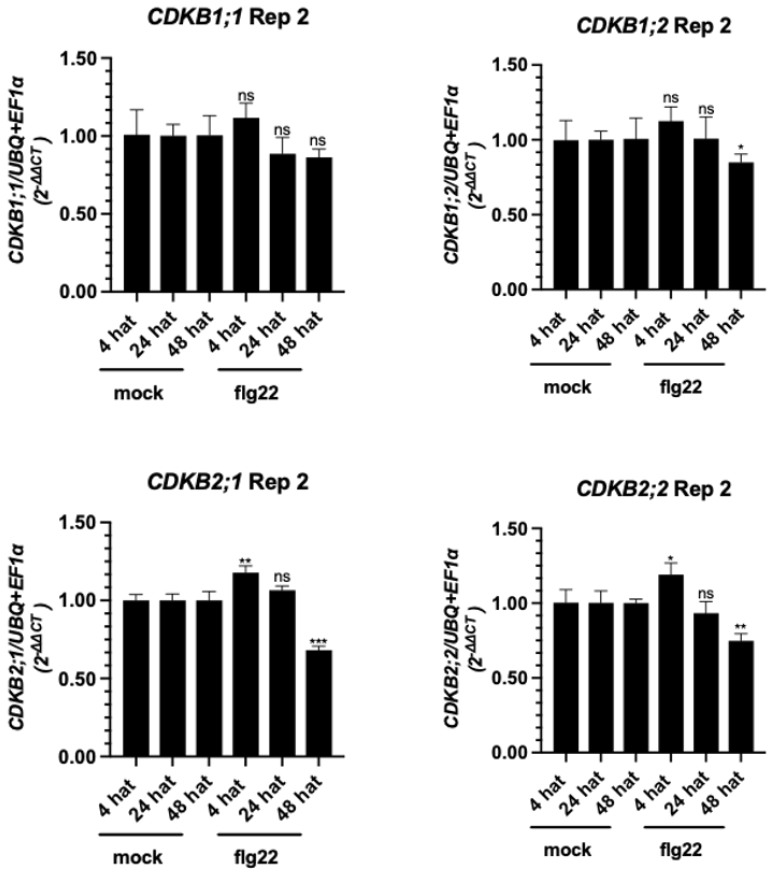

Figure S14: Expression of *CDKB* genes in *A. thaliana* roots after flg22 treatment: 12-day-old Col-0 seedlings were treated with 100 nM flg22 or with water (mock). Whole roots were harvested at 4, 24 and 48 hours after treatment (hat). Total RNA was extracted, reverse transcribed into cDNA and qRT-PCR was performed. The columns represent normalized mean values relative to the mock treated samples ($2^{-\Delta\Delta Ct}$). Housekeeping genes *AtUBQ5* and *AtEF1α* were used to normalize data. Error bars show SE of the mean. Asterisks indicate significant differences between mock and flg22 treated samples according to unpaired two-sided Student´s *t* test. $p < 0.001$ (***), $p < 0.01$ (**), $p < 0.05$ (*), ns: not significantly different.

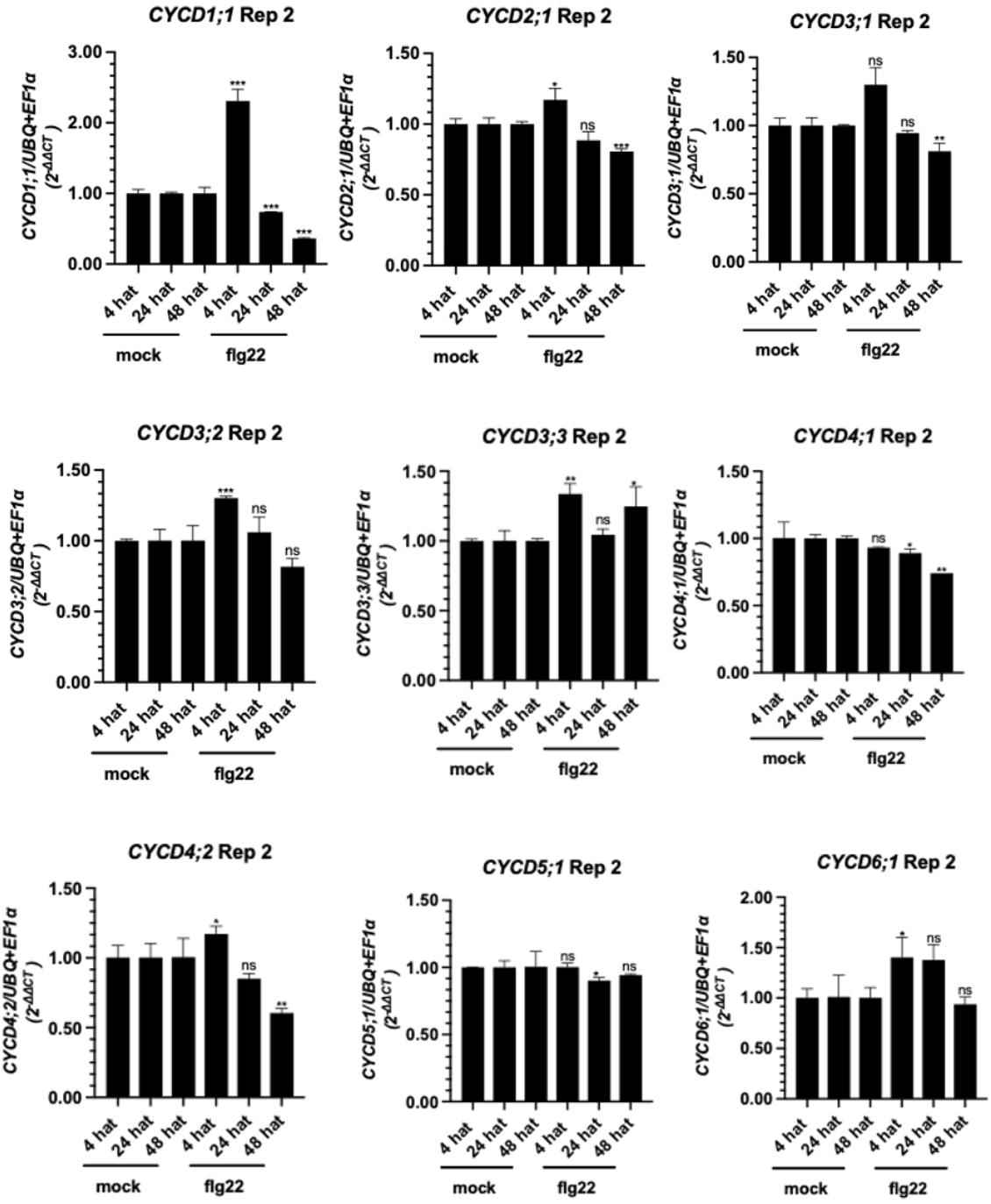

Figure S15: Expression of *CYCD* genes in *A. thaliana* roots after flg22 treatment: 12-day-old Col-0 seedlings were treated with 100 nM flg22 or with water (mock). Whole roots were harvested at 4, 24 and 48 hours after treatment (hat). Total RNA was extracted, reverse transcribed into cDNA and qRT-PCR was performed. The columns represent normalized mean values relative to the mock treated samples ($2^{-\Delta\Delta Ct}$). Housekeeping genes *AtUBQ5* and *AtEF1α* were used to normalize data. Error bars show SE of the mean. Asterisks indicate significant differences between mock and flg22 treated samples according to unpaired two-sided Student´s *t* test. $p < 0.001$ (***), $p < 0.01$ (**), $p < 0.05$ (*), ns: not significantly different.

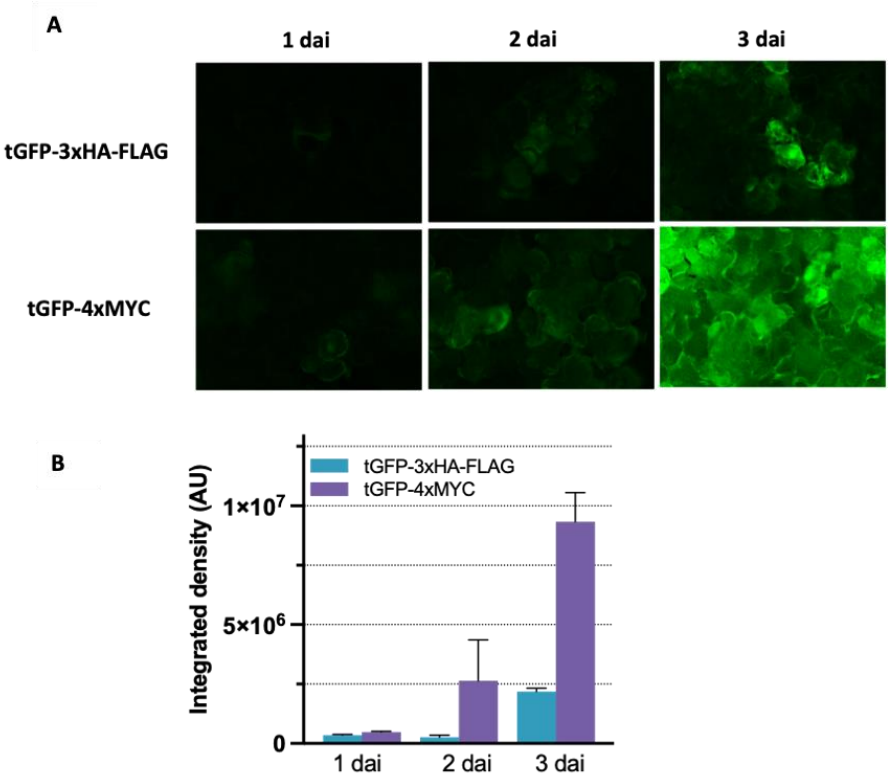

Figure S16: *tGFP* expression after *Agrobacterium* infiltration of *N. benthamiana* leaves: 4-5-week-old *N. benthamiana* leaves were co-infiltrated with *A. tumefaciens* carrying either the pL1P3_35S::tGFP-3xHA-FLAG or pL1P3_35S::tGFP-4xMYC plasmid and *A. tumefaciens* carrying a plasmid for the expression of the silencing suppressor p19. **(A)** 1, 2, and 3 days after infiltration (dai), leaf discs were collected and the abaxial sides of the leaves were investigated for the tGFP signal by using a fluorescence microscope. **(B)** Fluorescence signals in at least 2 images per condition were quantified by using the ImageJ image analysis software. AU: arbitrary unit.

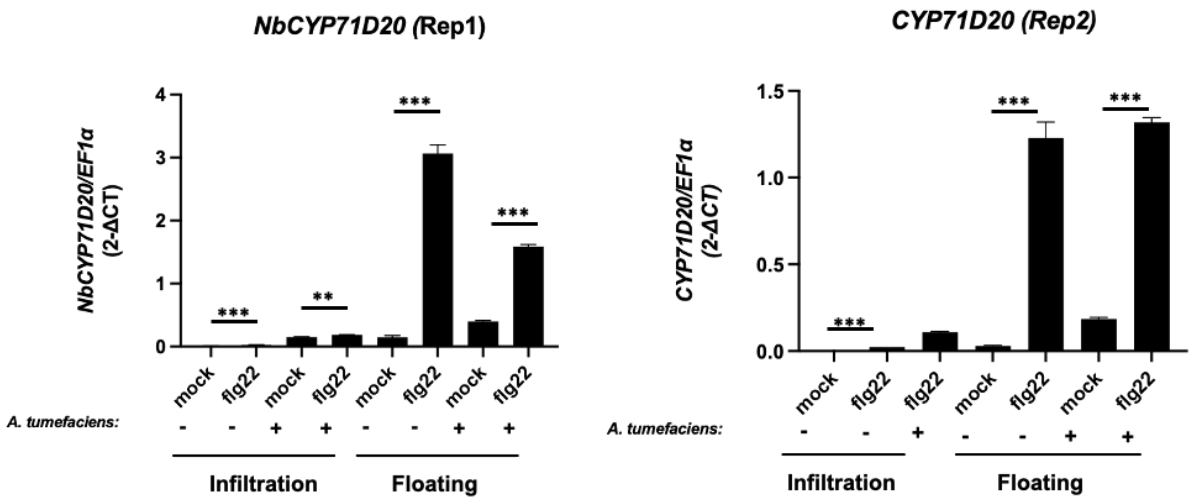

Figure S17: Upregulation on PTI marker genes in *N. benthamiana* leaf discs after flg22 treatment: 4-week-old *N. benthamiana* leaves were infiltrated with *A. tumefaciens* or infiltration buffer (control). 3 days after inoculation, 1 µM flg22 solution or water (mock) was infiltrated into some of the same leaves ("infiltration"). In parallel, leaf discs that were collected 2 days after *Agrobacterium* infiltration were treated with 1 µM flg22 solution in or water well plates ("floating"). 2 hours after treatment, samples were collected, total RNA extracted and reverse transcribed into cDNA before gene expression analysis by qRT-PCR was performed. The columns represent mean PTI gene expression values ($2^{-\Delta Ct}$), normalised against the house keeping gene, *NbEF1α*. Error bars show standard errors. Asterisks indicate significant differences between mock and flg22 treated samples according to unpaired two-sided Student´s *t* test. $p < 0.001$ (***), $p < 0.01$ (**).

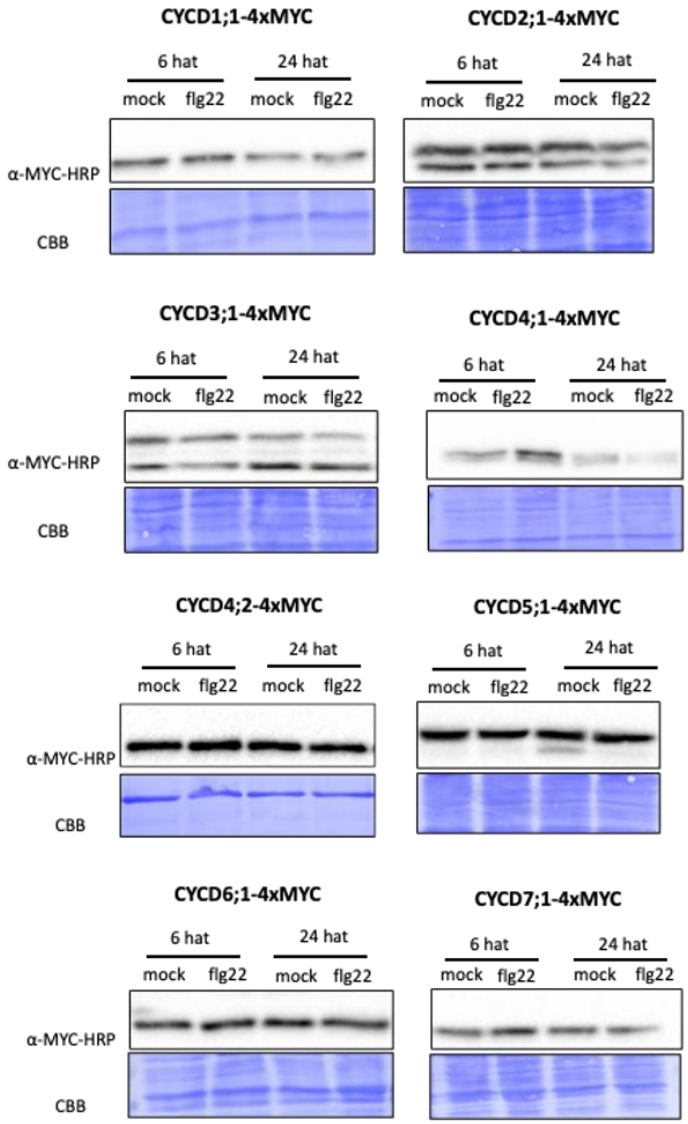

Figure S18: AtCYCD protein levels in *N. benthamiana* leaf discs after flg22 treatment: Experimental set-up: 4-week-old *N. benthamiana* leaves were co-infiltrated with *A. tumefaciens* carrying the plasmids for *AtCYCDs-4xMYC* expression and expression of the p19 silencing suppressor. 2 dai, leaf discs were collected and transferred into a 96-well plate containing water. On the next morning, leaf discs were treated with 1 µM flg22 solution or water. At 6 and 24 hours after treatment (hat), samples were harvested and proteins extracted. Western blot was performed with antibodies against HA- or MYC-tags. As loading control, membranes were stained with Coomassie brilliant blue (CBB).

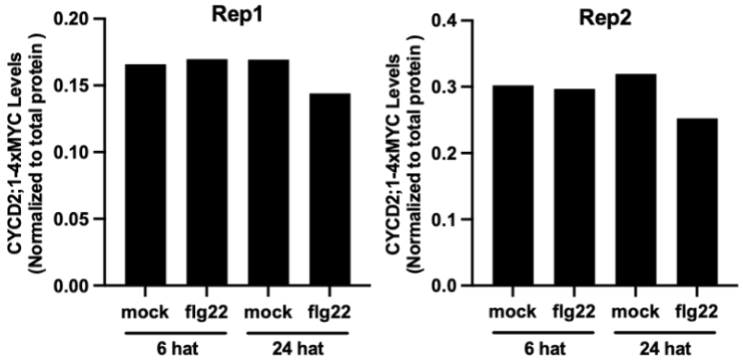

Figure S19: Quantification of CYCD2;1 protein levels: The Western blot band intensities of CYCD2;1-4xMYC protein shown in Figure 17 and Figure S18 (Rep 1 and Rep 2) were quantified using ImageJ/Fiji and normalized against the Coomassie brilliant blue stained total protein.

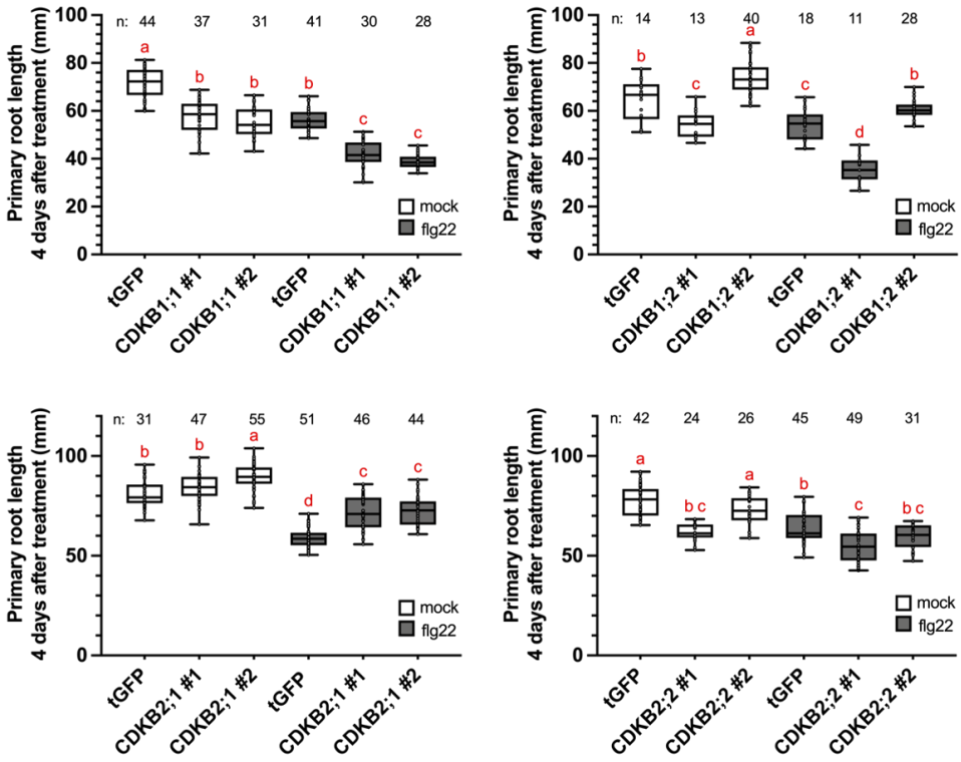

Figure S20: Root growth inhibition assay in *A. thaliana* plants overexpressing *B-type CDK*s: 10-day-old seedlings were treated with 100 nM flg22 or mock (water). After 4 days, primary root lengths were measured. Two lines each carrying one of the following constructs were selected: *35S::CDKB1;1-3xHA-FLAG::FASTR::AtAct2::tGFP-4xMYC* (*CDKB1;1*), *35S::CDKB1;2-3xHA-FLAG::FASTR::AtAct2::tGFP-4xMYC (CDKB1;2*), *35S::CDKB2;1-3xHA-FLAG::FASTR::AtAct2::tGFP-4xMYC* (*CDKB2;1*), *35S::CDKB2;2-3xHA-FLAG::FASTR::AtAct2::tGFP-4xMYC (CDKB2;2*). Plants expressing *35S::tGFP-3xHA-FLAG::FASTR::AtAct2::tGFP-4xMYC* (*tGFP*) served as controls. Box and whisker plots show mean absolute primary root lengths in one biological experiment (Rep 1). n: samples size. The letters above bars indicate significant differences as determined by ANOVA followed by Tukey´s honest significance test, or Kruskal-Wallis test followed by Dunn's multiple comparison test in case of non-normal distribution ($p<0.05$). Compact letter display was used for grouping statistical comparisons, where different letters denote significant difference ($p<0.05$) (performed using GraphPad). The experiment was repeated at least two times.

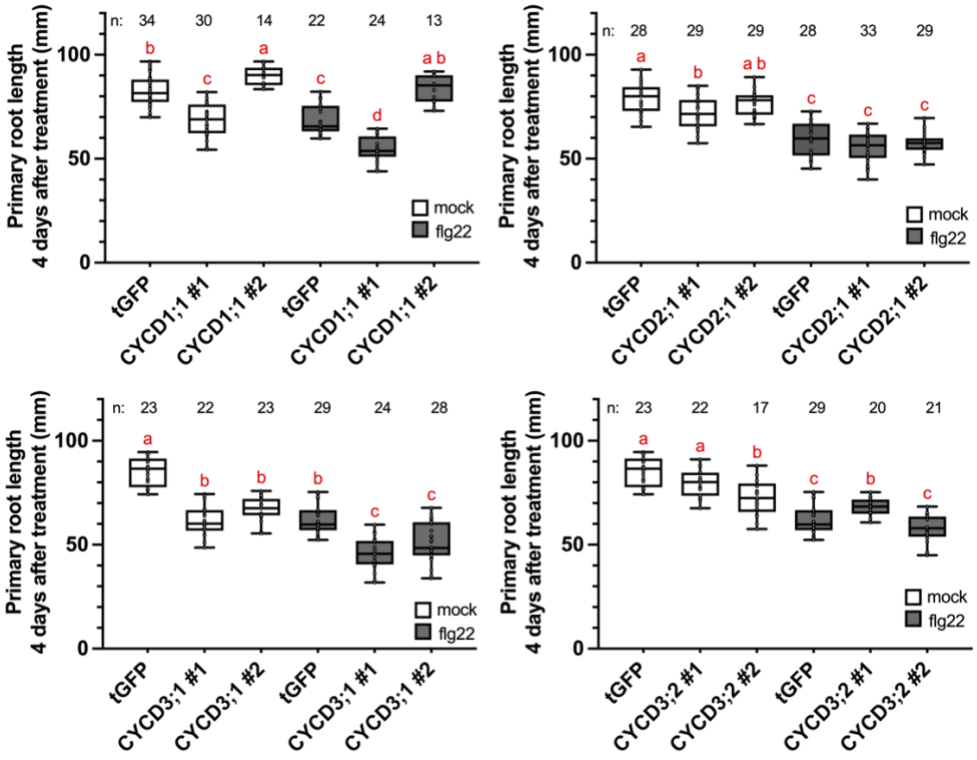

Figure S21: Root growth inhibition assay in *A. thaliana* plants overexpressing *D-type CYCs*: 10-day-old seedlings were treated with 100 nM flg22 or mock (water). After 4 days, primary root lengths were measured. Two lines each carrying one of the following constructs were selected: *35S::tGFP-3xHA-FLAG::FASTR::AtAct2::CYCD1;1-4xMYC (CYCD1;1), 35S::tGFP-3xHA-FLAG::FASTR::AtAct2::CYCD2;1-4xMYC (CYCD2;1), 35S::tGFP-3xHA-FLAG::FASTR::AtAct2::CYCD3;1-4xMYC (CYCD3;1), 35S::tGFP-3xHA-FLAG::FASTR::AtAct2::CYCD3;2-4xMYC (CYCD3;2).* Plants expressing *35S::tGFP-3xHA-FLAG::FASTR::AtAct2::tGFP-4xMYC* (*tGFP*) served as controls. Box and whisker plots show mean absolute primary root lengths in one biological experiment (Rep 1). n: samples size. The letters above bars indicate significant differences as determined by ANOVA followed by Tukey´s honest significance test, or Kruskal-Wallis test followed by Dunn's multiple comparison test in case of non-normal distribution ($p<0.05$). Compact letter display was used for grouping statistical comparisons, where different letters denote significant difference ($p<0.05$) (performed using GraphPad). The experiment was repeated at least two times.

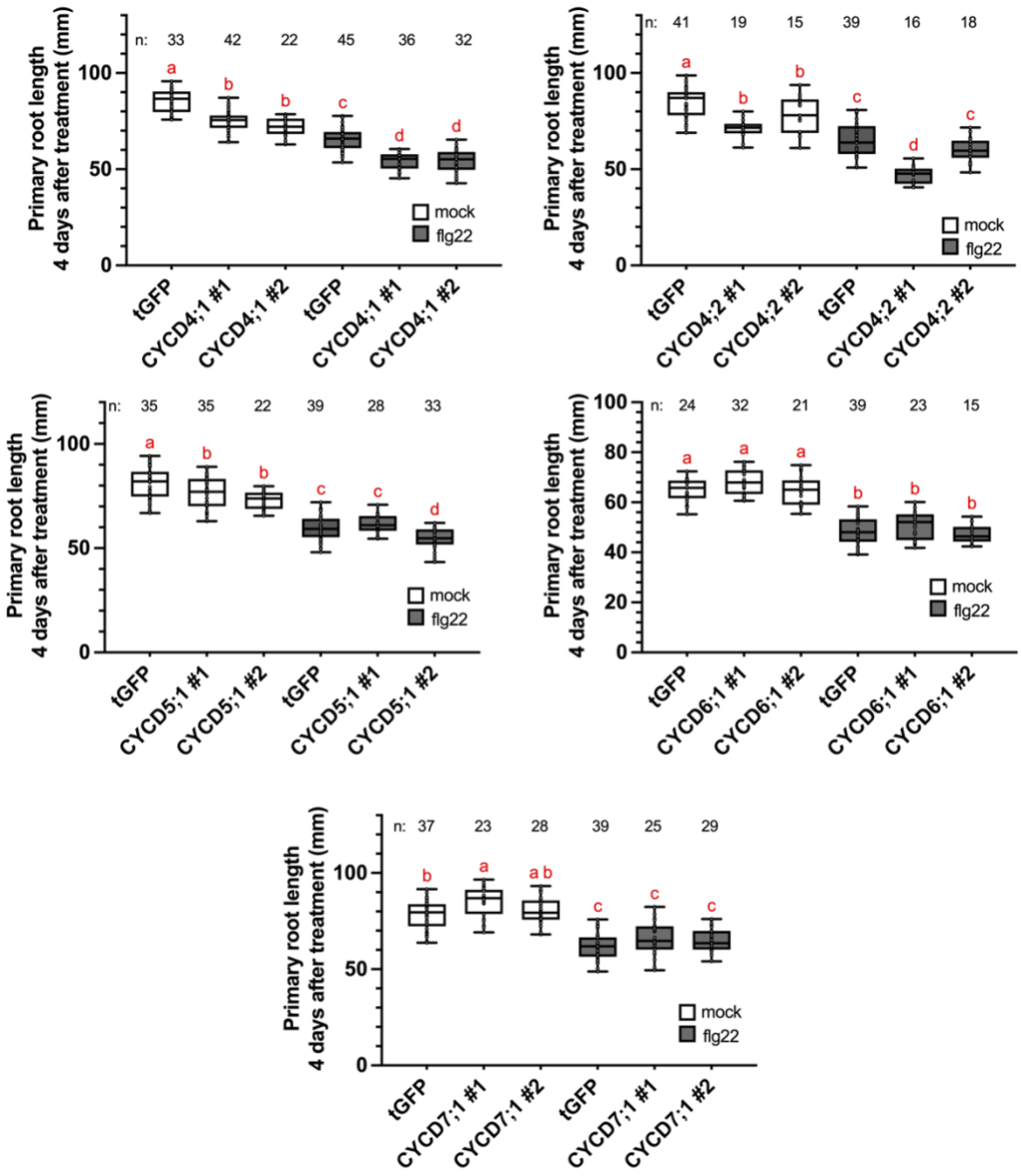

Figure S22: Root growth inhibition assay in *A. thaliana* plants overexpressing *D-type CYCs*: 10-day-old seedlings were treated with 100 nM flg22 or mock (water). After 4 days, primary root lengths were measured. Two lines each carrying one of the following constructs were selected: *35S::tGFP-3xHA-FLAG::FASTR::AtAct2::CYCD4;1-4xMYC (CYCD4;1), 35S::tGFP-3xHA-FLAG::FASTR::AtAct2::CYCD4;2-4xMYC (CYCD4;2), 35S::tGFP-3xHA-FLAG::FASTR::AtAct2::CYCD5;1-4xMYC (CYCD5;1), 35S::tGFP-3xHA-FLAG::FASTR::AtAct2::CYCD6;1-4xMYC (CYCD6;1)* and *35S::tGFP-3xHA-FLAG::FASTR::AtAct2::CYCD7;1-4xMYC (CYCD7;1)* . Plants expressing *35S::tGFP-3xHA-FLAG::FASTR::AtAct2::tGFP-4xMYC* (*tGFP*) served as controls. Box and whisker plots show mean absolute primary root lengths in one biological experiment (Rep 1). n: samples size. The letters above bars indicate significant differences as determined by ANOVA followed by Tukey´s honest significance test, or Kruskal-Wallis test followed by Dunn's multiple comparison test in case of non-normal distribution ($p<0.05$). Compact letter display was used for grouping statistical comparisons, where different letters denote significant difference ($p<0.05$) (performed using GraphPad). The experiment was repeated at least two times.

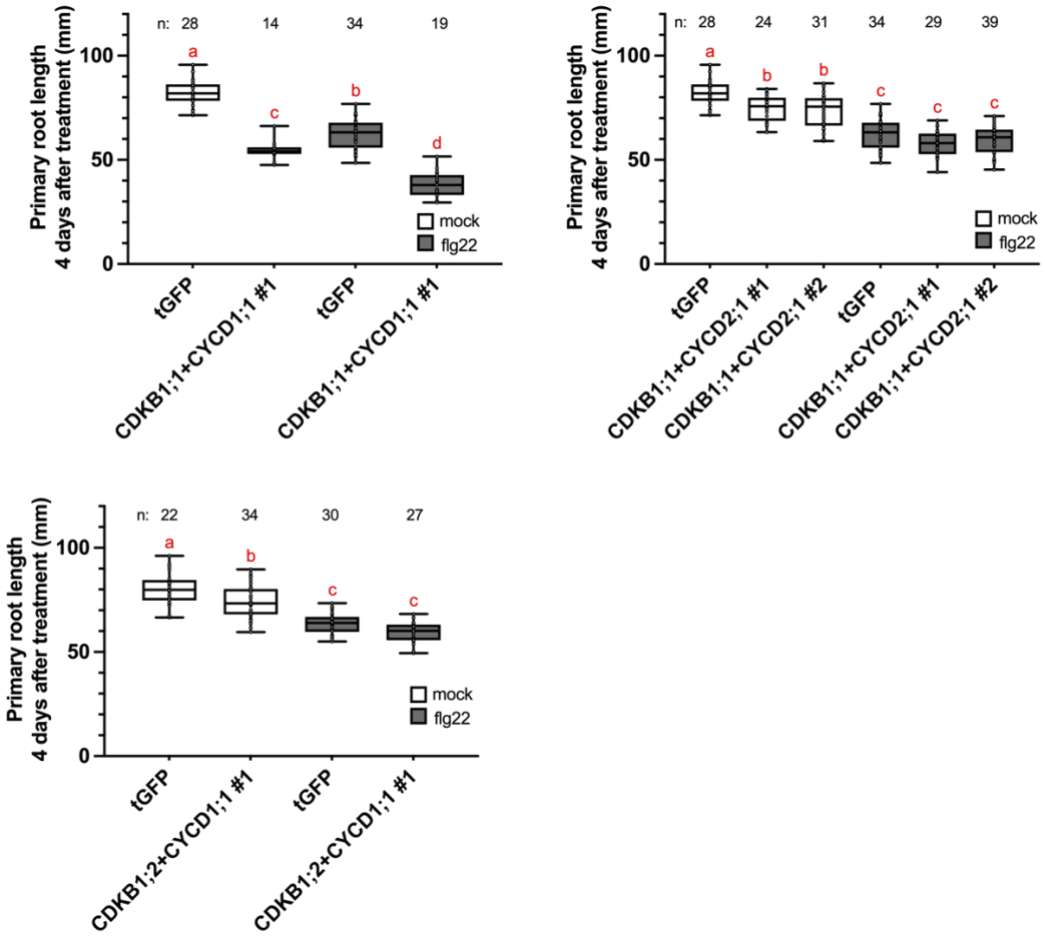

Figure S23: Root growth inhibition assay in *A. thaliana* plants double overexpressing *B-type CDK*s and *D-type CYC*s: 10-day-old seedlings were treated with 100 nM flg22 or mock (water). After 4 days, primary root lengths were measured. Two lines each carrying one of the following constructs were selected: *35S::CDKB1;1-3xHA-FLAG::FASTR::AtAct2::CYCD1;1-4xMYC* (*CDKB1;1+CYCD1;1*), *35S::CDKB1;1-3xHA-FLAG::FASTR::AtAct2::CYCD2;1-4xMYC (CDKB1;1+CYCD2;1*), *35S::CDKB1;2-3xHA-FLAG::FASTR::AtAct2::CYCD1;1P-4xMYC* (*CDKB1;1+CYCD1;1*). Plants expressing *35S::tGFP-3xHA-FLAG::FASTR::AtAct2::tGFP-4xMYC* (*tGFP*) served as controls. Box and whisker plots show mean absolute primary root lengths in one biological experiment (Rep 1). n: samples size. The letters above bars indicate significant differences as determined by ANOVA followed by Tukey´s honest significance test, or Kruskal-Wallis test followed by Dunn's multiple comparison test in case of non-normal distribution ($p<0.05$). Compact letter display was used for grouping statistical comparisons, where different letters denote significant difference ($p<0.05$) (performed using GraphPad). The experiment was repeated at least two times.

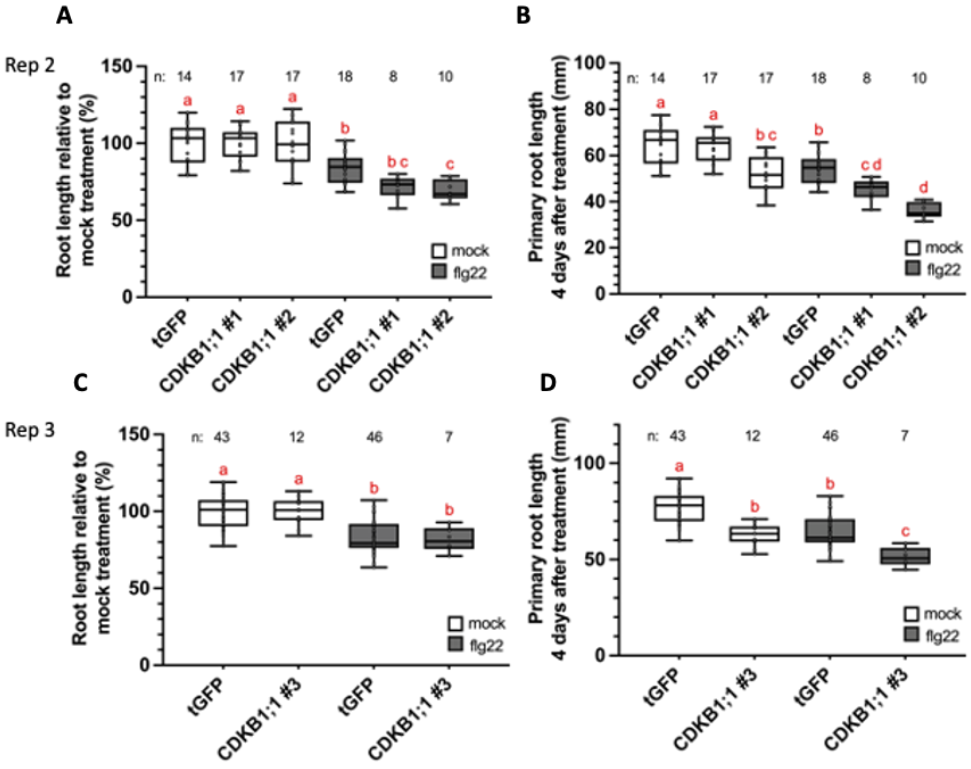

Figure S24: Root growth inhibition assay of *CDKB1;1*-overexpressing *A. thaliana* plants: Two independent *35S::CDKB1;1-3xHA-FLAG::FASTR::AtAct2::tGFP-4xMYC (CDKB1;1)* lines were selected. Col-0 wildtype or *35S::tGFP-3xHA-FLAG::FASTR::AtAct2::tGFP-4xMYC* (tGFP) plants served as controls. 10-day-old seedlings were treated with 100 nM flg22 or mock (water). After 4 days, primary root lengths were measured **(B,D)**. Box and whisker plots show mean primary root lengths in % relative to mock treated roots **(A,C)**. n: samples size. The letters above bars indicate significant differences as determined by ANOVA followed by Tukey´s honest significance test, or Kruskal-Wallis test followed by Dunn's multiple comparison test in case of non-normal distribution. Compact letter display was used for grouping statistical comparisons, where different letters denote significant difference ($p<0.05$) (performed using GraphPad). The experiment was repeated at least three times.

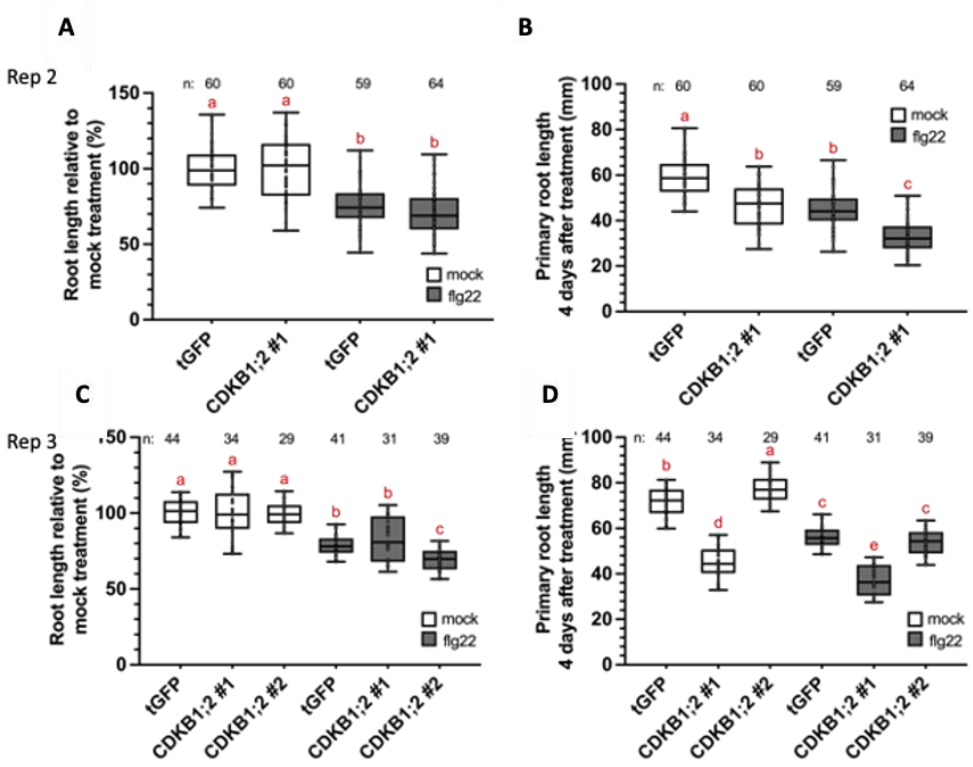

Figure S25: Root growth inhibition assay of *CDKB1;2*-overexpressing *A. thaliana* plants: Two independent *35S::CDKB1;2-3xHA-FLAG::FASTR::AtAct2::tGFP-4xMYC (CDKB1;2)* lines were selected. Col-0 wildtype or *35S::tGFP-3xHA-FLAG::FASTR::AtAct2::tGFP-4xMYC* (tGFP) plants served as controls. 10-day-old seedlings were treated with 100 nM flg22 or mock (water). After 4 days, primary root lengths were measured **(B,D)**. Box and whisker plots show mean primary root lengths in % relative to mock treated roots **(A,C).** n: samples size. The letters above bars indicate significant differences as determined by ANOVA followed by Tukey´s honest significance test, or Kruskal-Wallis test followed by Dunn's multiple comparison test in case of non-normal distribution. Compact letter display was used for grouping statistical comparisons, where different letters denote significant difference ($p<0.05$) (performed using GraphPad). The experiment was repeated at least three times.

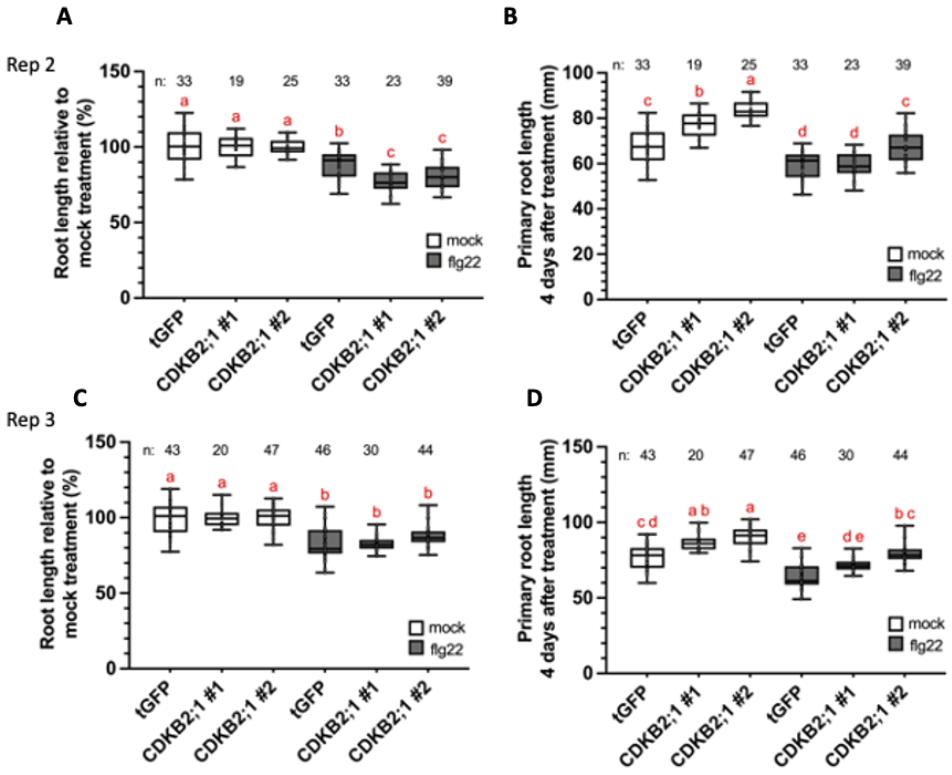

Figure S26: Root growth inhibition assay of *CDKB2;1*-overexpressing *A. thaliana* plants: Two independent *35S::CDKB2;1-3xHA-FLAG::FASTR::AtAct2::tGFP-4xMYC (CDKB2;1)* lines were selected. Col-0 wildtype or *35S::tGFP-3xHA-FLAG::FASTR::AtAct2::tGFP-4xMYC* (tGFP) plants served as controls. 10-day-old seedlings were treated with 100 nM flg22 or mock (water). After 4 days, primary root lengths were measured **(B,D)**. Box and whisker plots show mean primary root lengths in % relative to mock treated roots **(A,C)**. n: samples size. The letters above bars indicate significant differences as determined by ANOVA followed by Tukey´s honest significance test, or Kruskal-Wallis test followed by Dunn's multiple comparison test in case of non-normal distribution. Compact letter display was used for grouping statistical comparisons, where different letters denote significant difference ($p<0.05$) (performed using GraphPad). The experiment was repeated at least three times.

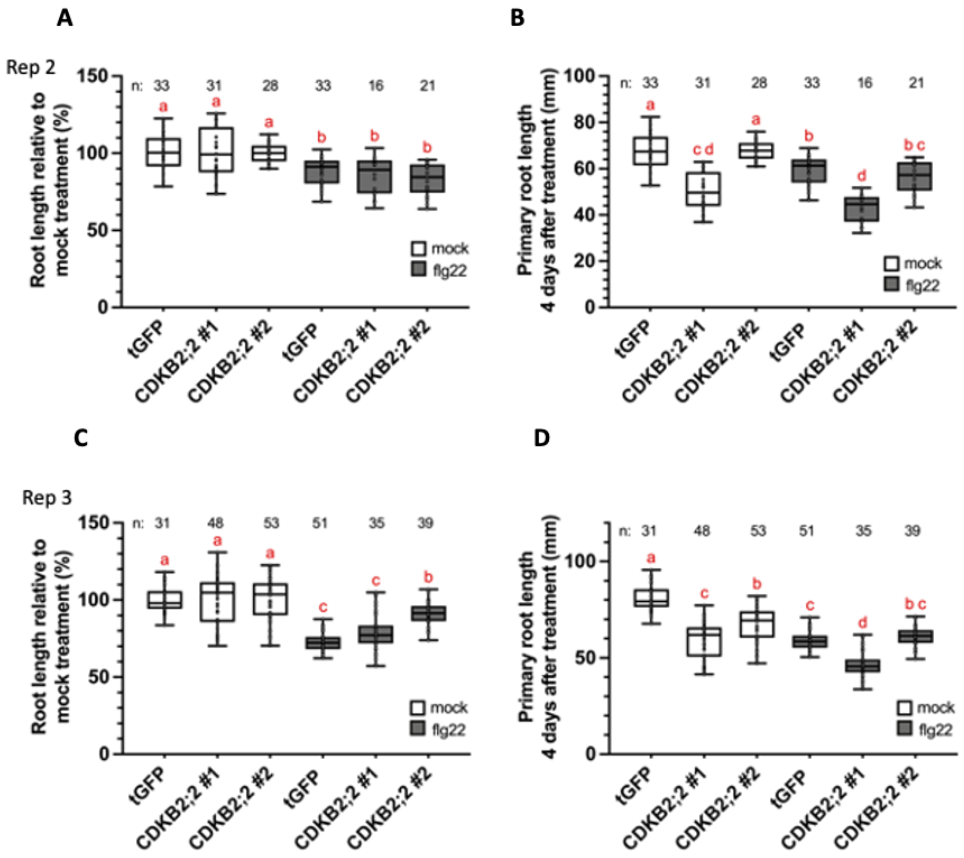

Figure S27: Root growth inhibition assay of *CDKB2;2*-overexpressing *A. thaliana* plants: Two independent *35S::CDKB2;2-3xHA-FLAG::FASTR::AtAct2::tGFP-4xMYC (CDKB2;2)* lines were selected. Col-0 wildtype or *35S::tGFP-3xHA-FLAG::FASTR::AtAct2::tGFP-4xMYC* (tGFP) plants served as controls. 10-day-old seedlings were treated with 100 nM flg22 or mock (water). After 4 days, primary root lengths were measured **(B,D)**. Box and whisker plots show mean primary root lengths in % relative to mock treated roots **(A,C)**. n: samples size. The letters above bars indicate significant differences as determined by ANOVA followed by Tukey´s honest significance test, or Kruskal-Wallis test followed by Dunn's multiple comparison test in case of non-normal distribution. Compact letter display was used for grouping statistical comparisons, where different letters denote significant difference ($p<0.05$) (performed using GraphPad). The experiment was repeated at least three times.

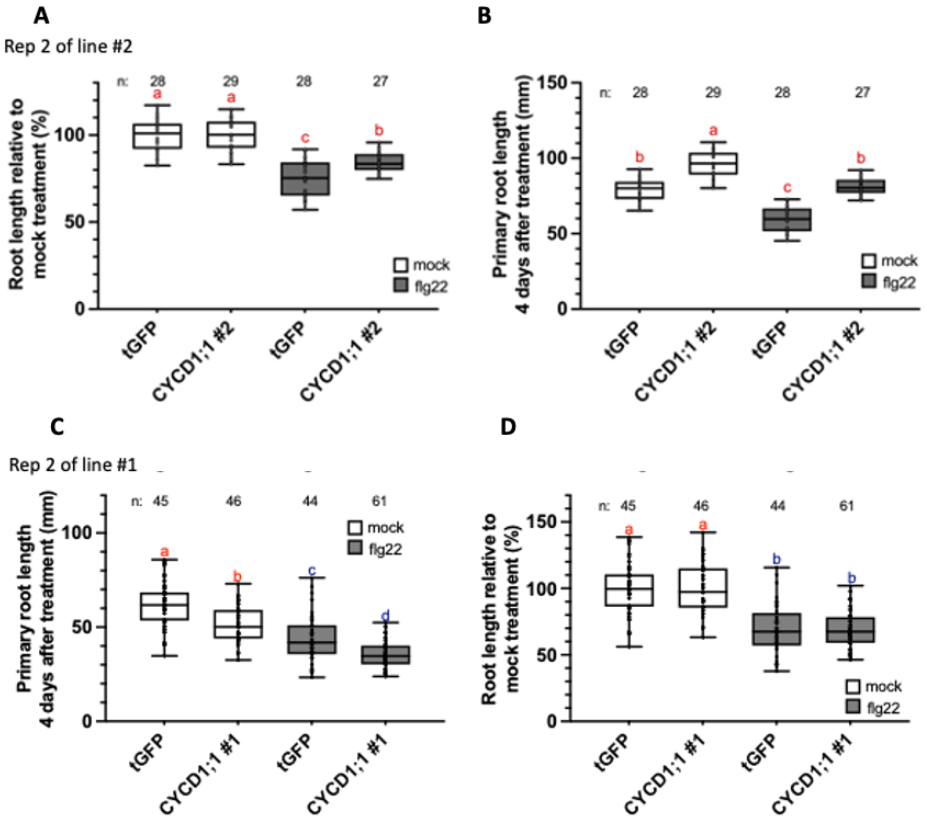

Figure S28: Root growth inhibition assay of *CYCD1;1*-overexpressing *A. thaliana* plants: Two independent *35S::tGFP-3xHA-FLAG::FASTR::AtAct2::CYCD1;1-4xMYC (CYCD1;1)* lines were selected. Col-0 wildtype or *35S::tGFP-3xHA-FLAG::FASTR::AtAct2::tGFP-4xMYC* (tGFP) plants served as controls. 10-day-old seedlings were treated with 100 nM flg22 or mock (water). After 4 days, primary root lengths were measured **(B,D).** Box and whisker plots show mean primary root lengths in % relative to mock treated roots **(A,C)**. n: samples size. The letters above bars indicate significant differences as determined by ANOVA followed by Tukey´s honest significance test, or Kruskal-Wallis test followed by Dunn's multiple comparison test in case of non-normal distribution. Compact letter display was used for grouping statistical comparisons, where different letters denote significant difference ($p<0.05$) (performed using GraphPad). The experiment was repeated at least three times.

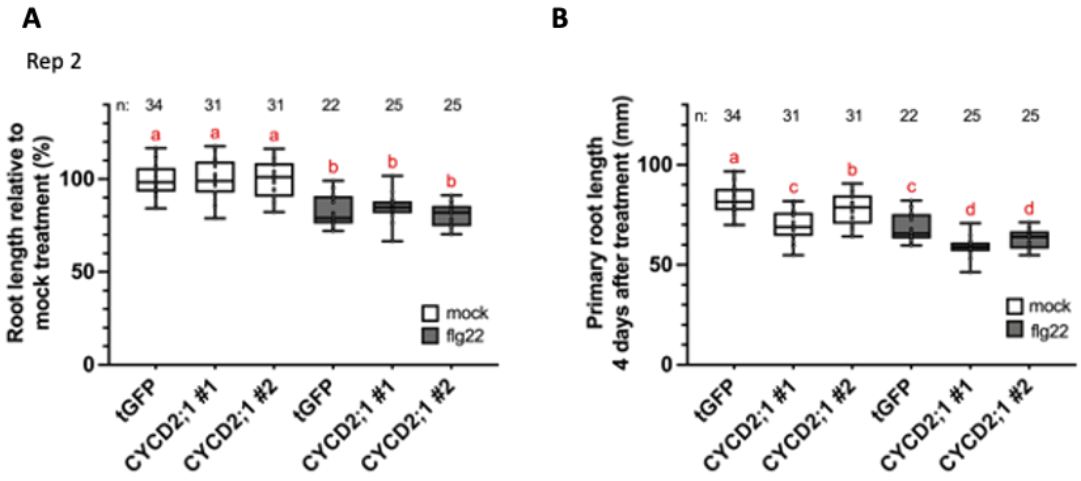

Figure S29: Root growth inhibition assay of *CYCD2;1*-overexpressing *A. thaliana* plants: Two independent *35S::tGFP-3xHA-FLAG::FASTR::AtAct2::CYCD2;1-4xMYC (CYCD2;1)* lines were selected. Col-0 wildtype or *35S::tGFP-3xHA-FLAG::FASTR::AtAct2::tGFP-4xMYC* (tGFP) plants served as controls. 10-day-old seedlings were treated with 100 nM flg22 or mock (water). After 4 days, primary root lengths were measured **(B)**. Box and whisker plots show mean primary root lengths in % relative to mock treated roots **(A)**. n: samples size. The letters above bars indicate significant differences as determined by ANOVA followed by Tukey´s honest significance test, or Kruskal-Wallis test followed by Dunn's multiple comparison test in case of non-normal distribution. Compact letter display was used for grouping statistical comparisons, where different letters denote significant difference ($p<0.05$) (performed using GraphPad). The experiment was repeated at least two times.

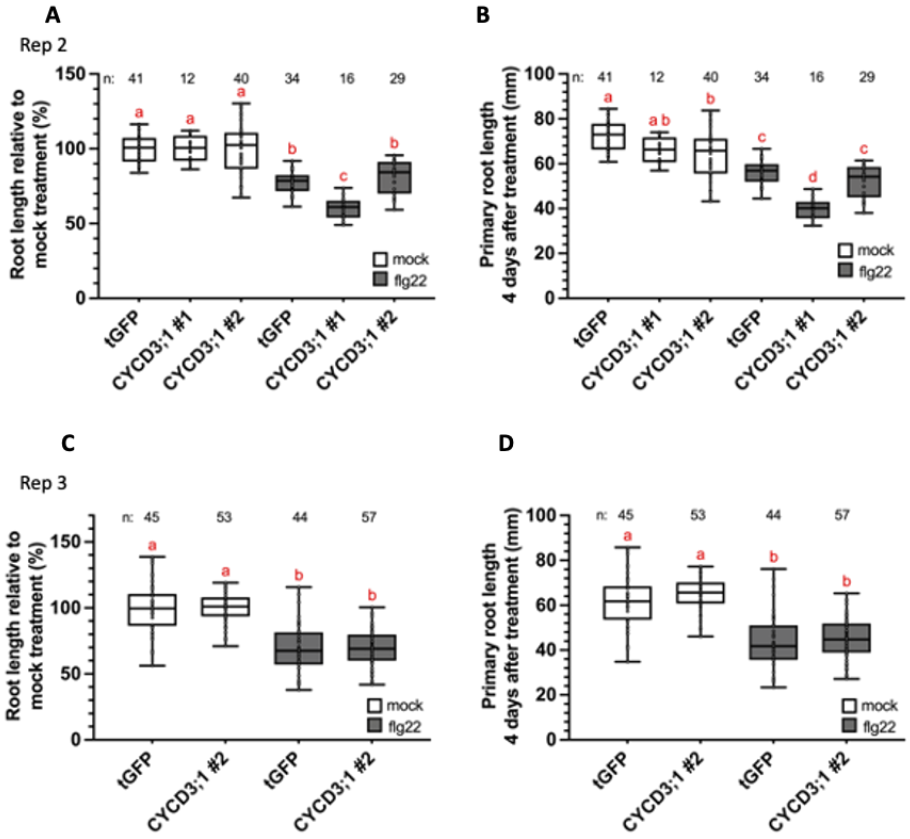

Figure S30: Root growth inhibition assay of *CYCD3;1*-overexpressing *A. thaliana* plants: Two independent *35S::tGFP-3xHA-FLAG::FASTR::AtAct2::CYCD3;1-4xMYC (CYCD3;1)* lines were selected. Col-0 wildtype or *35S::tGFP-3xHA-FLAG::FASTR::AtAct2::tGFP-4xMYC* (tGFP) plants served as controls. 10-day-old seedlings were treated with 100 nM flg22 or mock (water). After 4 days, primary root lengths were measured **(B,D)**. Box and whisker plots show mean primary root lengths in % relative to mock treated roots **(A,C)**. n: samples size. The letters above bars indicate significant differences as determined by ANOVA followed by Tukey´s honest significance test, or Kruskal-Wallis test followed by Dunn's multiple comparison test in case of non-normal distribution. Compact letter display was used for grouping statistical comparisons, where different letters denote significant difference ($p<0.05$) (performed using GraphPad). The experiment was repeated at least three times.

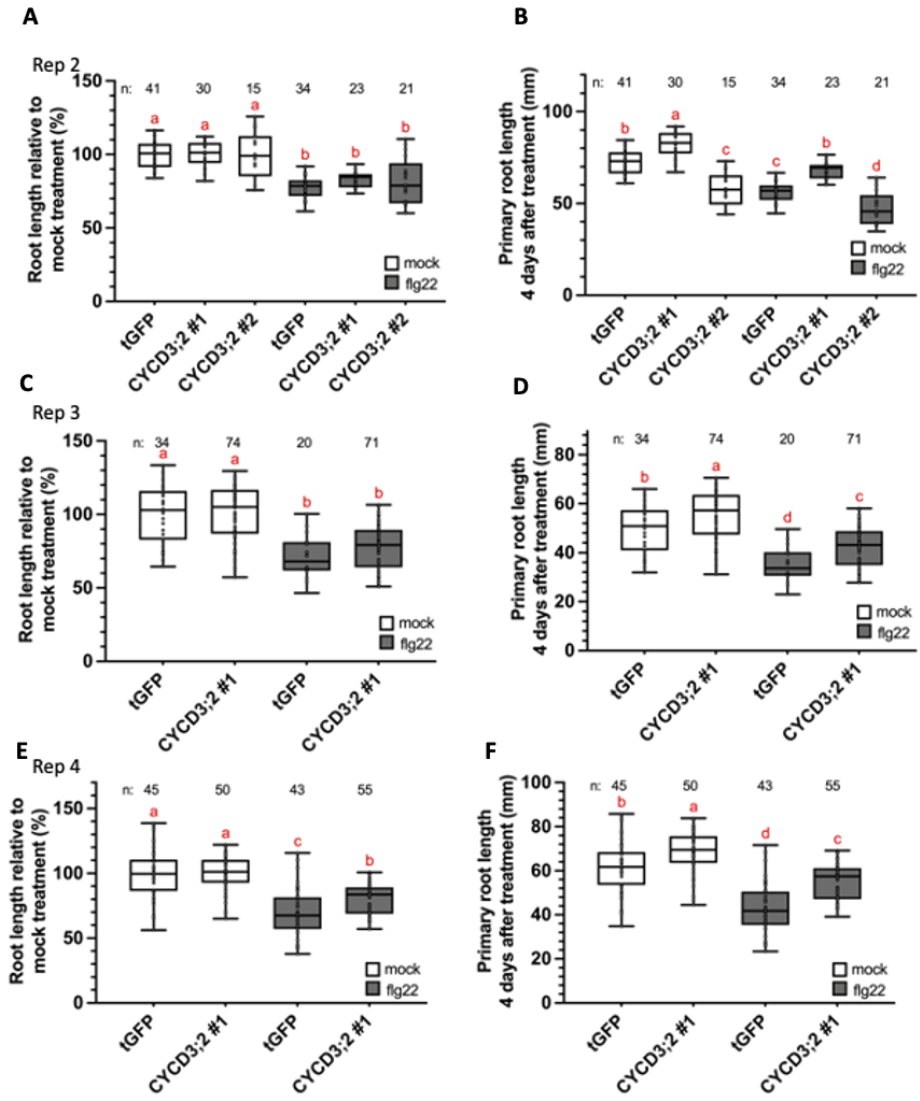

Figure S31: Root growth inhibition assay of *CYCD3;2*-overexpressing *A. thaliana* plants: Two independent *35S::tGFP-3xHA-FLAG::FASTR::AtAct2::CYCD3;2-4xMYC (CYCD3;2)* lines were selected. Col-0 wildtype or *35S::tGFP-3xHA-FLAG::FASTR::AtAct2::tGFP-4xMYC* (tGFP) plants served as controls. 10-day-old seedlings were treated with 100 nM flg22 or mock (water). After 4 days, primary root lengths were measured **(B,D,F)**. Box and whisker plots show mean primary root lengths in % relative to mock treated roots **(A,C,E)**. n: samples size. The letters above bars indicate significant differences as determined by ANOVA followed by Tukey´s honest significance test, or Kruskal-Wallis test followed by Dunn's multiple comparison test in case of non-normal distribution. Compact letter display was used for grouping statistical comparisons, where different letters denote significant difference ($p<0.05$) (performed using GraphPad). The experiment was repeated at least three times.

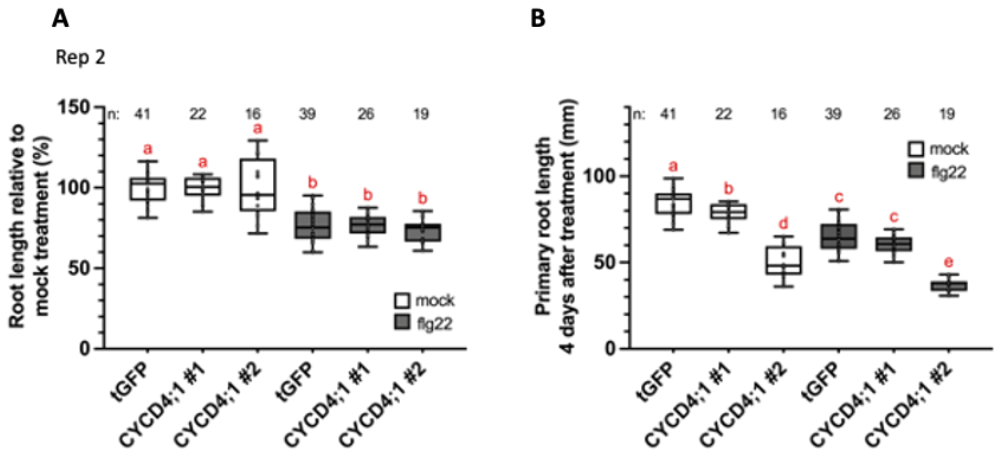

Figure S32: Root growth inhibition assay of *CYCD4;1*-overexpressing *A. thaliana* plants: Two independent *35S::tGFP-3xHA-FLAG::FASTR::AtAct2::CYCD4;1-4xMYC (CYCD4;1)* lines were selected. Col-0 wildtype or *35S::tGFP-3xHA-FLAG::FASTR::AtAct2::tGFP-4xMYC* (tGFP) plants served as controls. 10-day-old seedlings were treated with 100 nM flg22 or mock (water). After 4 days, primary root lengths were measured **(B)**. Box and whisker plots show mean primary root lengths in % relative to mock treated roots **(A)**. n: samples size. The letters above bars indicate significant differences as determined by ANOVA followed by Tukey´s honest significance test, or Kruskal-Wallis test followed by Dunn's multiple comparison test in case of non-normal distribution. Compact letter display was used for grouping statistical comparisons, where different letters denote significant difference ($p<0.05$) (performed using GraphPad). The experiment was repeated at least two times.

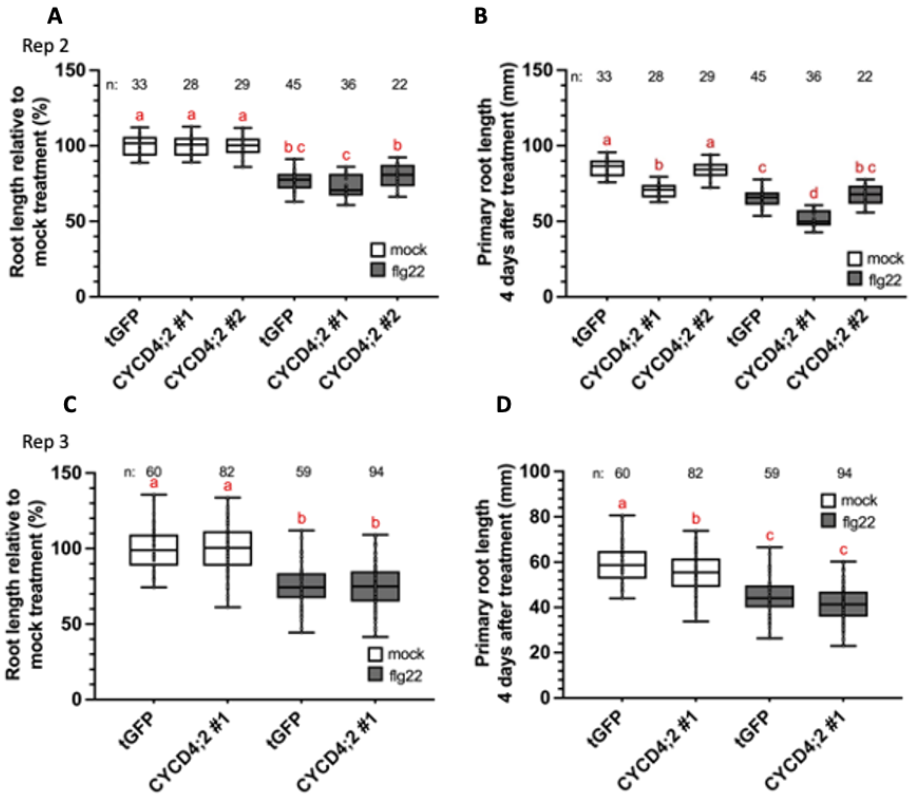

Figure S33: Root growth inhibition assay of *CYCD4;2*-overexpressing *A. thaliana* plants: Two independent *35S::tGFP-3xHA-FLAG::FASTR::AtAct2::CYCD4;2-4xMYC (CYCD4;2)* lines were selected. Col-0 wildtype or *35S::tGFP-3xHA-FLAG::FASTR::AtAct2::tGFP-4xMYC* (tGFP) plants served as controls. 10-day-old seedlings were treated with 100 nM flg22 or mock (water). After 4 days, primary root lengths were measured **(B,D)**. Box and whisker plots show mean primary root lengths in % relative to mock treated roots **(A,C)**. n: samples size. The letters above bars indicate significant differences as determined by ANOVA followed by Tukey´s honest significance test, or Kruskal-Wallis test followed by Dunn's multiple comparison test in case of non-normal distribution. Compact letter display was used for grouping statistical comparisons, where different letters denote significant difference ($p<0.05$) (performed using GraphPad). The experiment was repeated at least three times.

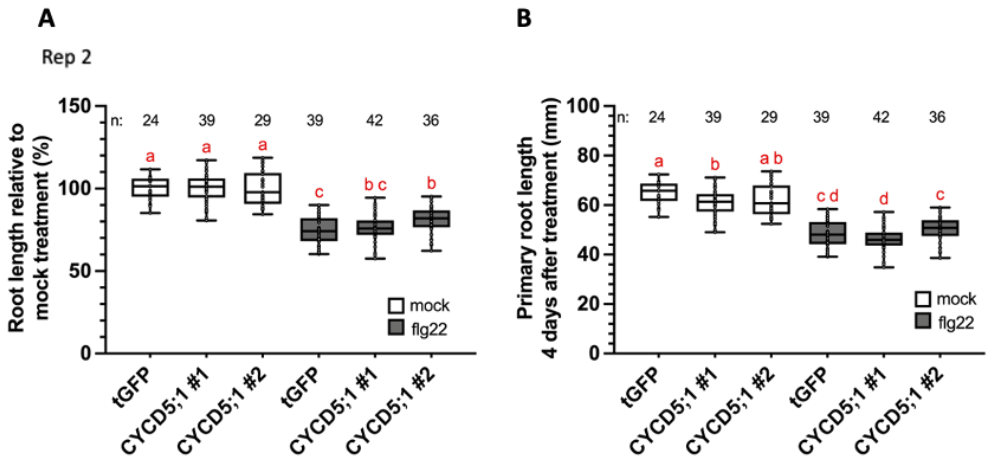

Figure S34: Root growth inhibition assay of *CYCD5;1*-overexpressing *A. thaliana* plants: Two independent *35S::tGFP-3xHA-FLAG::FASTR::AtAct2::CYCD5;1-4xMYC (CYCD5;1)* lines were selected. Col-0 wildtype or *35S::tGFP-3xHA-FLAG::FASTR::AtAct2::tGFP-4xMYC* (tGFP) plants served as controls. 10-day-old seedlings were treated with 100 nM flg22 or mock (water). After 4 days, primary root lengths were measured **(B)**. Box and whisker plots show mean primary root lengths in % relative to mock treated roots **(A)**. n: samples size. The letters above bars indicate significant differences as determined by ANOVA followed by Tukey´s honest significance test, or Kruskal-Wallis test followed by Dunn's multiple comparison test in case of non-normal distribution. Compact letter display was used for grouping statistical comparisons, where different letters denote significant difference ($p<0.05$) (performed using GraphPad). The experiment was repeated at least two times.

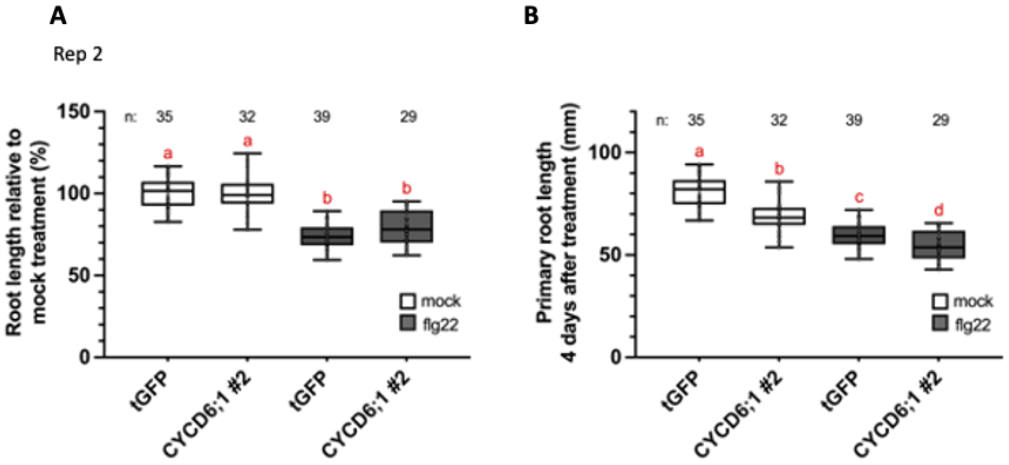

Figure S35: Root growth inhibition assay of *CYCD6;1*-overexpressing *A. thaliana* plants: Two independent *35S::tGFP-3xHA-FLAG::FASTR::AtAct2::CYCD6;1-4xMYC (CYCD6;1)* lines were selected. Col-0 wildtype or *35S::tGFP-3xHA-FLAG::FASTR::AtAct2::tGFP-4xMYC* (tGFP) plants served as controls. 10-day-old seedlings were treated with 100 nM flg22 or mock (water). After 4 days, primary root lengths were measured **(B)**. Box and whisker plots show mean primary root lengths in % relative to mock treated roots **(A)**. n: samples size. The letters above bars indicate significant differences as determined by ANOVA followed by Tukey´s honest significance test, or Kruskal-Wallis test followed by Dunn's multiple comparison test in case of non-normal distribution. Compact letter display was used for grouping statistical comparisons, where different letters denote significant difference ($p<0.05$) (performed using GraphPad). The experiment was repeated at least two times.

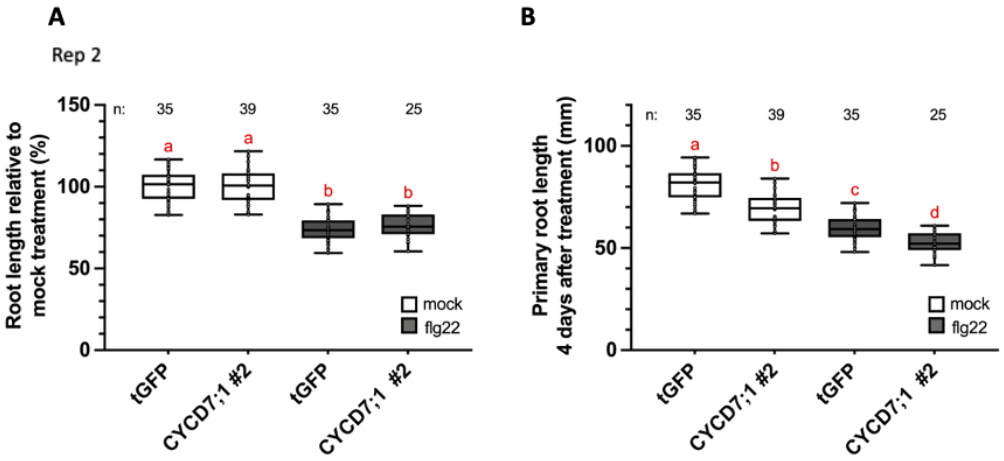

Figure S36: Root growth inhibition assay of *CYCD7;1*-overexpressing *A. thaliana* plants: Two independent *35S::tGFP-3xHA-FLAG::FASTR::AtAct2::CYCD7;1-4xMYC (CYCD7;1)* lines were selected. Col-0 wildtype or *35S::tGFP-3xHA-FLAG::FASTR::AtAct2::tGFP-4xMYC* (tGFP) plants served as controls. 10-day-old seedlings were treated with 100 nM flg22 or mock (water). After 4 days, primary root lengths were measured **(B)**.Box and whisker plots show mean primary root lengths in % relative to mock treated roots **(A)**. n: samples size. The letters above bars indicate significant differences as determined by ANOVA followed by Tukey´s honest significance test, or Kruskal-Wallis test followed by Dunn's multiple comparison test in case of non-normal distribution. Compact letter display was used for grouping statistical comparisons, where different letters denote significant difference ($p<0.05$) (performed using GraphPad). The experiment was repeated at least two times.

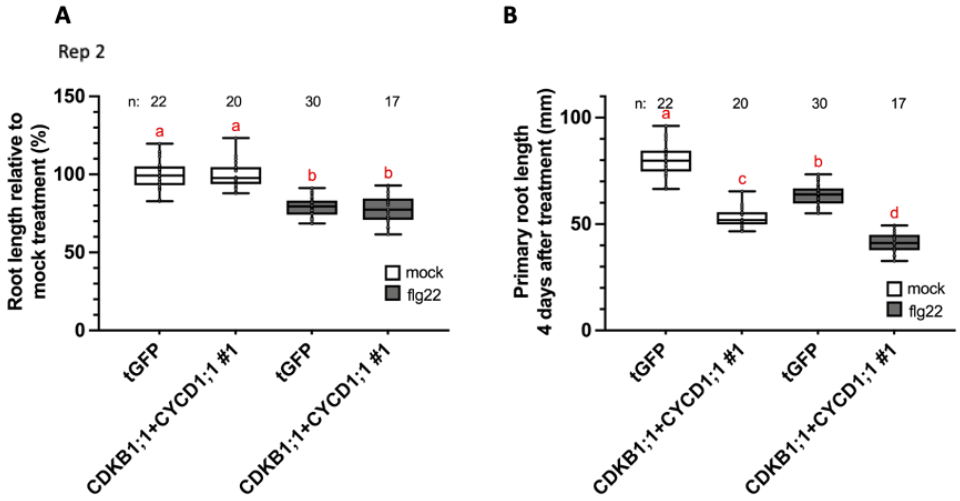

Figure S37: Root growth inhibition assay of *CDKB1;1* and *CYCD1;1*-overexpressing *A. thaliana* plants: Two independent *35S::CDKB1;1-3xHA-FLAG::FASTR::AtAct2::CYCD1;1-4xMYC (CDKB1;1+CYCD1;1)* lines were selected. Col-0 wildtype or *35S::tGFP-3xHA-FLAG::FASTR::AtAct2::tGFP-4xMYC* (tGFP) plants served as controls. 10-day-old seedlings were treated with 100 nM flg22 or mock (water). After 4 days, primary root lengths were measured **(B)**. Box and whisker plots show mean primary root lengths in % relative to mock treated roots **(A)**. n: samples size. The letters above bars indicate significant differences as determined by ANOVA followed by Tukey´s honest significance test, or Kruskal-Wallis test followed by Dunn's multiple comparison test in case of non-normal distribution. Compact letter display was used for grouping statistical comparisons, where different letters denote significant difference ($p<0.05$) (performed using GraphPad). The experiment was repeated at least two times.

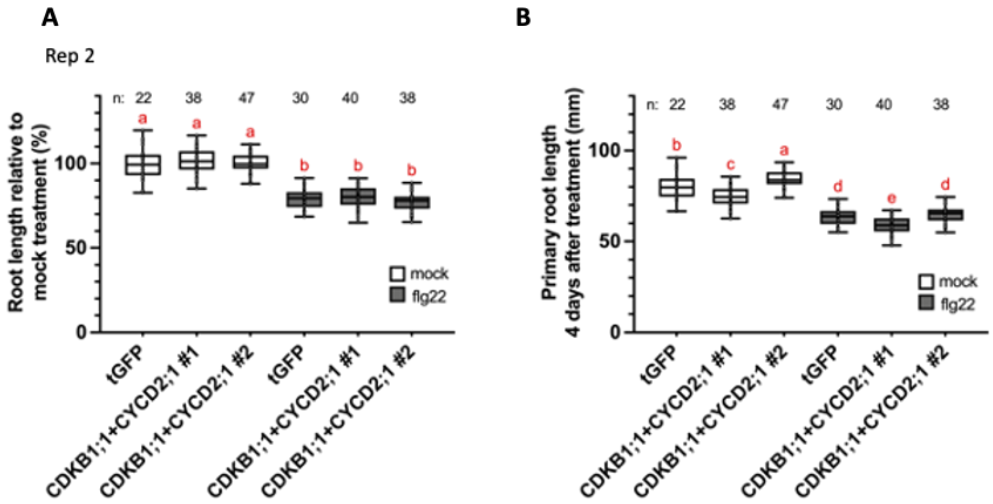

Figure S38: Root growth inhibition assay of *CDKB1;1* and *CYCD2;1*-overexpressing *A. thaliana* plants: Two independent *35S::CDKB1;1-3xHA-FLAG::FASTR::AtAct2::CYCD2;1-4xMYC (CDKB1;1+CYCD2;1)* lines were selected. Col-0 wildtype or *35S::tGFP-3xHA-FLAG::FASTR::AtAct2::tGFP-4xMYC* (tGFP) plants served as controls. 10-day-old seedlings were treated with 100 nM flg22 or mock (water). After 4 days, primary root lengths were measured **(B)**. Box and whisker plots show mean primary root lengths in % relative to mock treated roots **(A)**. n: samples size. The letters above bars indicate significant differences as determined by ANOVA followed by Tukey´s honest significance test, or Kruskal-Wallis test followed by Dunn's multiple comparison test in case of non-normal distribution. Compact letter display was used for grouping statistical comparisons, where different letters denote significant difference ($p<0.05$) (performed using GraphPad). The experiment was repeated at least two times.

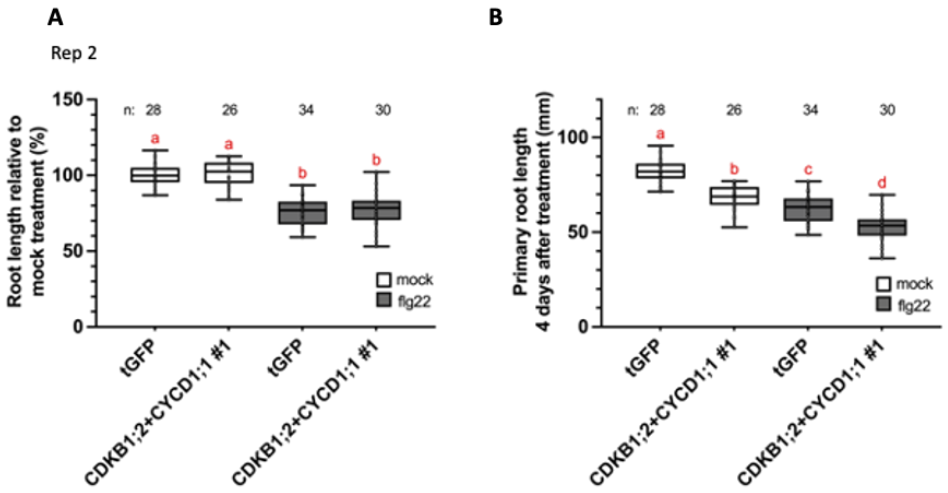

Figure S39: Root growth inhibition assay of *CDKB1;2* and *CYCD1;1*-overexpressing *A. thaliana* plants: Two independent *35S::CDKB1;2-3xHA-FLAG::FASTR::AtAct2::CYCD1;1-4xMYC (CDKB1;2+CYCD1;1)* lines were selected. Col-0 wildtype or *35S::tGFP-3xHA-FLAG::FASTR::AtAct2::tGFP-4xMYC* (tGFP) plants served as controls. 10-day-old seedlings were treated with 100 nM flg22 or mock (water). After 4 days, primary root lengths were measured **(B)**. Box and whisker plots show mean primary root lengths in % relative to mock treated roots **(A)**. n: samples size. The letters above bars indicate significant differences as determined by ANOVA followed by Tukey´s honest significance test, or Kruskal-Wallis test followed by Dunn's multiple comparison test in case of non-normal distribution. Compact letter display was used for grouping statistical comparisons, where different letters denote significant difference ($p<0.05$) (performed using GraphPad). The experiment was repeated at least two times.

Acknowledgements

This work would not have been possible without the help, support, and encouragement of several people, to whom I am deeply grateful.

First, I would like to thank my supervisor Prof. Dr. Patrick Schäfer for giving me the opportunity to work in this exciting project, as well as for his support and guidance during my PhD. I would also like to extend my thanks to my second supervisor, Prof. Dr. Annette Becker for accepting to be my second supervisor and providing warm support and valuable discussion.

I am deeply thankful to Dr. Ruth Schäfer for providing me with extensive mentorship during my PhD, which will have an important impact on my career. Thanks for training me in the lab, always being ready to answer my questions with patience, and engaging in stimulating discussions about the project. I am also grateful for her guidance during the writing process and for critically reading my work. Furthermore, I sincerely appreciate her help with bureaucratic issues outside the lab, and all the support she provided during challenging times.

I would like to thank all the technical and administrative staff, with whom I worked with during my PhD. Especially, I thank Martina Claar for helping with the experiments, Christina Neumann for answering my questions regarding the protein room, Juliette Kellermann and Eva Köpff for their help in harvesting the seeds, and Christina Birkenstock for taking care of the plants.

A special thanks to Maria Ladera-Carmona for being source of support during challenging times, offering encouragement and valuable advice that provided strength when it was most needed. I thank Xuesong, Ena, Sabrine, Laura, and all the members of the Phytopathology institute of the JLU Gießen, who made the laboratory a great place to work, for the wonderful lunches, drinks after work, stimulating discussions about science and life, and the continuous support. The delicious cakes have been a great treat.

Finally, I want to thank my family. This journey wouldn't have been possible without your unconditional love, support, and inspiration. My heartfelt thanks to my mother, Assoc. Prof. Dr. Fahriye Üstüner and my father, Prof. Dr. Yılmaz Üstüner, for supporting all my decisions, even when it meant we were 3000 km apart for years. Thank you for teaching me the importance of perseverance, always striving for growth and kindness. You both have inspired me intellectually and morally. I thank my husband Hakan for moving to Gießen for me, for his endless support, encouragement and patience. Thank you for feeding me during those long, hard-working days and raising my spirits. Your thought-provoking questions about biology and my research were incredibly stimulating. I truly appreciate the intellectual challenge and the great times we have shared together.